THE UNIVERSITY
of EDINBURGH

Modelling and Optimising the Mechanical Behaviour of Fractures Treated with Locking Plates

Alisdair Roderick MacLeod

Doctor of Philosophy

University of Edinburgh

2014

Declaration

This thesis and the associated research has been completed by Alisdair Roderick MacLeod and has not been submitted for any other degree or professional qualification. Where other sources are quoted full references are given.

Alisdair Roderick MacLeod

May 2014

"Death and life are in the power of the tongue"

– Proverbs 18:21

Acknowledgements

Thanks to my supervisor, colleague and friend, Dr. Pankaj, for relaxing on Greek beaches and deliberating over the word ‘however’. It is a blessing to learn from those wiser; I am pleased to report that Pankaj is definitely becoming more like me day by day.

Thanks to Prof. Hamish Simpson for his two-fold patience in taking the time to explain difficult and less difficult concepts and for his invaluable insights that have been inspirations.

Besides the many good friends and colleagues who have been sources of support and encouragement, I would specifically like to thank Noel and JP for their inclusiveness in the office (wanted or otherwise); Feng-Chen for his enthusiasm; Prashant and Francesc for sharing the same birthday; Reza for being there from the beginning of PhD-dom; Alberto Cuadrado for being a cool customer and Maria for being wonderfully irreplaceable.

My family: Mum, Dad, Dougie, Rowan and John Pokora provided a sanctuary of companionship and music and helped me with the English language (so the blame lies here); they also gave a unique slant on what is considered appropriate surgery.

Thanks to the workshop staff and School of Engineering IT department who have arguably been crucial to any research whatsoever, but also for their fast responses to many helpless emails.

The financial support of Orthopaedic Research UK is gratefully acknowledged. Also some aspects of this work would not have been possible without the financial aid of The Osteosynthesis Trauma Care Foundation. Thanks also to Stryker UK for providing the implants used in the experiments.

For the experimental work I must thank Nick Clement for helping to install the implants and Tim Stratford for providing support with software and testing equipment.

Finally, special thanks to Verena for raising the moral, ethical and tidiness standards in our home, being gentle, loving and kind in everything she does and for reminding me what is precious in life.

Abstract

A large number of bone fractures are treated with stabilisation devices that utilise metal wires or screws, which traverse the bone and are connected to an external frame or internal plate. Clinically, fixation devices are required to be able to: sustain loads; minimise patient discomfort and possible implant loosening; and promote healing. In the recent years locking plates have become increasingly popular for osteoporotic or complex fractures, which can be difficult to manage. It, however, remains unclear as to how these devices need to be configured for optimum clinical performance. This thesis investigates the mechanics of locking plates, factors that influence their performance and provides guidance to optimise the placement of screws. Finite element simulation and analytical models were developed and validated using lab-based experimental models.

The local behaviour around the screw-bone interface is considered and the implications of different modelling assumptions assessed. A novel method of simulating the effect of radial interference due to pilot-hole size is proposed. Different screw types are evaluated: osteoporotic bone is found to be particularly susceptible to the screw tightening preload used in compression screws; far-cortical locking screws are found to slightly reduce device stiffness but substantially increase strain levels around screw holes. Finite element simulations show that many of the local effects, such as preloads and contact modelling, can profoundly influence the prediction of strains around screws but do not generally influence the global load-displacement behaviour; the screw-plate connection and bone/plate material and geometric properties are found to have an influence on global stiffness predictions. The key determinants of load-displacement behaviour evaluated through models are the loading and restraint conditions, which explain the huge range of stiffness predictions in the literature (three orders of magnitude). An analytical model based on 7 bone-plate construct parameters is developed. Despite its simplicity, the model is found to be able to predict the axial stiffness for experimental

tests conducted and for 16 other cases from five previous studies with an average error of 20%. The manner of load application, not considered in the literature, is shown to dramatically alter predictions of plate stress, strains within the bone and conclusions regarding screw placement. Even with the inclusion of muscles forces, the choice of restraint condition dominates the mechanical behaviour. Using the models, the influence of screw position is systematically evaluated in varying bone qualities under axial loading and torsion and guidance for optimising fixation is developed.

Contents

List of Figures

List of Tables

Summary of Chapters

Chapter 1 introduces the concept of locking plates, their role in fracture fixation and potential complications that can arise. The process of fracture healing and the problems associated with different pathologies are reviewed and the research questions of the thesis summarised.

Chapters 2 & 3 evaluate the impact of different finite element (FE) modelling assumptions at the screw-bone interface and the impact of radial preload produced during screw insertion.

Chapter 4 uses FE simulation to compare locking plates with conventional plating and provides biomechanical evidence to support the improved performance of locking plates in osteoporotic bone.

Chapters 5 & 6 investigate the influence of loading and restraint conditions in the testing of tibial mid-shaft osteotomies in vitro and using FE simulation.

Chapter 7 develops an analytical model of the bone-plate system and evaluates the importance of various aspects of construct geometry and screw placement in predictions of mechanical response.

Chapter 8 assesses the impact of different locked plating screw configurations on the strains within varying qualities of host bone.

Chapter 9 compares alternative uses of locked plating such as uni-cortical fixation and far-cortical locking in osteoporotic bone under axial and torsional loading.

Chapter 10 attempts to simulate the in vivo mechanical environment within the femur during walking gait. A range of locking plate screw configurations for different fracture locations are evaluated throughout the course of healing in a distal femoral fracture.

1

Introduction to Fracture Fixation Using Locked Plating

The primary goal of fracture management is to enable the fracture to heal. This involves stabilisation of the fractured bone in order to achieve healing within a given time period but also to control the position of the bone for functional outcome (Taljanovic et al., 2003).

Several fracture management options are available to the orthopaedic surgeon:

1. Non-operative immobilisation by means of a cast, splint or brace.

2. External fixation where the bone is stabilised through the skin using pins or wires and the device remains outside of the body.

3. Internal fixation where the entire device is implanted.

Non-operative options remain the most prevalent treatment, particularly in children, in all except specialised trauma hospitals (Court-Brown et al., 2010). This is chiefly because they do not entail the risks of surgery; however, there are several reasons why they are not always preferred. Not all fractures will go on to union using a cast and when union is achieved they are more prone to shortening or rotational deformities (Newman et al., 2010, McGrath and Royston, 2003). The use of a cast is avoided in open fractures which require wound access.

External fixation allows wound access and, as the device can be incrementally changed, is often used to correct deformities. While the more flexible Illizarov tensioned wire fixator has been particularly successful for limb lengthening procedures, other devices such as monolateral and multiplanar fixators have higher malunion and non-union rates, which have been attributed to the complexity of the devices and sensitivity to the configuration (McGrath and Royston, 2003). All external fixation, however, carries a significant risk of pin-site infection. In the femur and tibia screw loosening or infection has been reported to affect one third of patients (Moroni et al., 2002). In 2011, a Cochrane review concluded that there was "no strong evidence that one pin care technique was better than any other for reducing the chance of infection and other complications" (Lethaby et al., 2011). The device itself is also cumbersome and intrusive, and requires considerable patient cooperation and responsibility with respect to pin-site care (McGrath and Royston, 2003).

Internal fixation has the advantage of enabling precise anatomical reduction, which is essential for fractures near articular surfaces (Strauss et al., 2008). At present most internal fixation procedures are performed by open reduction, however, minimally invasive techniques where the plate is inserted and fracture reduced percutaneously (through the skin) are becoming more common (Mushtaq et al., 2009). In practical terms, internal fixation is less obtrusive than external fixation and allows earlier mobilisation; however, it is also limited by the size of the device that can be implanted

demanding a higher degree of engineering. Two of the most common internal fixation implants are: intramedullary (IM) nails where a metal rod is inserted into the central cavity of the bone; and metal plates, which are applied to the external surface of the bone. Both are fastened to the bone using screws. Plates are considered to be more surgically demanding than IM nails and their success is largely dependent upon preoperative planning and implant configuration (Gautier, 2009). The use of plates and screws for internal fixation will form the focus of this thesis.

1.1 Historical Internal Fixation

Internal fixation, in the form of screws and pegs, has been used since the mid-nineteenth century with plates and intramedullary nails being introduced at the turn of the twentieth century (Uhthoff et al., 2006, Bartonicek, 2010). Prior to this amputation was the most frequent operative solution due to the justifiable fear of surgery and, in particular, the risk of infection (Bartonicek, 2010). Problems with corrosion in metal implants, and insufficient strength of other materials meant that improvements in internal fixation were stalled until the advent of the compression plate in the 1950s (Uhthoff et al., 2006). The novelty with this system (discussed below) was in compressing the bone fragments together so that the bone transmitted a large component of the load, not the plate. This system has been widely successful in the form of the dynamic compression plate (DCP), but still suffers from some inherent problems.

1.2 Plate Fixation

The types of plate fixation most commonly used differ primarily in the screw design (Gautier, 2009). The dynamic compression plate (DCP) uses compression screws that tighten the plate to the bone (Figure 1.1a). Additionally, some have angled screw holes in the plate to induce a preload between fracture fragments during screw insertion (Gardner et al., 2004). The ‘dynamic’ in the title refers to the ‘dynamic compression’

induced between bone fragments either generated using a tensioning device or generated by the screws within the holes during insertion. This aids in fracture reduction and helps eliminate any gaps between fractured bone ends. A newer type of plate, the locking compression plate (LCP), uses locking screws that have a threaded head enabling the screw to fasten into the plate as well as to the bone (Figure 1.1b) (Perren, 2002). This connection means that the plate is not tightened against the bone and can even be offset from it, helping to preserve the periosteum (Perren, 2002, Mushtaq et al., 2009). Compression screws can also be mixed with locking screws when using the LCP (Frigg, 2001).

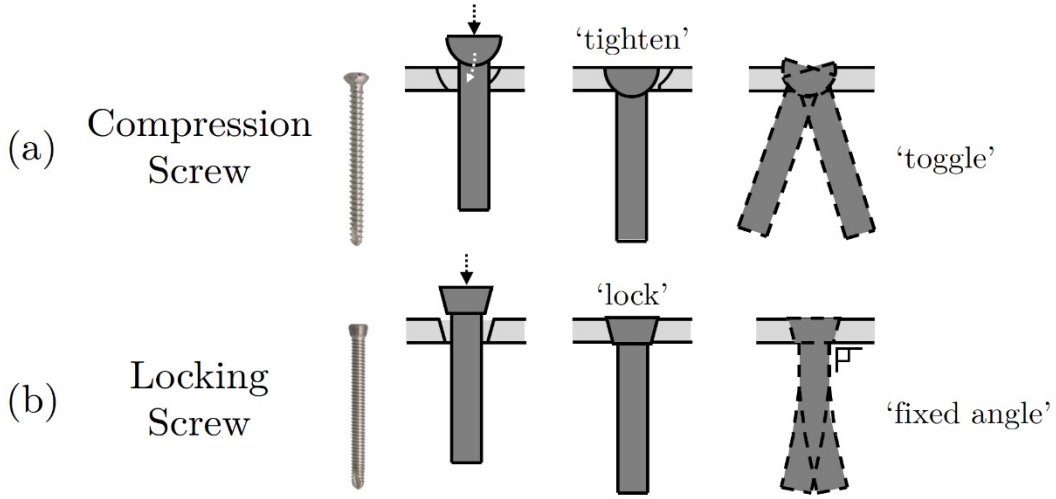

Figure 1.1 - Depiction of (a) compression screws migrating towards the fracture during tightening and (b) locking screws fastening during tightening.

Although the first coining of the phrase 'locking compression plate' (LCP) was only 13 years ago (Frigg, 2001), the LCP is now being researched intensively; the number of published research articles in the period 2006-2010 was greater than the DCP which has existed for nearly 50 years (Allgöwer et al., 1970) (Figure 1.2). Nevertheless, due to their ability to compress fractures, compression screws are still the most commonly used of all internal fixation devices (OrthoInfo, 2007).

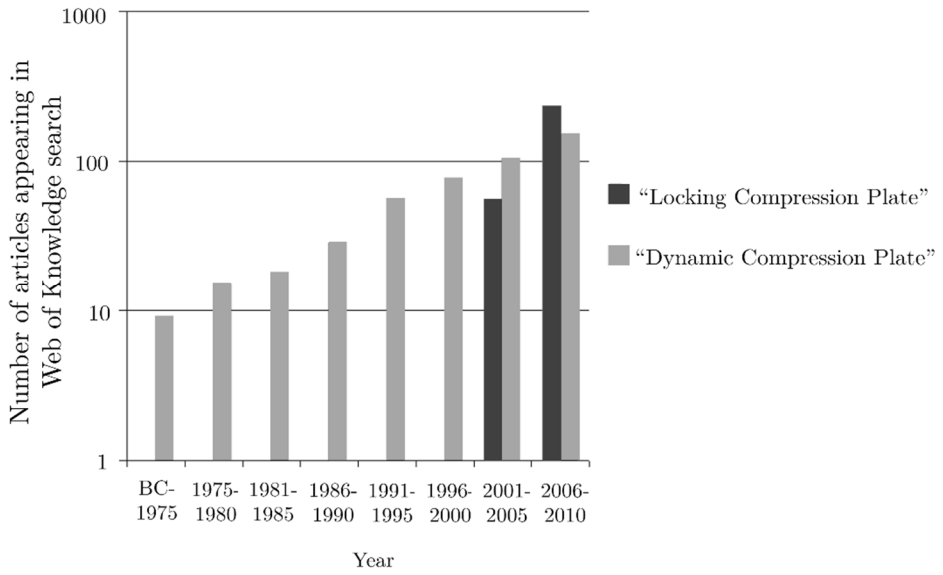

Figure 1.2 – Number of published articles appearing in Web of Knowledge search with the terms "dynamic compression plate" and "locking compression plate".

1.2.1 Fracture Repair

Bone is not inert; it is continually undergoing turnover and is known to adapt to changes in loading (Doblaré et al., 2004). Fractures can occur either by a sudden traumatic loading event that exceeds the strength of bone or by gradual accumulation of damage at a rate greater than can be repaired (Doblaré et al., 2004). Fracture healing can take two courses. Direct or primary bone healing is where the bone fragments are in close enough proximity to allow the metabolic bone cells to bridge the gap and heal the bone 'directly' (Uhthoff et al., 2006). Indirect or secondary bone healing, representing the majority of cases, is where the bone fragments are separated by a greater distance. In this situation, the formation of a haematoma (blood clot) ensues, gradually solidifying into fracture callus and eventually mature bone uniting the fracture fragments (Gaston and Simpson, 2007). During healing the fracture callus passes through different phases which are associated with tissue type: initially a blood clot forms soft granulation tissue; this develops into hyaline cartilage and woven (or immature) bone and is gradually replaced with aligned lamellar (or secondary) bone (Doblaré et al., 2004, Claes et al.,

1998). Different tissues are able to form at different levels of strain and deviatoric strain is thought to govern this (Carter et al., 1988, Isaksson et al., 2006). The final phase is remodelling where the bone is adapted to the original bone stress/strain contours (Murray et al., 1996).

1.2.2 **Philosophy of Fixation**

Compression plating aims to achieve direct bone healing using so-called 'absolute stability'[1] whereby minimal interfragmentary motion occurs (Reeves et al., 2007). In cases where the fracture pattern is segmental or comminuted absolute stability of all fragments may be too difficult to achieve; in this case 'relative stability' is the goal, where the primary fragments are secured and the remaining fragments or debris are untouched. This is also known as bridge plating (Gautier, 2009). In all cases, unless all fracture displacement is completely abolished, indirect bone healing ensues. Direct healing is slower (Woo et al., 1983, Perren, 2002) and requires a more invasive surgical procedure, which consequently entails higher risk of delayed healing and infection (Perren, 2002, Strauss et al., 2008). As a result, there has been a shift towards more 'biological' fixation, which aims to reduce the detrimental impact of the implant on the bone, utilise indirect healing and improve vascularisation (Perren, 2002).

[1] The term 'stability', as used in clinical practise, is often misleading when used as a synonym for stiffness or rigidity, rather than the engineering usage 'the ability of a structure to carry a given load'. Two structures may be equally stable and one may be more flexible; therefore the engineering usage has been used herein. The unstable definition of stability has been previously noted in relation to spine biomechanics (Reeves *et al.* 2007).

1.2.3 **Interfragmentary Strain**

Provided that the fracture region is sufficiently vascular, the principal factor that governs indirect bone healing is the amount of relative motion between bone fragments at the fracture site (Claes et al., 1998). For optimum healing, therefore, the amount of interfragmentary movement (IFM) allowed by a fixation device is critical (Gaston and Simpson, 2007, Epari et al., 2007). Too little motion and there is insufficient mechanical stimulation (Goodship and Kenwright, 1985); too much and the healing callus tissue can sever, disrupting healing (Claes et al., 1998). The type of motion that occurs is also important. Moderate axial motions have been shown to be beneficial (Epari et al., 2007, Goodship and Kenwright, 1985, Cunningham et al., 1989) whereas excessive shear motions are thought to be disruptive (Epari et al., 2007, Augat et al., 2003). The mechanical stimulation is often expressed as interfragmentary strain (IFS) which is defined as the axial IFM relative to the total fracture gap size (Kim et al., 2010, Miramini et al., 2013), or percentage gap closure as

$$IFS\ (\%) = \frac{IFM}{Fracture\ Gap\ Size} \tag{1.1}$$

The amount of IFM generated at the fracture site is strongly dependent on the rigidity of the device and healing can be impaired if the system is too rigid or too flexible (Gardner et al., 2009). The IFM, however, must be appropriate for the fracture gap size (Perren, 2002). The immediately post-operative IFS exposure at the fracture site is strongly correlated with speed of healing (Comiskey et al., 2010) and the optimal strain range, in the early stages of healing, appears to be 10-40% (Goodship A and Cunningham J, 2001).

1.2.4 **Mixing Fixation Philosophies**

Although locked screws and compression screws can be used in the same plate, using the LCP, they represent a contradiction in biological healing environments (Egol et al.,

2004, Perren, 2002). Locking screws cannot compress the fracture and rely on IFM to stimulate indirect healing; compression screws aim to eliminate motion and allow direct healing. Clearly, when choosing a device for a patient, it is important to consider whether it is direct or indirect healing that is being sought. The danger of mixing fixation philosophies has been previously demonstrated in a study by Krettek et al. (1991), which showed that external fixators used in combination with lag screws had a higher rate of re-fracture and more frequent need for bone grafting. Another contradiction between the screw types is at the bone-plate interface: compression screws pull the plate towards the bone; locking screws secure the bone at a fixed distance. These differences have resulted in essential surgical safeguards; for example, when using hybrid devices, with both screw types, locking screws must be inserted last (Apivatthakakul et al., 2012). This prevents undesirable preload being induced in the plate or screws. Nevertheless, compression screws can still be used safely as a tool to control plate positioning and restore fragment alignment in devices aiming to achieve indirect healing; likewise, locking screws can also be added to improve fixation in constructs aiming to achieve direct healing with compression screws (Gebhard et al., 2008).

1.2.5 **Stiffness**

The stiffness of a device is generally defined as the load required to produce a unit displacement. This makes it sensitive to the location at which movement is monitored; for example, the displacement at the fracture site is not the same as the movement at end of the bone. Indeed, the displacement varies across the entire fracture site (Bottlang et al., 2009b). Stiffness predictions can also vary with increasing load due to nonlinear load-displacement behaviour. The stiffness of Illizarov devices is known to change rapidly as the wires sag (Zamani and Oyadiji, 2009) and in plating the eccentricity of the load increases as the plate bends, also producing a nonlinear mechanical response.

1.3 Demand for Orthopaedic Research

Any implant will alter the natural load distribution within the host bone. Indeed, the intention is to redirect load and shield the bone from undesirable motion while supporting motion beneficial for callus formation until healing has occurred (McKibbin, 1978, Gaston and Simpson, 2007). This redirection of load also results in other unwanted effects: stress-shielding and stress concentration at the bone-implant interface. Stress-shielding, in which the implant unloads a region of bone, has received much attention (Uhthoff et al., 2006). If shielding occurs, the load that has been removed from one area must be transferred somewhere else; hence, overloading of the device can also occur. On the other hand, stress concentrations in the bone arise because loads are transferred via the screws inducing large stresses/strains at the bone-implant interface (MacLeod et al., 2012). Locking plates represent a considerable engineering challenge as they are eccentric to the dominant loading axis, thus inducing additional bending and shear (Huiskes et al., 1985). The mechanical evaluation of locking plates will form the focus of the thesis.

1.3.1 Mechanical Requirements of Fixation

There are three clinical requirements made of a device and mechanical demands arising from them:

- **The device must promote healing.** As discussed, the correct level of IFM is crucial for healing; this can be controlled by selection of an appropriate stiffness of device.

- **The device must sustain the applied loads for the duration of healing**. This concerns the strength and potential failure of the device itself. Stresses within implants are of interest as breakage can occur; this is more likely if healing has been delayed (Vallier et al., 2006).

- **The device should minimise its detrimental impact on the limb and any patient discomfort resulting from it**. If a device is painful then the patient is unlikely to weight-bear. Moreover, excessive stress at the screw-bone interface can cause loosening and infection resulting in device failure.

The requirements can be interdependent, for example, faster healing may reduce the fatigue strength demanded of a device; minimising damage to host bone around the screws will prevent discomfort and loosening and will, therefore, lead to faster healing. Therefore, the key variables of interest in biomechanical studies of orthopaedic devices are: IFM, device strength and screw-bone interface damage.

1.3.2 Failure Modes in Locked Plating

Besides failure to heal, locked plating can fail in other ways:

1.3.2.1 Plate Breakage

Failure of plates is generally due to fatigue and not a single traumatic event, meaning small differences in stress can have a significant effect on the lifespan (Ellis et al., 2001). Plate breakage is often attributed to poor screw placement or delayed healing (Gardner et al., 2009, Button et al., 2004, Hunt and Buckley, 2013).

1.3.2.2 Screw Breakage

Under physiological activities, screws are exposed to bending forces. Although other forces are present within screws, peak bending stresses in compression screws have been found to occur close to the screw head within the near cortex, and this is where clinical failures are seen (James and Andrade, 2013). While locking screws can also break at this location, it is more common for them to fail at the screw-plate junction (Leahy, 2010).

1.3.2.3 Screw Loosening

Excessive stress at the screw-bone interface is known to cause loosening around screw holes and carries a risk of infection (Fragomen and Rozbruch, 2007, Moroni et al., 2002). Screw loosening is more common in osteoporotic bone, compression plating and uni-cortical fixation (Gautier and Sommer, 2003); however, bi-cortical locking screws have a unique failure mode described as "cut-out" or "the windscreen wiper effect" where a swath of bone is gradually removed (Leahy, 2010).

1.3.2.4 Peri-Prosthetic Fracture

Fracture of the bone at the end of a plate can occur and is associated with osteoporotic bone and bending or torsional loading (Gardner et al., 2009, Bottlang et al., 2009a, Fitzpatrick et al., 2009). When it does occur it is usually around the last screw at the end of the plate. Additionally, compromising the integrity of the bone due to screw holes or bone atrophy can lead to periprosthetic fracture during fixation or re-fracture after device removal (Perren, 2002).

1.3.3 **Fracture Locations**

The tibia is the most commonly injured long bone in the body (Konowalchuk et al., 2009, Alho et al., 1992, McGrath and Royston, 2003). Fracture management can be controversial due to the wide range of possible treatments and complications (Bhandari et al., 2001, Mushtaq et al., 2009, Newman et al., 2010). Some authors have recommended that locked plating is indicated in the first instance for comminuted, osteoporotic or periarticular fractures but also for revision surgery where other devices have failed (Hunt and Buckley, 2013, Smith et al., 2007). In a survey of 169 fractures treated with locked plating, Sommer et al. (2003) found that the tibia was the most frequently treated bone and that 67% of the fractures treated were diaphyseal. In this study the main causes of failure (and percentage of incidence) were: non-union/ delayed union (3%); loosening (3%); plate breakage (2.4%); and re-fracture (2.4%). Complication

rates can be as high as 20% in the distal femur (Forster et al., 2006, Button et al., 2004, Henderson et al., 2011) and 26% in periprosthetic fractures (Ebraheim et al., 2012). Failure is generally associated with inappropriate application and can therefore be avoided with improved understanding and consistency in treatments (Sommer et al., 2003, Gautier, 2009, Leahy, 2010, Button et al., 2004, Gardner et al., 2009). Reducing the incidence of plate failure would also reduce the significant cost burden of revision surgery (Gerber et al., 1990).

Two fracture locations were adopted for the purposes of this thesis: the tibial diaphysis and distal femur. In the tibia during gait the dominant loading direction at the joints is axial (Wehner et al., 2009). Muscle forces also generally act axially, but are considerably smaller in magnitude than the joint reactions (Duda et al., 2002) meaning that physiological gait loading can be reasonably well approximated even in models that ignore muscles. The femur, however, is subject to greater bending and the multidirectional muscle forces are thought to be vital for realistic modelling (Sverdlova and Witzel, 2010, Phillips, 2009).

1.3.4 **Device Configuration**

One of the main concerns with locked plating is that they can become too stiff thereby generating insufficient motion for optimal healing (Kubiak et al., 2006, Bottlang et al., 2009b, Leahy, 2010). The arrangement of screws in the plate dramatically changes the stiffness of locked plating (Stoffel et al., 2003); however, the optimum number of screws and their placement depends on many factors and is still a matter of debate for orthopaedic surgeons (Izaham and Kadir, 2010, Mushtaq et al., 2009, Sommer et al., 2003, Williams and Schenk, 2008). In a study of 86 distal femur fractures, Henderson et al. (2011) found those which failed to heal were significantly ($p = 0.01$) more likely to have used screws placed immediately adjacent to the fracture site. Despite the importance of screw placement, there appears to be a wide variability in the configurations used by different surgeons even when using the same device. A recent

study in the US showed that the bridging span and number of screws employed by different surgeons using locking plates varied significantly for similar fracture scenarios (Fitzpatrick, 2009). There are also large differences in healing rates reported for similar devices using different materials (Lujan et al., 2010) indicating that this is something which is not appropriately accounted for.

Postoperatively, recommendations for weight bearing also vary widely (Granata et al., 2012) and there is a large variability in the weight bearing of individuals (Vasarhelyi et al., 2006). This means that the strain exposure at the fracture site is not optimised for an individual patient's fracture pattern and/or implant. If a method of providing simple, patient-specific guidance could be developed it would represent one of the most economical ways to improve mechanobiologic environment of the fracture (Schnaser and Vallier, 2013).

1.3.5 **Biomechanical Studies**

The compressive, bending and torsional stiffness of bone implanted with various devices is extensively studied due to its importance for bone healing; however, predictions are highly variable and there appears to be large inconsistencies between studies (Schmidt et al., 2013). For example, estimates of axial stiffness for locking plates can vary by three orders of magnitude (Stoffel et al., 2003, Bottlang et al., 2009b). The influence that device configuration and fixator choice has on strains within the bone and stresses within the implant is less well studied, but receiving growing attention (Salas et al., 2011b, Anitha et al., 2013, Arnone et al., 2013, Chen et al., 2013, Nassiri et al., 2013, Luo et al., 2013). While there is strong consensus that locking screws are superior to compression screws in osteoporotic bone (Miller and Goswami, 2007, Smith et al., 2007, Sommer et al., 2003), it is debatable whether they are advantageous in healthy bone (Kim et al., 2007). Additionally, there are variations in the application of locking screws that include uni-cortical and far-cortical locking screws; the optimum usage of which is

less clear (Bottlang et al., 2009b, Moazen et al., 2013, Davenport et al., 1988, Beaupre et al., 1992, Hunt and Buckley, 2013).

1.3.6 **Osteoporosis and Obesity**

Osteoporosis is a bone wasting disease defined by the World Health Organisation as a bone mineral density that lies 2.5 standard deviations or more below the average value for young healthy women (a T-score of <-2.5 SD) (WHO, 1994). It is characterised by structural deterioration of bone tissue, with a consequent increase in bone fragility and susceptibility to fracture (NICE, 2012). Osteoporosis occurs due to an imbalance in the activity of bone cells, which govern bone turnover resulting in a more rapid thinning and retreating of the endocortical surface. Although endosteal thinning occurs naturally, in men it is compensated for by periosteal apposition, increasing the total bone cross-sectional area and maintaining the overall structural integrity of the bone, in terms of cortical thickness and second moment of area (Russo et al., 2006). While increases in the medullary cavity size are similar for women, the total bone area does not increase and the net loss is taken by a reduction in cortical thickness.

Osteoporosis is currently considered to be an epidemic (Tan and Balogh, 2009) with over 250,000 fractures every year in the UK alone (NHS); moreover, with 23 per cent of the UK population projected to be aged 65 and over by 2034, the incidence of osteoporotic fractures are likely to increase further (ONS, 2011). Many conventional implants are known to perform poorly in osteoporotic bone, with a higher incidence of implant failure and reduced functional outcome (Schneider et al., 2005, Giannoudis and Schneider, 2006). Locked plating is being widely promoted as offering safer fixation for osteoporotic patients (Yanez et al., 2010, Kim et al., 2007, Cronier et al., 2010); the use of locking plates is therefore expected to increase (Zhang and Ge, 2009). At present, however, there appear to be no studies that incorporate the effect of the porous micro-architecture of osteoporotic bone when evaluating the performance of locking plates using computational simulation. The deterioration and thinning of bone due to

osteoporosis can increase its susceptibility to damage at the screw-bone interface (Donaldson et al., 2012b) and compromise its resistance to particular types of loading such as torsion or screw pull-out (Donaldson et al., 2012a).

Obesity is also a growing concern in orthopaedics as obese people are more likely to have fractures of the extremity, particularly around the knee and ankle (Sabharwal and Root, 2012). They are also more likely to have joint replacement due to osteoarthritis, which then puts the patient at risk of periprosthetic fracture. Interestingly, although obese and overweight people have been shown to have increased apparent bone mineral density, when normalised for body mass it was significantly lower (Templeton et al., 2010). This may be caused by the relative inactivity of the group, and hence lack of dynamic loading, despite having larger body mass' (Lanyon and Rubin, 1984).

The presence of increased loading from obesity or poorer bone quality due to osteoporosis may alter the performance of fixation device; however, there is no accepted methodology for selecting or configuring a locking plate for patients with different bone properties or weights.

1.3.7 **Finite Element Simulation**

There are several reasons why finite element (FE) modelling is being used to evaluate devices. Parametric evaluation of devices is fast as many more variations can be tested, often by changing only a single value. In vitro testing is limited in the loading that can be applied to a bone and is often not representative of the in vivo scenario (Phillips, 2009). FE modelling can predict and, sometimes more importantly, visualise results, which may be difficult or impossible experimentally or with elementary mechanics. This can improve the understanding of physical experiments and help inform lab experiments for more productive research (Cristofolini et al., 2010).

Recent advances in imaging and software have made the production of three-dimensional computer models from CT-scans much easier, faster and more readily

available. This has hugely positive implications for incorporation of realistic geometry in FE models; however, it has also been voiced that it can lead to an over-emphasis on the visual similarity of the models, which, in itself, is no guarantee of a good model (Prendergast, 1997). To ensure the validity of FE models every aspect of them must be tested. This thesis is predominantly simulation-based and throughout it every aspect of the models was investigated including: solution convergence and mesh sensitivity; contact effects arising from the assumed interactions between the bone, screws and plate; geometrical effects due to specimen size, positioning and device configuration; and the influence of the test set-up involving loading and boundary conditions. Additionally, FE models were developed in parallel with analytical models and experimentally conducted lab tests for direct validation.

1.4 Thesis Aims

The aim of this thesis is to provide guidance on the following:

- How to produce the optimum mechano-biological environment at the fracture site when using locking plates.
- How to prevent failure of locked plating devices.
- How to mitigate the detrimental impact that locked plating has on varying bone qualities and reduce the incidence of screw loosening.

These questions encompass many complexities including: the physiological loading of the body, the non-uniform material and geometrical characteristics of bone, which are unique to each individual and change with age, the time dependent nature of fracture healing and the vast number of possible fracture scenarios to name a few. Lastly, in what is a relatively new field, there is a large amount of uncertainty associated with biomechanics. To measure the true mechanical environment within the body directly, although it has been done in the form of telemetric implants for the hip and knee, presents many difficulties. Consequently, the thesis also hopes simply to improve our understanding of bone-plate systems.

2

Screw-Bone Interface Modelling

2.1 Introduction

A significant proportion of fractures are treated by stabilisation devices that utilise screws or pins, which traverse the bone and are attached to an external frame or internal plate. When using these devices two key biomechanical predictions are of clinical interest: motion at the fracture site, which is important for healing (Goodship and Kenwright, 1985, Gaston and Simpson, 2007); and the potential for loosening or failure at the screw-bone interface (Ahmad et al., 2007, Park et al., 2000). The bone-implant interface is the location where complications and failure most often occur (Compte and Straumann, 1985); therefore appropriate modelling of the bone-implant interface is essential for quality biomechanical predictions when using numerical models. The choice of contact interaction will clearly influence bone-implant interface motions and has been previously reported to alter bone remodelling predictions in dental implants (Eser et al., 2010). It is likely that it would also alter predictions of screw loosening, bone damage, and even fracture risk (periprosthetic fractures are usually at a bone-implant interface).

Behaviour of the bone-implant interface is one of the most uncertain aspects of contemporary computational modelling. This is primarily due to the difficulties in measuring relevant information such as contact pressure and because of the variation that can occur over time and with patient-specificity. Board et al. (2007) found that different external fixators (uni-lateral and Illizarov) produce very different stress environments at the screw-bone interface indicating that each fixation device needs to be evaluated individually.

2.2 Previous Studies

In previous studies, computational models of plate fixation the screw-bone interface has been represented using a range of approaches. The most common approach is to assume a fully-bonded interface wherein the surfaces of the screw and the bone are assumed to be tied (Krishna et al., 2008, Wirth et al., 2010, Stoffel et al., 2003, Baggi et al., 2008, Genna et al., 2003, Koca et al., 2005, Veziroglu et al., 2008, Chen et al., 2009, Shah et al., 2011, Dubov et al., 2011, Kim et al., 2011b, Wieding et al., 2012, Bottlang et al., 2010a). This approximation simplifies the analysis by making it linear. It also inherently assumes full osseointegration between the screw and the bone, which is unlikely to be the case particularly in the short-term after the treatment (Pessoa et al., 2010). This assumption has been criticised for providing an inaccurate representation of the contact interaction as no separation between screw and bone can occur (Natali, 1992, Huiskes et al., 1985).

Several studies have used a frictional interface ignoring screw threads (Kim et al., 2010, Fouad, 2010, Mathurin et al., 2009, Izaham and Kadir, 2010, Alonso-Vazquez et al., 2004, Moazen et al., 2012, Eser et al., 2010, Ramakrishna et al., 2004) while some others incorporate screw threads (Karunratanakul et al., 2010, Gefen, 2002). The reason for ignoring screw threads and simplifying screws to cylinders is for computational speed and ease of meshing. Coefficients of friction used vary widely from 0.1 to 0.9 with the

larger values generally used to simulate screw-bone interaction in models without threads.

While the majority of previous studies use three-dimensional models they are generally idealised hollow cylindrical representations of bone (Krishna et al., 2008, Kim et al., 2011b, Kim et al., 2011a, Stoffel et al., 2003, Bottlang et al., 2010a, Karunratanakul et al., 2010), which means that the system maintains two planes of symmetry. Some asymmetric three-dimensional exceptions exist where the full geometry of the bone was modelled; however, they all use simplified screw representations – in the form of a tied interface (Nassiri et al., 2012, Chen et al., 2009, Shah et al., 2011) or 'structural' screws modelled as beam elements (Duda et al., 2002, Wieding et al., 2012)

This chapter considers different three-dimensional interface modelling approaches: a fully-bonded assumption; and sliding contacts with varying frictional coefficients. Comparisons are made against simplified frictional and tied models that ignore the screw threads and treat the screw as a cylinder. In addition, the influence that varying the loading condition and the Young's modulus of bone has on the contact interaction is also examined.

2.3 Aim of the Chapter

The aim of the chapter is to examine the influence of different interface modelling strategies on the global load-deformation behaviour and the local stress-strain response within the bone in the vicinity of the screws.

2.4 Methods

2.4.1 Geometry

A three-dimensional finite element model was created in Abaqus (Simulia, Providence, RI, USA) using an existing tibia geometry available within the group (Donaldson et al., 2012a, MacLeod et al., 2012), which was acquired via the BEL repository freely available from www.biomedtown.org (now accessed through PhysiomeSpace[2]). A cross sectional slice of the tibial mid-shaft was taken and the internal and external surfaces scaled to match data from Russo et al. (2006) (Figure 2.1a). The bone had an average uni-cortical thickness and cross-sectional area of 5.1mm and 319mm^2 respectively, which is representative of a young female. The cross-sectional slice was then extruded to a length of 80mm. A fracture gap region of 10mm was left between the fracture surface and the plane on symmetry (Figure 2.1b). This produced a total specimen length of 180mm. The locking plates had cross-sectional dimensions 3.6 x 12.0 mm (Figure 2.2). Modelling helical screw threads results in slivers of bone at the cortex surface and subsequent meshing issues; for this reason, idealised rings were used. As diaphyseal fixation was considered, only cortical bone was modelled. When using locking screws there is no requirement for the plate to be in contact with the bone, indeed it is desirable for healing to off-set the plate from the bone. The models used a 2mm bone-plate off-set and no contact interaction was specified between bone and plate.

[2] Physiome Space Portal© 2013, Super Computing Solutions, www.physiomespace.com, last accessed 31st March 2014.

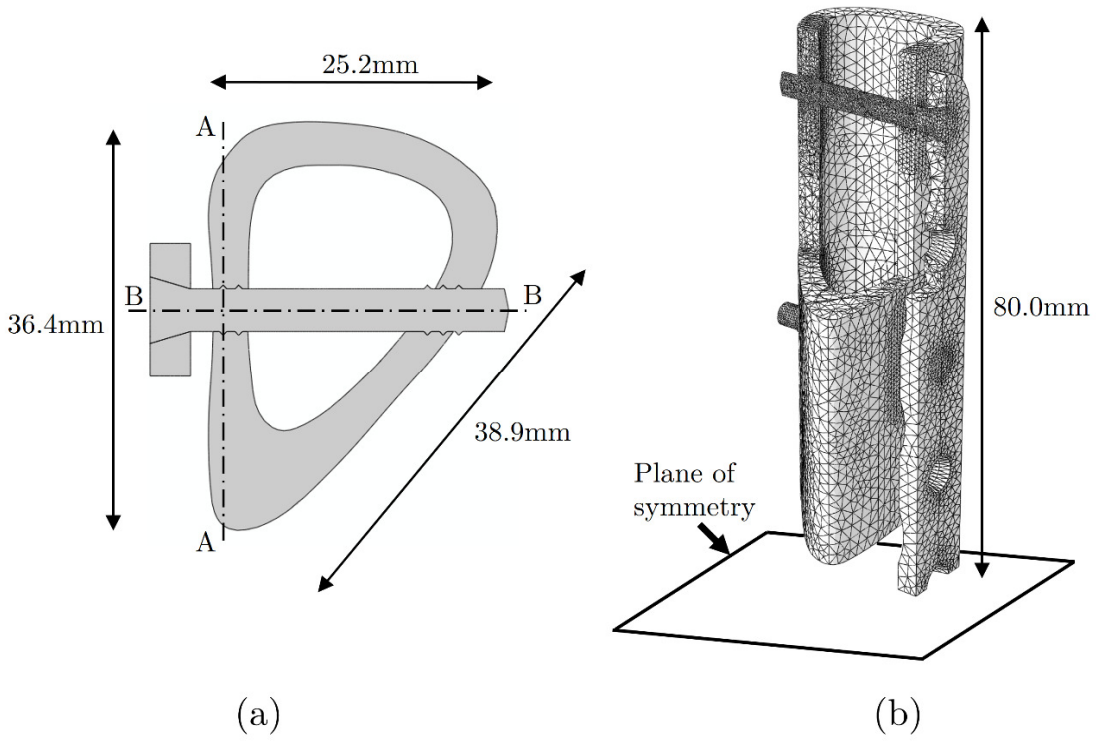

Figure 2.1 – (a) Model cross-section and (b) meshed finite element model showing refinement around screw holes.

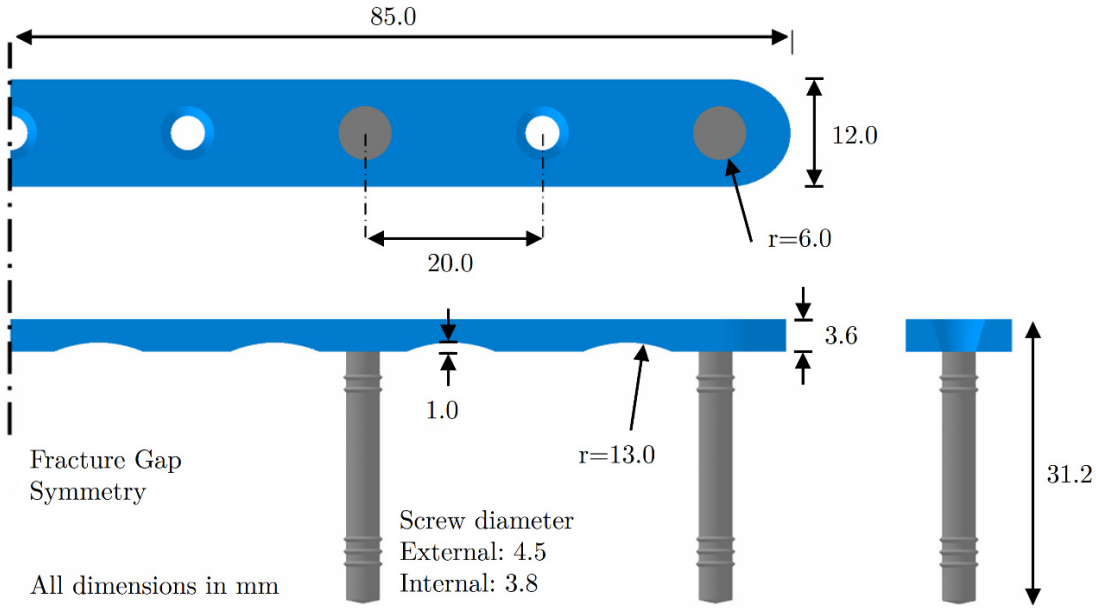

Figure 2.2 - Dimensions of the plate and screws.

Screws were inserted into holes two and four counting from the centre of the fracture gap ignoring the hole directly above the fracture zone (Figure 2.2). This left three holes free in the centre of the nine-hole plate, which is considered an appropriate ratio for a comminuted fracture of a long bone (Hertel et al., 2001, Gautier and Sommer, 2003). The influence of different screw configurations is evaluated in Chapter 8.

2.4.2 Material Assignments and Meshing

The material properties of bone and the steel plate/screws were assumed to be homogeneous, isotropic and linear elastic. The Young's moduli for bone and steel were 20.7GPa and 180GPa respectively (Benli et al., 2008, Fouad, 2010, Ganesh et al., 2005, Gefen, 2002). Poisson's ratio for both materials was taken as 0.3 (Benli et al., 2008, Ganesh et al., 2005, Oh et al., 2010).

The model used approximately 185,000 quadratic tetrahedral (10-noded) elements with refinement around screw holes (Figure 2.1b). In the region around screw holes the average element edge length was 0.4mm.

2.4.3 Loading and Boundary Conditions

In vivo load bearing measurements for internal fixation are extremely limited due to practical and ethical barriers (Stoffel et al., 2000, Gautier et al., 2000); however, there is more data for external fixation. Kershaw et al. (1993) found that mean ground reaction forces due to patients weight bearing reached 80% of body weight at 13 weeks post-surgery. A study by Cunningham et al. (1989) had similar results. Although for external fixation, these studies reflect AO literature with expected full normal weight-bearing for plating as early as 6 weeks post-surgery but bridging constructs taking longer at 16 weeks (Müller and Perren, 1991). The force within the bone, however, will be larger than the ground reaction force due to muscle forces. In a tibial plating study Duda et al. (2002) that included muscle forces, ankle reaction forces of 2070N (over 2.8 times bodyweight for 75kg) were used to represent toe-off during gait.

As healing progresses larger loads are carried by the bone-fixator system and an increasing proportion of the load is carried by the bone (Vijayakumar et al., 2006). In this chapter, however, the influence of the healing callus was not investigated. The worst case scenario for plating is where there is minimal callus formation and early weight-bearing, and this is when clinical failures are seen (Granata et al., 2012). For this reason the analysis was conducted up to a relatively large load of 1900N, which is approximately 2.6 times body weight for 75kg person. The applied load was axial and uniformly distributed across the cortical thickness as a pressure load (Figure 2.3).

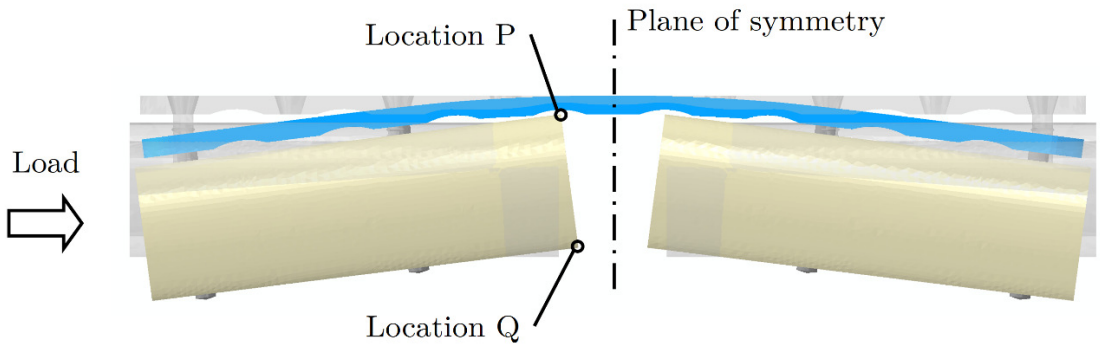

Figure 2.3 – Loading depiction of full model showing locations of interest at which displacement was monitored (deformed shape exaggeration x1)

The plate was fully restrained at the centre of the fracture gap on the plane of symmetry as shown in Figure 2.3. No other restraint was provided. Later in the chapter the effect of clamping the bone at either end during loading was represented by restraining transverse motion at the point of load application and ensuring that the loaded plane remained normal to the loading direction.

The effects of nonlinear geometrical deformations were included in all analyses. Implicit static general analyses were conducted using Abaqus 6.9 (Simulia, Providence, RI, USA).

2.4.4 Contact Interfaces

In a finite element model a surface interaction must be defined to describe the contact between the screw and the bone. A tied or fully-bonded interface does not allow relative motion between the surfaces. A frictional interface allows sliding or separation to occur, with a frictional penalty specified using the static coefficient of friction. The coefficient of friction was considered to be 0.3 in the threaded model and 0.9 in the model without threads (to represent the greater resistance provided by the macro-interlock of the threads). An additional frictionless analysis was conducted where the coefficient of friction was set to zero.

The cases considered were:

(a) Tied (bonded) interface without screw threads

(b) Frictional interface without screw threads (coefficient of friction 0.9)

(c) Tied interface with screw threads

(d) Frictional interface with screw threads (coefficient of friction 0.3)

(e) Frictionless interface with screw threads (coefficient of friction 0.0)

2.4.4.1 Contact Settings

While a tied interface is straightforward, sliding interfaces use parameters which can significantly influence the results of an interaction study. In all interaction cases surface-to-surface based contacts were used with the default Abaqus 6.9 (Simulia, Providence, RI, USA) settings (finite-sliding). The key behavioural characteristics of the default contact settings in Abaqus 6.9 are outlined (SIMULIA, 2009).

2.4.4.2 Penalty based contact

A penalty based contact interaction applies a pressure or traction to surfaces where a motion is to be resisted. This can be in the form of normal over-closure or tangential slipping. The magnitude of this reaction is determined by the extent of the over-closure.

The relationship between pressure and over-closure can be modified by Abaqus throughout the analysis to ensure that the required conditions are enforced.

2.4.4.3 Tangential motion and the 'elastic slip'

Standard coloumb friction relates the normal pressure of two contacting surfaces to a critical value of shear force at which sliding occurs using the static coefficient of friction. In the Abaqus implementation of this behaviour some motion is permitted, called elastic or allowable slip, before the critical value of friction has been overcome. In this study the default value of elastic slip, γ_i, was used, which is described as a fraction of the characteristic element edge length:

$$\gamma_i = F_f \bar{l}_i \tag{1.2}$$

Where $\bar{l}_i$ is the characteristic element edge length and the default value of $F_f = 0.005$

With a characteristic element edge length in the study around contacting surfaces of 0.4mm γ_i should be no greater than 0.002mm.

2.4.4.4 The hard normal contact

The penalty method is the default pressure-overclosure enforcement when using a 'hard' normal contact for finite sliding surface-to-surface contacts. As with the tangential motion Abaqus continually adjusts the interface 'penalty' in order to enforce this condition.

2.4.5 Model Verification

A mesh convergence study was performed and the results showed that doubling mesh density around screw holes resulted in a change of displacement at the fracture gap of less than 0.1%. Similarly, the variation of maximum compressive strain was less than 5% at matching locations around the screw holes.

In a study of discretisation error, Schmidt et al. (2009) measured the peak stress at the thread tips for different contact interactions in a pull-out test. They found no significant difference in max stress when varying the screw-bone interaction but did find different rates of convergence for differing interactions. Their loading condition, however, does not reproduce the loading environment that the screw is under when fastened in a plate. Pull-out tests produce dominantly axial stress within the screw; in the locked plating system the loading on the screw is largely bending. This is further investigated in a subsequent chapter of this thesis.

2.5 Results

2.5.1 Load-Deformation Behaviour

Deformed shape of the model was as expected (Figure 2.3) showing much greater motion at location Q than location P (Figure 2.4). There was less than 1.04% difference in predicted motion at location P and 0.4% at location Q between different contact interactions at the peak load of 1900N. Tied interactions had the smallest motions, whereas contacts that allowed separation to occur had slightly increased motions. It is noticeable from the load deformation curve that the apparent stiffness of location Q increases slightly with load– this is due to the pressure loading. If the load had been vertical the eccentricity would have increased and the stiffness would reduce with load. This is discussed further in Chapter 5.

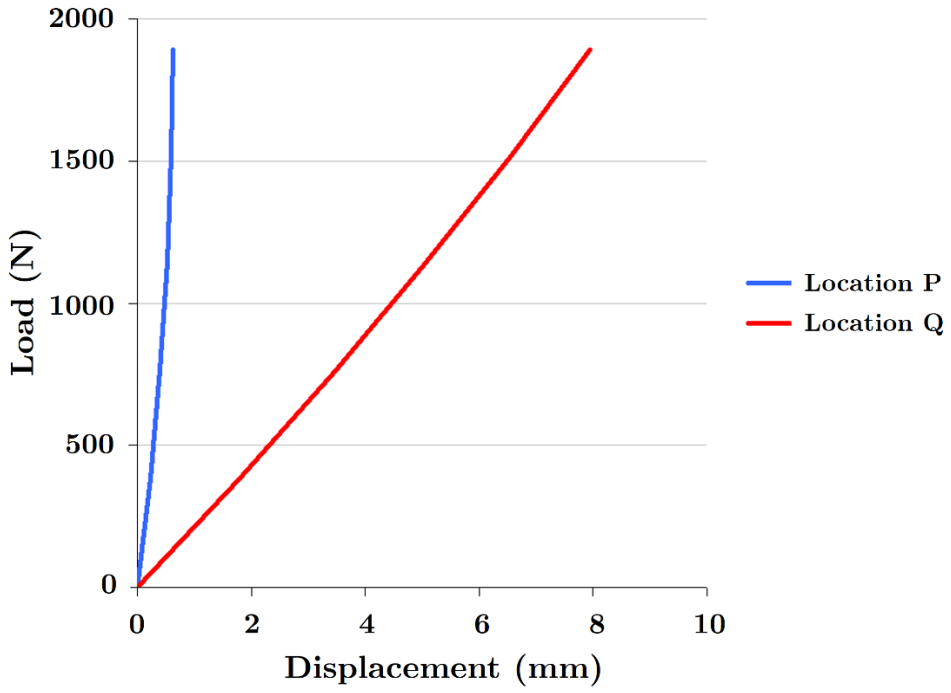

Figure 2.4 - Load-deformation behaviour of the bone-plate system

2.5.2 **Strain Distribution Around Screw Holes**

In terms of stress-strain distribution all models produced near identical results except in the vicinity of the screw-bone interfaces. For each case considered minimum principal strain contours were plotted (to identify the magnitude of compression generated) for the region of the screw-bone interface at the entry cortex of the screw hole closest to the fracture gap (Figure 2.5). All plots use section B-B from Figure 2.1 and are shown at an applied load of approximately 1900N. The limit of the scale was set to 0.8% compressive strain; the compressive yield strain of cortical bone has been shown to be from 0.7% to 1.0% strain (Leng et al., 2009, Mullins et al., 2009, Bayraktar et al., 2004, Reilly and Burstein, 1975).

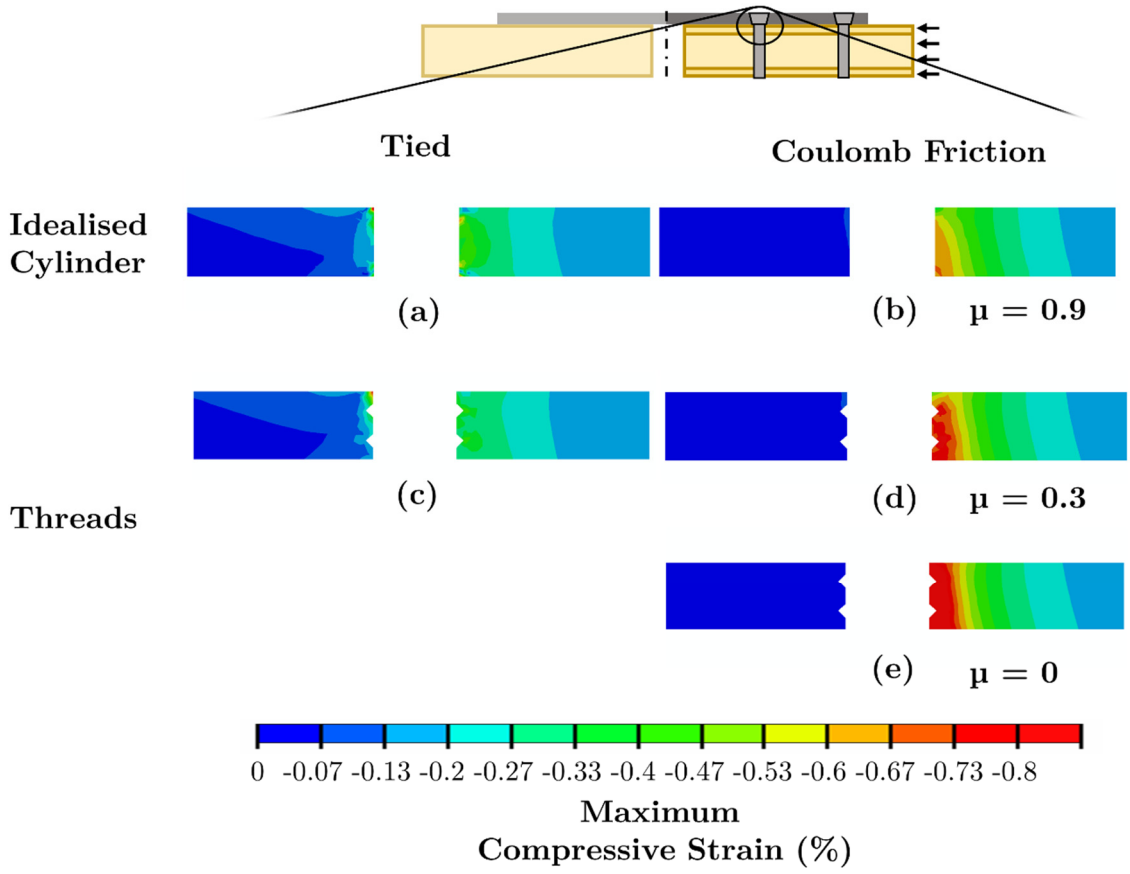

Figure 2.5 – Minimum Principal Strain at the entrant cortex of the screw nearest to the fracture site for the different contact models. The load is applied from the right.

When using a tied interface, the inclusion of threads makes negligible difference to either the magnitude or distribution of maximum compressive strain (Figure 2.5a and c). When using a sliding interface the inclusion of threads increases the strains around screw holes, particularly at the tips of the screw threads (Figure 2.5b and d). Peak strain magnitudes as seen to increase with decreasing coefficient of friction; the frictionless representation produces the largest strains both at the thread tips and further from the screw-bone interface (Figure 2.5e).

Compared to external fixation, locked plating produces a more uniform and therefore favourable stress distribution at the screw-bone interface (Figure 2.6). The uneven load

transfer associated with external fixation is due to the increased eccentricity producing a large bending moment that must be resisted at the screw-bone interface. This results in normal contact stresses that vary significantly through the cortex (Figure 2.6b) (Giotakis and Narayan, 2007, Huiskes et al., 1985, Donaldson et al., 2012a). In addition to more efficient transfer of normal contact stresses, pull-out forces are considerably reduced in locked plating compared with unilateral devices.

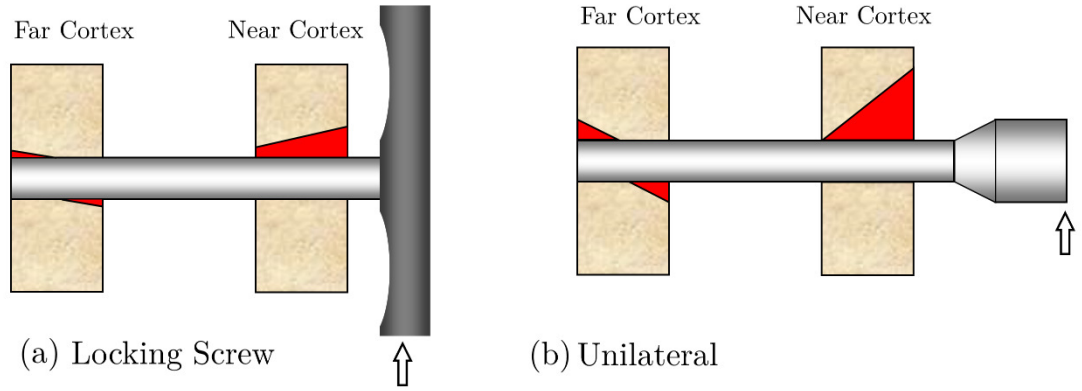

Figure 2.6 – Depictions of screw-bone interface stress distribution in: (a) locked plating; and (b) unilateral fixation.

Additional strain contours were plotted taking a cross-section through Section A-A (shown in Figure 2.1a) and are shown in Figure 2.7 and Figure 2.8. The plan view better illustrates the separation that occurs on the unloaded side of the screw in the sliding contacts (Figure 2.7b, d and e). In the tied models, where separation cannot occur, there are large tensile strains (Figure 2.7a and c). In the sliding contact models, the areas of tensile and compressive strain are in the same locations indicating that the tension is circumferential strain caused by radial compression. There is minimal difference between the tied models in either compressive or tensile strain.

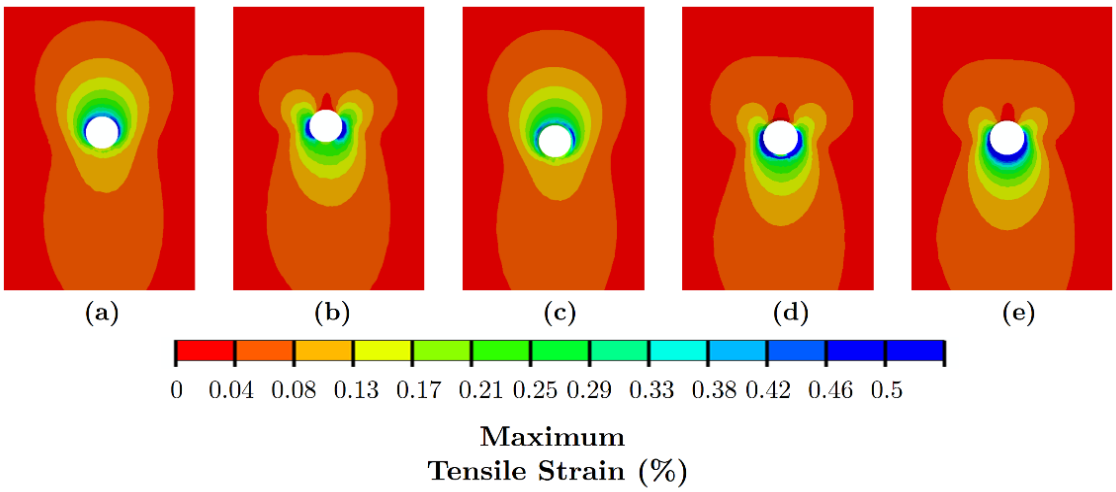

Figure 2.7 – Maximum principal strain contours for each of the contact interactions examined: (a) tied excluding threads; (b) frictional excluding threads; (c) tied including threads; (d) frictional including threads; and (e) frictionless including threads. The load acts from below.

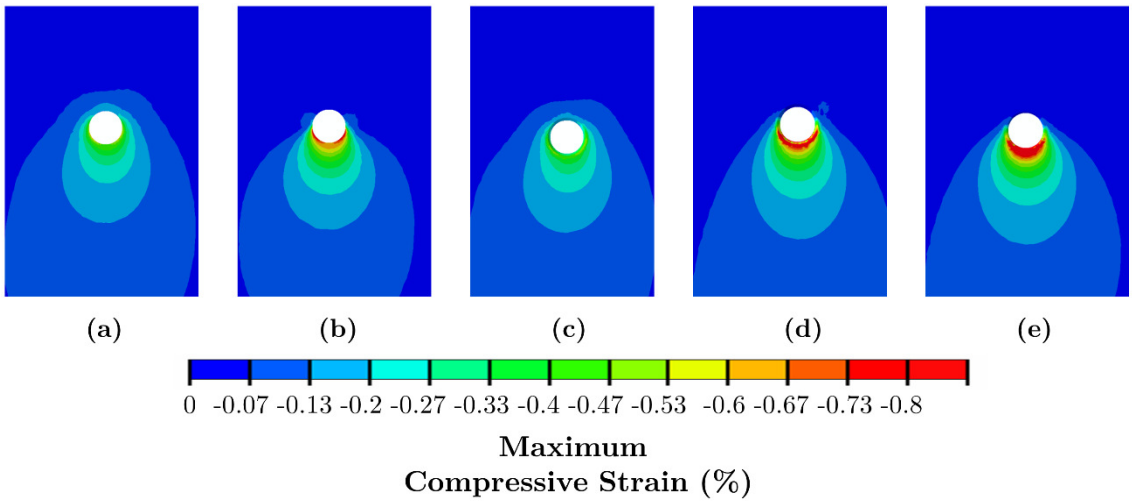

Figure 2.8 – Minimum principal strain contours for each of the contact interactions examined. : (a) tied excluding threads; (b) frictional excluding threads; (c) tied including threads; (d) frictional including threads; and (e) frictionless including threads. The load acts from below.

2.6 Influence of Clamped Boundary Conditions

Under pressure loading (considered in section 2.5.1) the small differences in fracture gap motion observed between different contact interactions models (tied, frictional, etc.) are insignificant. In this situation the plate is free to bend as there is no rotational support at the loaded end. Often, in vitro tests conducted by previous studies have applied a clamp or vice to at least one end of a loaded specimen (Bottlang et al., 2010a, Yánez et al., 2012, Fitzpatrick et al., 2009, Strauss et al., 2007, Ahmad et al., 2007, Filipowicz et al., 2009). This prevents rotation and translation at the point of load application (Figure 2.9), and results in a much stiffer mechanical environment (discussed further in Chapters 5 and 6). It was hypothesised that if the total global deformation became smaller due to a stiffer system, the differences between contact conditions would become more apparent. Additionally, a decreased Young's modulus of 7.6GPa was examined for comparison due to the possibility of increased gap formation around screw holes. The frictionless and tied cases were used as extreme cases to evaluate the maximum difference that could be obtained.

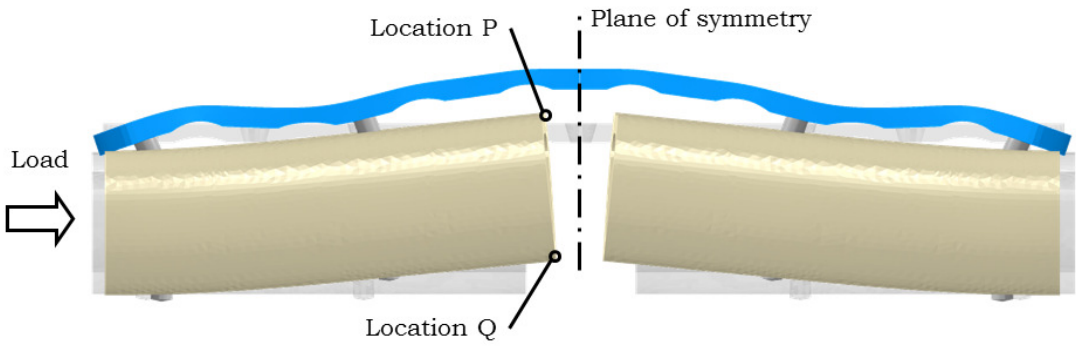

Figure 2.9 – Loading depiction and deformed shape of the clamped loading condition (exaggeration x 60).

2.7 Clamped Loading Condition Results

The fracture gap motion at location P and Q for each of the additional cases examined using the clamped loading condition are shown in Figure 2.10. Compared with the pressure loading condition the displacements at location P and Q were found to be much closer in magnitude. The ratio of P: Q motion was 1: 2.8 for the frictionless case and 1: 3.3 for the tied case. With the pressure loading condition the ratio was 1: 13.8 for all cases. The frictionless interaction increased motions compared with the tied model by 28.3% at location P and 6.1% at location Q (for E=20.7GPa). A lower Young's modulus of bone also exaggerates this effect and results in larger percentage differences in motion between tied and frictional contact interactions (9.8% at location Q) (Figure 2.10). For all cases the total motion at location Q was less than 0.22mm at a load of 1900N. Unlike the pressure loading conditions, the load-deformation behaviour was found to be linear when using a clamped condition. This indicates that geometric nonlinearity plays a very minor role and that the results can be linearly extrapolated.

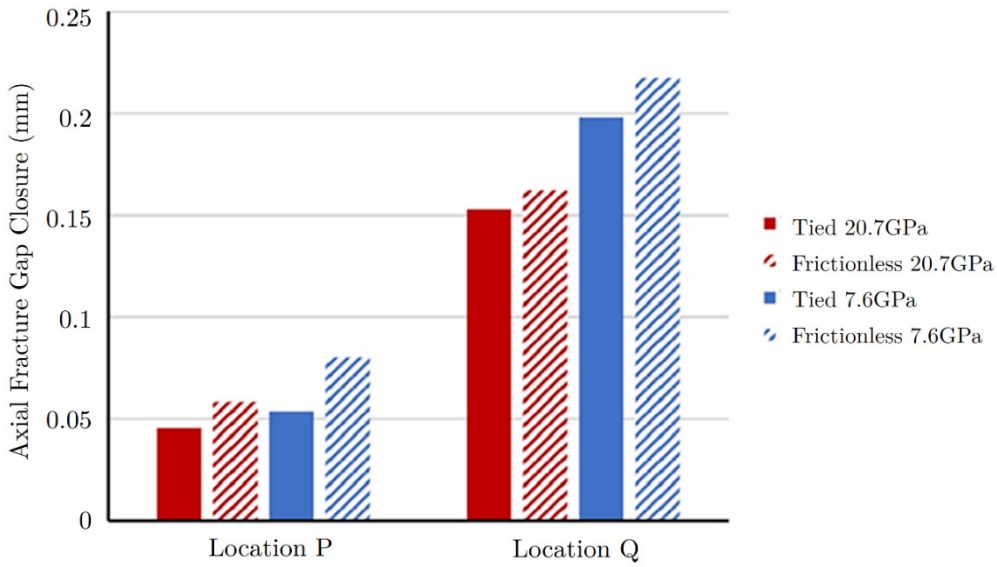

Figure 2.10 - Predicted fracture gap motions for a clamped loading condition under an applied load of 1900N.

While the absolute increase in maximal fracture gap motion due to the frictionless condition in the pressure loaded models was 0.044mm compared with 0.01mm in the clamped models, this represents a much larger percentage of the clamped models' motion (0.4% and 6.1% increase for pressure loaded and clamped respectively). At location P the relative increases for both loading conditions were greater with 1.04% under pressure loading and 28.3% under clamped conditions. Therefore the loading condition changes the relative importance of the contact interaction in terms of influencing the motion (loading conditions are evaluated and discussed further in Chapters 5 and 6).

2.8 Discussion

2.8.1 Local Behaviour

A tied screw-bone interface model predicts lower peak stresses around the screw holes than a frictional or frictionless interface. When using a tied contact, load can be transferred both where the screw is impacting against the bone and in tension locations where, in reality, separation would occur. When using a frictional interface screw-bone separation may occur; no tension can develop normally between the screw and bone, meaning load is predominantly transferred by compression in the portion of the screw in contact with the bone. This results in the bone being exposed to larger stresses throughout the whole cortex where contact occurs.

The difference in strain between frictional and frictionless cases with threads was minimal (Figure 2.8d and e). The models are, therefore, relatively insensitive to the choice of frictional coefficient when using explicitly modelled threads. This also demonstrates that shear deformation (allowing push-in or pull-out) is not significant compared with the normal deformation (causing gap opening). While the compressive strains in the frictional case without threads (Figure 2.8a) are similar to the threaded cases (Figure 2.8d and e) the position of the tensile strains indicate that larger shear forces are being transferred (Figure 2.7). This is expected as the coefficient of friction is

much larger than the cases with threads. The frictionless model had the largest strains of the interactions indicating that the choice of coefficient of friction is important when a model is used to predict damage or loosening around screw holes.

A study by Dammak et al. (1997) recreated the load-displacement behaviour of physical pull-out tests using non-linear frictional behaviour. As no threads were included their influence was approximated using modified properties. Pull-out tests induce large shear stresses at the screw-bone interface and these will be particularly high in the case of an un-threaded cylindrical bar with an interference fit, which relies entirely on the interface friction for stability. The screws in a bone-plate system under axial loading do not experience such pull-out forces; the majority of the load is transferred normally at the screw-bone interface—or through macro-interlock of the threads. It was, therefore, assumed that non-linear frictional properties would not significantly affect the results and were not included. This assumption was verified by the frictionless case, which produced results similar to those from the frictional case.

Other than in very close proximity to the screw (less than one hole diameter away) the frictional models without threads produced results very similar to those from the frictional threaded model. It should be noted that other load cases or configurations could produce higher pull-out forces where threads would be more influential. Previous studies have shown that the load distribution on each thread during screw pull-out is highly non-uniform (Gefen, 2002, Grewal and Sabbaghian, 1997); neglecting threads, therefore, results in load being more evenly distributed through the cortical thickness. If a tied interface is being assumed the inclusion of screw threads has negligible impact.

Away from the contact interface, the distribution is unaffected by the choice of contact interaction. The affected distance is approximately two times the diameter of the screw hole for the case evaluated.

2.8.2 Global Behaviour

In general, changing the contact interface model does not influence global load-deformation behaviour. When using more extreme boundary conditions (such as clamps that make the entire system more rigid), however, the contact interface model can begin to have more influence. The differences were also more observable by reducing the Young's modulus of the bone; even so, the largest difference in maximal fracture gap motion produced different contact interactions was only 16.4%. At location P the maximum difference achieved was larger at 52.8%; however, the absolute motion at this location was less than 0.1mm (Figure 2.10).

Karunratanakul et al. (2010) made a comparison of different contact interactions in external fixators and found that the choice of interaction affected the global stiffness of the construct. Interestingly, they found that while changes in contact interaction at the metalwork interfaces decreased stiffness by around 34%, similar changes at the screw-bone interface only decreased the stiffness prediction error by 20% (Karunratanakul et al., 2010). While this change in stiffness is larger than that predicted in this study (9.8% for bone with E=7.6GPa), it likely that the discrepancy can be explained by the use of hollow polyoxymethylene tubes, which had a Young's modulus equal to 3GPa. Unlike this study, however, Karunratanakul et al. (2010) found almost identical results when running a simulation with increased Young's modulus of bone (20.1GPa). They also show a linear stiffness relationship across the entire load range when using a tied contact—this makes it appear as though they have only incorporated contact nonlinearity and not geometrical nonlinearity. The absence of geometrical non-linearity may, therefore, be causing some of the discrepancy in deflection attributed to contact modelling.

For most studies focussing on fracture gap movement a simplified fully-tied interaction provides an acceptable model provided the Young's modulus of the bone specimen is

similar to cortical bone. It has been shown that the pull-out strength of screws increases up to 6 weeks of healing (Schatzker et al., 1975b); this is due to bony ingrowth (Schatzker et al., 1975a). When examining the interface between an implant and the host bone in the latter stages of healing, after full osseointegration has occurred, a simplified tied model may also be appropriate.

2.9 Limitations

The study used a homogeneous isotropic bone representation; however, the influence of orthotropic properties were tested and the observed differences in both fracture gap motion and strain were negligible. The addition of a callus is also likely reduce the differences seen between interactions as there would be more load transfer at the fracture site thereby reducing stress levels at the screw-bone interface.

The plate used was modelled on a typical 4.5mm narrow locking plate. The use of a stiffer plate would reduce the overall deformations but could increase the relative differences between contact representations. Deformation predictions could also be altered by the length of the specimen. This study used a 180mm long specimen; in reality long bones can be over 400mm. Chapter 6 demonstrates that an increase in bone length increases the motion produced at the fracture site; however, it is likely that there would be minimal change in the relative differences between the contact interactions.

The influence of changes to thread geometry was not considered. It has been shown that this can alter predictions of peak stress and change mesh convergence rates (Schmidt et al., 2009). Another aspect which was not included was a limiting shear value for the frictional contacts. This would be most influential in the unthreaded frictional case where the coefficient of friction is large leading to greater shear stresses.

2.10 Conclusions

The effect of the changing the contact interaction behaviour at the screw-bone interface was investigated. Fully-bonded, frictional and frictionless interfaces were considered. In addition, the effect of including screw threads in the model geometry was contrasted against idealised cylindrical screws. Several conclusions have been drawn regarding the choice of screw-bone interface representation[3]:

- Interface modelling has a significant impact on local behaviour within the bone – tied interfaces produce much lower strains than sliding interfaces.
- The inclusion of screw threads increases strains locally around thread tips and the use of a lower coefficient of friction increased strains through the entire cortical thickness.
- Globally, the load-deformation behaviour shows much less difference depending on the interface model. Different interactions changed the prediction by only 0.5% when using a distributed load that allowed free rotation of the bone ends.
- Generally, tie constraints can be used effectively for finite element models where the only interest is the global load-deformation.

[3] It should be noted that these conclusions relate only to locking screws and may not therefore apply to standard cortical screws which function very differently.

- Some validation experiments use rigid load application and a reduced Young's modulus of bone. Both of these aspects were shown to exaggerate the differences between the contact interactions. In these cases the maximal fracture gap closure could be altered by as much as 9.8% depending upon the interaction model and Young's modulus of bone.

3

Modelling Radial Preload at the Screw-Bone Interface

3.1 Introduction

Bone screws are used more often than any other type of implant (OrthoInfo, 2007). Many forms of fixation and implants rely on screws for anchorage to the bone (An et al., 2002). Pilot holes drilled in the bone are invariably of a smaller diameter than the screws and the resulting pressure between the screw and bone helps maintain a secure fit. This is also problematic, however, as it causes bone damage. Computer simulation of the screw-bone interaction can help to better understand this phenomenon with the ultimate goal of reducing bone iatrogenesis (inadvertent adverse effect or complication resulting from medical treatment). To accurately represent the screw-bone interface in a computational model, the mechanics of screw fastening must be appreciated. This chapter considers the effect of radial preload at the screw-bone interface. Unlike axial preload, which applies only to conventional screws, this phenomenon is applicable to all screw types. It is, however, locking screws that are considered in this chapter.

3.1.1 Types of Screw

Screws can be self-tapping or non-self-tapping. Self-tapping screws create their 'tap' with cutting threads as they are inserted. Both cases require pilot holes to be drilled but non-self-tapping screws require a drilled pre-tap in addition to this. While self-tapping screws are simpler to insert, non-self-tapping screws have the advantage of a more precise fit and the ability to remove and reinsert without the risk of creating a new tap or destroying an old one (Baumgart et al., 1993). Historically, self-tapping screws had a shallower tap (as they have to cut it themselves) and larger pilot hole dimension than non-self-tapping screws, making their pull-out resistance lower (Wheeless, Baumgart et al., 1993). As there are fewer torque losses from cutting and friction, non-self-tapping screws also generate higher screw tensile forces for the same torque (Hughes and Jordan, 1972). Although non-self-tapping screws are still superior, advances in screw design have produced self-tapping screws with the obvious operative advantages (reduction in time and the number of instruments that have to be used) and only marginal compromises with regard to pull-out strength (Bell and Ness, 2007, Andrea et al., 2002, Baumgart et al., 1993), insertion torque (Andrea et al., 2002, Bähr, 1990, Baumgart et al., 1993) and heat generated (Baumgart et al., 1993).

There are two processes by which a screw can self-tap: thread-cutting or thread-forming (Baumgart et al., 1993). Thread-cutting screws have sharp cutting edges which cut the bone while being driven. Similar to a pre-tap, this produces debris which is collected in flutes; however, pre-taps are usually cleaner as debris can be cleared more efficiently, which may be partially responsible for the differences in required insertion torque between the two (Bähr, 1990). Thread-forming screws create their tap by plastic deformation of the bone which does not produce debris but necessitates a larger amount of radial compression to form the threads (Kuhn et al., 1995).

Excessively large strains and damage in host bone will encourage resorpsion and compromise holding strength. It is therefore desirable to limit the damage caused to the

bone during screw insertion (Koistinen et al., 2011). Thread-forming screws were shown to cause the most damage during insertion in a study by Kuhn et al. (1995). They found that the maximum radial extent of plastic deformation was similar for thread-cutting and non-self-tapping screws, but the total area of plastic deformation was lowest in the non-self-tapping screws.

3.1.2 Pilot Holes

In order to maintain a secure fit, screws must be slightly larger than the hole into which they are inserted. The act of producing a tight fit between a component and host material due to a discrepancy in size is known as interference-fitting. Interference-fitting is used in manufacturing as a means of fastening and the principle has been adopted in orthopaedics with a desire to achieve a more secure fit between implant and bone. Loose screws or pins compromise the fixator and promote infection (Hyldahl et al., 1991). In addition, an interference-fit is often used in stemmed implants with the intention of reducing motion to levels where osseointegration can occur (Norman et al., 2006, Gebert et al., 2009).

Even when screws are initially snug, weight bearing is necessary for fracture healing stimulation and results in large strains at the screw-bone interface that can cause resorpsion, which leads to loosening (Giotakis and Narayan, 2007, Pettine et al., 1993). In external fixation, where loosening is a frequent complication (Biliouris et al., 1989, Hyldahl et al., 1991), 'bending' preload was historically used where the screws or pins were forced towards one another. Radial preload, however, has been shown to reduce resorpion around screw holes compared with bending preload or no preload (Hyldahl et al., 1991, Giotakis and Narayan, 2007).

The amount of radial preload produced is determined by the size of the pilot drill hole size relative to the screw (Defino et al., 2007, Kuhn et al., 1995); if a smaller pilot hole is used, the screw will have to displace more bone causing larger strains around the

screw. When using internal fixation such as plating, screws are supplied with manufacturer specified pilot hole sizes. Generally, manufacturers' recommendations are for pilot hole drill diameters to be equal to the core diameter of the screw; however, its influence on the pull-out strength of screws has been the subject of many studies (Shultz et al., 2006, Defino et al., 2007, Nagatani et al., 2010, Hughes and Jordan, 1972, Heidemann et al., 1998, Battula et al., 2008, Kunkel et al., 2011).

Pull-out strength has been shown in several studies to increase with decreasing pilot hole size (Nagatani et al., 2010, Defino et al., 2007, Hughes and Jordan, 1972, Heidemann et al., 1998); however, insertion torque also increases with decreasing pilot hole size (Heidemann et al., 1998, Battula et al., 2008, Steeves et al., 2005, Nagatani et al., 2010), as does radial and circumferential strain. In all cases pull-out strength tended to plateau at a certain size of pilot hole (Defino et al., 2007, Nagatani et al., 2010, Heidemann et al., 1998, Hughes and Jordan, 1972). Biliouris et al. (1989) attributed this to local bone damage preventing an increase in preload due to the tensile yield strain of bone being reached. There is therefore a compromise between pull-out strength and the risk of bone-damage and screw breakage during insertion.

When assessing screw performance many factors other than the pilot hole size influence the pull-out strength, including screw design features such as inner and outer diameters, thread pitch, flank angle and bone quality (Tsai et al., 2009, Thiele et al., 2007, Firoozabadi et al., 2012). Screw external diameter and bone density have been shown to positively influence pull-out strength (DeCoster et al., 1990) as both will increase shear strength (Shultz et al., 2006, Hughes and Jordan, 1972). Other screw design features have less influence than the external diameter (DeCoster et al., 1990, Halsey et al., 1992). Clearly external variables such as the type of loading and the dimensions of the host material will also influence predictions of screw holding strength.

Several studies have quoted 75-85% of the screw external diameter as the critical pilot hole size above which pull-out strength loss is considered unacceptable or statistically significant (Gantous and Phillips, 1995, Heidemann et al., 1998, Defino et al., 2007, Hughes and Jordan, 1972), with Heidemann et al. (1998) advocating that a slightly smaller hole should be specified due to surgical error increasing the hole size. Battula et al. (2008) also suggest that pilot holes should be as small as 71.5% of the screw external diameter in osteoporotic bone. Unfortunately these studies used synthetic bone and did not observe any cracking even at small pilot hole sizes showing that the plastic used is not representative of bone, which is more brittle (Steeves et al., 2005, Kunkel et al., 2011). It is also likely that cancellous bone would allow for smaller pilot hole sizes than cortical bone due to its decreased stiffness (DeCoster et al., 1990).

3.1.3 **Bone Damage**

In cadaveric studies Kuhn et al. (1995) and Biliouris et al. (1989) showed that drill diameters approaching those advocated in the synthetic bone studies (around 75% screw external diameter) can cause large amounts of plastic deformation and macroscopic fractures. Biliouris et al. (1989) found that cracking was observed in interferences greater than 0.1mm and no further preload was achieved beyond 0.3mm. In another cadaveric study Norman et al. (2006) experienced specimen fractures at interferences as small as 0.35mm in press-fit femoral stems, which have a much larger diameter than bone screws. When considering threaded screws as opposed to solid cylinders, however, thread penetration means that the resulting strains may be lower for the same interference. As a consequence, recommended pilot hole sizes produce interferences much larger than the limit of 0.5% suggested by Kuhn et al. (1995); manufacturers pilot drill specifications range from 71.1-86% of the screw external diameter, with the higher values for the larger screws (Synthes®, 2002, Synthes®, 2000, Stryker, 2007, DePuy, 2009, DePuy, 2005b).

Self-tapping screws have been shown to cause slightly higher levels of bone damage than pre-tapped (Andrea et al., 2002, Bell and Ness, 2007, Biliouris et al., 1989). Some

companies provide the option of self-drilling, self-tapping screws that do not require a pre-drilled pilot hole (Synthes®, 2002); however, these are only suitable for mono-cortical fixation due to the drill portion of the screw preventing threads near the tip. Nevertheless, all the same principles of pilot hole size also apply to these screws. Some screws may be made using materials of different stiffness which will also affect the optimal pilot hole size (Nagatani et al., 2010).

Newer composite bone replicas have bulk elastic properties close to those of cadaveric bone and match well in terms of Young's modulus (Pacific Research Laboratories, 2013) and average bending stiffness; the torsional stiffness, however, has been consistently shown to be much lower (Cristofolini et al., 1996, Cristofolini and Viceconti, 2000). While the elastic properties are well matched, it seems unlikely that the post-elastic properties would be as well represented; nevertheless, similar screw pull-out strengths and stripping torques have been predicted (Zdero et al., 2007, Nicayenzi et al., 2012). The longer-term response of real bone is an added complication which is beginning to receive more attention. Bone exhibits significant viscoelasticity which reduces the radial preload over time (Shultz et al., 2006, Norman et al., 2006); furthermore, the speed of the viscoelastic response increases non-linearly beyond the yield strain of bone (Brown et al., 2002, Norman et al., 2006). As well as causing damage, therefore, the improvement in security of fit when using larger interferences is limited due increased creep (hoop strain) and stress relaxation (radially).

Giotakis and Narayan have considered the effect of pilot hole size, major and minor diameters and expressed the effective 'interference' as a normalised proportion of the thread depth (Giotakis and Narayan, 2007):

$$Interference = \frac{major\ diameter - pilot\ hole\ diameter}{major\ diameter - minor\ diameter} \quad \textbf{(3.1)}$$

This, however, provides no information for stress or strain prediction at the screw-bone interface.

3.1.4 Previous Numerical Models of interference fitting

Screw-bone interference fits have been modelled using finite element previously in the literature (Shultz et al., 2006, Dawson and Bartel, 1992, Dammak et al., 1997, Mauntler et al., 2008); however, to the author's knowledge, screw threads have never been included in such models despite detailed threaded models being used for pull-out test simulation (Hsu et al., 2003, Schmidt et al., 2009, Gefen, 2002). This is due to the difficulties arising from the complex geometry of a screw – sharp edges can be problematic in FE during contact analysis with meshing difficulties (Schmidt et al., 2009), penetration errors or extremely high stress common (Hsu et al., 2003). It is much more straightforward to model the interference-fit of a cylinder; moreover, closed-form solutions exist for such problems.

Dammak et al. (1997) reproduced pull-out out response of interference-fitted, threaded screws using non-linear friction despite not incorporating threads. This approach relies on having an experimental model in order to replicate the pull-out response and is likely to be sensitive to changes in both loading direction and magnitude. The macro-interlock of threads produces a very different local environment to that of an un-threaded cylinder where pull-out is resisted solely by interface shear (see section 2.5.2).

In an axisymmetric idealised cylindrical model of a press-fit stem in the femoral medullary cavity, Shultz et al. (2006) demonstrated that the stress-relaxation behaviour of bone can significantly reduce the interference generated and therefore load carrying capacity of the press-fitted tube model. Interestingly, they predicted an interference threshold above which push-out load was not increased; for their case the plateau was reached at 0.1mm. As the model included no threads, however, the pull-out force was determined simply by the maximum shear capacity (a product of the coefficient of

friction and the contact pressure or the ultimate shear value beyond which slip occurs). Nevertheless, this showed that increases in pull-out strength due to a reduction in pilot hole size may be limited due to visco-elastic effects in addition to bone damage.

Dawson and Bartel (1992) noted that while bone yielding will occur due to interference, the stresses dissipate quickly with distance from the pin-bone interface meaning that the region of high stress is relatively small. While significant bone loss has been predicted in remodelling simulations of reamed hip replacement implants (Weinans et al., 1993, García et al., 2002), they argue that larger interferences may be beneficial as bony in-growth will occur short-term and the larger strains, which cause longer-term remodelling, will dissipate over time anyway. On the other hand, when viscoelastic effects are included, misfits larger than 0.1mm have been shown to have little advantage in terms of interface pressure after twenty-four hours (Shultz et al., 2006, Brown et al., 2002).

3.1.5 **Study Outline**

In locking screws there is no significant plate-bone preload caused by the screws. All screws, however, exert pressure on the surrounding bone during fastening causing substantial pre-stress even before loading due to weight-bearing occurs.

It is very complex to model a screw being driven into bone; however, interference is a fundamental aspect of screw mechanics which must be accounted for if strains within the bone are to be correctly predicted. Because of the associated difficulties with numerical modelling of interference fits with complex geometries, an alternative approach to representing this phenomenon using thermal expansion is proposed. Thermal expansion of the screw causes very similar forces to those during insertion; the screw is displacing surrounding bone. The desired interference is then generated by specifying an appropriate coefficient of thermal expansion. This approach also allows

for the inclusion of screw threads, something which has been neglected in previous numerical modelling (Dammak et al., 1997).

3.1.6 Chapter Aims

This chapter aimed to replicate the effect of an undersized screw hole by using thermal expansion to represent the interference.

3.2 Closed Form Solution

3.2.1 Idealised Cylindrical Misfit

Assuming that the screw is infinitely more rigid than the bone, the increase in circumference for an increase of radius, U_t, given original and expanded circumferences C_r and C_{r+u_t} the increase in circumference $C_{r+u_t} - C_r$ is:

$$C_{r+u_t} - C_r = 2\pi(r + u_t) - 2\pi r = 2\pi u_t \quad \textbf{(3.2)}$$

The circumferential strain at the screw-bone interface is dependent on the original and expanded circumferential length:

$$\varepsilon_c = \frac{2\pi u_t}{2\pi r} = \frac{u_t}{r} = \frac{misfit}{\phi_H} \quad \textbf{(3.3)}$$

Where the total $misfit = 2u_t$ and the diameter of the hole $\phi_H = 2r$.

Therefore a larger misfit is tolerable with a larger screw diameter; this is reflected in the manufacturers' specified pilot hole sizes (DePuy, 2009, DePuy, 2005b, Stryker, 2007, Synthes®, 2002, Synthes®, 2000).

3.2.2 Thick-Walled Cylinder Representation

A convenient representation of screw-bone interference is that of thick-walled cylinders interference, which allows for compression of the screw and incorporates an amount of surrounding bone (Figure 3.1).

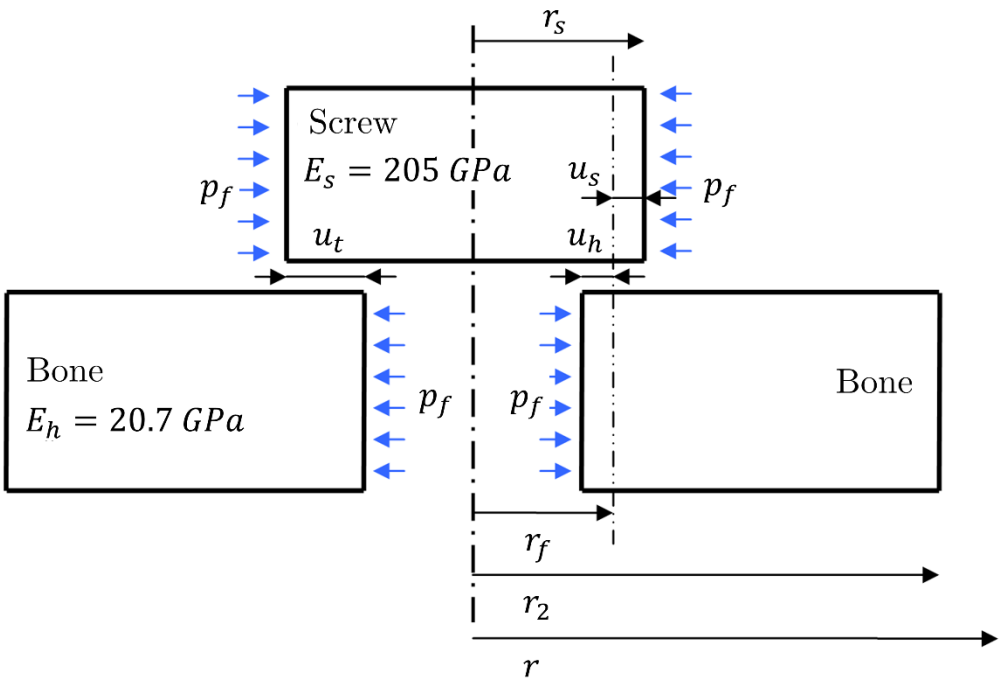

Figure 3.1 - Screw-bone interference diagram

Using the circumferential strain expression from Hooke's law:

$$\epsilon_c E = \sigma_c - v\sigma_a - v\sigma_r \tag{3.4}$$

Substituting the circumferential strain expression (Equation 3.3) into Hooke's law:

$$\epsilon_c E = E\frac{u_t}{r} = \sigma_c - v\sigma_a - v\sigma_r \tag{3.5}$$

Ignoring axial stress, σ_a, and rearranging for the interference, u_t:

$$u_t = \frac{r}{E}(\sigma_c - v\sigma_r) \tag{3.6}$$

The total interference, u_t, at the screw bone interface (Figure 3.1) will be applied to the screw and the hole is in relation to the Young's moduli where:

$$u_t = u_s + u_h \tag{3.7}$$

Therefore the increase in hole diameter, u_h, and decrease in screw diameter, u_s, depends of the Young's modulus of the material and can be expressed as:

$$u_h = \frac{r_f}{E_h}(\sigma_c - v_h\sigma_r) \qquad u_s = \frac{r_f}{E_s}(\sigma_c - v_s\sigma_r) \tag{3.8}$$

Where r_f is the distance to the screw-bone interface.

Lame's equations for thick walled cylinders give the radial and circumferential stresses (Beardmore, 2013, Bower, 2010) at a distance r from the centre of the section:

$$\sigma_r = \left(\frac{p_1{r_1}^2 + p_2{r_2}^2}{{r_2}^2 - {r_1}^2}\right) + \left(\frac{(p_2 - p_1){r_1}^2{r_2}^2}{r^2({r_2}^2 - {r_1}^2)}\right) \tag{3.9}$$

$$\sigma_c = \left(\frac{p_1{r_1}^2 + p_2{r_2}^2}{{r_2}^2 - {r_1}^2}\right) - \left(\frac{(p_2 - p_1){r_1}^2{r_2}^2}{r^2({r_2}^2 - {r_1}^2)}\right) \tag{3.10}$$

Where the internal and external dimensions of the bone cylinder are r_1 and r_2 and internal and external pressures are p_1 and p_2.

Considering a bone cylinder with zero external pressure, $p_2 = 0$:

$$\sigma_r = \frac{p_1{r_1}^2}{r^2}\frac{(r^2 - {r_2}^2)}{({r_2}^2 - {r_1}^2)} \tag{3.11}$$

$$\sigma_c = \frac{p_1{r_1}^2}{r^2}\frac{(r^2 + {r_2}^2)}{({r_2}^2 - {r_1}^2)} \tag{3.12}$$

A hollow cylindrical screw with zero internal pressure simplifies to:

$$\sigma_r = p_2 \frac{{r_2}^2}{r^2} \frac{(r^2 - {r_1}^2)}{({r_2}^2 - {r_1}^2)} \tag{3.13}$$

$$\sigma_c = p_2 \frac{{r_2}^2}{r^2} \frac{(r^2 + {r_1}^2)}{({r_2}^2 - {r_1}^2)} \tag{3.14}$$

If the screw is solid $r_1 = 0$

$$\sigma_r = \sigma_c = -p_2 \tag{3.15}$$

At the screw-bone interface we know that the radial stress is equal to the interface pressure, which we will call p_f. The pressure exerted on the screw and bone will be equal therefore:

$$\sigma_r = p_1 = p_2 = -p_f \tag{3.16}$$

Substituting $r = r_f$ and $r_1 = r_f$, the circumferential stress within the bone at the screw-bone interface is given by:

$$\sigma_c = p_f \frac{{r_2}^2 + {r_f}^2}{{r_2}^2 - {r_f}^2} \tag{3.17}$$

Equation 3.17 can be substituted into Equation 3.7:

$$\mathrm{u}_t = \mathrm{u}_h + (-\mathrm{u}_s) = \frac{r_f p_f}{E_h}\left[\left(\frac{{r_2}^2 + {r_f}^2}{{r_2}^2 - {r_f}^2}\right) + v_h\right] + \frac{r_f p_f}{E_s}(1 - v_s) \tag{3.18}$$

Arranging for p_f:

$$p_f = \frac{u_t}{\frac{r_f}{E_h}\left[\left(\frac{{r_2}^2 + {r_f}^2}{{r_2}^2 - {r_f}^2}\right) + v_h\right] + \frac{r_f}{E_s}(1 - v_s)} \tag{3.19}$$

Equations 3.19, 3.13 and 3.14 can be used to get the value of stress within the bone for a given interference at a distance, r, away from the screw-bone interface.

3.3 Verification of Thermal Expansion Representation

3.3.1 Idealised Cylinder

To ensure that the thermal expansion approach was producing the same behaviour as an interference fit, a finite element (FE) model was compared with the analytical solution. A fully three-dimensional model was created so that it was representative of the models used in the Chapter 2, into which it will later be incorporated. The methodology involved assigning anisotropic thermal expansion coefficients in which the coefficients corresponding to axial lengthening and shear expansions were set to zero and expansion was only allowed in the radial plane of the screw. Isotropic expansion of a screw would cause not only an increase in screw diameter, but also unrealistic lengthening along the length of the screw shaft (see section 3.5.1).

The benchmark test used a 4.5mm cylindrical un-threaded screw in a 9mm cylindrical bone section Figure 3.2. The Young's modulus of the steel and bone were 205GPa and 20.7GPa respectively. The Poisson's ratio for the materials was 0.3 and 0.25 respectively. A frictionless screw-bone interface was assumed. 42,445 linear tetrahedral elements were used. Coefficient of thermal expansion and applied temperature were specified to produce a 1% expansion; expansion was only allowed in the radial plane in order to prevent unrealistic lengthening of the screw. A static, temperature-displacement coupled analysis was conducted using Abaqus 6.10 (Simulia, Providence, RI, USA). The inclusion of nonlinear geometrical effects did not influence the result.

The maximum and minimum principal stresses correlated well with the analytical circumferential and radial predictions (Figure 3.3).

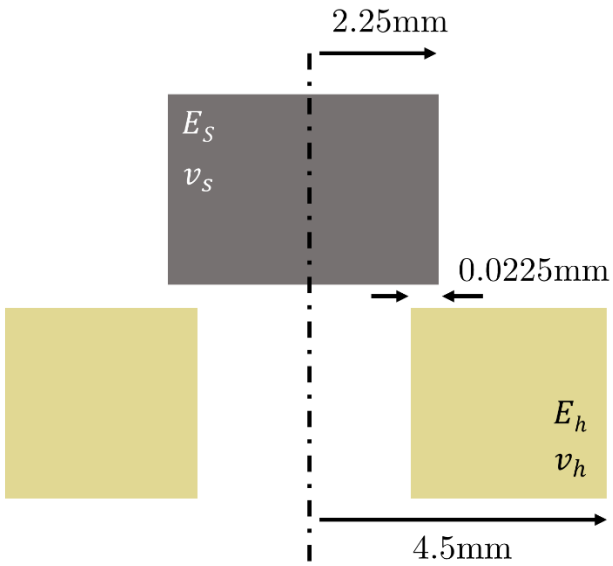

Figure 3.2 – Sketch of the benchmark test used to compare the thermal expansion approach with the analytical results.

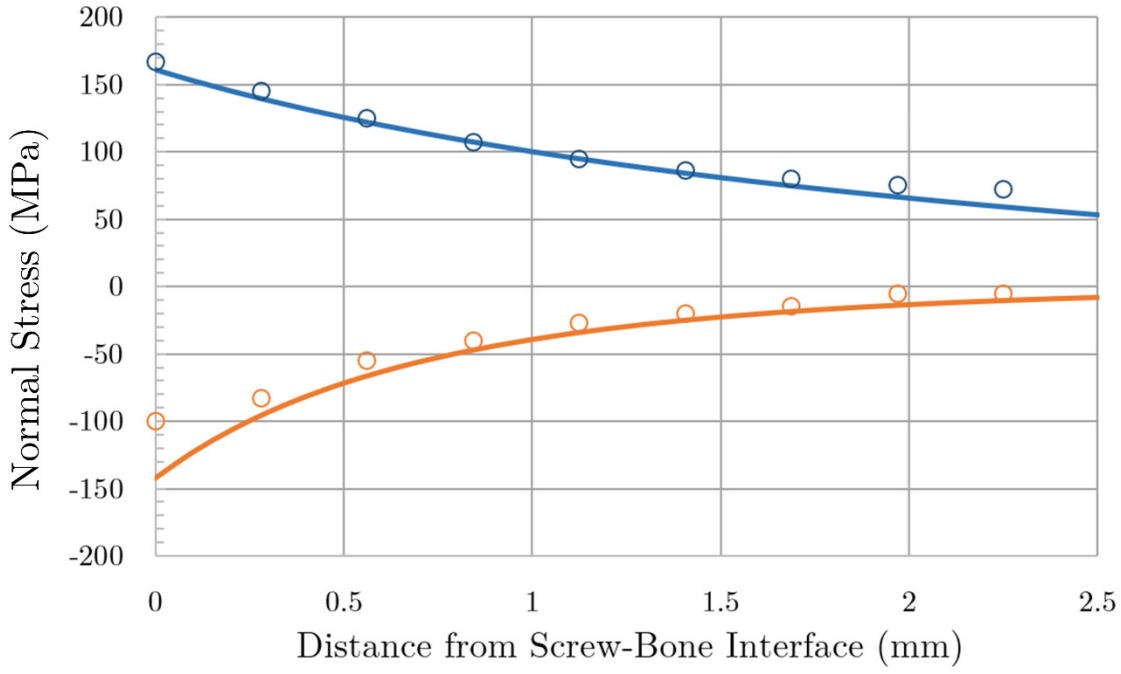

Figure 3.3 – Analytical and finite element results for radial and circumferential stress within the bone at a distance from the screw-bone interface.

3.3.2 Solution Simplification

Assuming the steel to be infinitely stiffer than the bone and for $r_2 \rightarrow \infty$, Equation 3.19, simplifies to the formula described by Kuhn et al. (Kuhn et al., 1995):

$$p_f = \frac{u_t E_h}{r_f(1 + v_h)} \tag{3.20}$$

This formula gives a value of stress at the screw-bone interface of 159.2MPa for the system considered in section 3.3.1. Accounting for screw deformation and a bone outer radius of 4.5mm (in reality this distance is around the bone cross section so is not directly comparable) predicts 167.8MPa. The error is only 5.4%.

3.3.3 Incorporating Screw Threads and Pilot Holes

The analytical solution does not account for screw threads, which will increase strain locally at thread tips. The FE simulation was extended to include threads identical to those considered in the previous chapter in order to examine their influence on strain within the bone (see section 2.4.1). Two cases were examined, further to the original idealised case, (a) (Figure 3.4a):

(b) A 'perfect fit' where the outer profile of the screw and threads exactly matches the inner geometry of the bone (Figure 3.4b)

(c) A 'realistic' case with a pilot hole diameter of 4.15mm; larger than the core diameter of the screw but smaller than the external diameter. (Figure 3.4c)

In all cases the threads and shaft of the screw were assigned frictionless sliding interactions with the bone (see section 2.4.6).

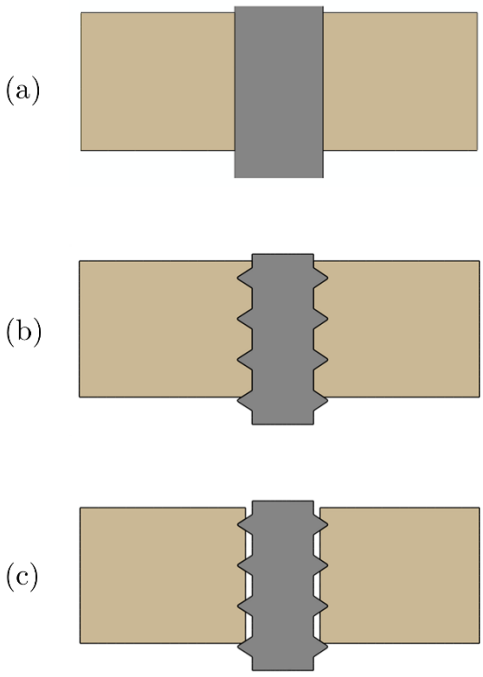

Figure 3.4 – Undeformed geometries of: (a) the idealised cylindrical representation; (b) the perfect fit and (c) the 'realistic' models.

As expected, the inclusion of screw threads increases the strains locally and the models produce similar radial strains both at the thread tips and further away from the screw-bone interface (Figure 3.5b and c). The area of high tensile strain extends furthest in model (b) as the pilot hole diameter is smaller, which effectively increases the interference producing larger circumferential strains throughout the depth (Figure 3.5b). The gap around the screw core in model (c) means that when the screw core expands it does not immediately exert pressure on the surrounding bone. Nevertheless, the peak maximum and minimum principal strains were highest for model (c) due to more local deformation.

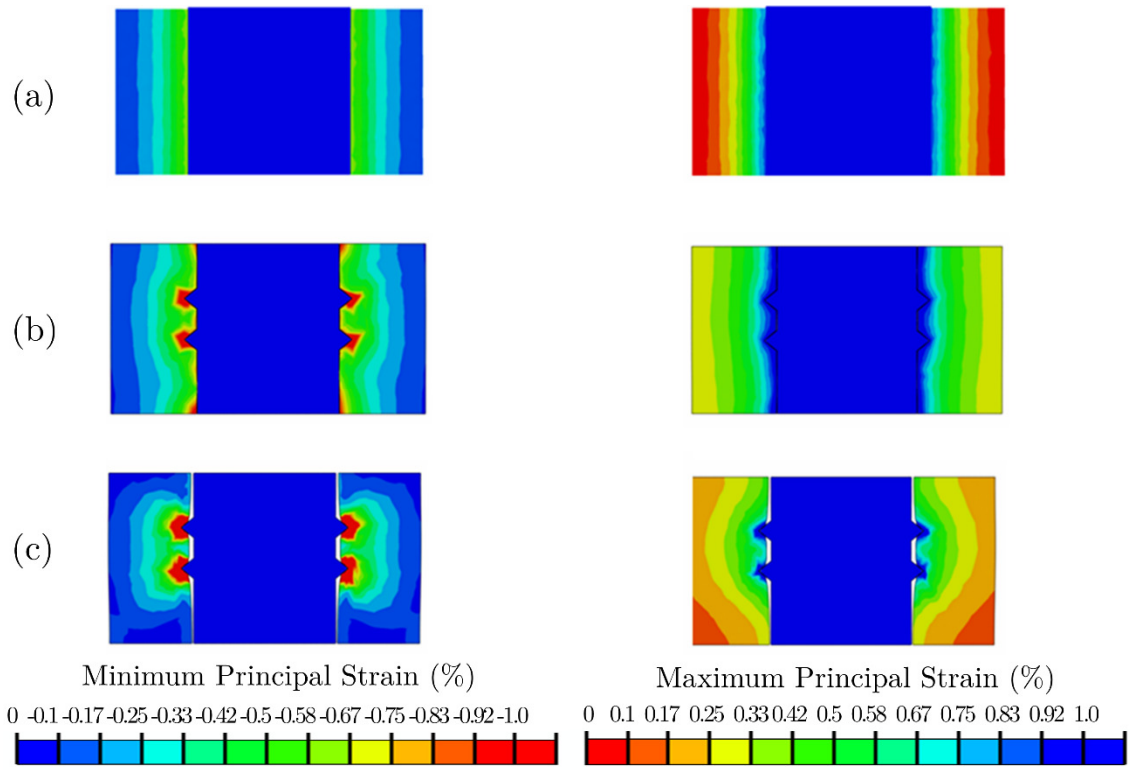

Figure 3.5 - Maximum and minimum principal strains at 1% expansion for (a) idealised cylindrical screw; (b) threaded screw with 'perfect fit'; (c) screw with realistic pilot hole.

3.4 Inclusion of Inelasticity

The amount of interference generated from screw expansion is not directly comparable to the interference values quoted in the literature as inelastic deformation and thread penetration will reduce the actual interference and interface pressure. This means that the idealised cylindrical representation is likely to over-estimate stress prediction and the damage caused to the bone.

A study by Kuhn et al. (1995) compared the damage caused by different screw types; those which caused the least damage were pre-tapped and self-tapping (Figure 3.6). Both screws had an outer diameter of 2.0mm and were predrilled with a pilot hole of 1.5mm. The pre-tapped screw had a core diameter of 1.3mm and the self-tapping screw had a core diameter of 1.4mm. An axisymmetric finite element model of the self-tapping screw used by Kuhn et al. (1995) was made. An expansion of 33.3% was imposed to represent the undersized pilot hole in both cases.

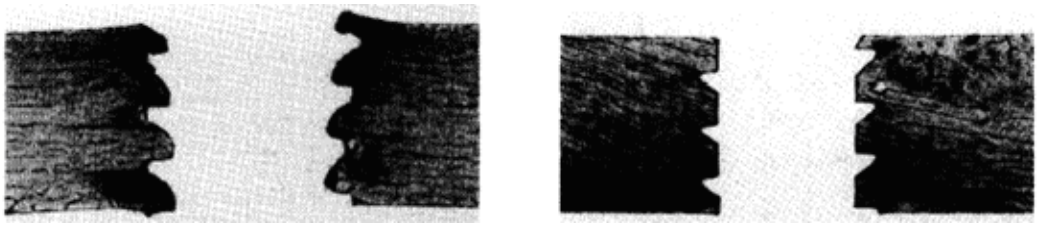

Figure 3.6 – Deformation caused by (a) the self-tapping screw and (b) the pre-tapped screw in a study by Kuhn et al. 1995.

To incorporate inelastic deformations, plasticity was included in the models using the Drucker-Prager yield criterion (Feerick and McGarry, 2012, Mullins et al., 2009) with a friction angle of 14° and flow stress ratio and dilation angle equal to zero (Goffin et al., 2014). These values were evaluated to give an appropriate tensile-compressive yield strain ratio. The compressive yield stress of 144.9MPa was derived from the Young's modulus and a typical yield strain of 0.7% (Bayraktar et al., 2004, Ebacher et al., 2007). Axisymmetry was used in the plasticity models in order to improve mesh resolution and decrease run time. The threads tips were filleted with a 0.05mm radius.

3.4.1 Strain Environment

Although the idealised cylindrical case has the same external diameter, it produced greater plastic deformation as there is no subsidence of the threads (Figure 3.7a). The region of plastic deformation extends furthest from the screw-bone interface in the cylindrical case followed by the 'perfect fit' and the 'realistic' model (Figure 3.7). Both the 'perfect fit' and 'realistic' models capture the localised compressive plastic strains around screw threads (Figure 3.7b and c); however, the 'perfect fit' case produces larger tensile strains between screw threads. This is due to the screw's core diameter being in contact with the bone.

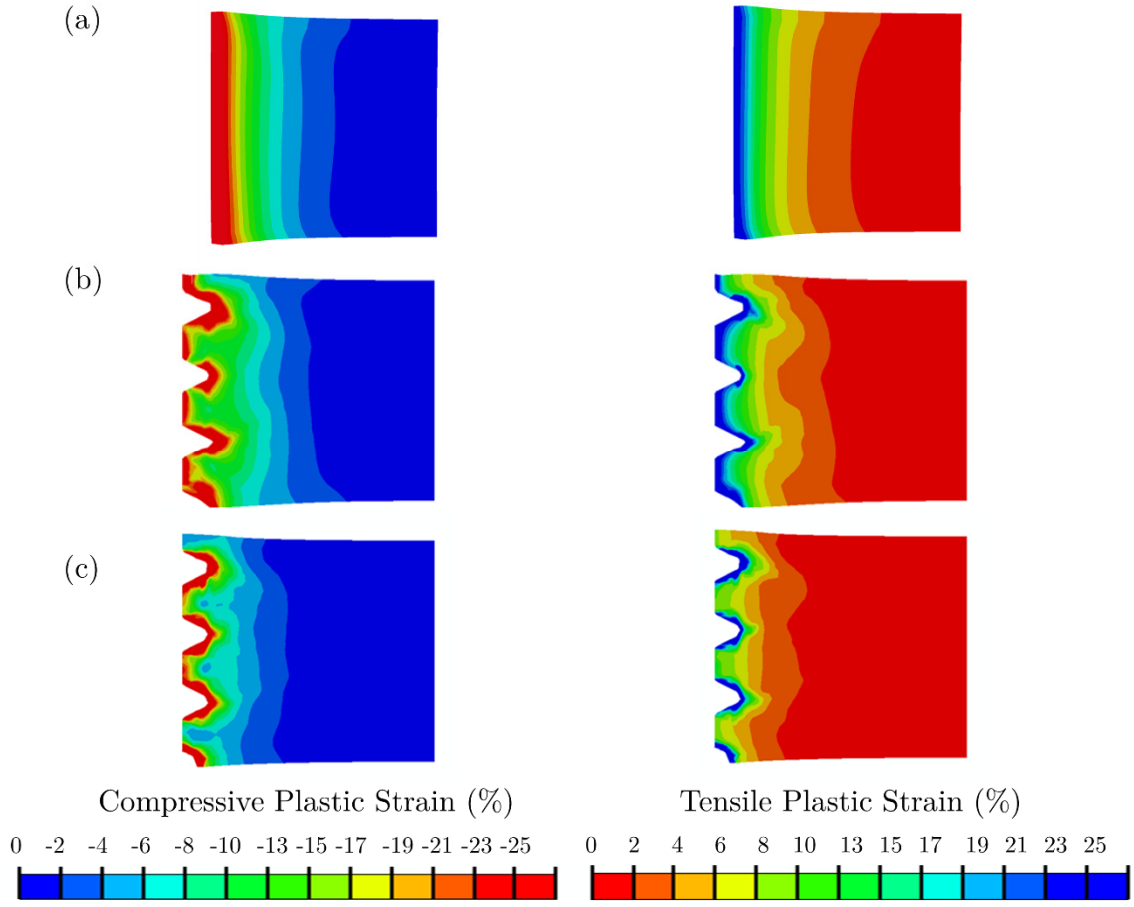

Figure 3.7 - Maximum compressive and tensile plastic strains for (a) idealised cylindrical; (b) the 'perfect fit' model and (c) the 'realistic' model at 33.3% screw expansion. All cases are shown with a deformation scale factor of 1.

3.4.2 Deformed Shape

The deformed shapes produced due to the screw expansion are shown for an idealised cylindrical case, the 'perfect fit' case and the 'realistic' case (Figure 3.8a-c). The permanent deformation produced from the 'perfect fit' and 'realistic' models are both similar to each other and to the experimental deformation shown by Kuhn et al. (1995) for self-tapping screws (Figure 3.8a). While only qualitatively similar, this demonstrates that by using only the external screw diameter and pilot hole size the thermal expansion can produce the deformation caused by self-tapping screws. Pre-tapped screws, however, can greatly reduce the effective interference and may require a reduced level of expansion to account for this. As the difference between models (b) and (c) was considered to be small, and creating the 'realistic' pilot hole was more time consuming, the 'perfect fit' approach is used herein.

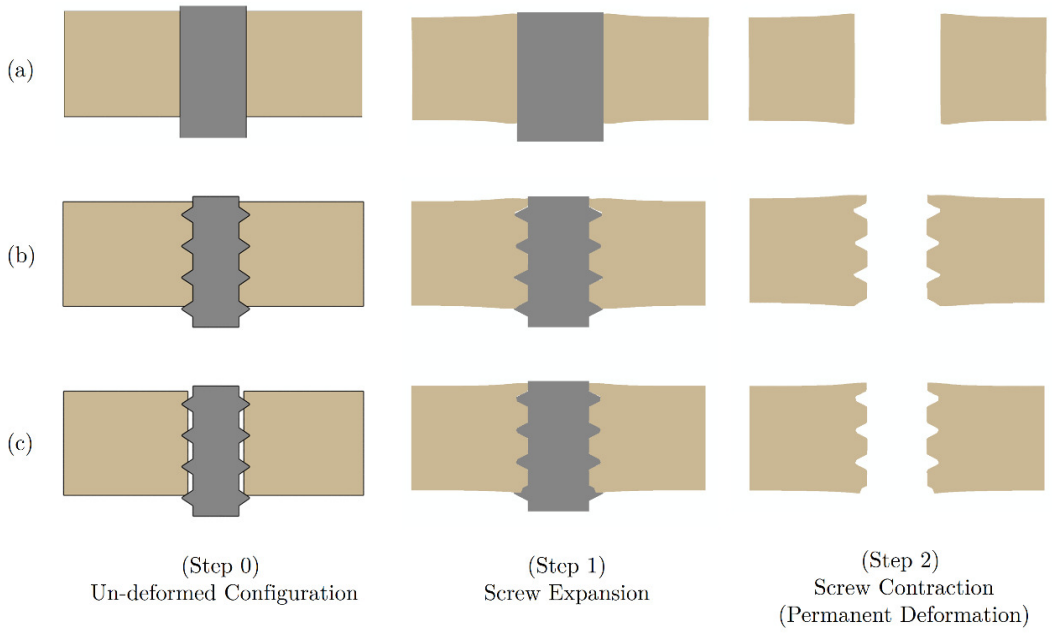

Figure 3.8 - The initial, expanded and final deformed profiles of: (a) the idealised cylindrical representation; (b) the perfect fit and (c) the 'realistic' models. All cases are shown with a deformation scale factor of 1.

3.5 Implementing the Radial Preload Representation in Bone-Fixator Systems

The thermal expansion approach to representing screw-bone interference was incorporated in plated bone models identical to those described in Chapter 2. The coefficient of thermal expansion used was 0.01 with a 1° increase in temperature corresponding to a 1% increase in size. A 'perfect' geometrical fit between the screw and bone was employed prior to expansion (see sections 3.3 and 3.4). Although temperature and thermal expansion was used, the temperature effects included did not influence the analysis in any way other than causing material expansion.

The analysis was conducted in two steps:

Step 1: a thermal step where the screw was heated causing expansion. No external loading was applied in this step; forces arise from the expansion alone.

Step 2: the temperature was maintained from Step 1 and the mechanical weight-bearing loads were applied.

Heating the entire length of the screw meant that there was compression in the plate around the screw heads. To avoid these stresses the temperature boundary condition was set to heat only the screw shaft inside the bone. The screw head was subsequently unheated and no thermal strains were induced.

3.5.1 Orthotropic Expansion

When a screw is driven into bone, it causes radial compression. Isotropic thermal expansion coefficients would cause unrealistic lengthening of the screw. Instead, thermal expansion coefficients were given for all directions with axial lengthening of the screw and shear expansions set to zero; expansion was only allowed in the radial plane of the screw. A cross-section of the original and expanded screw profiles is shown in Figure

3.9. The strains resulting from isotropic expansion compared with orthotropic expansion are shown in Figure 3.10.

Figure 3.9 - Original and expanded screw profiles (deformation exaggerated twenty times).

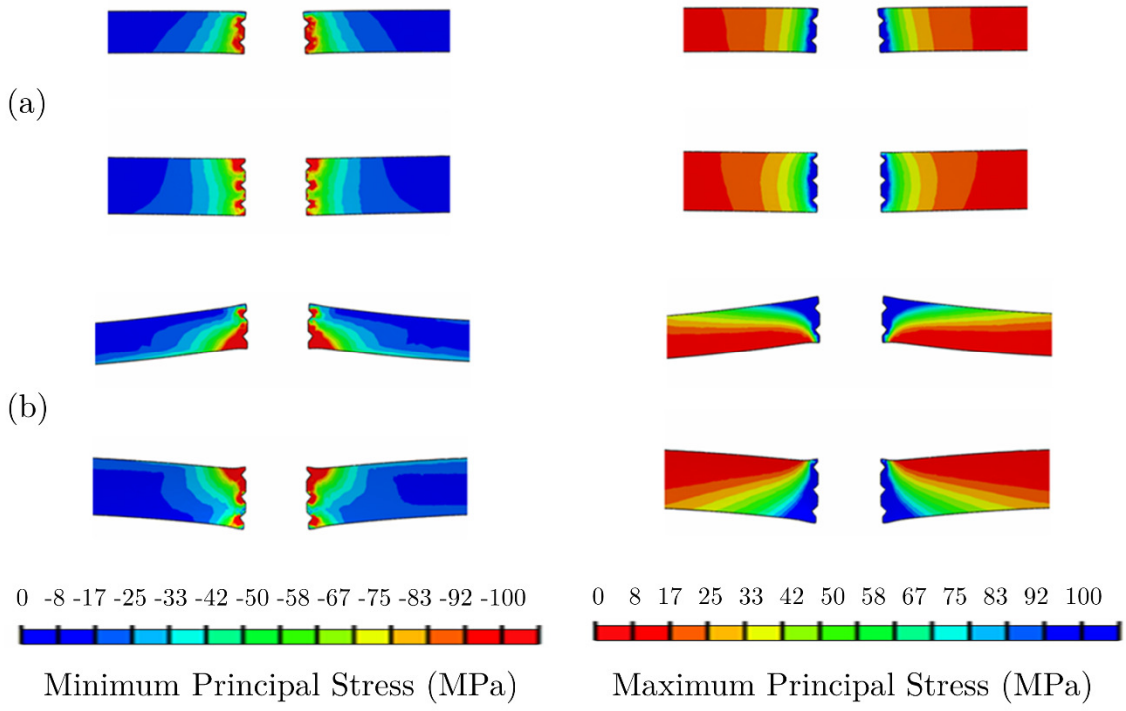

Figure 3.10 – Minimum and maximum principal stress in the bone due to expansion stresses only for (a) orthotropic expansion and (b) isotropic expansion. Deformation exaggeration times 20.

3.6 Results

The inclusion of preload due to screw expansion was seen to make very little difference to load-deformation behaviour of the bone-plate construct (less than 0.5% difference compared with the tied representation in section 2.5.1). The maximum and minimum principal strains were plotted through section A-A (see section 2.4.1) and are shown in Figure 3.11 (MacLeod et al., 2012, Pankaj, 2013).

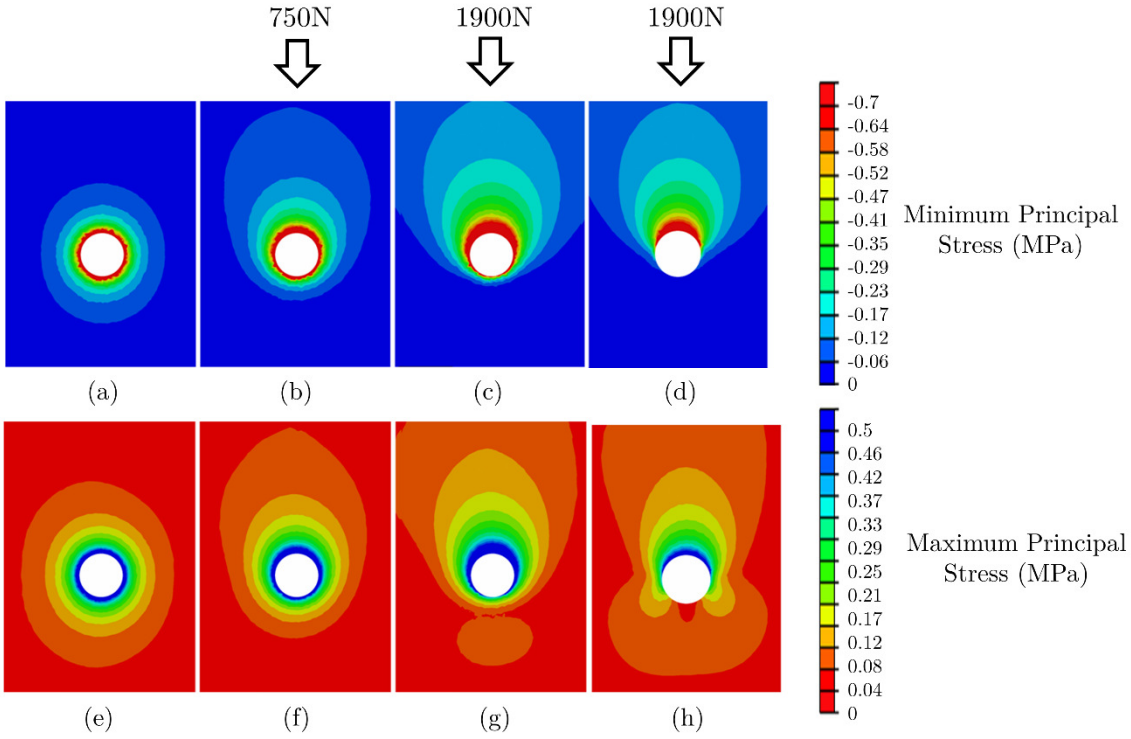

Figure 3.11 - Minimum and maximum principal strains due to expansion alone (a and e); including expansion different levels of load (b, c, f, g) and neglecting expansion (d, h) (MacLeod et al., 2012, Pankaj, 2013).

3.7 Discussion

The stress pattern and magnitude around the threads of a screw are indicators of screw loosening, bone damage and stress shielding. It is one of the most important aspects of implant performance. Screws cause prestress within the bone due to the discrepancy in size between screw and hole; thermal expansion is a convenient method of incorporating this. This can be done using a pre-loading step in the finite element analysis.

In the isotropic expansion model there are significantly larger tensile strains at the periosteum and compressive strains at the endosteum compared with the orthotropic expansion model (Figure 3.10). This is due to the pull-out style loading occurring because of the screw lengthening. The inclusion of orthotropic material expansion was found to change the environment locally around the screw holes but elsewhere is similar to the model without expansion. Isotropic expansion resulted in much larger strains throughout the bone. Both the compressive and tensile prestresses were seen to migrate towards to applied load under loading (Figure 3.11). Despite only using 1% expansion, the stresses arising in step 1 due to screw expansion were seen to be larger than those produced by 100% body weight (Figure 3.11b and f). At larger loads (250% B.W.) the prestress starts to be overcome on the side of the hole distal to the load (Figure 3.11d and h). Although the amount of expansion is small, the stresses induced approach the yield stress of bone and could not exceed this in reality. Therefore, with increased interference, the region of high stress would likely extend further from the screw-bone interface but otherwise the pattern would remain similar. This, however, would require the inclusion of plasticity.

3.7.1 Interference Fit Applied Through Contact Settings

Abaqus has a built-in interaction setting that allows interferences or overlaps to be resolved and the resulting strains imposed. This feature can work well for simple geometries, however, was found to be heavily mesh dependant when screw threads were

included. Using anisotropic thermal expansion to produce the interference fit has several advantages: it simplifies the modelling process, particularly where screw threads are included; it allows several levels of interference to be simulated by changing only a single value; and is straightforward to implement.

3.7.2 Limitations

The prestresses caused during screw fastening will recede over time. In the early stages of healing these may well be the dominant forces that a bone is exposed to due to the avoidance of weight-bearing; nevertheless, inclusion of viscoelastic effects would reduce the prestress observed over time. In order to predict the true stress-strain environment case plasticity would also be required to allow subsidence around thread tips, which would reduce the peak stresses.

Screw expansion means that the screw will be bigger at the end of the analysis than at the beginning. While this effect is negligible for the small interferences considered in this study, it may become unrealistic when representing very small pilot holes. A possible way of overcoming this would be to model a smaller hole and screw, taking into account the amount of expansion needed, then to expand the screw shaft to the real size. This, however, requires a unique geometry of model for a given interference.

3.8 Conclusions

- Orthotropic thermal expansion is a convenient method of representating screw-bone interference. The method of allows for the inclusion of screw threads, which are a crucial aspect of screw fixation but often neglected in computational models.

- Even small interferences can produce extremely large preload. An interference of 1% of the diameter of the screw can produce stresses at the screw-bone interface larger than due to 100% of body-weight.

4

Locking Screws in Osteoporotic Bone

4.1 Introduction

Studies have suggested that the locking compression plate (LCP) performs better than the dynamic compression plate (DCP) in older or weaker bone (Kim et al., 2007, Yanez et al., 2010, Gardner et al., 2004) (Davis et al., 2012, Kim et al., 2007, Yanez et al., 2010, Miller and Goswami, 2007, Szypryt and Forward, 2009, Gardner et al., 2004, Grawe et al., 2012). Locked plating has been reported to have increased fatigue strength and ultimate failure loads (Zehnder et al., 2009, Uhl et al., 2008, Seide et al., 2007) and are still considerably more expensive than the DCP (Smith et al., 2007). On the other hand, studies have shown that the pull-out strength of compression screws increases with bone density (DeCoster et al., 1990, Thiele et al., 2007), and they can perform better than locked plating in healthy bone (Kim et al., 2007).

The reasons for the differences in failure loads between the plating types are not straightforward as there are multiple factors to consider. The preloads involved in compression screw tightening increase stress levels at the screw-bone interface even

before physiological loads are applied, whereas locking screws have negligible screw tightening preload (Gardner et al., 2004). During physiological loading, however, the DCP allows for frictional load transfer at the plate-bone interface; locked plating, on the other hand, transfers all physiological loads via the screw-bone interface. Therefore, the local environment around screws in a DCP is influenced by a mix of effects, whereas the mechanics related to locking screws is more straightforward – similar to a unilateral external fixation device.

4.1.1 Previous Studies

Many experimental tests have been conducted comparing locking and compression screws (Kim et al., 2007, Uhl et al., 2008, Yanez et al., 2010, Seide et al., 2007); while the experimental tests have been able to compare the performance, they have not been able to fully explain the mechanics associated with the difference. This study uses finite element simulation, which permits evaluation of the local stress/strain response around screws; this is difficult, if not impossible, to measure in a lab experiment.

Few computational simulations have been attempted as DCPs are complex to model due to the screw insertion producing axial preload in the screw (pulling the plate towards the bone) and interfragmentary compression caused by preload within the plate (compression screws are inserted off-centre in plate holes, which forces the bone towards the fracture gap) (Gardner et al., 2004). While compression plate preloads have been included in some previous numerical studies (Kim et al., 2010, Cheal et al., 1985, Rybicki and Simonen, 1977, Beaupre et al., 1988, Ferguson et al., 1996, Zand et al., 1983), their inclusion is via application of concentrated loads or as prescribed displacements. The effect produced by such techniques is not completely realistic; for example, an applied displacement to the bottom of a screw does not induce loads akin to screw fastening as the threads closest to the displacement will carry larger loads. Moreover, screw threads are rarely modelled and can have considerable influence on the local strain environment.

Gefen (2002) noted the high proportion of load taken by the first thread in a study where screw tightening preload was modelled.

While the majority of previous studies assume homogeneous and isotropic material properties for bone (Duda et al., 2002, Anitha et al., 2013, Benli et al., 2008, Fouad, 2010, Ganesh et al., 2005, Moazen et al., 2012, Stoffel et al., 2003, Chen et al., 2013, Ma et al., 2013, Ebrahimi et al., 2012, Luo et al., 2013, Dubov et al., 2011), more complex models generally include either homogeneous orthotropic (Kim et al., 2010, Krishna et al., 2008, Taheri et al., 2012) or heterogeneous isotropic typically derived from CT attenuations (Wieding et al., 2012, Gray et al., 2008, Schileo et al., 2007). Depending on the parameters of interest, simplified material properties may be justified. For example, predictions of fracture gap motion, have been shown to be relatively insensitive to changes in bone material properties (Uhl et al., 2008, Donaldson et al., 2012a); however, when examining localised region response, such as strains through the cortex, simplifications can have greater consequences (Prendergast, 1997).

It has been previously shown that the fracture gap size affects the strain within the plate (Oh et al., 2010, Stoffel et al., 2003); however, to our knowledge, the influence of a fracture gap on the strains in the bone around screw holes has not been investigated. Aseptic loosening of screws is a significant clinical problem, which is generally attributed to over or under exposure to strain (Evans et al., 1990, Stoffel et al., 2003, Huiskes et al., 1985, Turner et al., 1997). Moreover, this threshold may be below the yield strain of bone (Sugiura et al., 2000) and osteoporotic bone is thought to be more susceptible to loosening than healthy bone (Gardner et al., 2004). High levels of strain around screw holes are therefore strong indicators of potential loosening.

Locking plate fixation is becoming an increasingly popular choice for complex and osteoporotic fractures but has not completely replaced compression plating, which

remains the standard choice for many indications including articular fractures (Gardner et al., 2004).

4.1.2 Chapter Aim

This chapter attempts to model the mechanical environment in dynamic compression plate fixation in a more realistic manner than has previously been achieved. For the purposes of the study, the exclusive use of each screw type was considered. The local strain environment around screw holes and the stresses within the implants is predicted for varying bone qualities and fracture patterns. The results are compared with those for a locking plate. The aim of the chapter is to provide a biomechanical basis for the reported improved performance of locking plates in poorer bone quality.

4.2 Methods

4.2.1 Geometry

For both compression plating and locked plating, models were developed to represent a fracture gap scenario where no interfragmentary contact can occur and for a fully reduced fracture. The DCP is not generally used as a bridge plate, however, complete reduction of the fracture may not always be achieved leaving a fracture gap. Both plating systems and fracture gap scenarios were modelled for healthy and osteoporotic bone using representative cross-sectional geometries and material properties. As the study examined the tibial diaphysis, only the cortical bone was included in the models.

Two reference tibial cross-sections with a cross-sectional areas 319 mm^2 and 265 mm^2 with an average unicortical thickness of 5.1 mm and 3.64 mm (Russo et al., 2006, Donaldson et al., 2012b) were considered for healthy and osteoporotic bone. These tibial cross-sections were extruded longitudinally to a length of 110mm for three dimensional finite element modelling (Figure 4.1a-d). We considered a transverse fracture of the tibial diaphysis and assumed symmetry on either side of the fracture (Figure 4.1c).

Locking plates are generally used with an off-set between the plate and the bone (Figure 4.1b); therefore, we assumed no interaction between these two components and a 2mm off-set in the locking plate models. Callus or soft tissue was not included in any of the models.

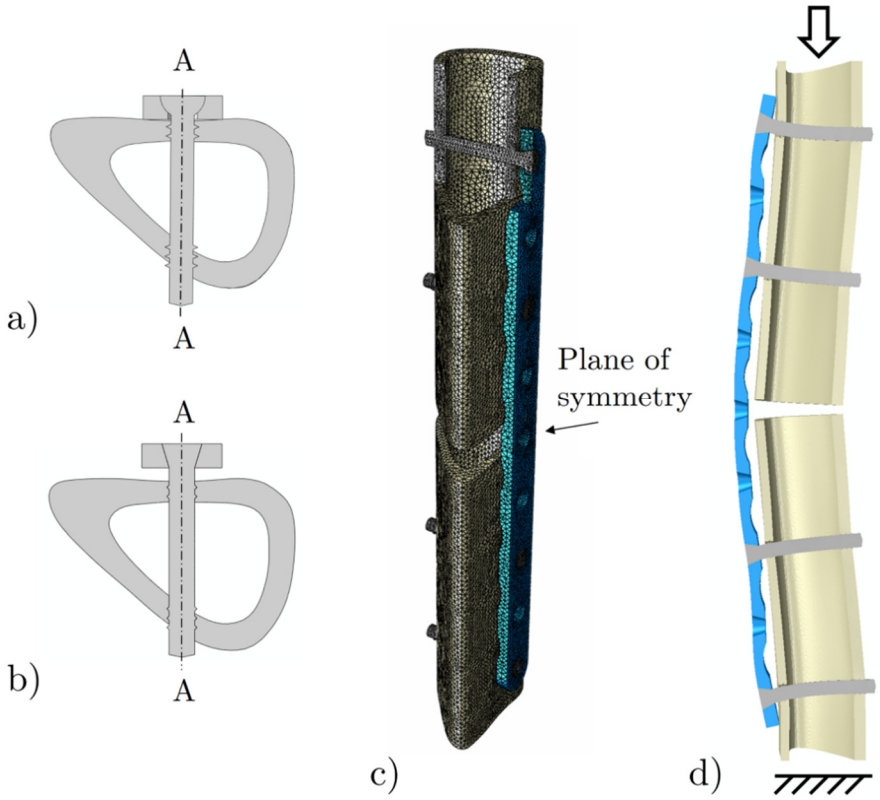

Figure 4.1 - a) Cross-section of a healthy tibia with DCP; b) cross-section with LCP; c) finite element model geometry of the LCP with section through the centre line of the plate showing the mesh refinement around screw holes; and d) deformed shape of the LCP model (scale factor x40).

The plate dimensions were the same for the DCP and LCP and based on typical industry standard: 9-hole plate with a cross-section 3.6x12 mm; hole spacing of 20 mm. Screws were placed in the second and fourth holes from the fracture gap (Figure 4.1d). The screws had an external diameter of 4.5 mm and a core diameter of 3.84 mm and 3.5mm for locking and compression screws respectively. Threads, with a spacing of 1.4 mm, were modelled as idealised rings rather than helical, an approach which has been

previously used (MacLeod et al., 2012, Donaldson et al., 2012a). This assumption eased meshing and was thought to be unlikely to affect the results. For simplification only the threads in contact with the bone were modelled.

4.2.2 **Material Properties**

The cortical bone properties used were linear elastic, orthotropic and heterogeneous (variable through the cortical thickness) and are shown in Table 4.1. Two groups of bone properties employed were representative of female cortical bone and based on a past study (Donaldson et al., 2012b). The anisotropy was incorporated using cylindrical axes for each segment of the cross-section (Figure 4.2a), where E11 is the radial, E22 is the circumferential and E33 is the longitudinal direction. Table 1 provides values at the periosteum and the endosteumn (Donaldson et al. 2012b); the variation in orthotropic elastic properties through the thickness was evaluated using tensor interpolations (Yang et al., 1999) and is illustrated in Figure 4.2b. A comparison of tensoral interpolation against component-wise interpolation for the case of osteoporotic bone is included in Appendix A.1. Cortical thinning and periosteal apposition were also incorporated for osteoporotic models as shown in Figure 4.2c (Russo et al., 2006, Donaldson et al., 2012b). The plate and screws were assumed to be homogeneous, isotropic and linear elastic steel. The Young's modulus for both was 1.80×10^{11} N/m^2 (Fouad, 2010, Gefen, 2002, Benli et al., 2008, Ganesh et al., 2005). Poisson's ratio for steel was taken as 0.3 (Oh et al., 2010, Benli et al., 2008, Ganesh et al., 2005).

Table 4.1 – Orthotropic heterogeneous material properties assumed for different bone qualities.

	Young / Healthy		Old / Osteoporotic	
(GPa)	periosteum	endosteum	periosteum	endosteum
E11	18.6	16.6	12.9	3.2
E22	18.8	17.1	14.6	6.0
E33	22.4	21.4	19.3	11.2
G12	7.2	6.6	5.4	1.8
G13	6.9	6.4	5.4	2.2
G23	7.0	6.5	5.7	3.0
v12	0.29	0.27	0.24	0.16
v13	0.26	0.24	0.20	0.07
v23	0.26	0.24	0.22	0.14

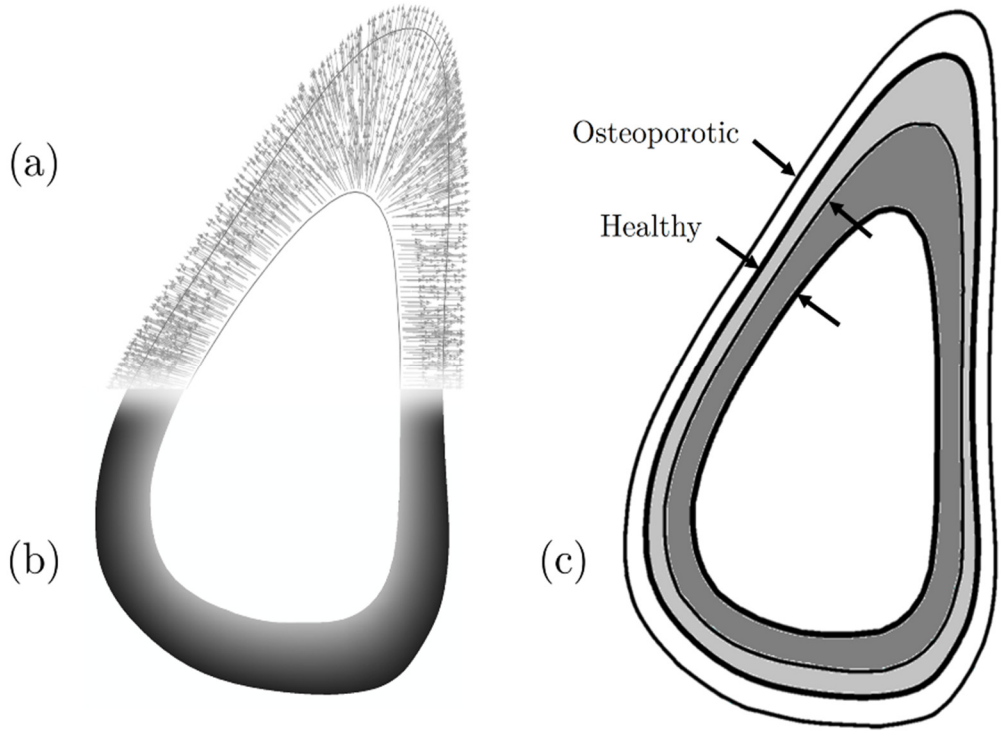

Figure 4.2 - The material properties incorporated showing a) orthotropic material orientations; b) heterogeneity—gradient from endosteal to periosteal surfaces; and (c) the geometrical changes—periosteal apposition and endocortical resorption associated with osteoporosis.

4.2.3 Contact Interactions

The screw-bone interaction at the entrant cortex was modelled as frictional using a standard Coulomb friction coefficient of 0.3 based on some recent studies (Eser et al., 2010, Pessoa et al., 2010, MacLeod et al., 2012). As the majority of load is transferred at the screw holes on the entrant cortex the screw-bone interaction at the exit cortex was modelled as tied for analysis simplification. The plate-bone interaction for DCP used a frictional coefficient of 0.4 (Kim et al., 2010, Perren, 2002).

4.2.4 Loading

The load was applied using uniform displacement control at the free end as shown in Fig. 1d. The analysis was conducted up to a load of 1200N (approximately 1.6 times bodyweight for a 75kg person), which has been shown to be the force in the tibial mid-shaft at 7 weeks post-surgery (Vijayakumar et al., 2006).

4.2.5 Mesh

The models used approximately 220,000 linear tetrahedral elements with refinement around screw holes (Figure 4.1c). In the region around screw holes the average element edge length was 0.3mm. A mesh convergence study was performed and the results showed that doubling mesh density of the plate increased the displacement at the fracture gap by 6.78% in healthy bone and 6.85% in osteoporotic bone. In the bone the change in peak minimum (and maximum) compressive strain was less than 3.22% (3.07%) when doubling the mesh resolution. Geometrically nonlinear analyses were conducted using Abaqus 6.10 (Simulia, Providence, RI, USA).

4.2.6 Incorporation of Preloads

The screw fastening preload was simulated using ‘bolt load’ in Abaqus 6.10. This preload was applied to a slice of the screw shaft, below the head and above the first thread (Figure 4.3a). Other methods such as ‘body forces’ or ‘tractions’ were not suitable as

they are applied over volumes or external surfaces. This novel application induces normal stresses in the axial direction of the screw and does not require any artificial constraints or prescribed displacements. Values of preload vary widely in the literature; a value of 500N was chosen based on an average of some previous studies (Cheal et al., 1985, Perren, 2002, Kim et al., 2010, Zand et al., 1983, Rybicki and Simonen, 1977, Beaupre et al., 1988, Ya'ish et al., 2011). This value may appear to be large, however, pull-out forces for cortical screws in human bone are around 1200N (DeCoster et al., 1990). In the DCP models where the fracture was completely reduced this approach was also used to simulate a 500N tensile preload in the plate (Figure 4.3b). As radial interference preload is likely to be present in both screw types (MacLeod et al., 2012) it was not included to better highlight the differences between the two plating systems.

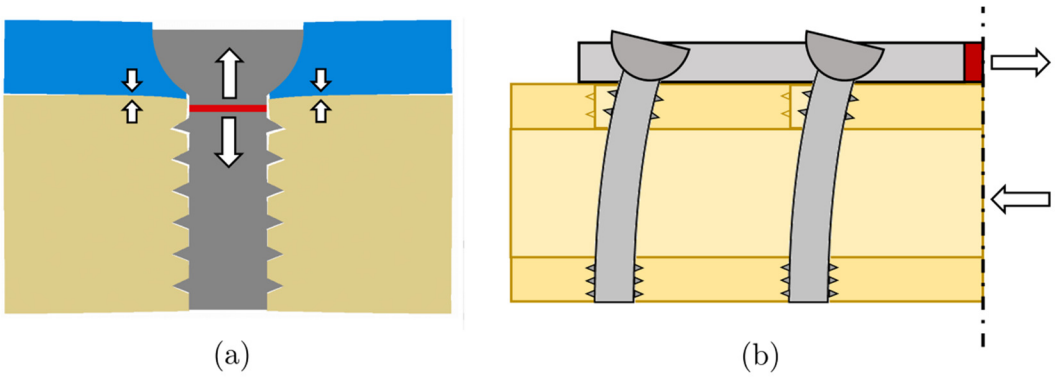

Figure 4.3 – Depictions of the preloads used in the DCP models: (a) screw tightening and resulting bone-plate compression; (b) plate tensioning and resulting interfragmentary compression. The red regions are where the preload was specified and white arrows indicate the direction of the preloads.

4.2.7 Boundary Conditions for Pull-out Tests

Several studies have simulated axial pull-out of screws (Yu et al., 2011, Ruffoni et al., 2012, Wirth et al., 2010, Feerick and McGarry, 2012); however, the boundary conditions imposed can vary significantly between studies. The influence of several boundary conditions was examined (Figure 4.4). If the bone is restrained proximally, strains will be nearer the screw head (Figure 4.4a); restraint distally increases the concentration of strain closer to the tip of the screw (Figure 4.4d). Restraint throughout the depth of the sample increases shear resistance (Figure 4.4b); an effect that is only slightly diminished by removal of lateral restraint (Figure 4.4c). Condition (a) was adopted for comparisons against the screw tightening procedure.

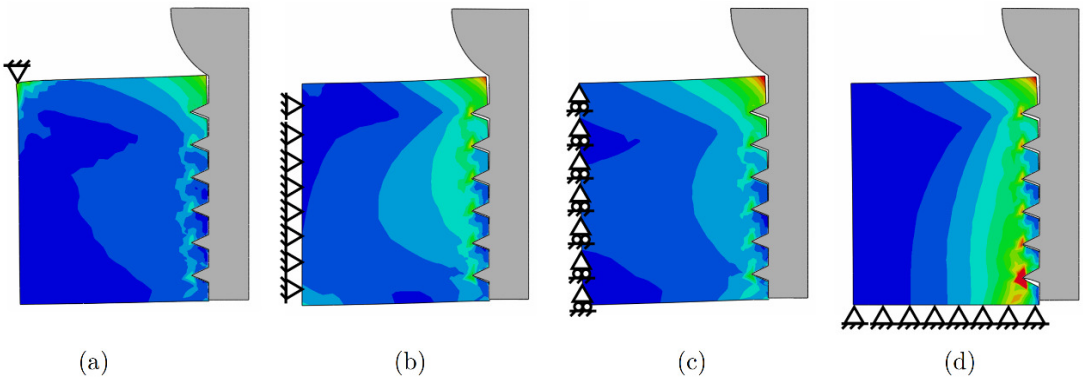

Figure 4.4 – Pull-out test simulations using different restraint conditions and the pattern of maximum principal strain produced around screw threads.

4.3 Results

4.3.1 Screw Fastening Representation

In the first instance the stresses induced due to screw tightening preload (for DCP) were compared with those due to simple screw pull-out. The von Mises stresses produced are shown in Figure 4.5 for the two cases. In both cases the largest stresses occur in the vicinity of the first screw thread, which also transmits the most load (Figure 4.5c). However, the region of bone with high stresses was found to be larger in the case of plate tightening simulation in comparison to screw pull-out.

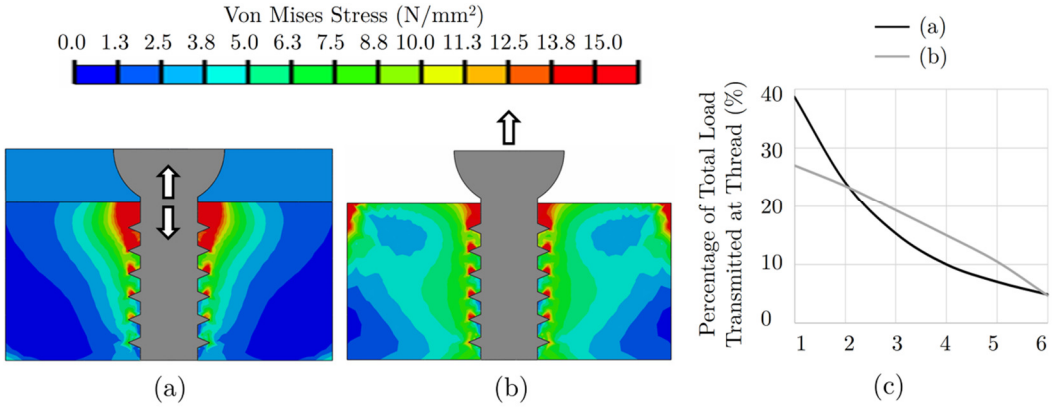

Figure 4.5 – Von Mises stress distribution in the bone due to (a) the bolt preload representation of screw fastening with a plate; (b) pull-out style loading; and (c) the percentage load transferred at each thread counting from the screw head for the two loading cases.

4.3.2 Comparison of Plating Types and Bone Qualities

Minimum and maximum principal strain contours were plotted using section A-A (Figure 4.1a and b) in the vicinity of the screw hole on the proximal side of the fracture (Figure 4.6 and Figure 4.7). The plots compare strains in: the LCP (a, c, e, g); the DCP (b, d, f, h); healthy bone (a, b, c, d); osteoporotic bone (e, f, g, h); a fully reduced fracture (a, b, e, f); and a fracture gap (c, d, g, h). Principal strain rather than stress was used for the comparisons (Pankaj, 2013) and the limits of the scale were chosen to be 0.5% and 0.7% for tensile and compressive strain respectively. These values represent yield values for cortical bone found in the literature (Bayraktar et al., 2004, Ebacher et al., 2007). For the DCP large compressive and tensile strains occur around the full perimeter of the DCP screws (particularly apparent in Figure 4.6f and h and Figure 4.7f and h). These arise due to the screw tightening preload. Large principal strains in the LCP are primarily confined to the loaded side of the perimeter (Figure 4.6c and g and Figure 4.7c and g). For the LCP these arise due to screw-bone interface compression, in the direction of the load, and consequent circumferential tension and pull-out effects. For both types of plating larger principal strains are located in the periosteal region; however, this effect is more pronounced for DCP particularly at the periosteal side of the first screw thread (Figure 4.7f and h).

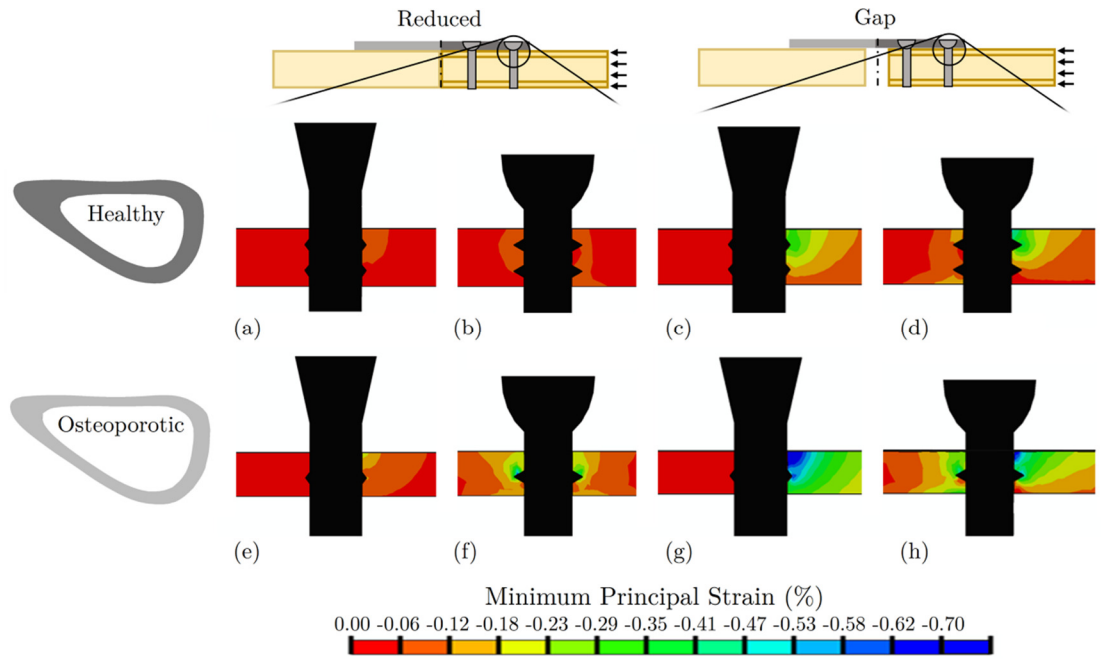

Figure 4.6 – Minimum principal strain around the screw hole furthest from the fracture gap in the LCP (a,c,e,g) and DCP (b,d,f,h) taking a transverse section through the centre line of the plate.

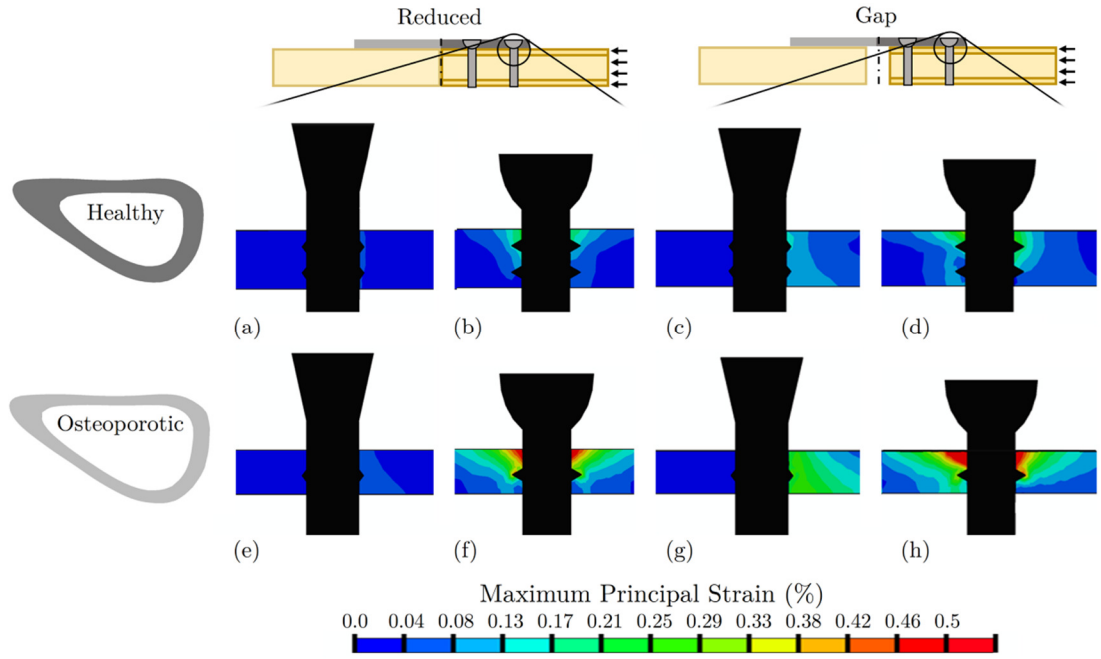

Figure 4.7 – Maximum principal strain around the screw hole furthest from the fracture gap in the LCP (a,c,e,g) and DCP (b,d,f,h) taking a transverse section through the centre line of the plate.

The volume of bone with maximum (and minimum) principal strain greater than 0.2% (-0.2%) was termed MaxEV (and MinEV) was determined for each of the healthy (Figure 4.8a) and the osteoporotic (Figure 4.8b) bone models. This value is close to the upper limit of physiological strain and therefore represents regions susceptible to loosening (Sugiura et al., 2000, Turner et al., 1997). In healthy bone with a reduced fracture, both plating types result in negligible MinEV and MaxEV (Figure 4.8a); this is also apparent from Figure 4.6a, b and Figure 4.7a, b. However, for osteoporotic bone with reduced fracture gap the MaxEV and MinEV are substantially larger for DCP in comparison to LCP (Figure 4.8b); an effect also apparent from Figure 4.6e, f and Figure 4.7e, f. Both types of plating produced larger regions of high strain in the presence of a fracture gap (Figure 4.8), wherein DCP results in larger tensile region (MaxEV) and a slightly smaller compressive region (MinEV). For healthy bone with a fracture gap the LCP produced 35% more MinEV and 67% less MaxEV than the DCP (Figure 4.8a). For osteoporotic bone with a fracture gap the LCP produced 4% more MinEV than the DCP (Figure 4.8b), while the MaxEV region was found to be 53% smaller and restricted to the side of the screw hole proximal to the load (Figure 4.6g and h). The DCP produced larger regions of MaxEV than the LCP in all cases and this was most pronounced in osteoporotic bone (Figure 4.8b).

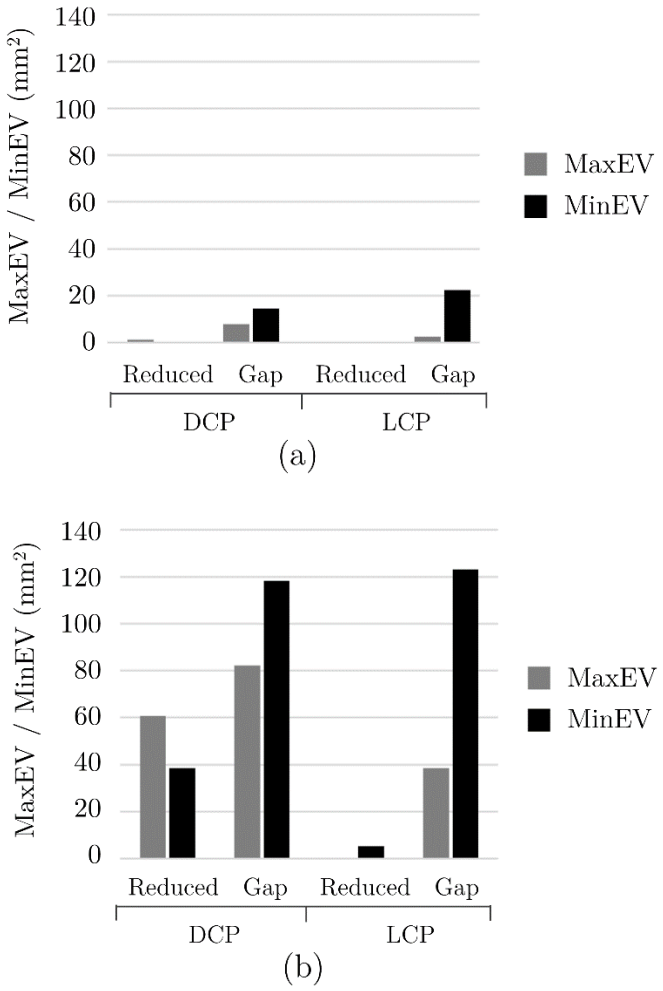

Figure 4.8 – Volume of bone with principal strain magnitude greater than 0.2% (MaxEV or MinEV) for: (a) healthy bone and (b) osteoporotic bone.

4.3.3 Stress within the Screws

The von Mises stress distribution along the length screws is shown in Figure 4.9. Compression screws developed larger stresses than locking screws and osteoporotic bone was found to increase the bending stress within both screw types. The stress distribution along the length of the screws are consistent with those predicted by James and Andrade (2013) in an analytical model.

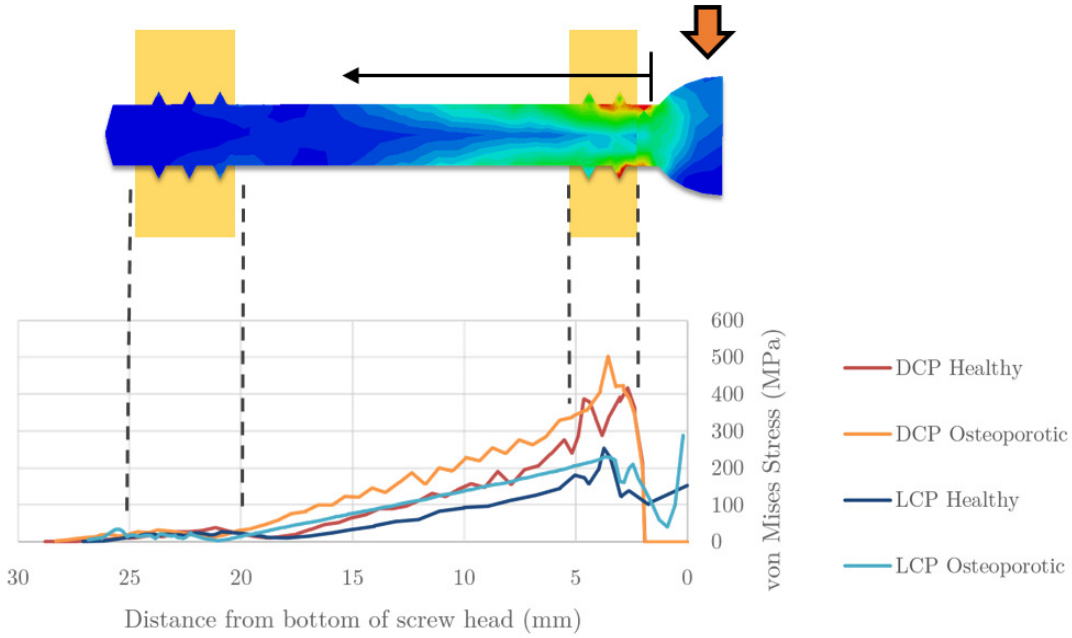

Figure 4.9 – Von Mises stress distribution along the screws. All cases are for the fracture gap model at a load of 1200N. The load depicts the reaction force of the plate on the screw head.

4.3.4 Load Transmission

The relative proportion of load transmitted through the fracture site and by the plate for a reduced fracture is shown in Figure 4.10. Locking plates redirect a greater proportion of the load than the DCP, thereby shielding the fracture site from some of the weight-bearing loads. This is due to the induced interfragmentary compression and is more significant at lower loads. Both plate types take a slightly larger proportion of the load in osteoporotic bone.

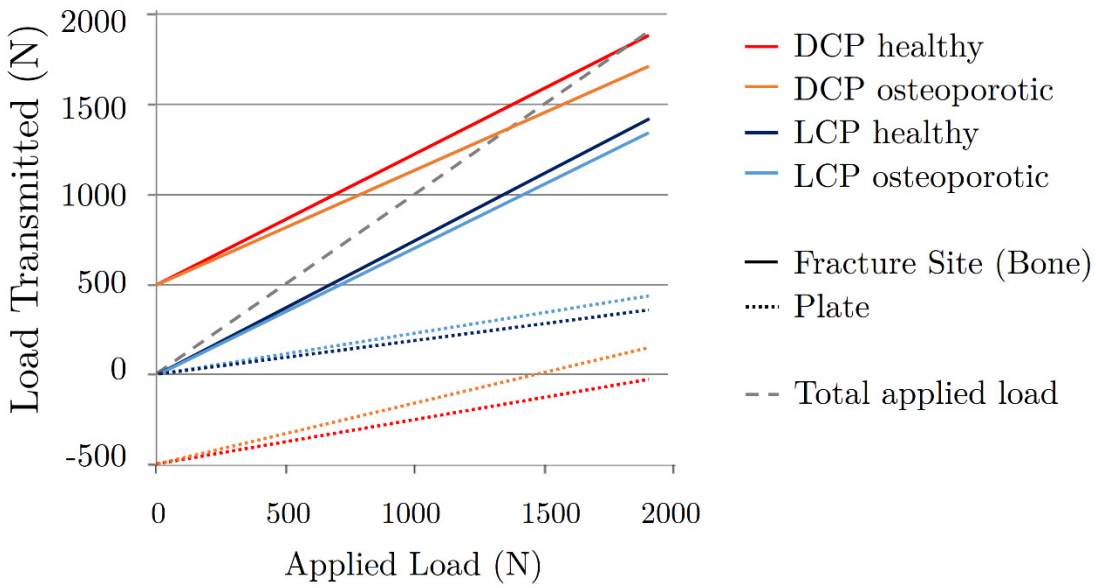

Figure 4.10 - Proportion of load transmitted by the plate and bone in the two plating types with varying bone quality

4.4 Discussion

The bolt preload representation of screw fastening used in this study was found to produce results similar to a study by Gefen (2002) and to the analytical models of Grewal et al. (1997) and Chen et al. (2010b). Screw tightening results in compression of the bone against the plate; this compression increases the proportion of load taken in the vicinity of the first thread compared to pull-out style loading.

This study shows that locking plates produce lower tensile strains around screw-hole locations in osteoporotic bone than DCPs. In healthy bone, there was a much smaller difference between the two types of plating. In both types of plating, an incomplete fracture reduction or a fracture gap resulted in increased strain concentration around screw holes. These results support clinical conclusions that simple fractures should be treated with reduction and absolute stability (Leahy, 2010). Compression plated osteoporotic bone, however, resulted in regions of very high tensile strain – even with complete fracture reduction. While strains due to weight-bearing may be reduced by the addition of more screws (Donaldson et al., 2012a), the strains caused by screw fastening in DCPs will be present regardless of the number of screws used. Another major difference in strain distribution between the screw types was that locked plating mainly produced strains on the side of the screw proximal to the load; compression plating produced strains all around the perimeter. Screw-tightening preloads are therefore fundamental to modelling the strain environment produced by the DCP.

In the reduced fracture pattern interfragmentary preload was included in the DCP models. This increased the proportion of load transmitted through the bone via interfragmentary contact compared to locking plates. In reduced fractures, therefore, an LCP shields the bone from load at the interfragmentary contact location by redirecting it through the plate. This aspect of compression plating, however, only applies when the fracture is fully reduced. In models with a fracture gap, the strains were largest in the periosteal surface in the screw entrant cortex (Figs. 5g and 5h). This is similar to

strain distributions seen in external fixators (Huiskes et al., 1985, Donaldson et al., 2012a).

4.4.1 Limitations

This study has some limitations. The preloads induced by the DCP will dissipate over time due to remodelling, damage or the viscoelasticity of bone (Beaupre et al., 1988, Allgöwer et al., 1970); our models, however, were not equipped to predict such behaviour. It is also likely that surgeons would not be able to fasten the screws as tightly in osteoporotic bone and therefore the screw tensile preload would be smaller than in healthy bone. To make the models comparable, however, the same value was used in this study.

Material non-linearity was not included in the models. This has been shown to have a negligible influence on fracture gap motion (Donaldson et al., 2012a) but could influence the stress-strain environment around screw holes. Nevertheless, even in the model with the largest strains, only 0.02% of the volume of the bone was above the compressive yield strain (0.7%) and 0.04% above the tensile yield strain (0.5%). Even with material non-linearity included the locations of peak strain are likely to remain unchanged.

Finite element modelling can provide information such as strains around screw holes, which can be difficult or impossible to measure in a physical experiment. This study predicted that locked plating produced far smaller tensile strains around screw holes in osteoporotic bone than compression plating. This provides a mechanical basis for the improved performance of locking plates in poorer bone quality and explains previously reported higher incidence of screw loosening using the DCP (Bottlang et al., 2009a). These differences in strain at the screw-bone interface were achieved using more realistic modelling of screw fastening produces in the DCP; this will be important in any further studies with an aim to understand bone remodelling, fatigue behaviour or loosening of screws.

4.5 Conclusions

- Conventional screws cause similar strains to locking screws if the bone is of good quality and the fracture is fully reduced.

- In poorer quality bone compression screws produce much larger tensile strains at the periosteal surface than locking screws. This explains the mechanism behind the high rates of loosening seen when using conventional screws in osteoporotic bone.

- Inclusion of accurate material properties and geometry is vital to observe the differences caused by the screw systems in varying bone quality. Osteoporosis causes both a deterioration in the cortical thickness and material properties.

5

Loading & Boundary Conditions in In Vitro Testing of the LCP

5.1 Introduction

This chapter considers experimental testing of locking plate constructs. It is important to predict the amount of axial movement a fixator will produce at the fracture site as too much or too little can inhibit healing (Gaston and Simpson, 2007, Kenwright and Gardner, 1998). In the fixation literature, 'stiffness' can have a variety of meanings; the vast majority of studies use stiffness to denote the ratio of applied load to displacement at a chosen location. Clearly, the location at which displacement is being monitored can considerably influence the value of stiffness. In this chapter, the term 'axial stiffness' will be used to imply actuator displacement, whereas the 'gap stiffness' will use the maximal fracture gap closure. Stiffness is useful for comparisons between studies because comparing the interfragmentary movement (IFM) alone does not take into account the level of loading. A careful survey of the literature indicates that the range of values of stiffness reported in the literature vary by three orders of magnitude for locking plates (Stoffel et al., 2003, Hoffmeier et al., 2011, Ahmad et al., 2007, Bottlang et al., 2009b,

Uhl et al., 2008, Filipowicz et al., 2009, Fitzpatrick et al., 2009, Bae et al., 2011, Dobele et al., 2010, Hogel et al., 2012, Strauss et al., 2007, Duda et al., 2002, Schmidt et al., 2013, Chao et al., 2013, Liang et al., 2012, Yánez et al., 2012, Assari et al., 2013, Gardner et al., 2010, Wähnert et al., 2011). Studies by Bottlang et al. (2009b), Fitzpatrick et al. (2009), Gardner et al. (2010) and Assari et al. (2013) represent values at the upper end of the predictions at over 1000N/mm; studies with stiffness predictions less than 100N/mm include: Stoffel et al. (2003), Dobele et al. (2010) Hoffmeier et al. (2011) and Schmidt et al. (2013). Several factors have been shown to influence the IFM produced by a locking plate: the material properties (Kim et al., 2010, Fouad, 2010) and geometry of the plate and screws, the bone-plate off-set (Ahmad et al., 2007) and the position of screws within the plate (Stoffel et al., 2003). In studies using similar loading regimes, but different implant materials and geometries, the range of stiffness values found was considerable, but generally contained within a single order of magnitude (Schmidt et al., 2013, Stoffel et al., 2003, Uhl et al., 2008, Hogel et al., 2012, Hoffmeier et al., 2011, Dobele et al., 2010). The wide variation of stiffness values presented in the literature, therefore, cannot be readily explained solely on the basis of studies' differing materials and geometries. The impact that the choice of boundary condition has in such situations has not been previously discussed, yet studies continue to use inconsistent boundary conditions. This chapter used experimental models of the bone-plate system to examine the influence that the method of load application has on the IFM produced.

5.1.1 Chapter Aim

This chapter aimed to evaluate how the choice of loading condition influences the prediction of IFM in an experimental locked plating model.

5.2 Methods

Fourth generation large composite sawbones tibias were implanted with Stryker AxSOS 5.0mm Narrow and Broad steel locking plates (Figure 5.1). There were four specimens in total: two were fitted with narrow plates and two with broad plates. The plates were fitted by an orthopaedic surgeon and off-set 2mm from the bone. A 10mm osteotomy of the diaphysis was created (Uhl et al., 2008, Krishna et al., 2008, Schmidt et al., 2013). The specimens were 405mm long with an outer bone width at the fracture site of 28mm (Figure 5.1e). The cortical thickness at the fracture zone was approximately 5mm. The locking screw dimensions were 5.0mm external and 4.3mm core diameter. The drill bit used was the same size as the internal diameter as recommended by the manufacturer. Threads had depth of 0.7mm and a spacing of 1.2mm.

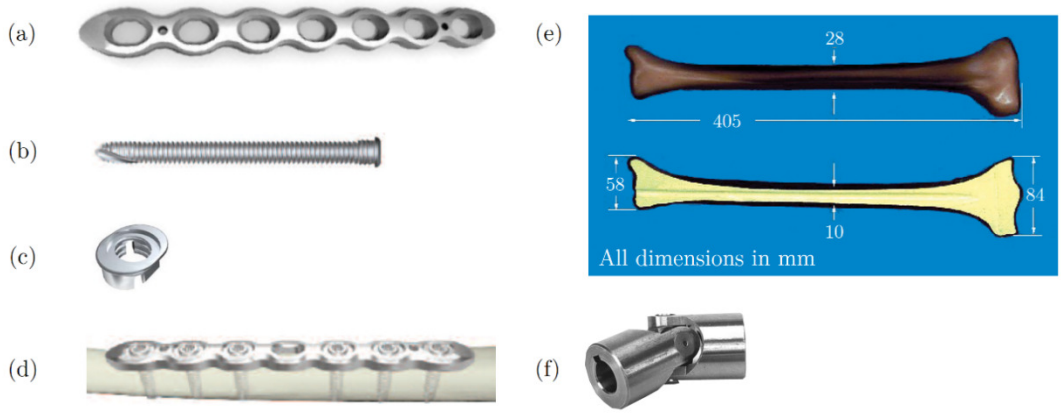

Figure 5.1 – Consumables used in the study showing (a) a Stryker AxSOS basic fragment plate; (b) a 5.0mm locking screw; (c) a locking insert; (d) the full assembly into host bone; (e) a large fourth-generation sawbones tibia with key dimensions; and (f) the universal joints used. Images are taken from Stryker AxSoS basic fragment brochure[4], Sawbones.com[5] and RS-online.com[6].

[4]www.osteosynthesis.stryker.com/medias/pdf/982295_Rev_4_AxSOS_Straight_Plate_Optech.pdf
[5] www.sawbones.com/products
[6] uk.rs-online.com/web/p/universal-joints/4924045/

Four loading conditions that have been previously used were examined as shown in Figure 5.2a-d:

(a) *Clamped Proximally-Clamped Distally*—where both ends of the bone are restrained against rotation (Figure 5.2a) (Ahmad et al., Yanez et al., Liang et al, Filipowitz et al. and Strauss et al.).

(b) *Clamped Proximally-Pinned Distally*—where the proximal tibia is restrained against rotation and the ankle is free to rotate (Figure 5.2b) (Bottlang et al., Fitzpatrick et al, Gardner et al., Bae et al., Chao et al.).

(c) *Pinned Proximally-Pinned Distally*—where both ends of the bone are free to rotate (Figure 5.2c) (Stoffel et al, Hoffmeier et al., Schmidt et al., Hogel et al., Dobele et al., Uhl et al., Duda et al. and Wahnert et al.).

(d) *Hinged Proximally-Pinned Distally*—medial and lateral condylar restraint was provided permitting rotation in the sagittal plane proximally and free to rotate distally (Figure 5.2d) (Assari et al.).

In all load cases lateral translation was restrained at both bone ends.

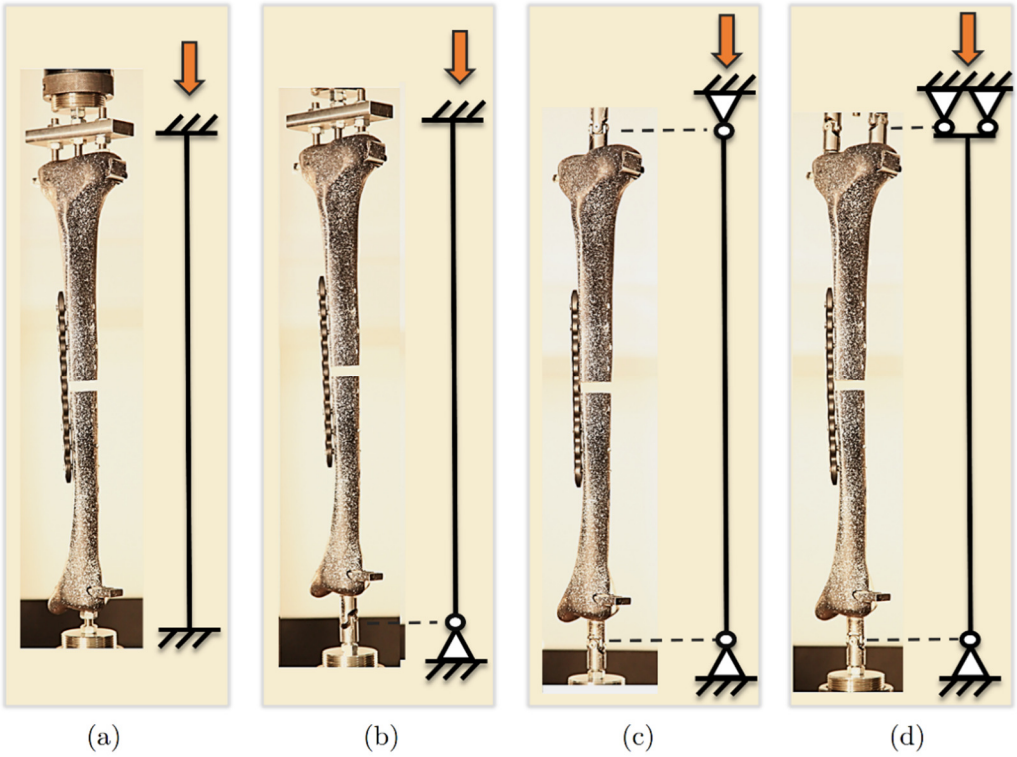

Figure 5.2 - Experimental test set-up showing the four loading conditions tested and the speckled pattern used for DIC.

While many studies examine idealised bone models such as cylinders (Bottlang et al., 2009b, Dobele et al., 2010, Yánez et al., 2012, Uhl et al., 2008, Fitzpatrick et al., 2009, Stoffel et al., 2003), the reason for modelling the whole tibia was to situate the boundary conditions at the relevant anatomical locations; the bone length was found to alter the stiffness prediction in the analytical model in Chapter 4. Moreover, the IFM predictions were also found to be dependent upon the transverse width of the fracture site. For the clamped conditions, (a) and (b), the bone was bolted (using M8 bolts) to 8mm thick steel plates slotted through the metaphases. In loading conditions (b), (c) and (d) universal joints were used to allow free rotation (Figure 5.1f). The universal joints used were 40mm long and positioned so that the centre of rotation was 20mm from the articular surfaces of the tibia (representing the centre of the femoral condyles and the tibiotalor joint) thereby making the effective length of the specimens 445mm. The

universal joints had a nominal peak torque capacity of 10Nm (RS, 2003). Using the outer dimension of 16mm, the maximum permissible load on each side of the joint was calculated to be approximately 625N.

Three sets of experiments were conducted for each loading condition using symmetrical screw configurations; these are summarised in Figure 5.3. In all cases the central hole above the fracture site was left empty. The configuration numbers relate to the filled screw holes counting outwards from the centre of the plate. In configuration C1234 screws were placed in all plate holes other than the single central hole directly above the fracture site; configuration C234 had the two screw holes closest to the fracture site empty; and in configuration C34 screws were only placed in the last two holes on either end of the plate. In order to re-use samples screws were incrementally removed to test all configurations. The influence of the residual screw holes under the working length portion of the plate was considered to be negligible as this part of the bone is not transmitting any load.

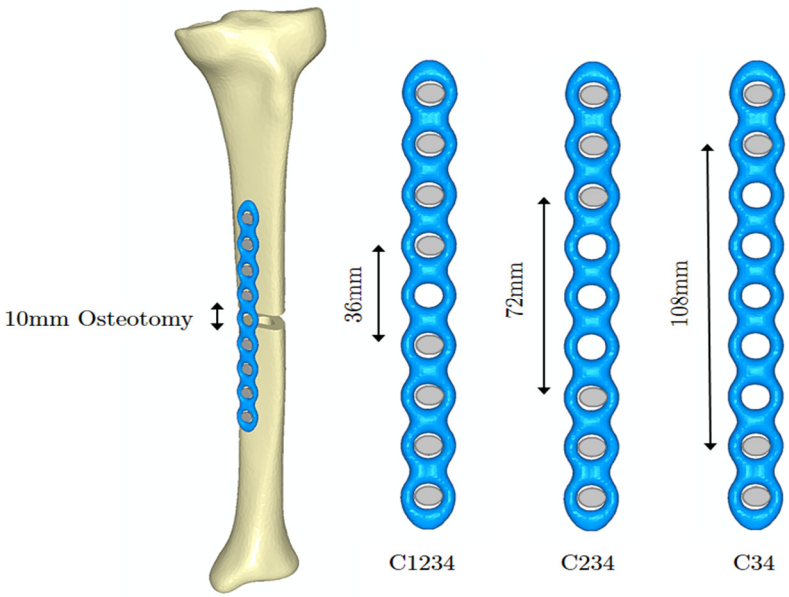

Figure 5.3 – Depiction of the implanted sawbones tibia with 10mm osteotomy and the three screw configurations tested showing the working length of each.

In all cases the displacement controlled load was applied proximally and quasi-statically using a loading rate of approximately 5N/s using an Instron 4505 (Instron, Norwood, MA, USA). Load-displacement data were recorded at the load actuator. Loading was stopped once the actuator displacement went beyond 1mm or the load above 200N. This was to ensure that the test did not cause failure of the plate; using the analytical model (to be discussed in Chapter 7) initiation of yielding of the plate was predicted at around 250N for the largest working length.

The study used digital image correlation to assess the motion at different locations across the fracture site. The IFM was calculated as the net closure of the fracture site at the far cortex. The cameras used were Canon 5D EOS mark ii 21.1 megapixel. The digital image correlation software used was a matlab module called GeoPIV[7]. The sensitivity of the set-up was tested using a rigid body motion test where the entire specimen was displaced by controlled amounts in the axial direction (the displacement in the transverse direction is zero). The absolute error in the transverse direction was below 0.001mm for all levels of motion; in the axial direction the largest error was found to be around 0.045mm (Figure 5.4). This is 0.0093% of the total length of the photo (~485mm) gives an accuracy of 0.52 pixels.

[7] White DJ, Take WA & Bolton MD (2003) Geotechnique 53(7):619-631

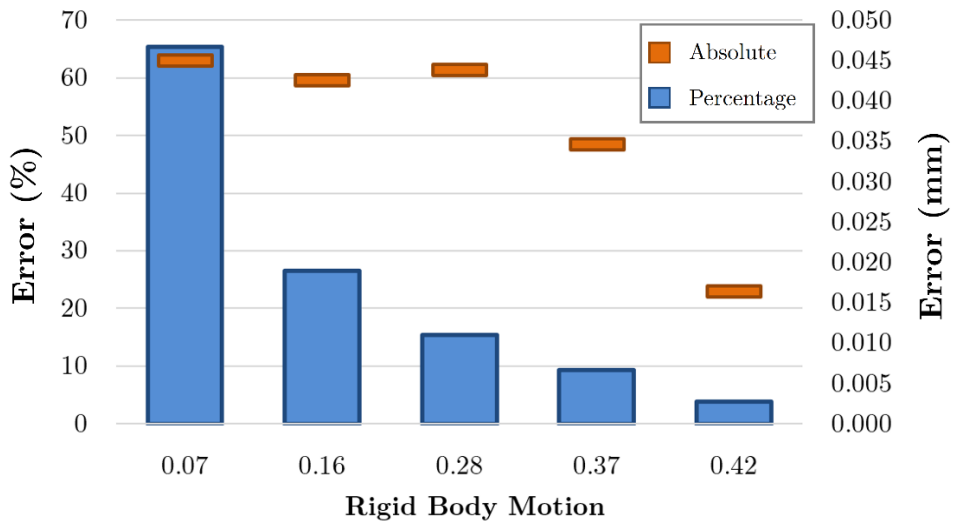

Figure 5.4 - Measured errors in the axial direction from a rigid body motion test

5.3 Results

The load-deformation response for each of the loading conditions using screw configuration C34 is shown in Figure 5.5. The IFM at the near and far cortices and the loading actuator displacement are plotted. IFM was defined as the difference in motion between proximal and distal fragments. Interestingly, the most rigid loading condition, (a), shows linear load-deformation behavior, whereas the more flexible conditions produce a geometrically non-linear response. It can be seen that the near cortex motion for loading condition (c) becomes greater than the far cortex motion in condition (a) and (b) at loads of approximately 100N.

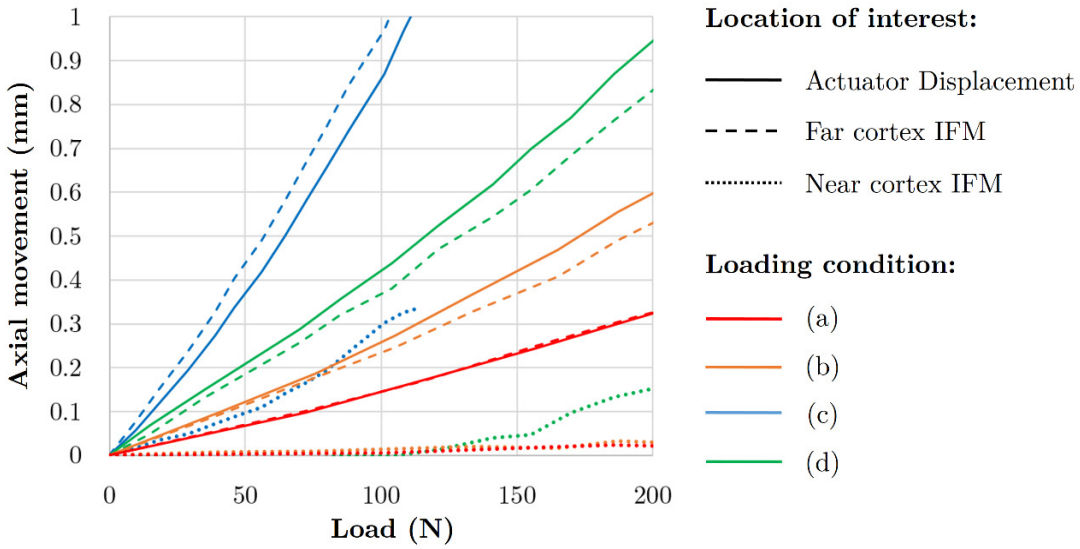

Figure 5.5 – Load-displacement data measured at different locations within the specimen for the different loading conditions. The data is for screw configuration C34.

The experimentally measured range of fracture gap motion (axial and transverse) for each loading condition is shown in Figure 5.6 (narrow plates) and Figure 5.7 (broad plates). Net transverse motion at the fracture site was defined as the difference between locations of maximum and minimum motion. The lowest value for each loading

condition uses the far cortex IFM produced using screw configuration C1234; the intermediate value is with C234; and the highest is with C34.

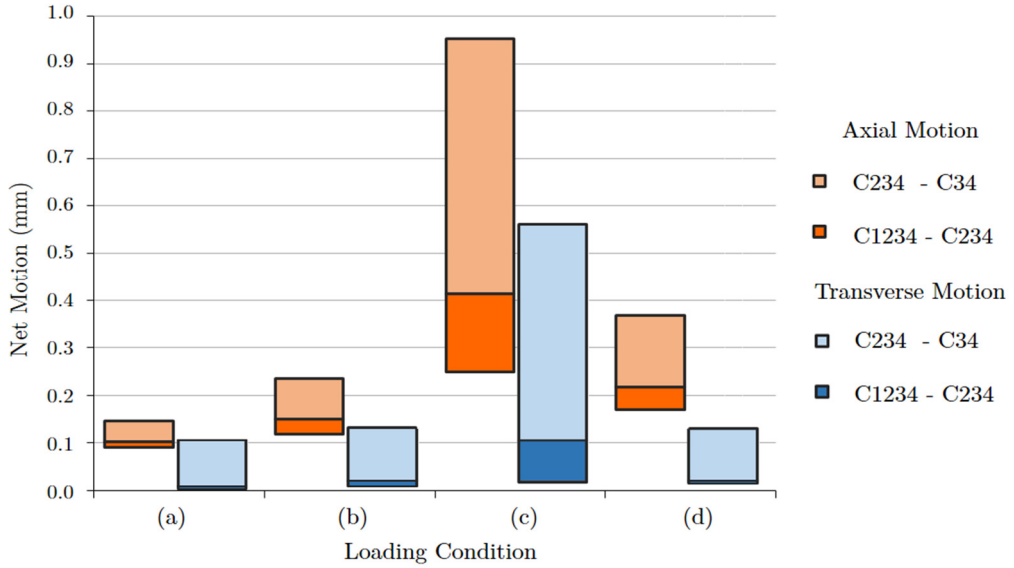

Figure 5.6 - Axial and transverse fracture gap motion measured at the far cortex for the four loading conditions using the narrow plates at a load of 100N

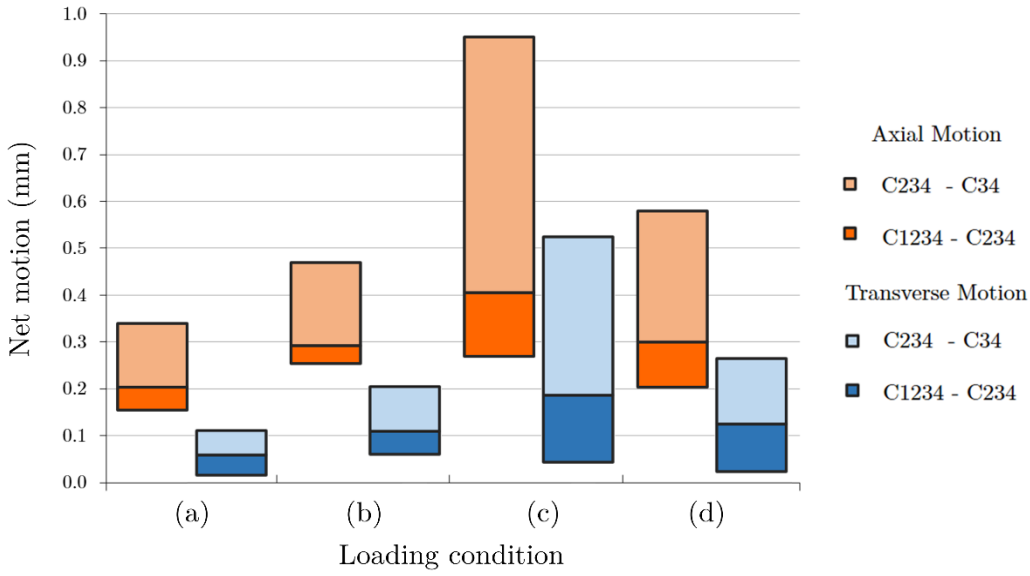

Figure 5.7 - Axial and transverse fracture gap motion measured at the far cortex for the four loading conditions using the broad plates at a load of 200N

Gap stiffness was calculated for the narrow plates using the fracture gap motions for the narrow plate shown in Figure 5.6. The stiffness predictions for the various loading conditions was compared with previous studies and are shown in Figure 5.8 (Stoffel et al., 2003, Hoffmeier et al., 2011, Ahmad et al., 2007, Bottlang et al., 2009b, Uhl et al., 2008, Filipowicz et al., 2009, Fitzpatrick et al., 2009, Bae et al., 2011, Dobele et al., 2010, Hogel et al., 2012, Strauss et al., 2007, Duda et al., 2002, Schmidt et al., 2013, Chao et al., 2013, Liang et al., 2012, Yánez et al., 2012, Assari et al., 2013, Gardner et al., 2010, Wähnert et al., 2011). The last four bars correspond to the four loading conditions used in the present study and have the upper value of stiffness evaluated from screw configuration C1234 and the lower value derived from C34 (i.e. the extreme values from Figure 5.6).

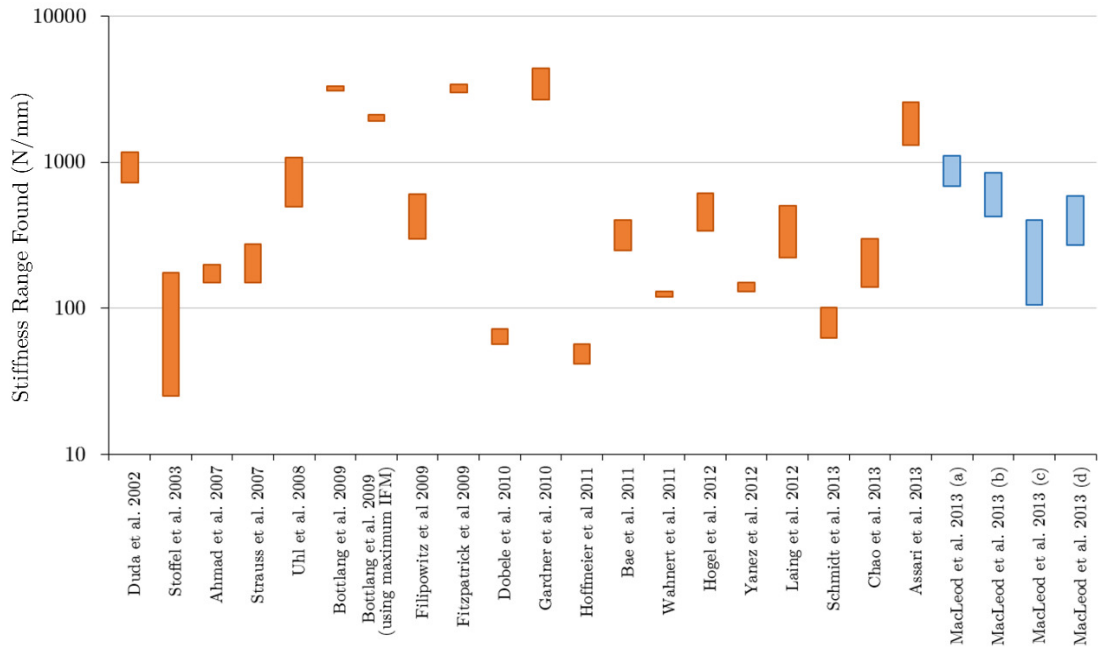

Figure 5.8 - Gap stiffness (or axial stiffness if not available) predictions of previous LCP studies and the present study

Additional screw configurations C124, C134 and C14 were tested for both narrow and broad plates for loading conditions (a) and (c). The bones were re-used for these additional tests; however, screws were only ever re-inserted once into the same screw

hole. The values of axial stiffness (using actuator displacement) for all screw configurations tested are shown in Figure 5.9. As the axial stiffness changes rapidly with applied load, the initial value of stiffness was used in these comparisons. The initial values of stiffness also had the best correlation with the predictions of the analytical model in Chapter 7; this was found to be due to local subsidence around the universal joints (Chapter 6). The results show the influence that the loading condition has regarding the plate type, number of screws and working length. When using loading condition (a), the use of a broad plate increased axial stiffness predictions by an average of 7.9% compared with the narrow plate; using loading condition (c) the stiffness values increased by 58%. Loading condition (a) also had a slightly stronger correlation between the total number of screws used and stiffness (r^2=0.67 vs. r^2=0.53); whereas loading condition (c) had a much stronger correlation between the working length and the stiffness (r^2=0.82 vs. r^2=0.11).

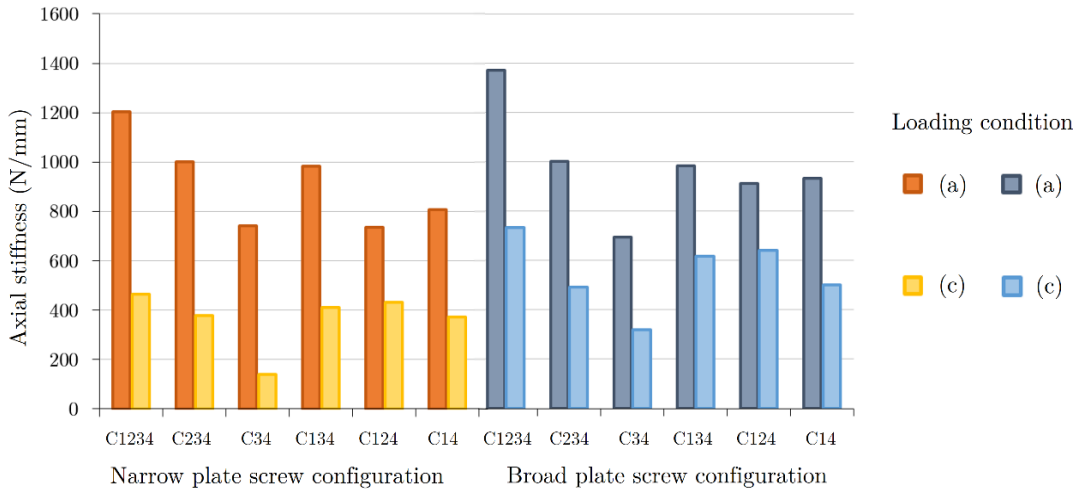

Figure 5.9 - Axial stiffness for different screw configurations

5.4 Discussion

Experimental biomechanical models are frequently used for prediction of IFM produced by fracture fixation devices. This study has shown that the method of load application has a profound effect on the IFM produced by locking plates; by changing only the

loading condition the prediction of gap stiffness was altered by over six and a half times (Figure 5.6). The choice of loading condition had the largest impact on the screw configurations with larger working lengths, indicating that more flexible systems are most affected. The loading condition can also substantially change the relative importance of working length. Considering axial motion, condition (c) is most sensitive to changes in working length while conditions (a) and (b) are relatively insensitive (Figure 5.6 and Figure 5.7). The transverse motion is similar for all loading conditions except condition (c), which has increased movement due to lack of rotational restraint.

The *clamped* approach (Figure 5.8a) produces the highest gap stiffness due to predominantly axial deformation of the plate. The *pinned* approach, on the other hand, (Figure 5.8c) produces the smallest gap stiffness due to bending of the plate. Each of the loading conditions examined in this study have been used in previous studies. The lowest stiffness values predicted (Stoffel et al., 2003, Hoffmeier et al., 2011, Dobele et al., 2010) all appear to have used the *pinned* loading condition (c) whereas the highest values predicted (Bottlang et al., 2009b, Bottlang et al., 2010a, Fitzpatrick et al., 2009, Kim et al., 2010) have used one of the *clamped* conditions—(a) or (b). The deformation response of condition (b) is very similar to that of condition (a) as both have almost zero near cortex motion (Figure 5.5a and b). This shows that the *clamped* boundary condition dominates the behaviour. Bottlang et al. (2010a, 2009b) used an average value of IFM for their stiffness prediction but also provided the maximum value; using the maximum value reduces their axial stiffness prediction by approximately 40% but it still remains much larger than the majority of the studies (Figure 5.8). Condition (d) – *hinge proximally – pinned distally* provides stiffness values in between the extremes represented by the other loading conditions (Figure 5.8d). While the studies considered in Figure 5.8 are not directly comparable, the difference in stiffness quoted varies by three orders of magnitude—much larger than would be expected from varying material properties and geometries alone.

Although the use of fully restrained boundary conditions in biomechanical systems has been criticised previously in the literature (Phillips, 2009, Speirs et al., 2007, Polgar et al., 2003) many studies continue to use them in fracture fixation modelling, often, when an idealised bone is used (Bottlang et al., 2009b, Fitzpatrick et al., 2009, Gardner et al., 2010, Yánez et al., 2012). In a study of various unilateral fixators, Epari et al. (2007) found that fixators which had moderate axial stiffness (2000N/mm) and high shear stiffness (500N/mm) produced the best healing outcomes in terms of residual torsional stiffness. These values are at the upper end of the stiffness range presented in the literature and must be taken in the context of the loading condition used to evaluate them; both ends of the bones were potted in polymethylmethacrylate clearly representing a clamped condition. In locked plating, the use of a clamped condition restricts plate bending and therefore cannot be used for predictions of fracture gap motion. This is because the IFM produced is largely determined by how much restraint is provided by the clamp. Some studies have used a clamped condition comparing far-cortical locking or slotted locking plates against standard locking plates (Bottlang et al., 2009b, Fitzpatrick et al., 2009, Gardner et al., 2010). In these studies the plate bending will be restricted and will exaggerate the differences in IFM found between the types of screw tested (to be discussed further in Chapter 9).

This study used a hinged condition similar to Assari et al. (2013) where the hinge axis is coincident with the centres of the femoral condyles (Morrison, 1970, Smidt, 1973). Unfortunately, the hinged condition suffers from the same major limitation as the clamped conditions; the restraint can never be truly encastre and therefore the observed IFM is largely a result of how much motion the restraint condition allows. Moreover, the stiffness prediction will depend on the angle of the plate relative to the hinge axis. The *pinned proximally-pinned distally* loading condition, (c), is the only condition tested which is not influenced by the rigidity of the rotational restraint, and can therefore provide results which can be compared meaningfully with other studies.

It is recommended that the *pinned proximally-pinned distally* loading condition should be used for in vitro testing of tibias under axial loading. The use of this loading condition is advocated primarily for reproducibility and meaningful comparisons between studies. In the subsequent chapter, however, there is some discussion as to why this loading conditions is also more physiological (Section 6.4.4). This loading condition also allows for bending moments to be incorporated by eccentric positioning of the loading joints, something which studies are already beginning to incorporate (Hogel et al., 2012, Schmidt et al., 2013, Gaebler et al., 2001).

5.5 Limitations

Applied to the present study, the analytical model developed in Chapter 7 predicted much smaller axial stiffness than gap stiffness (around 40% lower). The experimentally measured values of the two stiffnesses, however, were very similar. This increased actuator displacement was attributed to deformation around the slot in the metaphysis created for the steel plate and bolted connection. This cavity may have allowed subsidence and increased actuator displacement. Subsequent finite element simulations confirmed that this region of reduced stiffness would increase actuator motions while having minimal impact on IFM (discussed in Chapter 6).

Gradual loosening of the screws may have occurred as bones and screw holes were re-used for testing different loading conditions and different configurations. A screw was only ever re-inserted once and the fourth screw was never extracted. The testing order was C1234, C234, C34, C134, C124 and C14. Although the sample size was small the results are as expected (increased working length increased fracture gap motions) and the values of stiffness are within those reported by the literature. The results also closely match the analytical predictions made using the model developed in Chapter 7.

During the testing it became clear that the tightness of the fittings could also influence the results. Over-tightening can cause fracture of the bone and so the tightness of the

connection is limited and can never approach 'ideally rigid'. Compared with pinned end conditions, clamped end conditions greatly reduced rotation at the ends of the specimen, but movement was still visible from DIC imaging. Therefore, if tighter clamps or a different method of restraint were used, much greater differences in axial stiffness and IFM could be observed.

The resolution of the digital image correlation could have been much improved if the region monitored had been reduced to the fracture site only.

5.6 Conclusions

- The loading condition was found to greatly influence the predicted stiffness of locked plating systems.

- Loading conditions change the relative importance of screw positioning variables. Working length is the primary determinant of axial stiffness when using flexible load application; the number of screws is more important when using rigid load application.

- It is recommended that, for axial load tests of tibias, future studies should use loading condition (c) for reproducibility and meaningful comparisons with other studies.

6

Modelling Loading Conditions in LCP fixation

6.1 Introduction

This chapter develops finite element models based on the experimental models in chapter 5. The importance of the loading conditions in biomechanical modelling is well known. Many studies show dramatic differences depending on the extent of muscle inclusion on strain within the bone (Duda et al., 1998, Phillips, 2009, Phillips et al., 2007, Polgar et al., 2003, Taylor et al., 1996, Viceconti et al., 2003, Helwig et al., 2013, Pankaj, 2013) and therefore remodelling predictions (Bitsakos et al., 2005, Kerner et al., 1999). Some of the studies note the detrimental influence of fixed boundary conditions in finite element models (Polgar et al., 2003, Phillips, 2009, Phillips et al., 2007).

Although computer simulations can include multiple bones and muscle forces, for practical reasons, experimental models almost exclusively test a single bone in isolation without muscle forces. This reduces the complexity of the model; however, assumptions must be made as to how it is held in position. Strategies employed in previous studies for restraining long bones include:

- ‘Fixed’ boundary conditions where a large number of nodes (3 or more) of the same region are restrained against motion in 1 or more directions. This results in rotational movements being restrained at the ‘fixed boundary’. In experiments, ‘potting’ of samples in clay or clamps are both fixed boundaries despite the clay being softer.
- Restraining a single node on the surface of the bone, preventing translation in selected directions (axial or transverse) while permitting rotation. At least three nodes must be restrained in the model with a total of six degrees of freedom to maintain a stable structure.

In cases where ‘balanced’ muscle forces are used restrained nodes are still necessary to prevent rigid body motion.

While it is obvious that ‘fixed’ boundaries are unrealistic, restraining the cortex at a single location does not represent the in vivo situation either (Phillips, 2009). The ‘free’ boundary condition presented by Phillips required a hip and knee structure to be modelled in addition to the femur. These acted to restrain the joint surfaces through contacting surfaces, albeit in a less direct manner than direct nodal restraint. The ‘improved’ case used by Speirs et al. (2007) used a single reaction node on the surface of the bone. This is a practical and convenient assumption; however, it ignores the anatomical situation of the bone presenting two problems:

- The joint is forced to rotate about the restrained node on the articular surface. In reality, the femoral head rotates within the acetabulum and the femoral condyles within the tibial tray. The centre of rotation of both of these joints lies within the femur. Likewise, at the knee, the tibia rotates around the same location within the femoral condyles.
- It ignores the bi-condylar restraint provided by the knee.

Many of the studies discussed considered an intact bone, however, biomechanical models are frequently used to assess the performance of fixation devices in the presence of a defect or implant (Duda et al., 2002, Chen et al., 2013, Salas et al., 2011b, Moazen et al., 2013). Extramedullary devices, such as locking plates, are placed under eccentric loading being located some distance from the dominant loading axis, which makes them sensitive to changes in loading. In the previous chapter it was demonstrated that the loading condition can dramatically alter experimental predictions of motion and stiffness when using these devices; it is therefore also likely that the strains within the bone and the stresses within the implant will be affected by the choice of loading condition. This study examines the most commonly employed boundary conditions in previous experimental and computational models. In particular, their impact on the strain distribution within the bone and the stress within the implant is assessed in the context of locked plate fixators.

6.1.1 Chapter Aim

This chapter aimed to evaluate the influence of different boundary conditions used in computer simulation and the impact each has on predictions of strain within the bone and stress levels within the implant. The four boundary conditions (a-d) examined in Chapter 5 were considered. The chapter also addresses some finite element issues relating to realistic modelling of the bone-implant system, which can considerably influence the load-deformation predictions.

6.2 Methods

6.2.1 Geometry

A three-dimensional finite element model was developed based on previous studies conducted by the authors (Figure 6.1) (MacLeod et al., 2012). The geometry of the tibia and plates (section 5.2) were obtained using a desktop 3D laser scanner (NextEngine, Inc., Santa Monica, CA, USA). The screw was drawn using computer aided drawing

software in Abaqus 6.10 (Simulia, Providence, RI, USA) and the dimensions are detailed in section 5.2. The outer surface of the scanned tibia (Figure 6.1a) was off-set to produce a unicortical thickness of 5mm (Figure 6.1c). As the simulated fracture was in the tibial diaphysis (Duda et al., 2002) screw anchorage is provided by cortical bone; as such, only the cortical bone was included in the models (Figure 6.1c) (Donaldson et al., 2012b). Similar to previous studies, the fibula was ignored as it transmits between 6.4-16.7% of the load transmitted in the lower leg and is often fractured along with the tibia (Takebe et al., 1984).

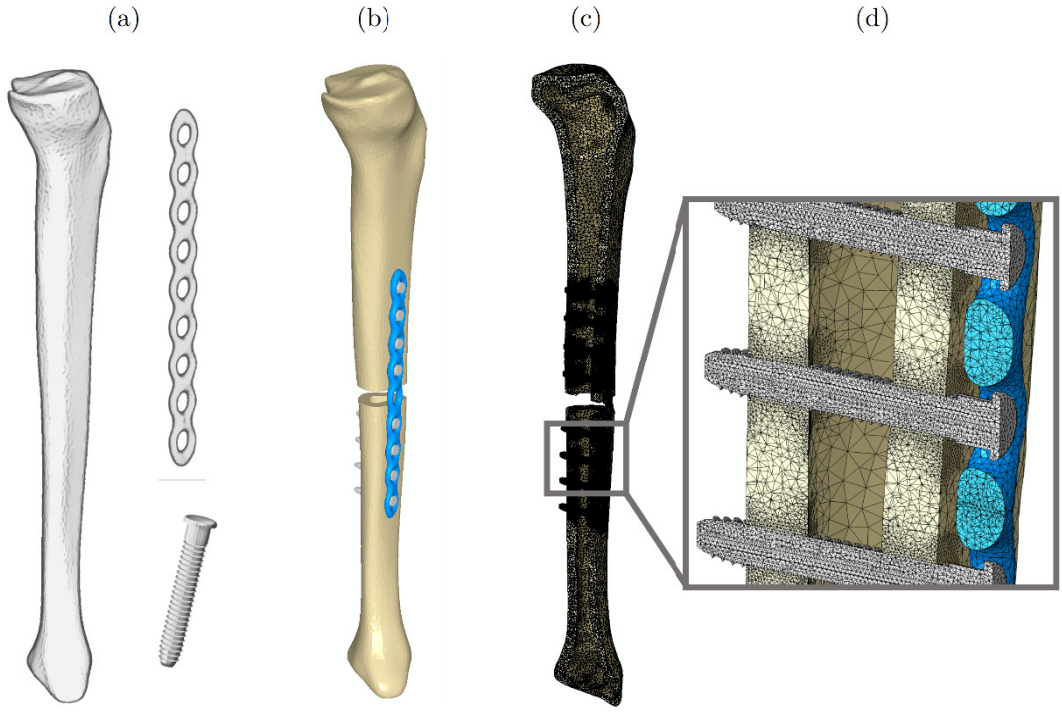

Figure 6.1 - Development of the finite element model showing (a) the scanned 3D geometry of tibia, narrow locking plate and screw; (b) the virtually implanted tibia with 10mm osteotomy full assembly; (c) a sectional view of the mesh used; and (d) the local mesh around the threads of the screws

6.2.2 Boundary Conditions

In this chapter the experiments described in Chapter 5 were examined using finite element simulation. The four loading conditions and their finite element implementation are outlined in Figure 6.2. It was essential to validate the implanted case (as opposed to the intact case only) as there are many more aspects which require modelling attention; the non-linear contact interactions between the screw and the bone; interactions between the screw and the plate; and the non-linear geometrical changes which occur during large-scale deformation. Moreover, the loading conditions are likely to have greater influence when testing implanted orthopaedic devices as the bone-fixator system is more flexible than the intact bone.

As well as fixed boundary conditions (Figure 6.2a and b), joints which allowed rotation in three degrees of freedom (Figure 6.2c) and a single degree of freedom (Figure 6.2d) were considered. Joint rotations were implemented by constraining the articular surfaces to a single point in space considered to be the centre of the joint (Figure 6.2b-d). This allowed the bone to be modelled in isolation while permitting motion across the entire articular surface. The effect of bi-condylar restraint was also incorporated using this method (Figure 6.2d).

In all cases the distal restraint allowed axial translation as the load was applied distally. The position of the joints and the loading axis were located as closely as possible to the experimental tests.

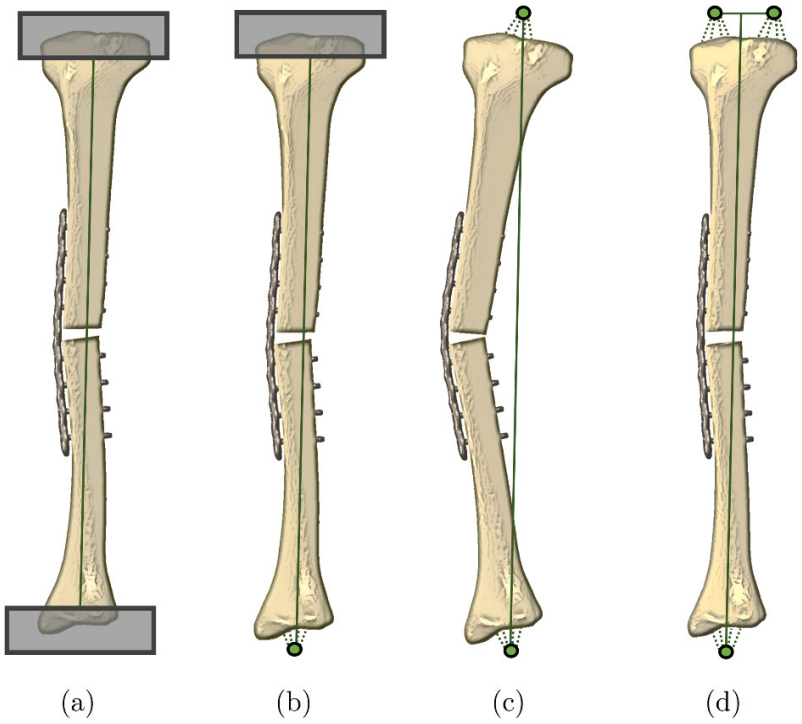

Figure 6.2 - Depiction of the loading conditions used in the study with (a) clamped proximally and distally; (b) clamped proximally and pinned distally; (c) pinned proximally and pinned distally; and (d) hinged proximally and pinned distally. Grey regions represent fully restrained regions and green dots are the centres of rotation of the joint and are restrained against translation only. The solid green line shows the loading axis the dashed green lines are constraints to the bone. Deformed shapes are exaggerated 40x, 40x, 4x, and 6x respectively.

6.2.3 Material Properties

The tensile and compressive moduli of the glass reinforced epoxy used in sawbones cortical bone was 16.7GPa and 16GPa respectively (from manufacturer's datasheet). An average value of 16.35GPa was adopted. The steel was assigned a Young's modulus of 205GPa. All materials were assumed to be homogeneous, isotropic and linear elastic and were assigned a Poisson's ratio of 0.3 (Oh et al., 2010, Ganesh et al., 2005, Duda et al., 2002).

6.2.4 **Contact Interactions**

6.2.4.1 Screw-Bone and Bone-Plate Interactions

The screw threads were modelled as idealised rings rather than helical—an approach that has been previously used (Figure 6.1a and d) (Donaldson et al., 2012a, MacLeod et al., 2012, Karunratanakul et al., 2010). The screw-bone interaction at the entrant cortex was modelled as frictional using a standard Coulomb frictional coefficient of 0.3 (Eser et al., 2010, Pessoa et al., 2010). As the majority of load is transferred at the screw holes on the entrant cortex the screw-bone interaction at the exit cortex was modelled as tied for analysis simplification. The screw-bone interface representation has been shown not to significantly influence the interfragmentary motion prediction but alter the strain around screw holes (MacLeod et al., 2012). As the stress-strain environment at the screw bone interface was of interest non-linear screw-bone interactions were used. No interaction between the plate and the bone was included in the computer models.

6.2.4.2 Development of Screw-Plate Interaction

To the authors knowledge, all previous studies have assumed the screw-plate interaction to be completely rigid and modelled using tie constraints in the manner shown in Figure 6.3a (Moazen et al., 2013, Kim et al., 2010, Arnone et al., 2013, Salas et al., 2011b, Chen et al., 2013). Therefore, initially, the threaded 'locking inserts' of the plate (Chapter 5, Figure 5.1c) were ignored in the FE model and the screws were assumed to be tied to the surrounding hole in the plate. Although this assumption had less influence in the clamped conditions, it increased the gap stiffness by around eight times in the pin-pin loading condition. This modelling error was also sensitive to the size of the region being tied together determined by the *allowable distance* parameter in the Abaqus constraints settings (Figure 6.3a). To avoid this, the screw-plate interaction was modelled using four spring elements around the screw head connecting to the plate (Figure 6.3b). A linear spring stiffness of approximately 10,000N/mm was derived using

experimental tests including cantilever screw bending (Figure 6.4) and simply supported bending of the plate (discussed later in section 6.4.7.3). Unfortunately, like other spring-based contact approaches, this constant does not have a physical meaning as it arises from the spring element configuration. Nevertheless, it is a straightforward representation of the screw-plate continuity that can be experimentally derived. The requirement for this approach was confirmed by the relative movement between the screw and the plate detected in the DIC analysis and is shown in the quiver plot (of selected locations) in Figure 6.4a. It is also supported by that fact that many previous experimental studies show similar global stiffness predictions for locking and unlocked screws (Yanez et al., 2010, Bottlang et al., 2010a), which suggests that locking screws do not contribute to the bending rigidity of the plate.

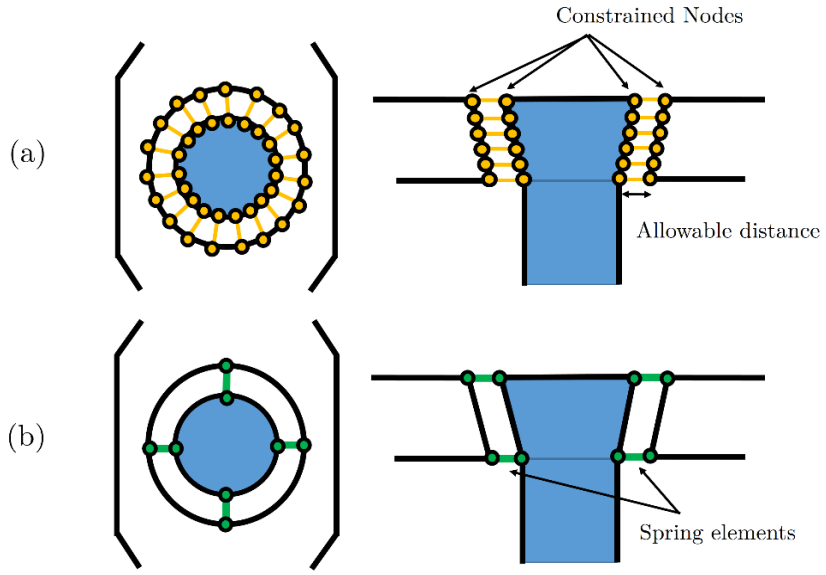

Figure 6.3 – Examples of screw-plate interactions showing (a) tie constraints and (b) spring elements

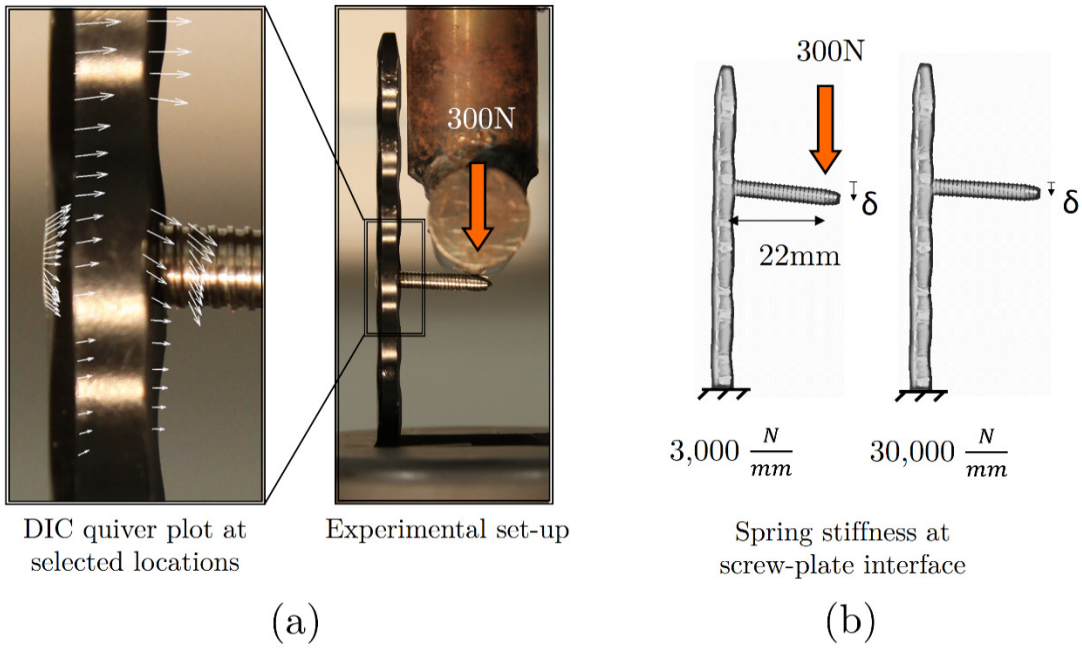

Figure 6.4 –Cantilever bending test used to evaluate the spring stiffness constant showing: (a) the experimental test and movement detected using digital image correlation (DIC); and (b) the finite element simulation using different values of spring stiffness at the screw-plate interface.

6.2.5 Meshing

The models used over one million linear and ninety thousand quadratic tetrahedral elements with refinement around screw holes. The element type and number for each region in the model are summarised in Table 6.1. Within the bone, the region around screw holes had an average element edge length of 0.3-0.4mm.

Table 6.1 – Number and order of elements used for each region of the model

Region	Number of elements	Element order
Bone	694,323	linear
Screw	39,125	linear
Plate	90,381	quadratic

6.2.6 Convergence

A mesh convergence study was performed and the results showed that doubling mesh density of the plate (quadratic elements) only increased the fracture gap motion by 0.3%. When the number of elements in the bone was increased to 1,200,385 (73% increase), the actuator displacement increased by 2.4% and fracture gap motion reduced by 1.3%. These small changes can be attributed to variations in local strains around the actuator caused by the differences in mesh. Similarly, change in peak minimum (and maximum) compressive strain was 3.0% (2.1%) around screw hole locations.

6.2.7 Loading

The finite element simulation was conducted up to 500N. This load was selected to cover the range of the experimental predictions in Chapter 4.1. The load was applied along the loading axis used in the experiment and this direction was maintained through the analysis (it did not follow nodal rotation).

6.2.8 Analyses

The three screw configurations used in Chapter 5 (Figure 5.3) were tested using the finite element models. The analyses were conducted using geometrical non-linearity using Abaqus 6.10 (Simulia, Providence, RI, USA).

The net axial movement at the fracture gap (IFM) was evaluated at the far cortex (furthest away from the plate) for each loading configuration and screw configuration. The movement was also recorded at the loading actuator.

6.3 Results

The load-deformation predictions of the finite element models were found to be similar to the experimental results in Chapter 5. The IFM at the far cortex was compared to the experimental tests using loading condition (c) for narrow (Figure 6.5a) and broad locking plates (Figure 6.5b). The maximum errors ranged from 1-16% for all cases except C234 for the narrow plate which was 25%.

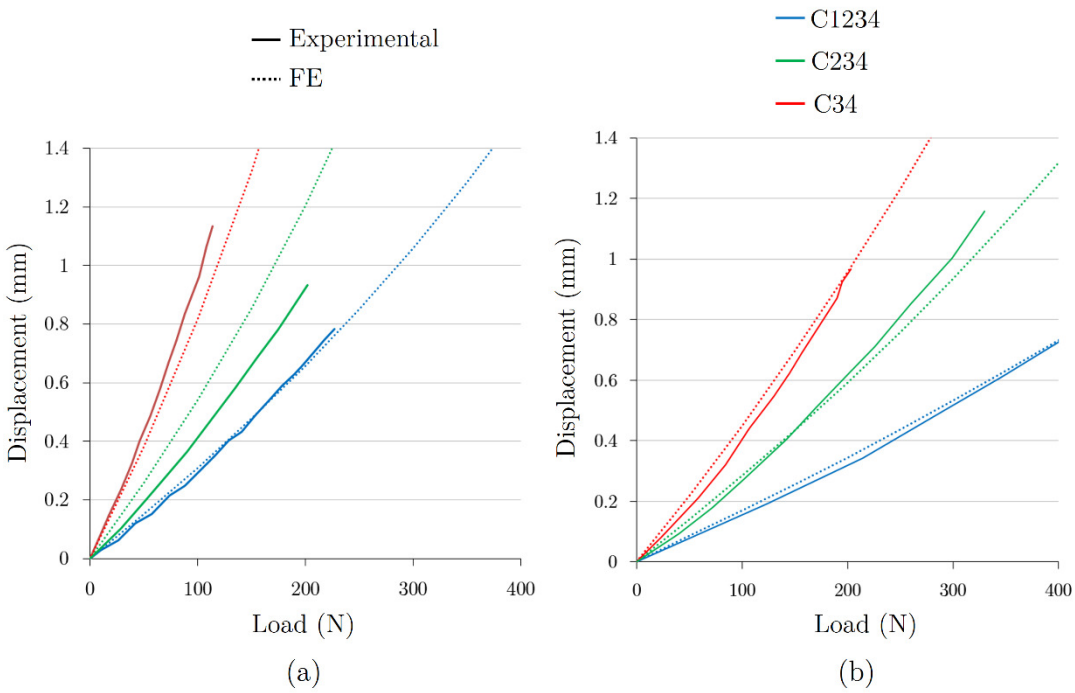

Figure 6.5 - IFM of the finite element models and the experimental tests from Chapter 5 for different screw configurations (C1234, C234 and C34) showing (a) the narrow locking plate and (b) the broad locking plate

While IFM predictions were similar to experimental tests, the predicted movement of the actuator was smaller in the finite element simulations. Figure 6.6 shows the actuator movement measured in the experimental test and predictions of the finite element.

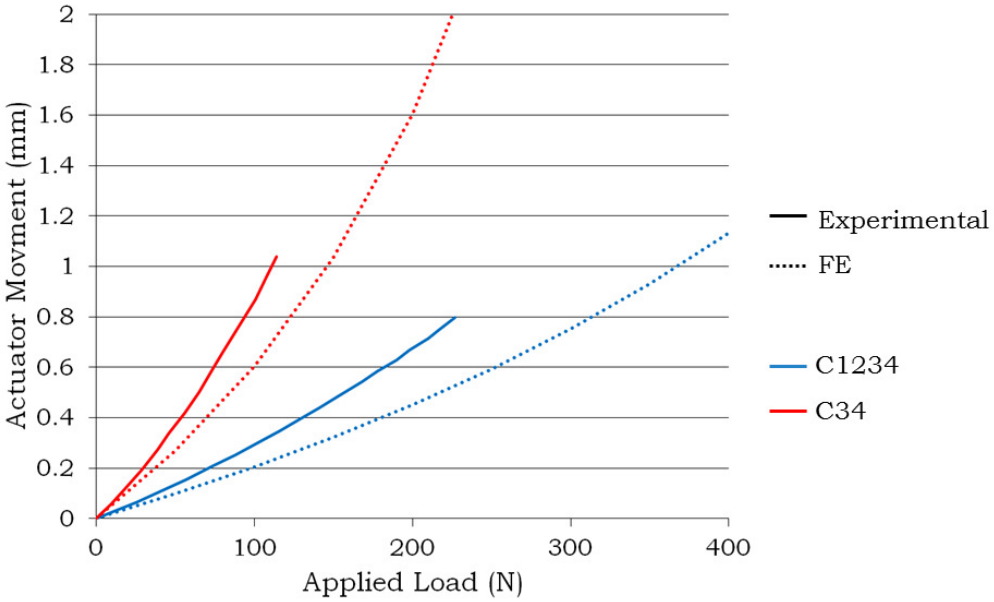

Figure 6.6 - Actuator motion predictions of the experimental, finite element and analytical models for screw configurations C1234 and C34 using the narrow locking plate

IFM was compared for the different loading conditions, plate types and screw configurations and is shown in Figure 6.7. Predictions of transverse motion showed similar trends to the axial predictions and have been included in Appendix B.1. The numerical clamped conditions produced much smaller motions than those of the experimental tests (Figure 6.7a and b). The motions produced by loading conditions (c) and (d) were much closer to the experimental results (Figure 6.7c and d).

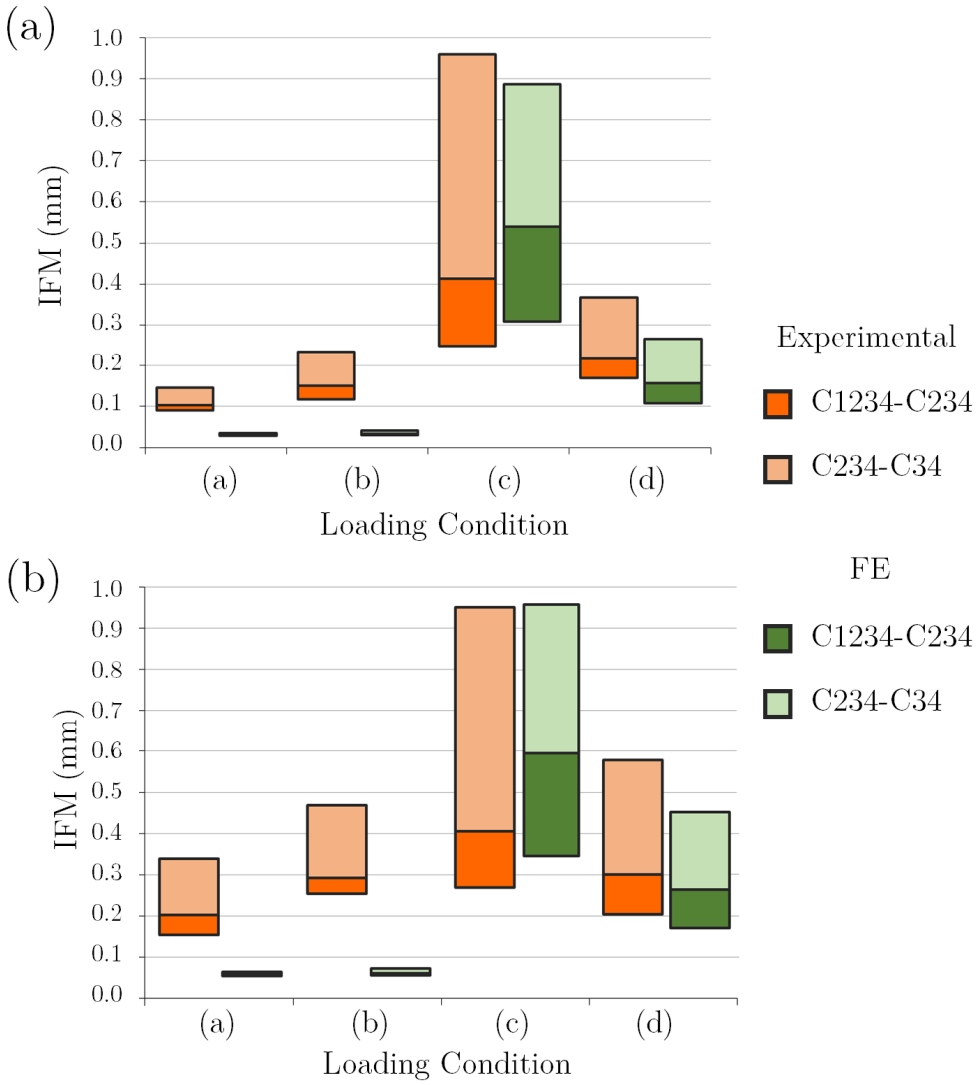

Figure 6.7 – IFM predictions of finite element models compared with the experimental tests in Chapter 5 for (a) the narrow plate at a load of 100N; and (b) the broad plate at a load of 200N. The influence of the different loading conditions (a-d) and screw positions (C1234, C234 and C34) is shown.

Minimum principal strain was plotted for the various loading scenarios on the surface of the bone underneath the plate (Figure 6.8). Minimum principal strain was chosen because compressive strains dominate within the bone under axial loading. It is now also recognised that bone yielding and failure is strain based (Pankaj and Donaldson, 2012) (rather than stress-based) and the yield strain is known to be approximately isotropic (Mercer et al., 2006, Ebacher et al., 2007). The plate and the screws removed from view and the limit of the scale has been set to 1000 microstrain or 0.1% strain to clearly illustrate the results. This value of strain is also considered to be the upper limit of physiological strain in the tibia during walking (Speirs et al., 2007, Duda et al., 2002, Chen et al., 2010a, Yang et al., 2011). It can be seen that the location of peak compressive strain for loading condition (a) and loading condition (b) is at the screw farthest from the fracture gap whereas for loading condition (c) it is the screw closest to the fracture gap. Loading condition (d) has high strains at screws both near and far from the fracture gap.

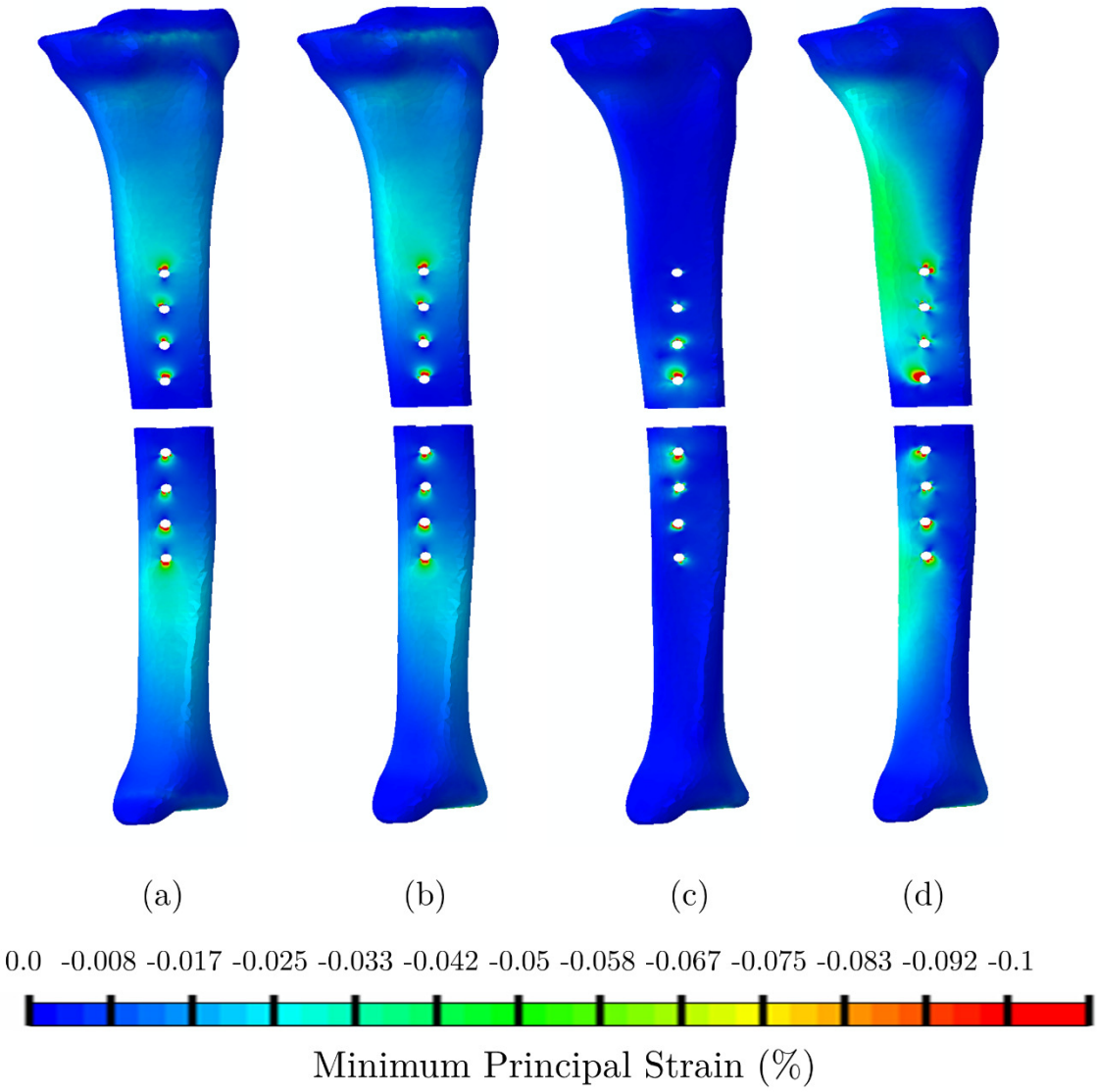

Figure 6.8 - Minimum principle strain in the bone for the different loading conditions (a-d) using the narrow locking plate with screw configuration C1234 at a load of 500N.

Von Mises stress was plotted for the screws and plate for each loading condition using screw configuration C1234 at a load of 500N (Figure 6.9). Loading condition (c) produces large regions with von Mises stress above 500MPa as the plate is free to bend. Loading conditions (a) and (b) result in much smaller plate stresses as it carries loads primarily in axial compression. Loading condition (d) results in bi-axial bending and has smaller regions of high stress compared with condition (c).

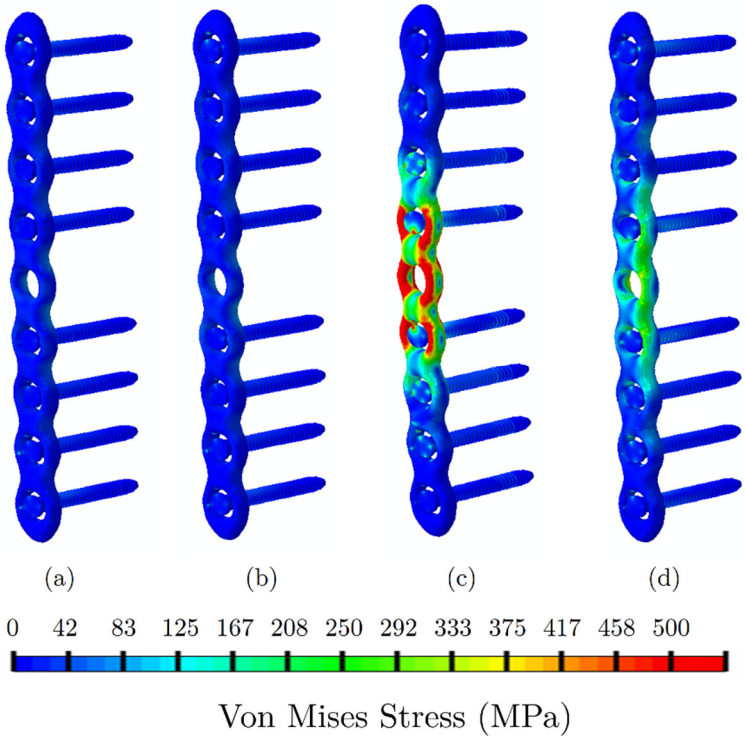

Figure 6.9 - Von Mises stress in the narrow locking plate and screws (C1234) for the different loading conditions (a-d) at a load of 500N.

6.4 Discussion

Biomechanical models are extensively used to predict differences in strength, stiffness and potential impact on the bone for different devices and device configurations. Some aspects of the bone-plate system have been shown to have a considerable influence on these parameters such as plate dimensions and material properties, working length, bone-plate off-set (Stoffel et al., 2003, Ahmad et al., 2007, Hoffmeier et al., 2011). In the previous chapter it was shown that the loading condition can considerably influence the IFM produced by the bone-plate system. Some aspects have been shown to have less influence. For example, Merino et al. (2013) showed that the orientation of screws does not significantly influence stiffness or load to failure. Bone properties and local bone failure do not significantly influence IFM predictions (Donaldson et al., 2012a). In Chapter 2 the choice of contact interaction was shown to have minimal influence in loading condition (c) but slightly more when using loading condition (a).

In this Chapter, the method of load application was found to greatly influence the strains within the bone and the stresses within the locking plate implant. Additionally, predictions of IFM are even more sensitive to the boundary conditions when using finite element simulation than in lab experiments.

6.4.1 Load-Deformation Response and IFM

Using loading condition (c), the predicted load-deformation response of the finite element models was similar to the experimental tests in Chapter 5 for three screw configurations and two types of plate (Figure 6.5). One exception to this was screw configuration C234 for the narrow plate. As the finite element model and the analytical model (discussed later in chapter 7) predictions of IFM are consistent, it is likely that the experimental value is wrong. The most likely cause of this increased stiffness in the experimental tests is unwanted bone-plate contact.

For all the loading conditions, the trends of IFM are consistent with the experimental findings; however, the clamped conditions produce much smaller motions numerically (Figure 6.7). In the previous chapter's experimental work, the choice of loading condition could increase the gap stiffness prediction by nearly 3 fold for the smallest working length; for the largest working length, this increase was over 6 times. In finite element simulations the observed differences can be even larger (as much as 24 fold) as the clamp is ideally rigid. In the experimental tests some motion was seen from the DIC imaging, which revealed that the clamp was not completely restraining movement. This finding highlights the sensitivity of the system to the tightness of the clamp. Studies which choose to use a clamped condition should, therefore, be aware that the rigidity of the clamp can be hugely influential.

The conclusions from Chapter 5 regarding the importance of working length and screw number are even more pronounced for the numerical results. This is to be expected as the encastre condition is much more difficult to enforce experimentally than numerically.

6.4.2 **Strain Environment within the Bone**

The peak strains within the bone around screw holes were found to be unique to the loading condition being used (Figure 6.8). Using loading condition (c) the largest strains were found at the screw closest to the fracture gap (Figure 6.8c). This is consistent with a recent study by Donaldson et al. (2012a) on unilateral fixators using similar loading conditions, which predicted highest degree of yielding and associated loosening at this location. A recent study by Bottlang et al. (2010a) predicted highest strains at the last screw when using loading condition (b) producing a pattern of strain as shown in Figure 6.8b. Loading condition (d) produces large strains both near and far from the fracture site. Away from screw hole locations, the largest strains within the bone occurred using loading condition (d), which used a hinged knee joint representation. Periprosthetic fractures are known to occur at the plate end (Leahy, 2010). It is likely that these fractures are caused by a reduction in bone quality—being located either in metaphseal

bone or an osteoporotic diaphysis, or due to an overly rigid plate. A simulation was run using a reduced Young's modulus of bone and this caused increased strain at the plate ends. Similarly, the broad plate resulted in larger end-of-plate strains than the narrow plate.

6.4.3 Stress Environment within the Implants

The differences in deformation behaviour result in radically different estimates stress within the implants. Loading condition (c) predicted plate stresses of over 500MPa; the peak stress in loading conditions (a) and (b) was around 50MPa as the plate is prevented from bending thus carrying predominantly axial stress. Condition (d) resulted in biaxial bending of the plate; this was because the plate was in a different plane to the rotation allowed at the knee.

6.4.4 Which Loading Condition is Most Realistic?

This chapter did not attempt to recreate an in vivo loading condition; it aims to inform those who are considering experimental or numerical bone tests on the importance of the loading condition when considering axial load tests of fractured bone-plate constructs. Nevertheless, these biomechanical tests of implants are used to predict in vivo performance. The results demonstrate that a loading condition using rigid restraint can be very sensitive to the rigidity of the connection or restraining body. These loading conditions predict unrealistically small IFM and plate stress and are therefore considered to be unphysiological. Loading condition (c) is similar to the 'improved' loading condition by Speirs et al. (2007) for the femur and used by Duda et al. (2002) for the tibia. In this chapter, rather than restraining nodes on the articular surfaces, the articular surfaces were constrained to a node considered to be the centre of the joint. This allowed the entire articular surface to rotate relative to the centre of the joint. Experiments and simulations using loading condition (c) can be compared against each other as there is no influence from artificial rotational restraint at the bone ends. In

loading condition (d) vertical restraint was defined at both condyles thereby producing a hinge. This was to imitate the condylar joint reactions at the knee and allow for medial-lateral load distribution to be predicted, as opposed to a single 'knee joint reaction'. A hinged loading condition using the centre of rotation of the joint was recently used in a study of a supracondylar femoral fracture by Assari et al. (2013). The justification for the use of a hinge is that the dominant rotation of the knee is in the stagittal plane; however, it is known to allow movement in all six degrees of freedom. Some studies have quoted rotations of up to ±6 degrees in the transverse plane although during mid-stance rotation does not exceed ±3 degrees (Scanlan et al., 2010, Halloran et al., 2005). Scanlan et al. (2010) and Li et al. (2009) also measured varus-valgus rotations of up to 4 degrees. Although the magnitude of the rotations are small, there can be a large lever arm due to the length of the bone making them significant. The hinge representation, loading condition (d), will therefore produce more rigid behaviour than the real knee, which has some additional freedom of movement that is not accounted for. Conversely, the stabilising influence of muscle wrapping, which could act to dampen motion produced, was neglected. Ideally, the inclusion of all muscles and appropriate joint reactions would reveal the true nature of the mechanical response but this is not straightforward to incorporate and the majority of experiments will continue to be conducted using simplified loading conditions so that the relevant bone can be tested in isolation. The allowable movement at the knee means that at smaller loads (where the allowable rotation has not been reached) loading condition (c) is likely to be most realistic; whereas at larger loads, the knee restraint could become significant and therefore loading condition (d) may be most appropriate. Similarly, the allowable movement permitted by the ankle would depend upon the direction and magnitude of the joint rotation. Although the pin condition allows unlimited rotation, it is unlikely that the loads involved in the immediately post-operative period would cause enough implant deformation to exceed the allowable movement at the joints. Additionally, the relative proportion of weight-bearing load transmitted by the device reduces as healing

progresses (Vijayakumar et al., 2006). Therefore, for the purposes of predicting fracture healing environment, the true in vivo condition is therefore likely to be much closer to loading condition (c) than loading condition (d).

6.4.5 Recommendation of Loading Condition

Predictions of stiffness, IFM, implant stress and strain within the bone are all substantially altered by the choice of loading condition, yet studies continue to use a wide range of loading and boundary conditions. Although it is possible that the hinge-pin loading condition (d) may be closer to the in vivo scenario at larger loads, the stiffness of the system is dependent on the angle of the plate relative to the hinge axis. This additional restraint limits the ability to make comparisons with other studies. Considering that the loads involved in the early stages of fracture healing are greatly reduced from full weight-bearing (Vijayakumar et al., 2006), the pin-pin condition is likely to produce the most realistic environment. For these reasons, in addition to its advantages in terms of reproducibility, the pinned loading condition is recommended for axial load tests of tibias. It should be noted that this loading condition is only relevant to axial loading; other loading types such as torsion or bending would require a different restraint conditions.

6.4.6 Limitations

This study has a few limitations. Material non-linearity was not included in the bone or the plate; however, the loading considered did not cause the metalwork to reach the yield stress or bone to reach yield strain. In addition, only short-term static loading was considered; for long-term predictions viscoelasticity or fatigue effects may play a role.

6.4.7 Modelling Discussion

Many modelling aspects were found to influence the model's ability to correctly predict motion. They are briefly discussed.

6.4.7.1 Bone Length & Positioning of the Joints

The universal joints were 40mm long with the pivot half way. This size was chosen to approximate the distance that the articular surface is away from the centre of the femoral condyles and the talus. As many of the studies considered in Chapter 5 had different lengths of test specimen the influence that bone length had on the motion prediction was investigated. The FE model using loading condition (c) was re-run positioning the end conditions closer to the fracture gap and constraining them to the shaft; a 42.6% reduction in bone length resulted in a 31% reduction in gap motion. In addition, positioning of the fracture closer to the end of the bone also altered IFM.

The results were also found to be sensitive to the transverse positioning of the pinned supports. This was also seen in the sensitivity of the model to bone-plate off-set and bone width in Chapter 5; both of these parameters increase the eccentricity of the load from the plate.

6.4.7.2 Subsidence around Joints

The finite element simulation predicted smaller actuator motion than the experimental model. Experimentally, the universal joints were bolted to a plate slotted through the metaphysis which required a cavity to be created; the actuator motion was predicted to be increased by subsidence. To test this, the finite element model was modified to incorporate an area of reduced Young's modulus around the joints (12GPa, 26.6% reduction in E). This resulted in a 4.16% increase in actuator displacement; the fracture gap motion, however, increased by only 0.26%.

6.4.7.3 Screw-Plate Connection

The screw-plate interaction had a profound influence on the fracture gap motion prediction: a non-continuous screw-plate interaction (using spring elements) increased gap motion by over 8 times the tied equivalent. As described in the methods section, the spring element screw-plate connection was developed based on experimental tests. In addition to the cantilever bending tests of screws within the plate (described in

section 6.2.4.2) the mid-span displacement of the locking plate under three-point bending load was measured with and without screws in the plate. It was found that the displacement was similar in both cases showing that filled screw holes do not significantly increase the bending stiffness of the plate. A replica model was created in FE and the displacement was not sensitive to the screw-plate spring stiffness used.

Several studies have examined the influence of filling unused plate holes with 'locking buttons' but have reached contrary conclusions regarding the predicted fatigue life of the locked plates (Eichinger et al., 2011, Tompkins et al., 2013, Firoozabadi et al., 2012). Similar to Eichinger et al. (2011) and Firoozabadi et al. (2012), this study found no difference in bending stiffness when using filled plate holes; it is therefore unlikely that the fatigue strength would be altered either. A recent finite element study examined plates without holes above the fracture zone and found greatly reduced plate stress (Anitha et al., 2013). In this case, however, the plate was considered to be solid rather than having 'filled holes', which would increase the bending stiffness and could therefore inhibit healing (Schnaser and Vallier, 2013).

Moazen et al. (2013) modelled the load-displacement response of an experimental locking plate model by Bottling et al. (2010a) using a spring-based screw-bone contact model. Their study used a tied plate-screw interface, which will greatly increase the stiffness of the plate; this implies that their screw-bone interface representation is likely to be overly-flexible.

6.4.7.4 Young's Modulus of Bone

The Young's modulus of bone has been previously shown to influence axial stiffness predictions (Uhl et al., 2008). To evaluate the influence of the Young's modulus models were re-run varying the elastic properties of the entire bone. The Young's modulus was seen to have a greater influence on axial stiffness than gap motion with both exhibiting strongly non-linear power law relationships. The results are described in Chapter 7 (section 7.3.1).

6.5 Conclusions

- The loading conditions can be even more influential in computational simulations than in experimental work.
- The locations of peak strains within the bone and plate stress are found to be unique to the loading condition.
- The restraint conditions used must be anatomically appropriate; the specimen length and transverse positioning of restraint at the joints can considerably influence stiffness predictions.

7

Development of an Analytical Model of the Bone-Plate System

7.1 Introduction

Having developed more complex three-dimensional models in previous chapters, this chapter attempts to reduce the bone-plate system to a two-dimensional representation, thereby greatly reducing the number of parameters required.

With locked plating, preoperative planning is key to the success of the surgery (Leahy, 2010, Strauss et al., 2008). Strauss et al. (2008) have shown that failures of the LCP occur when the wrong screw configuration is chosen for a fracture pattern; comments which are echoed by many other studies (Leahy, 2010, Cronier et al., 2010). These failures can occur when a mix of fixation philosophies are being used—i.e. a lag screw and a comminuted fracture pattern (Krettek et al., 1991); but also if the working length (distance between the two innermost screws) is inappropriate for the fracture pattern (Strauss et al., 2008, Leahy, 2010, Cronier et al., 2010). As depicted in Figure 7.1, insufficient working lengths in a simple fracture can cause large plate stresses (Ellis et al., 2001, Stoffel et al., 2003); conversely, excessive working lengths in a comminuted

fracture can result in large plate stresses (Wagner, 2003, Cronier et al., 2010). The reason for this is because once interfragmentary contact is made due to plate bending, the bone transmits load and the plate is shielded from further stress (Stoffel et al., 2003). In fracture patterns with wider gaps, the plate transmits the full weight-bearing loads until healing progresses. It is crucial, therefore, that a distinction is made between situations where bone-on-bone contact can occur, and those where it cannot (including gap opening situations which may occur in tension locations).

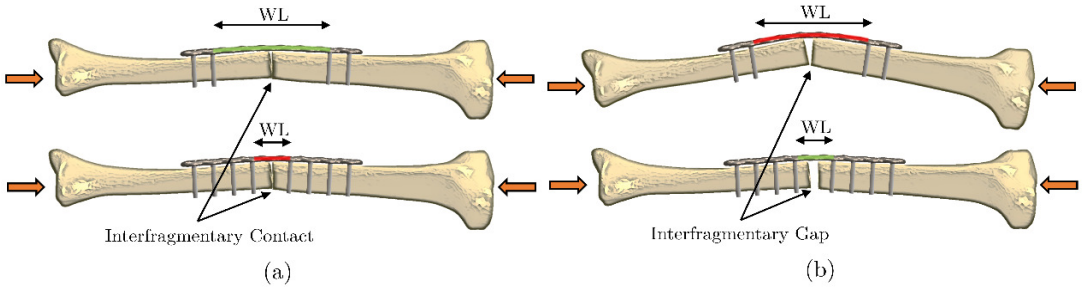

Figure 7.1 - Influence of working length (WL) on plate stress under axial load using different working lengths for (a) a small interfrangmentary gap and (b) a large interfragmentary gap.

For fractures where direct healing is the goal, fracture reduction is more important than screw placement (Leahy, 2010); however, for all fractures where indirect healing is the goal (or complete reduction is not achieved) screw placement influences stress within the plate (Ellis et al., 2001, Stoffel et al., 2003). Most failures are not due to a single traumatic event, but are the result of fatigue failure (Ellis et al., 2001); minimising stress in the plates and screws should, therefore, be one of the goals of internal fixation (Ellis et al., 2001). If healing progress more rapidly, however, the demands upon the fixation are also reduced (Schnaser and Vallier, 2013). The correct level of axial motion and minimal shear movements appear to be the most beneficial healing conditions (Epari et al., 2007, Augat et al., 2003). Previous studies have found that the IFM produced by locked plating can be altered by many variables: working length, the offset distance between the bone and plate (BPD) and the material properties of the plate (Stoffel et

al., 2003, Ahmad et al., 2007, Miramini et al., 2013). Despite this, no study has provided a formula to predict the fracture gap motion or plate stress for a given locking plate device and screw configuration. If the IFM and plate stress produced by a locking plate device could be accurately predicted then the likelihood of mechanical failure or delayed healing could be reduced by selection of an appropriate working length and informed weight-bearing guidance.

7.1.1 Chapter Aim

This chapter aimed to develop an analytical model of a fractured long bone implanted with locking plate capable of predicting IFM, axial stiffness and plate stress.

7.2 Methods

Locked plating is structurally similar to uni-lateral external fixation; however, the influence of the reduced bone plate offset is significant. As the length of screw free to bend is greatly reduced, the majority of the fracture gap motion is generated by plate bending. It also results in asymmetric fracture gap motion (Bottlang et al., 2010a). The bone fragments were initially assumed to be ideally rigid; the influence of this assumption was later evaluated. The system was assumed to be symmetrical with the total length of the loaded bone specimen, L_E, and working length, L_W (Figure 7.2a). The working length portion of the plate was idealised as an eccentrically loaded column (eFunda) (Figure 7.2b and c).

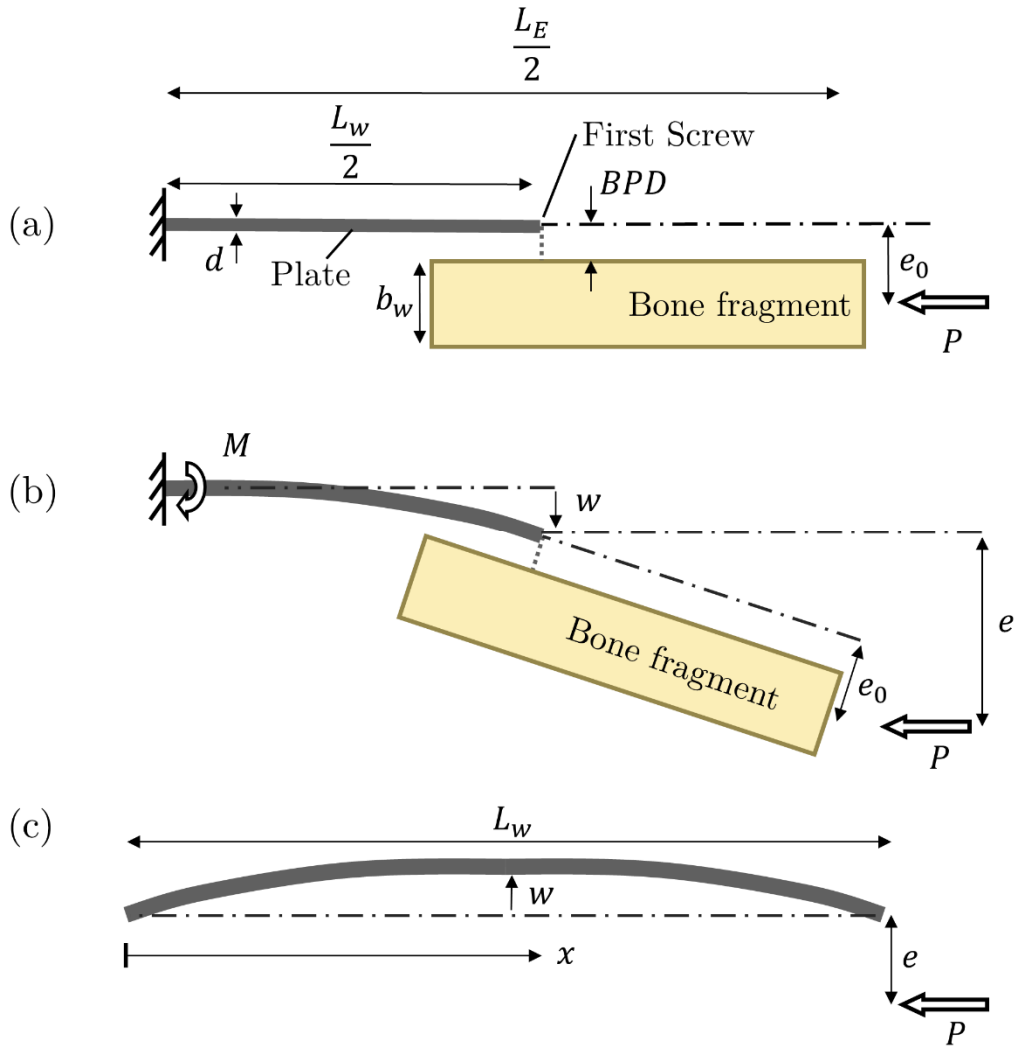

Figure 7.2 – Depiction of the idealised bone-plate system and the variables used showing: (a) the initial undeformed configuration; (b) the increased eccentricity due to plate bending and the bending moment produced at the centre of the plate; and (c) the working length portion of the plate idealised as an eccentrically loaded column.

The bending moment at the mid-span of the plate caused by the eccentricity, e, and lateral deflection of the plate, w, is given by (Figure 7.2b):

$$M = P(w + e) \tag{7.1}$$

Using the Euler-Bernoulli substitution for bending moment, $M = -EI\ \frac{d^2w}{dx^2}$, the equation governing transverse displacement of the column, w, is:

$$\frac{d^2w}{dx^2} + \frac{Pw}{EI} = -\frac{Pe}{EI} \tag{7.2}$$

Substituting $m^2 = \frac{P}{EI}$

$$\frac{d^2w}{dx^2} + m^2w = -m^2e \tag{7.3}$$

The general solution of the equation is:

$$w(x) = A\sin(mx) + B\cos(mx) - e \tag{7.4}$$

Using the pinned boundary conditions:

$$w(x) = 0\ at\ x = 0\ and\ x = L_w \tag{7.5}$$

Solving equation 7.4 for coefficients A and B:

$$B = e \tag{7.6}$$

$$A = e\left(\frac{1}{\sin(mL_w)} - \frac{1}{\tan(mL_w)}\right)$$

Recalling that $\tan\left(\frac{\theta}{2}\right) = \csc\theta + \cot\theta$

$$A = e\left(\tan\left(\frac{mL_w}{2}\right)\right) \tag{7.7}$$

Substituting A and B into equation 7.4 the solution for the column's lateral displacement, w, is:

$$w(x) = e\left(\tan\left(\frac{mL_w}{2}\right)\sin(mx) + \cos(mx) - 1\right) \tag{7.8}$$

Where the maximum lateral displacement will occur at $x = \frac{L_w}{2}$

The slope at the ends of the working length (or at the screw closest to the fracture) is given by $w'(x)$ at $x = 0 = L_w$

$$w'(x) = e\left(\tan\left(\frac{mL_w}{2}\right)m\cos(mL_w) - m\sin(mL_w)\right) \tag{7.9}$$

The displacement of the entire bone-plate system can then be found using the slope at the screw nearest to the fracture gap, θ (Figure 7.3).

The initial eccentricity, e_0, of the load is given by:

$$e_0 = BPD + \frac{d}{2} + \frac{b_w}{2} \tag{7.10}$$

Where BPD is the bone-plate distance, d is the depth of the plate and b_w is the width of the bone at the fracture site as shown in Figure 7.2a.

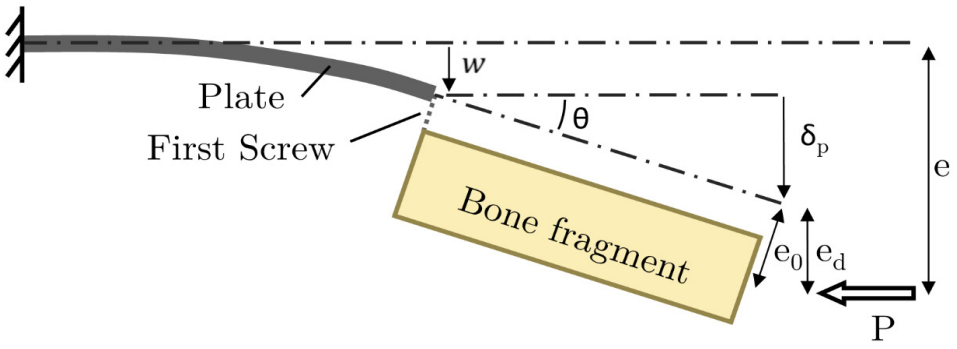

Figure 7.3 - Idealised bone-plate system showing the components of the increased eccentricity due to deformation.

Once the slope and horizontal displacement of the idealised column (plate) has been calculated, the horizontal deflection due to the rotation of the bone fragment is calculated using the slope at the first screw

$$\delta_P = \frac{(L_E - L_w)}{2}\sin\theta \tag{7.11}$$

The total horizontal deflection at the point of load application is (Figure 7.3):

$$u_{load} = w + \delta_P + e_d \tag{7.12}$$

Where

$$e_d = e_0 \cos\theta \tag{7.13}$$

In order to account for non-linear geometrical effects, the eccentricity must be updated with deformation. At the plate deforms, the bone rotates which increases the eccentricity of the load. This nonlinearity was accounted for by iteratively solving the equations, continually updating the initial eccentricity.

The initial eccentricity for the next iteration, e, is:

$$e = w + \delta_P + e_d \tag{7.14}$$

The maximum interfragmentary movement at the fracture site due to rotation of the bone is at the far cortex. This is calculated using the total bone depth, bone-plate offset and half of the plate thickness.

$$v_{frx} = \left(\frac{d}{2} + BPD + b_w\right)\sin\theta \tag{7.15}$$

The net closure of the fracture gap is double this value due to symmetry.

The axial motion at the position of the load is calculated using half of the bone fragment depth (where the load is assumed to be applied). There is also a contribution from the rotation of the bone fragment.

$$v_{load} = \left(BPD + \frac{d}{2} + \frac{b_w}{2}\right)\sin\theta + \left[\frac{(L_E - L_w)}{2} - \left(\frac{(L_E - L_w)}{2}\cos\theta\right)\right] \tag{7.16}$$

Again, the total displacement is double this value due to symmetry.

The bending stress in the plate, σ_b, can be found using the deformed eccentricity at the applied load, u_{load}, the applied load, P, plate depth, d, and the second moment of area, I:

$$M = u_{load}P \quad \sigma_b = \frac{Md}{2I} \tag{7.17}$$

Combining the bending stress with the axial stress from the applied load gives:

$$\sigma = \frac{F}{A} + \frac{Md}{2I} \tag{7.18}$$

Where A was assumed to be a product of the cross sectional width and depth of the plate.

7.2.1 **Solution**

This analytical model was solved using Matlab 7.6 (MathWorks inc., Cambridge, UK). Nonlinear geometrical effects were included by successive iterations of the script.

The variables required for the model are:

- Total length of the bone-plate construct from points of rotation (i.e. distance between centre of condlyes and centre of talus) (L_E)
- Bone width at fracture site (b_w)
- Plate: E value (E_P); I value (I); and depth (d)
- Working length—distance between the two innermost screws (W_L)
- Bone-plate offset (BPD)

The influence of including the Young's modulus of the bone, E_B, is evaluated in Section 7.3.1.

7.3 Results

Using the Styker narrow 5.0mm LCP ($I = 60.3\text{mm}^4$, $E = 180\text{GPa}$). The predicted IFM for a range of working lengths and applied loads demonstrates the high degree of non-linearity of both variables (Figure 7.4). The predicted stress in the plate due shows greater difference between working lengths at larger loads (Figure 7.5).

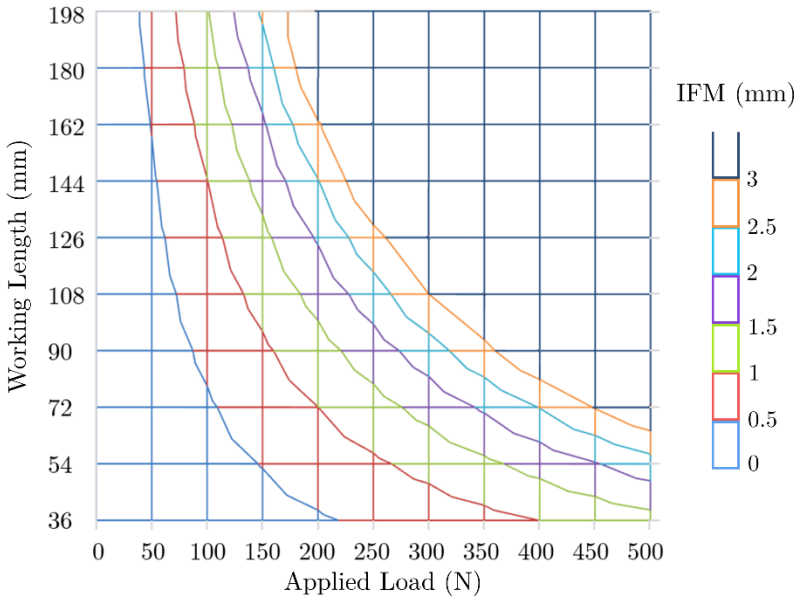

Figure 7.4 – Predicted IFM for increasing load and working lengths

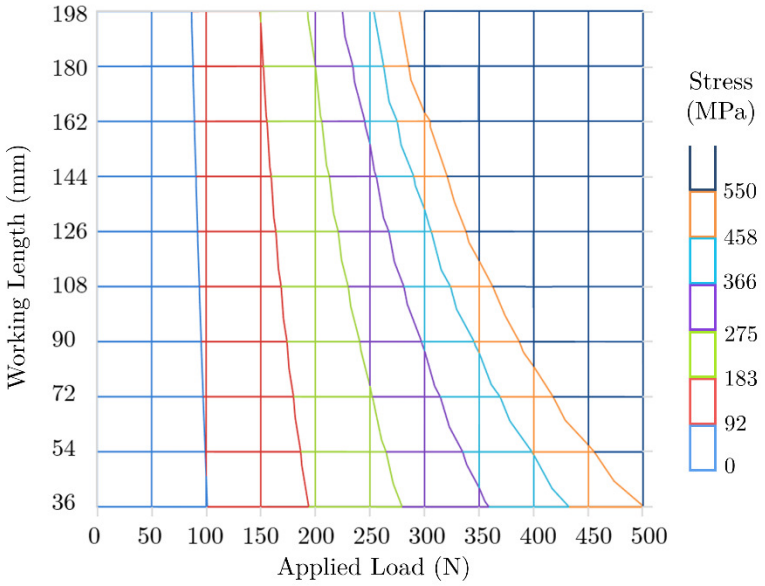

Figure 7.5 – Predicted stress within the plate for increasing load and working lengths

7.3.1 Incorporating the Effect of Bone Elasticity

In the analytical model, the bone was initially assumed to be ideally rigid for simplification. The finite element models developed in Chapter 6 were used to evaluate the influence of this assumption. Using a 5.0mm narrow locking plate, two screw configurations were examined (C1234 and C234) at a load of 100N. Models were run with varying values of Young's modulus for the bone: 200MPa, 1GPa, 5GPa, 16.375GPa (Sawbones) and infinitely rigid. The reduction in gap stiffness (load divided by IFM) and axial stiffness (load divided by actuator movement) for each value expressed as percentage decrease in stiffness relative to the idealised rigid case and plotted in Figure 7.6. There was a greater percentage reduction in axial stiffness than gap stiffness and two screw configurations produced similar reductions (maximum difference of 12% in axial stiffness and 2% in gap stiffness). For simplification, the correction factor for the smallest working length was adopted as it had the most influence. A best-fit power law relationship was used. This correction factor is likely to change with bone geometry, plate properties and the level of load applied; nevertheless, it provides a rough estimate for fractures of the tibial diaphysis.

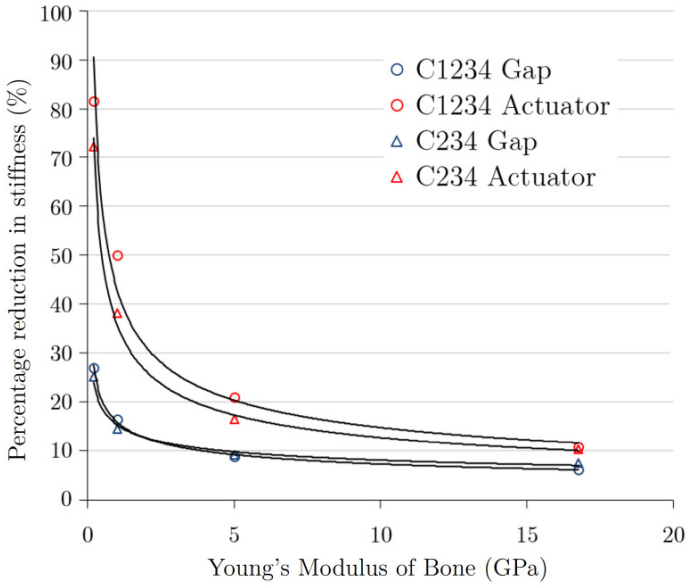

Figure 7.6 – Derived correction factor for axial stiffness and gap stiffness for different Young's moduli of bone for a 5.0mm narrow locking plate at a load of 100N

There are several reasons for the observed reductions in stiffness. The greater sensitivity of axial stiffness compared to gap stiffness can be attributed to axial deformation of the bone and local deformation in the region of load application. Some of the reduction in stiffness can be attributed to an increase in eccentricity produced by bending deformation of the bone proximal and distal to the plate (Figure 7.7); however, subsidence around the screws closest to the fracture was also found to be a major factor. This local deformation results in greater rotation at the first screw reducing both gap stiffness and axial stiffness. The increased deformation due to a reduction in Young's modulus and concentration of strain at the first screw are shown in Figure 7.7.

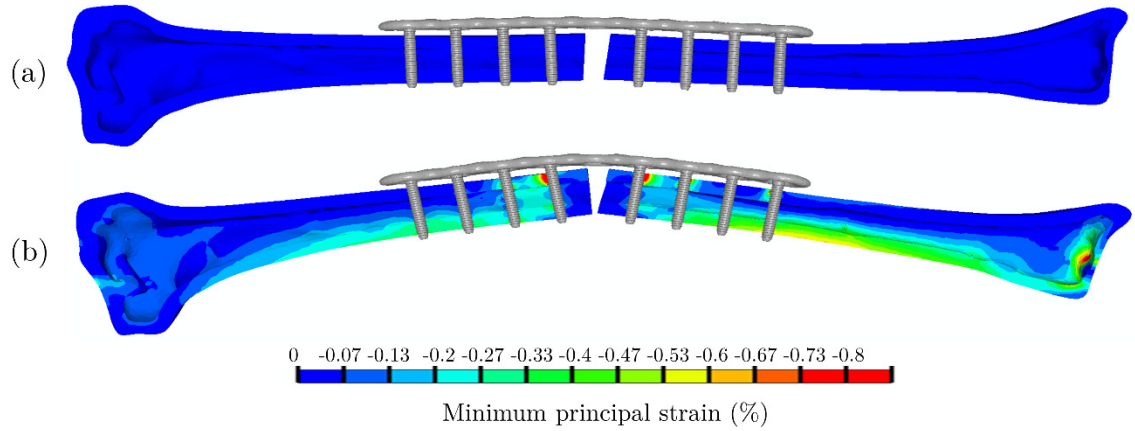

Figure 7.7 – Deformed shape (scale factor ×3) and minimum principal strain in the bone at a load of 500N for different Young's moduli: (a) ideally rigid and (b) 1GPa.

7.3.2 Validation

The model was used to predict the experimentally measured values of gap stiffness and axial stiffness from experimental tests conducted in Chapter 5. The load at which the value of stiffness was taken was 100N, 150N and 200N for screw configurations C34, C234 and C1234 respectively. As discussed earlier, two plate types were evaluated (Stryker ASoX 5.0mm narrow and broad LCPs obtained experimentally in Chapter 6) to ensure a correct representation for changes in second moment of are. The analytical model predicted the gap stiffness of the experimental models with an average mean error

of 22.8% for both plate types using three different working lengths (six cases). This error reduced to 16.5% when corrected for bone elasticity (Figure 7.8).

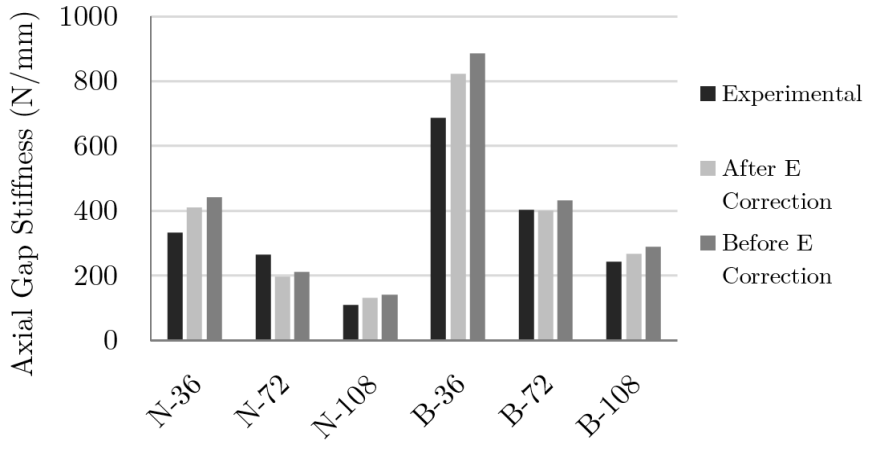

Figure 7.8 - Gap stiffness predictions of the analytical model versus the experimental validation tests where 'N' denotes the narrow plate type and 'B' the broad for the different working lengths (in mm).

The axial stiffness was less well predicted with a mean error of 73.8% reducing to 61.6% after correction for bone elasticity (Figure 7.9). The discrepancy was attributed to experimental subsidence around the bolted connections used. This was confirmed using finite element simulation (Chapter 6).

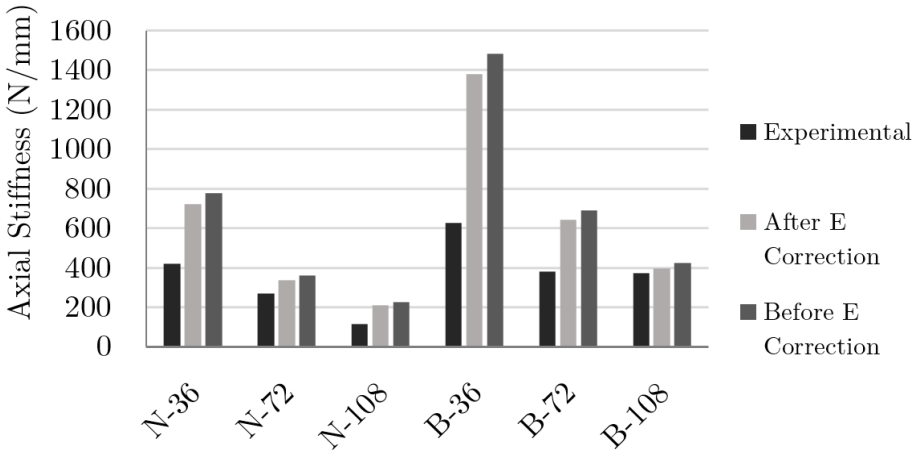

Figure 7.9 - Axial stiffness predictions of the analytical model versus the experimental validation tests where 'N' denotes the narrow plate type and 'B' the broad for the different working lengths (in mm).

7.3.3 Comparisons with Previous Studies

The analytical model was used to predict the axial stiffness and gap stiffness of the locking plate constructs in previous studies. In order for consistent comparisons to be made the studies included were reduced to those using:

- A loading condition where the bone ends were free to rotate.
- Locking plate devices with exclusively locking screws.
- A three-dimensional bone or surrogate

Five previous studies met the criteria and were used (Schmidt et al., 2013, Stoffel et al., 2003, Uhl et al., 2008, Dobele et al., 2010, Hogel et al., 2012). Each study and all the relevant variables are shown in Table 7.1 and Table 7.2. If a value in a study was not known, an appropriate assumption was made. Where a study provided stiffness results for multiple variables these have been included in the tables. As the only second moment of area data available was for Stryker ASoX 5.0 narrow and broad LCPs, each study was assumed to be one of these values. For consistency, steel and titanium were assumed to have $E = 205GPa$ and $E = 105GPa$ respectively. Where the load used for stiffness prediction was not known and load-deformation data was not given a load of 350N was used. Schmidt et al. (2013) and Hogel et al. (2012) used asymmetric models, where the fracture gap was not centrally positioned; for the purposes of the study they were assumed to be symmetrical and the total length of the bone-plate system was used. Material properties for the synthetic bones were obtained from matweb.com[8]. Where two values of Young's modulus were used in a model or the material had varying tensile and compressive moduli, an average was taken.

[8] www.matweb.com, MatWeb, LLC 1996-2014, last accessed 12/02/2014

Table 7.1 – Bone properties of previous studies

Study	Bone Properties						
	Fragment 1 L (mm)	Fragment 2 L (mm)	Fracture size (mm)	Additional length (mm)	Total L (mm)	Bone E (GPa)	Bone Width (mm)
Stoffel et al. 2003	125	125	6		256	17	35
Uhl et al. 2008	70	70	2		142	0.247 / 1.31	20
Dobele et al. 2010	120	120	3		243	3.1	30
Hogel et al. 2012	37.5	337.5	10		385	16.35	22
Schmidt et al. 2013	250	70	25	140	485	8.249	35
MacLeod et al. 2013	197.5	197.5	10	40	445	16.375	25

Table 7.2 – Plate properties of previous studies

Study	Plate Properties					Measured Stiffness Location
	BPD (mm)	Depth (mm)	I	E	WL (mm)	
Stoffel et al. 2003	2	4.9	Narrow	Titanuim	36, 72, 108	Gap
Uhl et al. 2008	0	4.9	Narrow	Steel	18	Gap, Actuator
Dobele et al. 2010	2	4.9	Narrow	Titanium	54	Gap, Actuator
Hogel et al. 2012	2	4.9	Narrow	Steel, Titanium	36	Gap, Actuator
Schmidt et al. 2013	2	4.9	Broad	Steel, Titanium	54	Gap
MacLeod et al. 2013	2.5	4.9	Narrow, Broad	Steel	36, 72, 108	Gap

The stiffness predictions of the analytical model for each of the previous studies are shown in Figure 7.10. Where a study provided results for different variables these have been included as separate entries. For example, Stoffel et al. (2003) give values for different working lengths; Uhl et al. (2008) give values of movement at the actuator as well as IFM for different bone densities. The results of the experimental tests from Chapter 5 are also included under the entries "MacLeod et al. 2013".

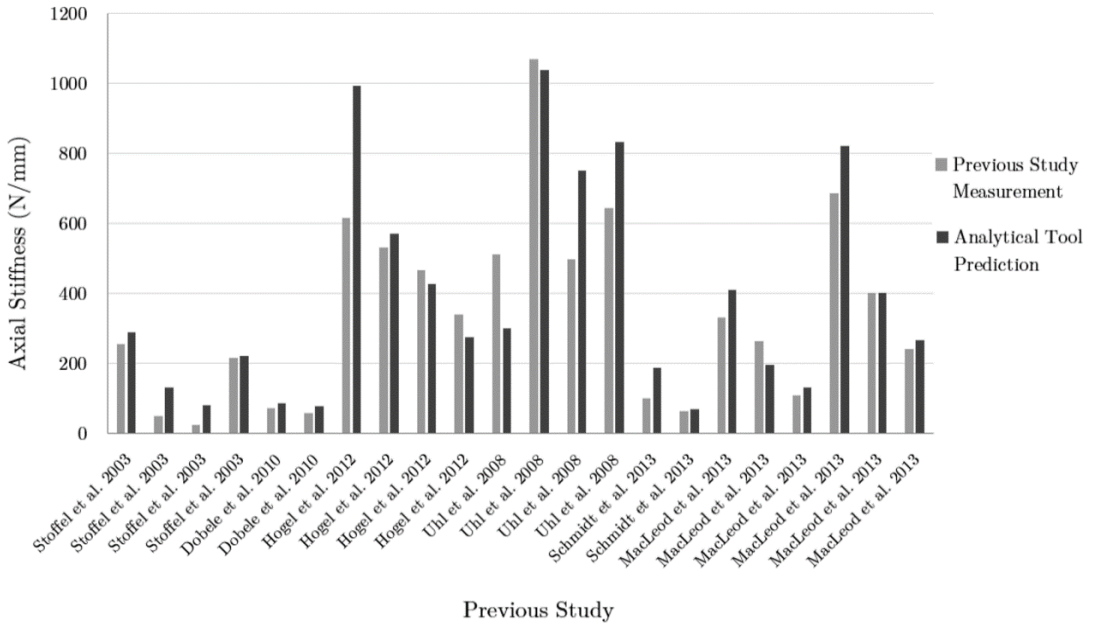

Figure 7.10 – Previous studies measured stiffness' compared with predictions of the developed analytical tool (corrected for bone Young's modulus).

The predictions of previous studies (excluding MacLeod et al. 2013) were predicted with an average mean error of 53% (78%); once corrected for bone elasticity the values reduced to 39% (48%). Median errors are lower at 30% and 20% once corrected for E (including MacLeod et al.). Additionally, the range of the experimental values is considerable (25-1069 N/mm) with the range of the predictions matching very closely (71-1038 N/mm). A linear best-fit line between experimental and predicted stiffness values produced an R^2 value of 0.86 (Figure 7.11).

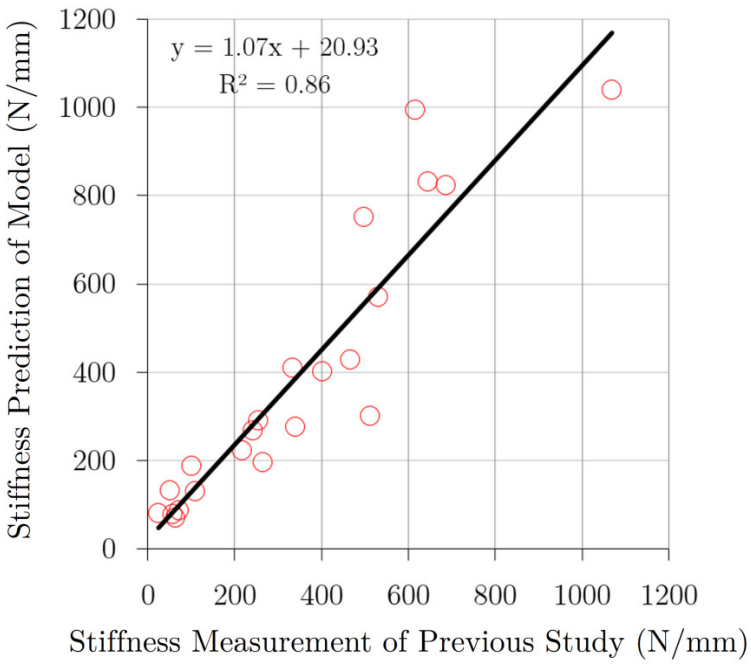

Figure 7.11 – Correlation of previous studies measured stiffness and predictions of the developed analytical tool (corrected for bone Young's modulus).

7.4 Discussion

The developed analytical model provides a tool for the prediction of IFM, axial stiffness, transverse motion and plate stress. The gap stiffness predictions of the model (based on IFM) were within 16% of the experimentally measured values (Chapter 5). The model predicted the stiffness values from five previous experimental studies with a median error of 20%. The required variables for this prediction are fracture gap size and cross-sectional width, bone length, bone-plate offset, working length and plate material and geometric properties (E and I). The Young's modulus of the bone can also be taken into account using a formula developed from finite element models in Chapter 6. This formula is currently limited to studies which test using a pinned loading condition (loading condition (c), Chapter 5). Not all of the variables were known for these comparisons and the predictions would improve with more precise data, in particular, for the second moment of area of the plate.

7.4.1 Plate Stress

Using a plate of similar dimensions to that used in this study and a working length of 40mm, Ellis et al. (2001) found that permanent plate deformation occurred at 600N axial load; for a working length of 36mm the current model predicted a value of around 550N. In experimental tests, the load-deformation behaviour changed considerably at around 500N indicating that yielding occurred (Figure 7.12). The prediction of bending stress is based on horizontal displacement and would therefore improve if the Young's modulus correction factor was incorporated in a similar manner.

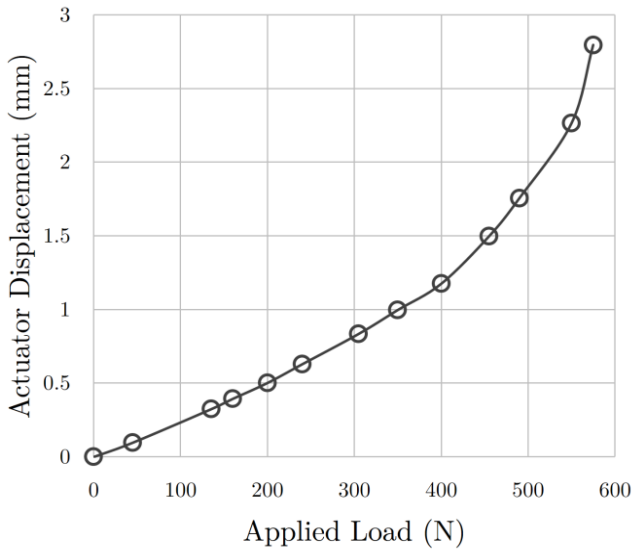

Figure 7.12 – Experimentally measured load deformation response of the narrow LCP

7.4.2 Bone Dimensions

In a finite element model of a fractured tibia Duda et al. (2002) predicted gradually increasing interfragmentary movements towards the mid-shaft, but also slightly increased movements in the metaphyses. Their analysis did not incorporate geometrically nonlinear effects so the values are not comparable; nevertheless, these increases can be explained by the analytical model. An increase in effective length of the bone-plate construct, L_E, was seen to increase IFM; by locating the fracture closer

to the mid-span there is a greater lever arm of rotation. Towards the metaphyses there is a flare in bone width, b_w, which increases the distance from the plate and, therefore, the IFM.

7.4.3 Bone Quality

The derived stiffness reduction factor based on Young's modulus showed that the bone elasticity has a much greater influence on axial stiffness than IFM; a study by Uhl et al. (2008) showed similar influence. For a Young's modulus of 1GPa the observed reduction in gap stiffness was 15% compared to around 7% for 16.4GPa (Sawbones cortical bone).

7.4.4 Verification and Validation

Verification of the model was performed using two and three-dimensional finite element simulation. The model was directly validated using the motion at the fracture site obtained from the experimental tests in Chapter 5. It was also indirectly validated by comparing predictions of previous studies.

7.4.5 Limitations of the Model

In reality, the screws will bend slightly between the plate and the bone. This would be more influential with larger bone-plate offsets. It would also be more apparent when using shorter working lengths as it would represent a larger proportion of the total deformation. The plate and screws will also have some deflection contribution from shear deformation and axial compression; neither have been accounted for in the analytical model. The model also assumes rigidity beyond the first screw. While the Young's modulus correction factor accounts for much of the influence that this has, screw configuration beyond the screws closest to the fracture can affect plate stiffness (Stoffel et al., 2003) and this was not accounted for. The Young's modulus correction factor could also be improved to account for the level of load.

The model is capable of predicting in vitro IFM and plate stress. It is not clear how muscle activity or callus healing would alter these variables in vivo. The model is likely be most representative of the tibia where joint reactions are the dominant loading and the largest muscle forces are axial. Although joint reactions also dominate loading in the femur, muscle loading is multidirectional and so the present model may not be as representative.

As the model is nonlinear, none of the output variables are linearly scalable. The importance of the geometric nonlinearity is illustrated in Figure 7.13 using different working lengths.

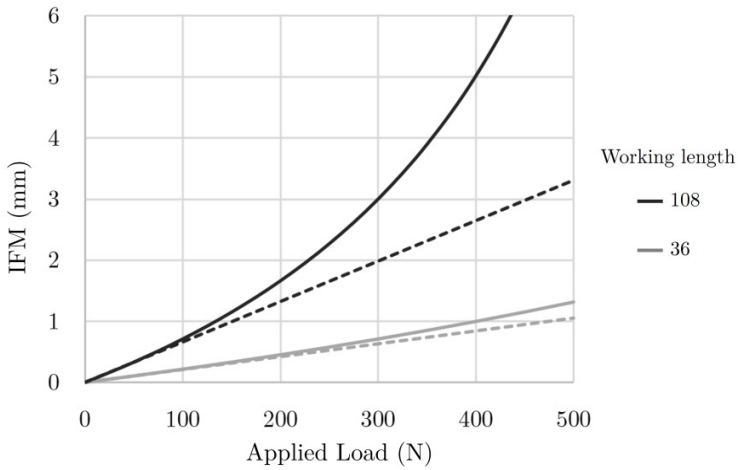

Figure 7.13 - The importance of nonlinearity for different working lengths.

7.4.6 Comparisons with Previous Studies

In some of the studies it was not clear what the total bone length was as the additional length of actuator attachments or connections was not specified (Hogel et al., 2012, Dobele et al., 2010, Uhl et al., 2008, Stoffel et al., 2003). This could account for some of the prediction error. All studies were assumed to be symmetric even when two were not (Schmidt et al., 2013, Hogel et al., 2012). This does not seem to have influenced the prediction significantly. In the study by Hogel et al. (2012) the position of the plate is not shown. As it is described as being positioned medially, it was assumed to be

positioned in the stagittal plane with a 2mm bone-plate offset. Their model used a 15mm offset proximally and 4mm distally; a weighted average value of 5.1mm was assumed (with the fracture described as being positioned 10% of the total length away from the ankle). As the bone was eccentrically placed (medially offset) and the plate was also located medially, this effectively reduced the bone-plate offset. Therefore, the effect of this loading eccentricity was subtracted from the total bone-plate offset to give an effective bone plate offset of -3.1mm. Unfortunately, the study by Hoffmeier et al. (2011) did not have sufficient bone-plate offset to utilise the full working length, resulting in all configurations producing similar values of stiffness. It could not, therefore, be used for comparison in this study.

7.5 Clinical Application

Current screw positioning guidance helps inform surgeons with regard to the appropriate plate length and the number of screws to use (Apivatthakakul et al., 2012). Unfortunately, there are no guidelines regarding working length, which is known to be the primary determinant of IFM in locking plates (Stoffel et al., 2003). Recommendations for postoperative weight-bearing vary widely (Granata et al., 2012); in addition, there is a large variability in the weight-bearing of individuals (Vasarhelyi et al., 2006). This tool can be used to select the appropriate working length to produce the most osteoinductive environment so that healing progresses more rapidly (Schnaser and Vallier, 2013). Moreover, it would make the guidance consistent and patient-specific, taking into account: fracture pattern, bone quality and implant properties. Clearly there are always external factors which cannot be accounted for, however, the tool could also safeguard against fixation failure by providing early-stage healing estimates of plate stress under a given load.

Locking plates can be used in complex fractures which are difficult to manage and have even been used as external fixators (Woon et al., 2010). The tool has the potential to

be used for guidance in more unusual situations to which surgeons may not be as familiar.

7.5.1 Implementation

This analytical model was developed with the aim of providing surgical guidance. Given the following two variables, a working length can be selected to prevent material failure of the plate and optimise the healing environment:

- How much IFM/IFS is desirable for the particular fracture pattern?
- How much load is the patient going to bear?

To assess the risk of plate failure, the expected weight-bearing loads can be used to evaluate the bending stress that the plate is exposed. A working length can be selected that reduces this risk to an acceptable level. If there is insufficient bone-plate offset, the working length is reduced to the size of the fracture gap regardless of the positions of the screws and cannot, therefore, be regulated (Chao et al., 2013, Hoffmeier et al., 2011). If this is the case, the model can still be used to provide an estimate of IFM and plate stress. The influence that bone-plate offset and fracture gap width have on working length and plate stress is summarised in Figure 7.14. The figure assumes that fractures gaps of greater than 1mm will not close under patient weight-bearing loads.

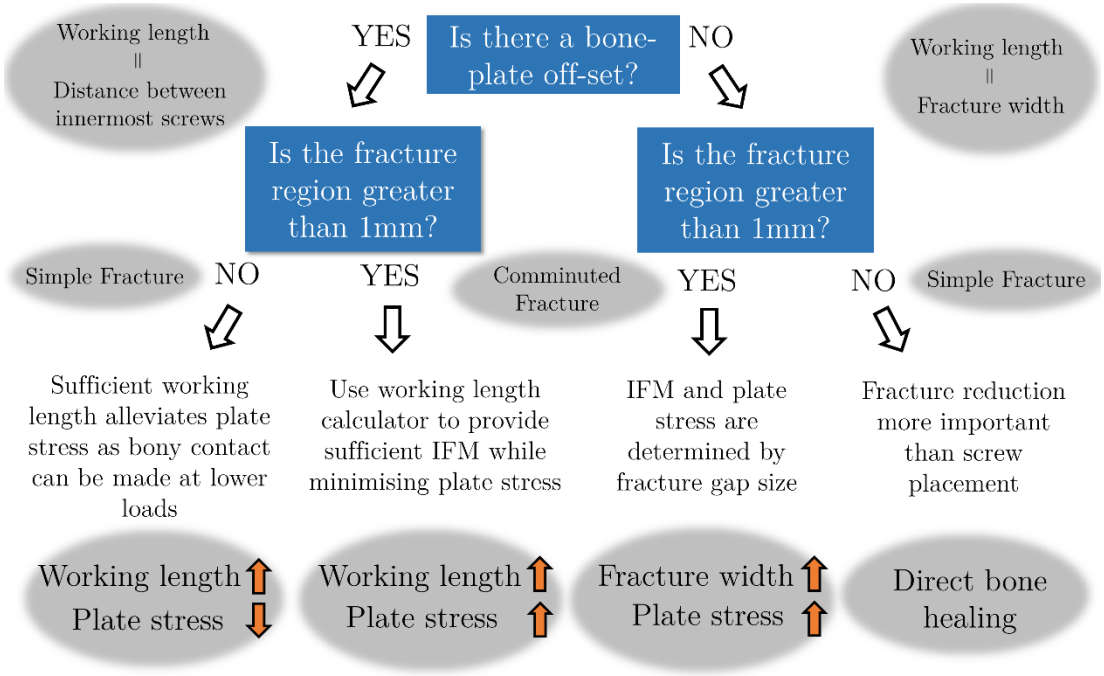

Figure 7.14 - The importance of working length in different fractures

7.5.2 Example

Using the bone dimensions of the experimental tests conducted and the Stryker ASoX 5.0 narrow steel plate the following examples illustrate the application and potential use of the model.

The beneficial range of interfragmentary strain is considered to be 10-40% (Goodship A and Cunningham J, 2001, Comiskey et al., 2010). For a 2.5mm fracture gap, therefore, 1mm of motion would be appropriate. This motion is predicted for a working length of 108mm at a load of 150N; using a smaller 36mm working length does not generate that level of motion until 450N (three-fold load increase).

Plastic deformation of a steel plate would be predicted to occur at a load of approximately 400N using a working length of 108mm. Using a working length of 36mm, this would not occur until 550N.

It is important to note that these values represent an over-estimate of strength as the current prediction of plate stress does not have the Young's modulus correction factor incorporated.

7.6 Conclusions

- The interfragmentary motion in the bone plate system can be well predicted with only eight variables using the developed analytical model.
- Axial stiffness is substantially altered by bone material properties; IFM is less sensitive.

8

The Influence of Screw Configuration on Pull-Out Risk in Locked Plating

8.1 Introduction

In the literature, general guidance exists for how to manipulate the stiffness of locking plate devices and protect against plate breakage (Cronier et al., 2010, Gautier and Sommer, 2003, Stoffel et al., 2003). This guidance has been used to inform clinical practise. For diaphyseal tibia fractures, the AO Foundation Surgery Reference Guide (Apivatthakakul et al., 2012), which refers to an article by Gautier and Sommer (2003), recommend a minimum of three well-spaced screws either side of the fracture with fewer than half of the holes filled by screws. Once screws are inserted at the plate ends, two screws should be positioned as close as practicable to the fracture zone ('near and far'). Plate length is selected based on the fracture pattern with 2-3 times the fracture length suggested for comminuted fractures and 8-10 times in simple fractures. When plating osteoporotic bone, additional screws either side of the fracture should be used. This guidance aids with the selection of plate length and number of screws but does not

provide any information regarding working length (the distance between the innermost two screws). The reason for this is probably due to the fact that the majority of plated internal fixations use compression screws, which are forced to be in contact with the bone; indeed, when using both types of screws, it is advised that placing locking screws adjacent to the bridged zone should be avoided (Apivatthakakul et al., 2012). In these situations, the working length is simply the size of the fracture. This highlights a key difference between the two screw types—the presence of a bone-plate off-set. The use of exclusively locking screws, therefore, requires a different approach to screw placement as they are behaving not like a plate, but an internal fixator (Leahy, 2010).

8.1.1 Incidence of Locked Plating Failure

In a survey of 169 fractures, Sommer et al. (2003) found that the main causes of revision operations in locking plates (and % incidence) were: delayed/non-union (3%); screw loosening (3%), re-fracture adjacent to the implant (3%) and plate breakage (2.4%). Many studies have investigated the influence of screw position on interfragmentary motion (IFM) (Stoffel et al., 2003, Ellis et al., 2001, Tornkvist et al., 1996) and stress exposure or fatigue strength of implants (Stoffel et al., 2003, Duda et al., 2002, Hoffmeier et al., 2011, Ellis et al., 2001). These studies can help to reduce the incidence of plate breakage and delayed or non-union. Periprosthetic fractures and screw loosening, however, are caused by strain concentrations within the bone. Infection, which can be a source of screw loosening, is relatively common in external fixation but rare in plating (Sommer et al., 2003). Therefore screw loosening in plating is related to bone damage or resorpsion caused by excessive strain exposure (Huiskes et al., 1985).

8.1.2 Screw Positioning in Fixators

Due to the presence of bone-plate off-set, locking plates are known to behave differently than conventional plates (Stoffel et al., 2003); this means that conventional screw positioning guidance does not always apply (Gautier, 2009). Similarly, external fixation

literature advocates the placement of screw and pins 'near and far' from the fracture site (Fragomen and Rozbruch, 2007); while this may be appropriate for external fixators, where the gap motion is mainly produced by deformation of the traversing elements, it results in very stiff locked plating constructs.

Huiskes et al. (1985) showed that reducing the bone-fixator off-set and increasing the distance between pins reduced the stress at the screw-bone interface in external fixators. For unilateral fixators, Donaldson et al. (2012a) showed that using three pins rather than two can substantially reduce the volume of yielded bone around screw locations in osteoporotic bone. Locked plate fixation is mechanically similar to unilateral external fixation and some of the same principles apply; however, there are additional considerations due to the bending of the plate. Screw positioning variables such as working length and plate properties (material and geometric) become influential (Stoffel et al., 2003).

While some studies have shown that the addition of locking screws can increase loads to failure (Erhardt et al., 2012), Hak et al. (2010a) found that the addition of a third screw could reduce the torque to failure in a humeral shaft model. Additionally, many studies state that too many screws can cause periprosthetic fracture (Leahy, 2010, Sommer et al., 2004, Tan and Balogh, 2009). Therefore, there is conflicting guidance regarding the impact of screws on the screw-bone construct.

A computational study by Duda et al. (2002) predicted that a longer working length reduced von Mises stress in the plate using a gap defect model. Stoffel et al. (2003) attributed this to increased total plate length; however, it is not clear why that should reduce the bending stress. It is more likely that this was due to the presence of callus (this issue is discussed further in Chapter 10). Although the concept of working length has been investigated previously by several studies with regard to the axial stiffness of devices (Stoffel et al., 2003, Hoffmeier et al., 2011, Ellis et al., 2001), the role of subsequent screws is less well investigated. Stoffel et al. (2003) found that the position

of the second screw from the fracture gap was influential in terms of stiffness. While Duda et al. (2002) also examined the strains within the bone due to different screw configurations, the biomechanical reasons for the differences were not clear. Changes to the stiffness of devices is likely to have an impact on the host bone and discerning screw placement may be able alleviate excessive stress.

8.1.3 Osteoporotic Bone

Locking screws have been promoted as having superior fixation in osteoporotic bone (Kim et al., 2007, Yanez et al., 2010, Gardner et al., 2004); however, different fixation techniques are often required in osteoporotic bone and it is not clear whether screw positioning guidance that applies to healthy bone also applies to bone of poorer quality (Giannoudis and Schneider, 2006). Osteoporotic bone can be more susceptible to screw cut-out and periprosthetic failure (Grawe et al., 2012, Leahy, 2010, Strauss et al., 2008). The healing process can be also be prolonged placing higher demands on the fixation than in healthy bone (Giannoudis and Schneider, 2006). Many biomechanical studies use osteoporotic bone models (Grawe et al., 2012, Bottlang et al., 2009a, Yánez et al., 2012); however, the influence that bone density has on choice of screw position has not been investigated.

8.1.4 Influence of Test Conditions

Several studies have used cantilever or bending tests to draw conclusions regarding screw placement. Perren (2002) and Gauiter et al. (2003) used cantilever bending diagrams to illustrate that increased distance between screws and thinner plates can reduce pull-out forces on screws. Using three and four-point bending examples, previous studies have stated that increased working length decreases stress in the plate (Gardner et al., 2004, Sommer et al., 2003, Tan and Balogh, 2009). In cantilever and bending tests only transverse loads are considered; whereas, in reality, transverse forces arise due to axial forces (Figure 8.1a). This can result in misleading conclusions. Under simply

supported bending, it is the distance between the applied loads not the working length that determines the plate stress (Ellis et al., 2001) (Figure 8.1b and 1c).

In Chapter 5 the loading regime was found to greatly alter the mechanical response and alter the locations of peak strain within the bone. Cantilever and bending experiments are straightforward to implement but do not represent the in vivo loading situation. The conclusions regarding screw placement, therefore, may not apply to axially loaded bone-plate constructs.

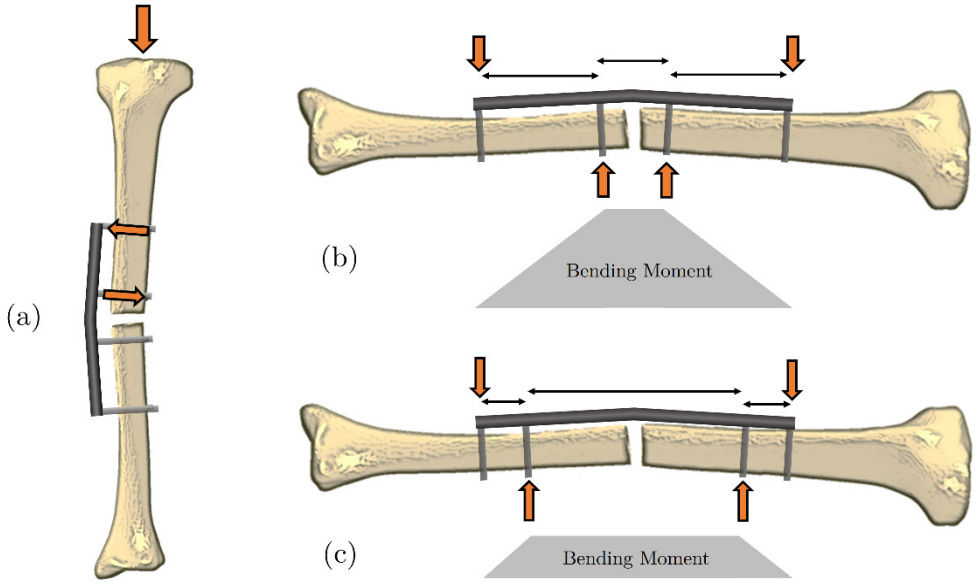

Figure 8.1 – Assumed loading conditions can greatly alter conclusions regarding screw placement showing: (a) transverse forces arising from axial loads in unilateral fixation; (b) bending moment due to a four-point bending arrangement; and (c) bending moment due to reduced spacing of loads.

The influence of screw positioning is not straightforward as there are multiple effects to consider. Techniques to reduce pull-out or push-in loading may not be the most important aspect in axially loaded bone where large normal loads are transferred at the screw-bone interface. An additional consideration is that of geometric nonlinearity, which means that the distribution of strain is likely to change with increasing load. The influence of screw position must, therefore, be systematically evaluated to isolate these

variables and properly understand the behaviour of locked plate constructs (Miller and Goswami, 2007).

8.1.5 Modelling Screws

Some previous studies evaluating fractured bone with osteosynthesis devices have simplified the screws to structural beam elements (Wieding et al., 2012, Seral et al., 2004, Blecha et al., 2005, Wilke et al., 2009). The beam elements are then tied to nodes on the bone and plate. Simplified analyses like these can be used for predictions of fracture gap motion but cannot provide information about strains within the bone around screws. Other studies have incorporated three-dimensional locking screws but have not considered the local strain environment within the bone caused by varying screw position (Moazen et al., 2013, Chen et al., 2013, Stoffel et al., 2003, Salas et al., 2011b).

8.1.6 Chapter Aims

This chapter aimed to evaluate the influence of screw positioning when using locked plating, with particular focus on levels of strain produced at the screw-bone interface. The influence that bone quality had on screw selection was also evaluated. This chapter considers the application of solely locking screws in a plate used as a bridging device.

8.2 Methods

A three-dimensional finite element model was developed using plate and screw geometries identical to those in Chapter 6 and the idealised bone geometry used in Chapter 4 (Figure 8.2). Symmetry was assumed at the centre of the plate and the bone was unrestrained at the fracture site. The total length of bone-plate construct (including symmetry) was 445mm. A bone-plate off-set of 2mm was used.

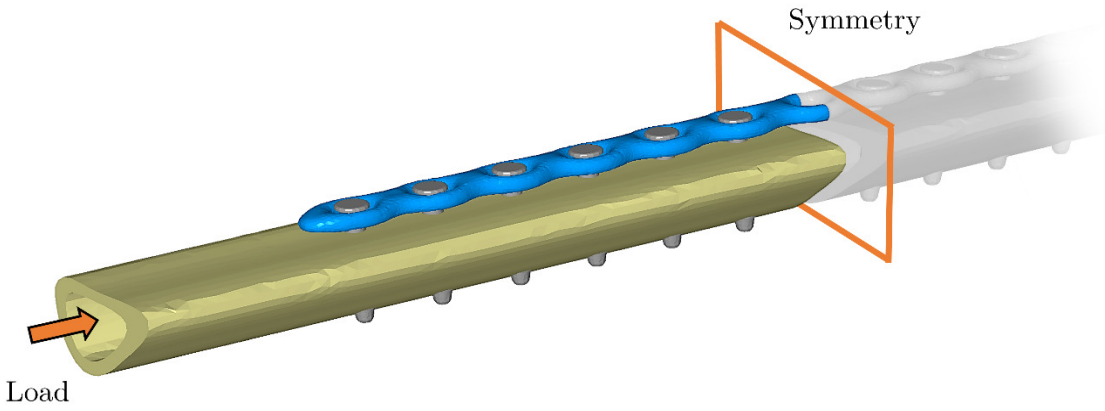

Figure 8.2 - Idealised model of the bone-plate system showing loading and boundary conditions.

8.2.1 Geometry and Material Properties

To evaluate the influence that bone quality had when using different screw configurations, healthy and osteoporotic bone geometry and material properties were incorporated in an identical manner to those described in Chapter 4 (section 4.2.2). These properties include: material orientations for orthotropy; heterogeneous variation in the radial direction; and geometrical changes associated with osteoporosis (Donaldson et al., 2012b).

8.2.2 Contact Interactions

Contact interactions were identical to those described in Chapter 6. These included frictional interactions (coulomb frictional coefficient of 0.3) at the near cortex and tied constraints at the far cortex. The screw threads were explicitly modelled as idealised rings.

8.2.3 Fracture Pattern

Locking plates are often used for comminuted fracture patterns where individual fragments and the fracture site are bridged (Smith et al., 2007). A 10mm osteotomy gap was used to represent this situation; the fracture pattern would be included in AO fracture classification 42C1-C3 (Apivatthakakul et al., 2012). This fracture pattern is often associated with high energy fracture such as car accidents where the fibula is also commonly fractured (Duda et al., 2002).

8.2.4 Loading

Stoffel et al. (2003) found that peak strains within the bone were located at the screw nearest to the fracture site whereas Bottlang et al. (2009b) predicted that strains within the bone are largest at the screw farthest from the fracture site. In Chapter 5 this variation was shown to be a consequence of the loading condition used. Loading in which the bone is permitted to rotate was primarily used in this study; the influence of modelling the knee as a hinge was also considered (discussed later in section 8.3.10). The bone was loaded axially up to 250N, which is similar in magnitude to previous studies (Stoffel et al., 2003, Hogel et al., 2012, Uhl et al., 2008). Torsional loading of 2Nm was also applied to the model. Both the axial and torsional loads were evenly distributed over the free end of the bone. The analysis was conducted using geometric nonlinearity in Abaqus 6.10 (Simulia, Providence, RI, USA).

8.2.5 **Influence of Screw Placement**

The influence of the following screw positioning variables was investigated:

- The total number of screws used;
- Plate span — the distance between the first and last screws on the same side of the fracture site;
- The working length — the distance between the two innermost screws on either side of the fracture;
- Screw spacing — the proximity of the first and second screws closest to the fracture site.

The influence of bone quality and plate rigidity were also examined. In all cases symmetrical screw configurations and the 5.0mm narrow locking plate (described in Chapter 5) were used. To quantify the impact of screw positioning on the bone, the stress-strain environment within the bone was examined around screw hole locations. The volume of bone above 3MPa Von Mises stress at the near and far cortices was quantified around each screw hole location (Equivalent stress volume—EqSV). Although this value is low (equates to around 0.02% strain) it is only intended to be an indication of regions of high stress where bone may undergo resorpsion and therefore loosening (Turner et al., 1997, Giannoudis and Schneider, 2006). As the majority of EqSV was found to occur at the first two screws, the use of a larger value would have also eliminated any comparisons of subsequent screws.

None of the screw configurations tested in healthy or osteoporotic bone produced maximum or minimum principal strains greater than the tensile or compressive yield strains of cortical bone (0.5% or 0.7% respectively). Increased loads could not be used as the yield strength of steel would be exceeded.

8.3 Results

8.3.1 Number of Screws

The influence of the total number of screws was examined using screw configurations C12, C123, C1234 and C123456, which have increasing numbers of screws either side of the fracture site (Figure 8.3).

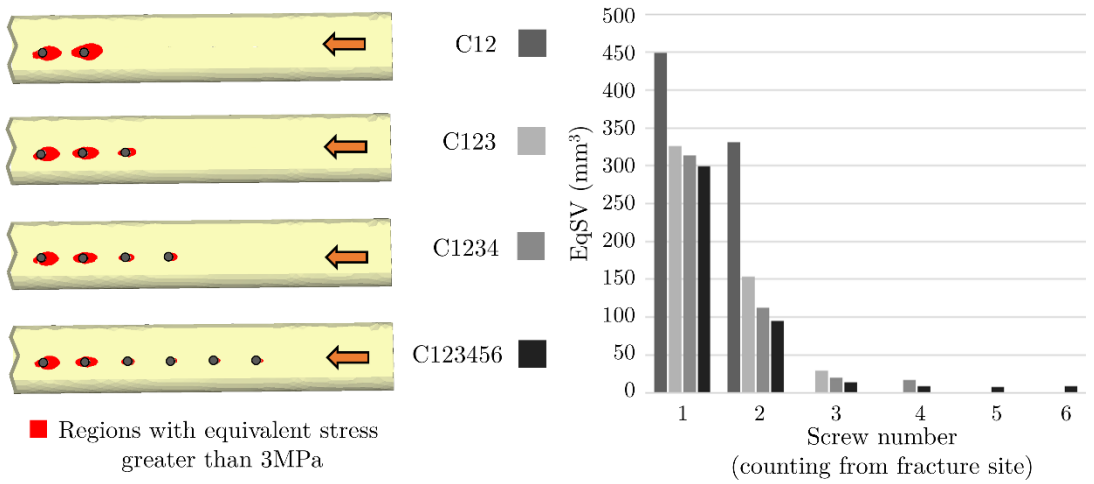

Figure 8.3 - Predicted volumes of bone above 3MPa equivalent stress for different numbers of screws using screw arrangements: C12; C123; C1234; and C123456. The load of 250N is applied from the right and the fracture is located on the left.

Increasing the number of screws was found to decrease EqSV at the first two screws; however, the extent of the decrease reduces sharply with increasing numbers of screw. This is similar to the numbers of engaged threads in a pull-out test, where no significant reduction is stress is attained beyond a certain number of threads (Grewal and Sabbaghian, 1997). It appears that, clinically, three screws are generally adequate but four screws could be considered for osteoporotic patients where the small reduction is strain attained may be more important.

8.3.2 Plate Span

The influence of plate span was examined using screw configurations C12, C13, C14. C15 and C16, which have incrementally increasing distances between the screws either side of the fracture site (Figure 8.4). The number of screws and working length are identical for the configurations.

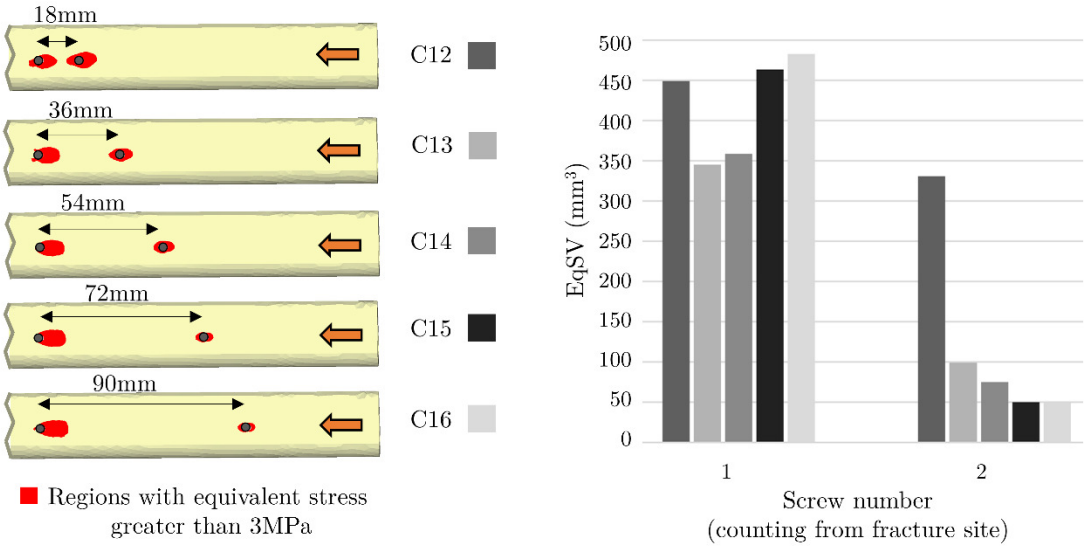

Figure 8.4 – Predicted volumes of bone above 3MPa equivalent stress for different plate span arrangements: C12; C13; C14; C15; and C16. The load of 250N is applied from the right and the fracture is located on the left.

Increased plate span was seen to decrease EqSV around the last screw hole but a decrease was only seen at the first screw in configurations C13 and C14. Previous models have predicted that increased plate span would reduce pull-out forces on the screws (Tan and Balogh, 2009, Perren, 2002). This comparison has shown that the reduction in EqSV at the screw closest to the fracture site is limited because, under axial loading, axial compressive forces dominate. At the last screw, however, tensile loading in the transverse direction (i.e. pull-out) is more significant and therefore a noticeable reduction in EqSV is observed with increased plate span.

8.3.3 Working Length

The influence of working length was examined using screw configurations C123, C234 and C345, which have incrementally increasing distances between the two inner screws either side of the fracture site (Figure 8.5). The number of screws and the screw spacing remained constant between configurations although there is an unavoidable increase in plate length.

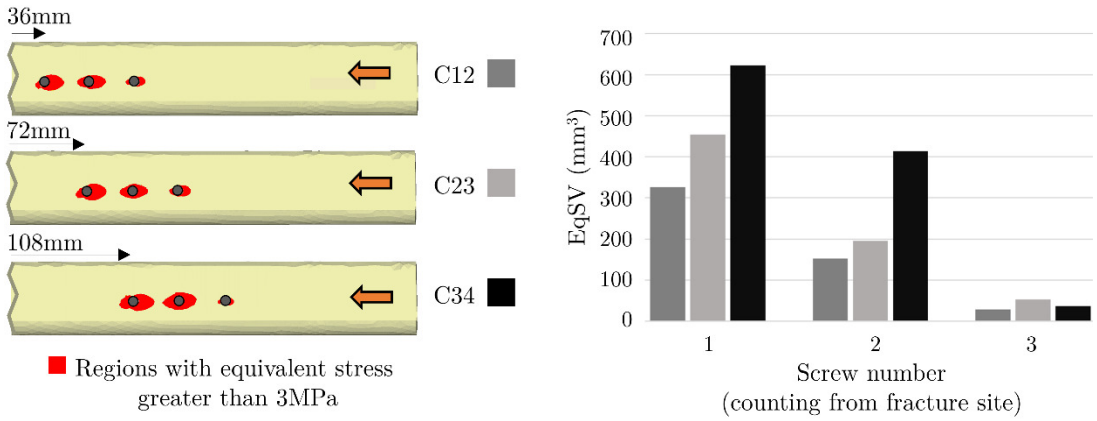

Figure 8.5 – Predicted volumes of bone above 3MPa equivalent stress for the different working lengths: (a) C123; (b) C234 and (c) C345. The load of 250N is applied from the right and the fracture is located on the left.

Increased working length was shown to increase EqSV around the first and second screw holes. These increases are caused by the additional bending of the plate resulting in larger pull-out forces. Sufficient working length is necessary for indirect bone healing; however, in the presence of a fracture gap, excessive working length will not only increase plate stress (Chapter 7) but also intensify the regions of high stress within the host bone.

8.3.4 Changes to Stress Distribution with Load

Von Mises stress contours were plotted for screw configuration C123456 (Figure 8.6). The location of peak stress can be seen to migrate toward the fracture site with increasing load. As discussed earlier, due to plate bending, locked plating exhibits a geometrically nonlinear load-deformation response (Chapter 7). The level of load, therefore, can alter the response and conclusions regarding screw placement.

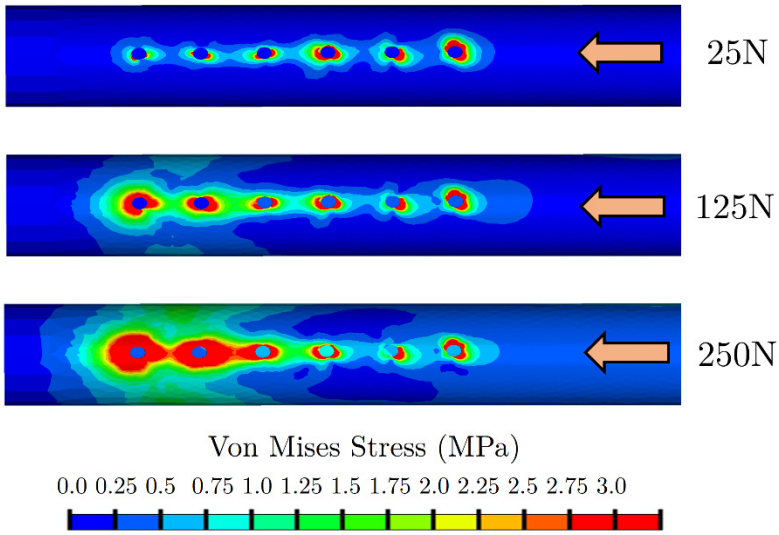

Figure 8.6 - Changes in von Mises stress distribution with increasing load for screw configuration C123456. The load is applied from the right and the fracture site is on the left.

In Chapter 6 it was seen that bone loaded in a restrained manner (i.e. clamped) produced the peak stresses within the bone at the end of the plate; whereas, the loading condition where the bone ends could rotate produced peak strains at the screws closest to the fracture site. Figure 8.6 shows that at very low loads the distribution of stress is more like a clamped loading condition; at larger loads, it migrate towards the fracture gap as seen in pinned loading conditions.

8.3.5 The Proximity of the First and Second Screws

The comparison of the number of screws (section 8.3.1) revealed that the first two screws closest to the fracture site have the largest EqSV associated with them, regardless of the number of screws (Figure 8.3). As three screws are the minimum recommended by AO guidelines, the influence of the position of the second screw was examined using screw configurations C126, C136, C146 and C156 (Figure 8.7). The number of screws, working length and plate length remained constant between configurations. Additionally, the EqSV regions are shown for loads of 125N and 250N (Figure 8.7).

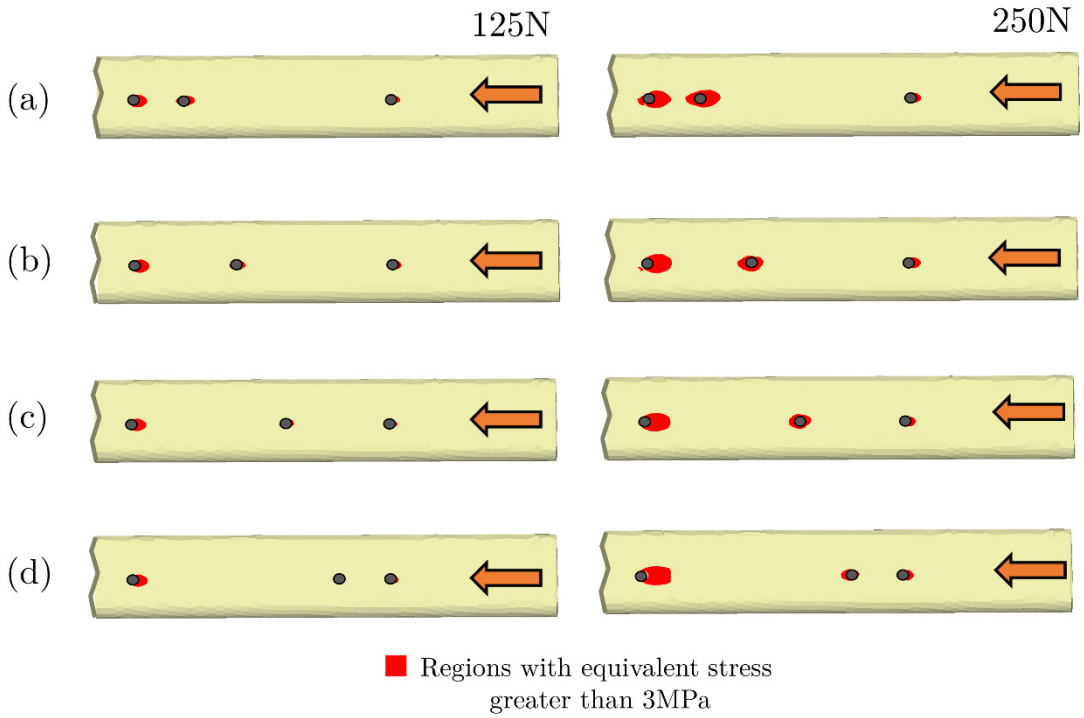

Figure 8.7 - The predicted EqSV depending upon the proximity of the second screw from the first: (a) C126; (b) C136; (c) C146; and (d) C156. Two levels of load are applied from the right and the fracture is located at the left.

The EqSV around each screw is quantified in Figure 8.8. At 125N there are only minimal differences between the screw configurations; however, at 250N an increased spacing between the first and second screws greatly reduces EqSV at the second screw. At the first screw, C126 and C156 produce the largest EqSV while C136 and C146 are approximately 15% lower; this is due to varying proportions of transverse and axial load transfer. Although a relatively small load was used, it is likely that larger loads would further increase the differences seen between configurations.

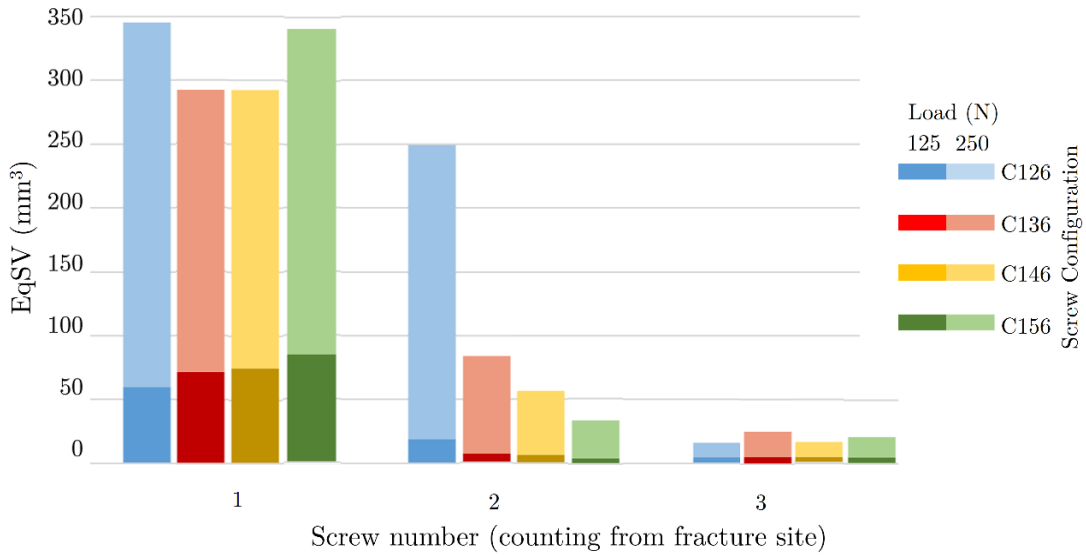

Figure 8.8 - EqSV predictions for different configurations in healthy bone where results for 125N are shown in the dark shade bars and results for 250N are shown in the lighter shade.

8.3.6 **Osteoporotic Bone**

The influence of the proximity of the first and second screws from the fracture site was evaluated for osteoporotic bone. The EqSV around each screw is shown in Figure 8.9. A similar pattern of EqSV is seen to that of healthy bone (Figure 8.8), but the total volumes are considerably larger. The relative differences between screw configurations are also larger with C136 reducing EqSV by 32% at the first screw compared with C126—double the reduction achieved in healthy bone.

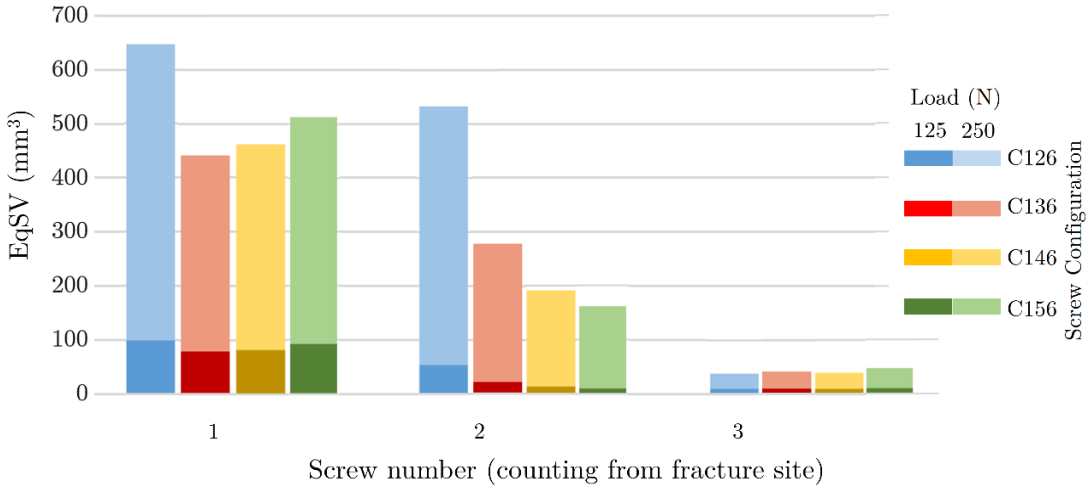

Figure 8.9 - EqSV predictions for different configurations in osteoporotic bone where results for 125N are shown in the dark shade bars and results for 250N are shown in the lighter shade.

Osteoporotic bone was also found to have a larger proportion of EqSV at the far cortex compared with healthy bone (Table 8.1). This supports previous studies' recommendations that bi-cortical fixation should be used in osteoporotic bone (Gautier and Sommer, 2003).

Table 8.1 - Proportion of EqSV at the far cortex in the first screw for selected screw configurations.

Screw Configuration	**Proportion of EqSV at the Far Cortex (%)**	
	Healthy	Osteoporotic
C123456	13.4	48.2
C1234	11.6	44.6
C123	10.4	40.5
C12	12.3	43.0
C126	13.9	47.7
C136	4.1	27.1
C146	4.3	19.1
C156	4.3	17.0
Average	9.3	35.9

8.3.7 **Stress in the Plate**

Although not the focus of the study, the peak von Mises stress at the centre of the plate was compared for the various screw configurations (Figure 8.10). It was found that working length was the primary determinant of plate stress while all other screw positioning variables had minimal influence of plate stress.

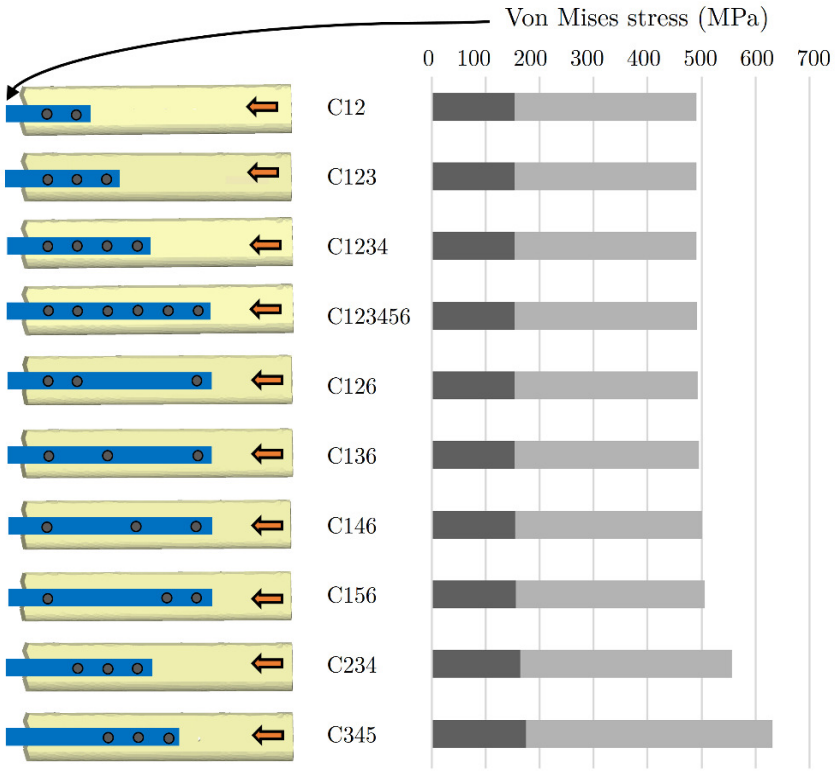

Figure 8.10 - Predicted Von Mises stress at the centre of the plate using different screw configurations. The load is applied from the right and the fracture site is on the left. The dark grey bar shows the stress at 125N and the lighter shade shows the value at 250N.

8.3.8 Plate Rigidity

To evaluate the influence of plate rigidity, screw configurations C126 and C136 were re-analysed using three different plate Young's moduli: 105 GPa, 205 GPa and 300GPa. These variations represent changes in the axial and flexural rigidity of the plate while Young's moduli of the screws remain unchanged at 205GPa. The EqSV predictions in Figure 8.11 show that reducing the plate rigidity to 105GPa increased EqSV around the first screw by as much as 83%. Similarly, increasing the plate rigidity to 300GPa reduced the EqSV around the first screw by 20%. The relative differences between configuration C126 and C136 at the first screw remain unchanged.

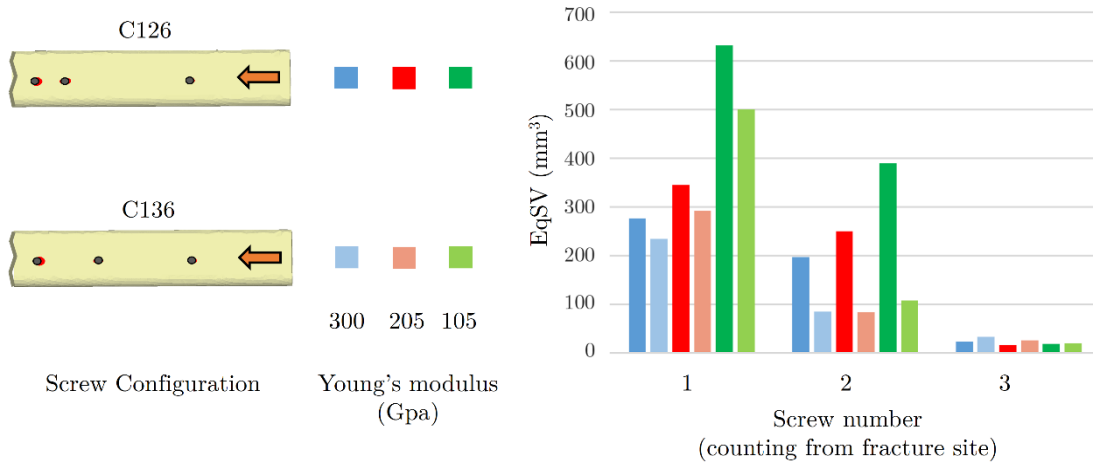

Figure 8.11 - Predicted EqSV using screw configurations C126 and C136 for differing plate rigidities. The dark bar shows the stress at 125N and the lighter shade shows the value at 250N.

8.3.9 Torsional Loading

Under torsional loading, positioning of screws closer to the fracture site reduced EqSV at the first screw. Therefore, in situations where torsional loading is critical (such as in the humerus) placing screws closer to the fracture gap may be the most beneficial configuration.

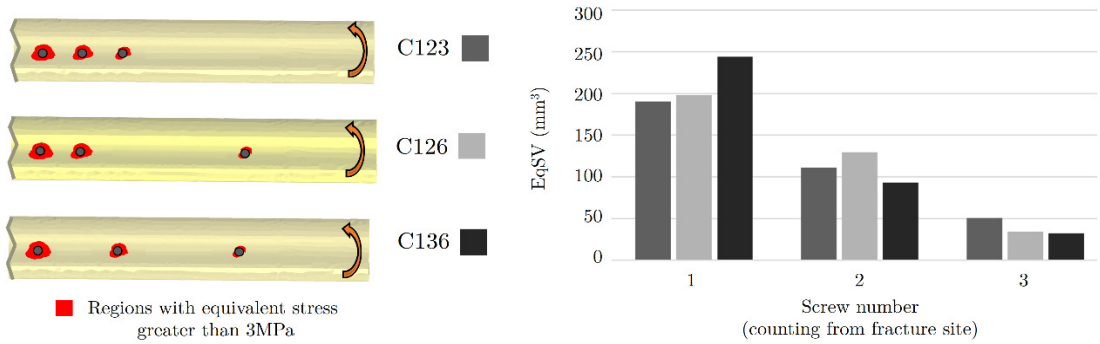

Figure 8.12 – Predicted EqSV under torsion for screw configurations C123, C126 and C136. The load is applied from the right and the fracture site is on the left.

The number of screws was the other major factor influencing EqSV under torsional loading (Figure 8.13). These results are similar to Stoffel et al. (2003) who found that torsional stiffness was related to the number of screws and not the position.

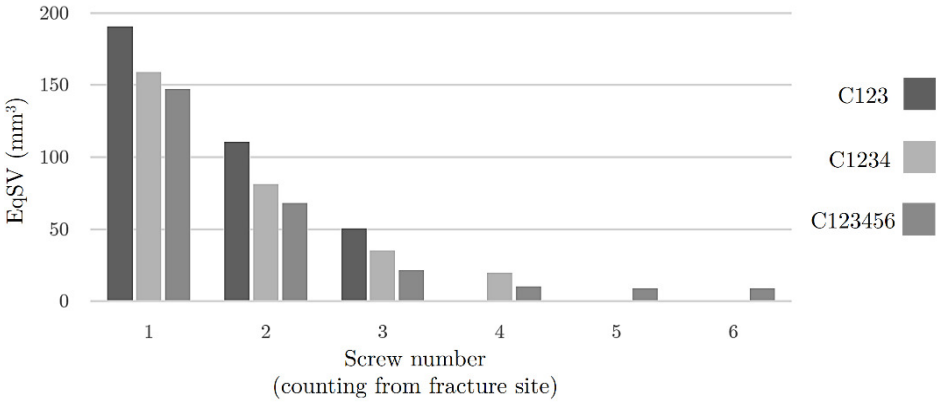

Figure 8.13 - Predicted EqSV under torsion for different numbers of screws using configurations C123, C1234 and C123456. The load is applied from the right and the fracture site is on the left.

8.3.10 **Use of a Hinge at the Knee**

In Chapter 6 the loading condition was shown to dramatically alter the locations of peak stress within the bone. Modelling the knee as a hinge increases the restraint provided to the bone-plate system as proximal rotation is only permitted in a single plane. The angle of the plate relative to the hinge is also influential as the plate is forced to bend bi-axially; this was chosen to be 45 degrees.

The use of a hinged loading condition was found to produce large regions of EqSV both near and far from the fracture site (Figure 8.14). Compared to the pinned loading case, the total magnitude of EqSV was reduced around screws close to the fracture site and was increased around screws far from the fracture site. The use of four screws instead of three reduced EqSV by 36% at the first screw and 41% at the last screw. Increasing the number of screws from four to six had less influence with 23% and 8% reductions in EqSV respectively. Similar to the pinned loading condition, positioning additional screws closer to the fracture site was found to increase EqSV around all screws.

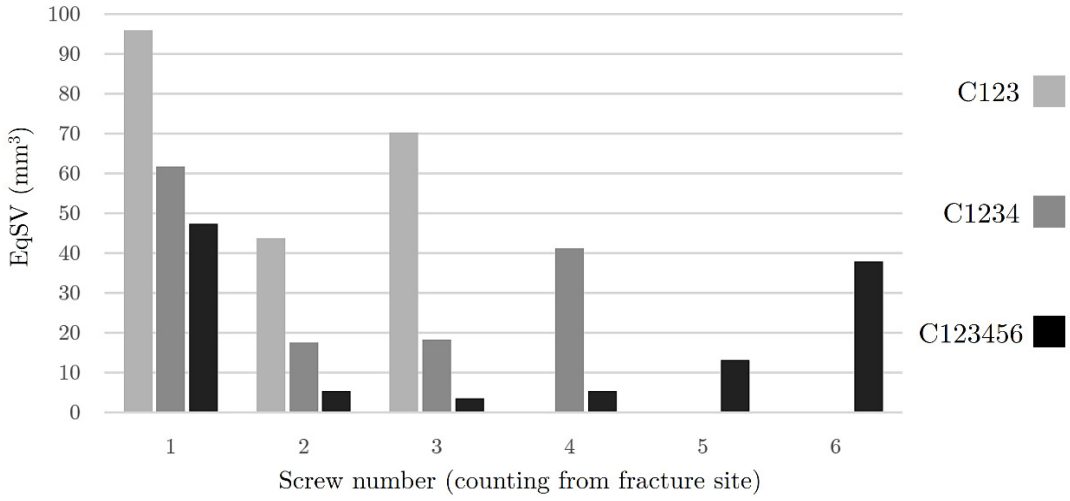

Figure 8.14 - Predicted EqSV under axial loading modelling the knee as a hinge for different numbers of screws using configurations C123, C1234 and C123456.

8.4 Discussion

In simple fractures where interfragmentary contact can occur, fracture reduction is more important than screw placement (Leahy, 2010). Nevertheless, when using locked plating, selection of the correct working length is crucial to mimimise plate stress and achieve the correct level of interfragmentary motion, as discussed in Chapter 7. In fractures that are bridged the locking plate must support the full weight-bearing loads. In these situations the demands upon the fixation are much greater and screw positioning can greatly influence the strains induced in the implants and the bone.

8.4.1 Working Length

In Chapter 7 additional working length was shown to increase the stress within the plate. This chapter has shown that greater working lengths also increased the strains within the bone around the screw holes. Therefore, there is a compromise between generating sufficient motion at the fracture site and reducing the demands upon the fixation. Once the required working length is selected, the total plate length, number of screws and position of the remaining screws must be determined.

8.4.2 Plate Length

This chapter found that plate length, in itself, did not influence EqSV; however, other variables such as working length, screw number and the proximity of the first two screws can influence EqSV and require additional plate length. Plate length did not have any influence of plate stress. The key determinant of plate stress was working length; increasing the working length by one screw either side of the fracture increased plate stress by 7% at 125N and 16% at 250N. These findings agree with the findings of Chapter 7 that geometric nonlinearity is fundamental to the prediction.

8.4.3 Placement of Additional Screws

This chapter found the largest regions of high stress within the bone at the screw closest to the fracture gap. These regions of high stress correspond to those reported by Stoffel et al. (2003) who suggested that placement of additional screws could alleviate this stress. This chapter presents contradictory findings that additional screws placed close to the fracture site actually increase the levels of stress within the bone. Therefore additional screws should be placed at least one screw hole away from the first screw. Although plate breakage is an issue, loosening of screws continues to be reported as the most frequent complication in locking plate constructs (Stoffel et al., 2003, Sommer et al., 2003).

8.4.4 Plate Material

This chapter has found that more flexible implants increase screw-bone interface stress. This was expected as Huiskes et al. (1985) and Donaldson (2012a) presented similar findings for reduced stiffness titanium screws in unilateral fixators. On the other hand, in a cadaveric distal femur study, Zlowodzki et al. (2004) found that titanium LISS implants had a lower incidence of distal cut-out than the more rigid angled blade plate under cyclic load. The reasons for this result are not clear as the implants have different geometries and so the influence of material or rigidity cannot be directly compared.

8.4.5 Bone quality

As would be expected, this chapter demonstrated that osteoporotic bone is more sensitive to screw placement than healthy bone. While the trends remain similar, the impact of the placement of the second screw from the fracture site is more pronounced than in healthy bone. A reduction in EqSV obtained at the first screw by using C136 compared with C126 was 15.4% in healthy bone; in osteoporotic bone the reduction was 32%. Bone quality can also considerably influence the distribution of load between the near and far cortices. In healthy bone the maximum proportion of EqSV at the far

cortex for any configuration was 13.9% (average of all configurations tested was 9.3%); in osteoporotic bone it was 48.2% (average of 35.9%). Therefore, screw position and bi-cortical fixation is clearly more critical in osteoporotic bone. Under axial loading the use of four screws instead of three was not substantial, only reducing EqSV at the first screw by 5.9% in osteoporotic bone compared with 3.9% in healthy bone. Under torsional loading, however, a 22% reduction in EqSV was observed from using the additional screw. Under torsional loading total volumes of the EqSV in osteoporotic were lower than and healthy bone. This may be due to the larger cross-sectional width of osteoporotic bone.

8.4.6 **Are Two Screws Enough for Selected Fractures?**

There is some discussion as to whether two locking screws may be enough in some selected scenarios such as humeral fractures (Hak et al., 2010a, Grawe et al., 2012). This study found that increasing the number of screws from two to three reduced the EqSV at the first screw by 27.3% and 35% in healthy and osteoporotic bone respectively. Humeral fractures are not exposed to the same level of axial load as tibial fractures; nevertheless, under torsion, similar decreases were observed (approximately 34%).

8.4.7 **Risk of loosening**

Under the loads used in this study (250N) no screw configuration produced strains within the bone that reached the yield strain of cortical bone (approximately 0.5-0.7%). While screw pull-out is rare in locked plating, screw cut-out has been observed clinically (Leahy, 2010), which results in two possible implications for the study: 1) the loads used in study are not large enough to cause material failure; or 2) loosening may occur at strains significantly lower than the yield strain of bone. The use of larger loads would have caused unrealistic stresses within the plate; however, the loading condition could be overly-flexible thereby generating plate stresses that are too high. Alternatively, the threshold strain for bone resorpsion has been reported to be as low as 0.36% (Sugiura

et al., 2000). The peak strains observed the study were approximately 0.3% occurring in osteoporotic bone, when using titanium plates and under torsional loading. As the incidence of screw loosening is low (Sommer et al., 2003) it should be expected that only specific cases indicate loosening. The reduction in bone stiffness under cyclic loading could also play a role in increasing the strain levels at the screw-bone interface (Turner and Burr, 1993). Moreover, micro-movement at the screw-bone interface may encourage loosening in addition to strain exposure (Evans et al., 1990, Uhthoff, 1973).

8.4.8 Mechanical Explanation for Observations

Cronier et al. (2010) demonstrated that, under bending loads, greater spacing of screws can distribute forces, reducing the localised strain within the bone (or surrogate) around screws. This study has shown that under axial loading the mechanical behaviour can be different. The first two screws on either side of the fracture site were found to have the largest EqSV associated with them under axial loading, regardless of the total number of screws or their position. This finding was investigated further; an explanation for this phenomenon is given in Appendix C.1.

8.4.9 Hinge at the Knee

When the knee is modelled as a hinge, the influence of screw positioning is altered. Similar trends were observed with regard to the number of screws; however, EqSV around the last screw in the plate became comparable to the first. This is due to the increased bending created by the hinge. Despite the changes to the loading, allowing a single hole space between the first and second screws closest to the fracture gap reduced EqSV in all screws by between 10-16%.

8.4.10 **Limitations**

Material nonlinearity was not included, but would not have influenced the results. If the long-term response of the system was required, healing within the fracture gap and cyclical loading would be necessary; in this case, material non-linearity could have greater influence. Cancellous bone was ignored as it was assumed to contribute minimally to the result; similar previous studies have shown that this is the case (Cheung et al., 2004).

Muscle forces were not included in the models. The influence of muscle forces was examined (Appendix C.2) using muscle force data from Duda et al. (2002) and was found to have minimal influence on stress within the plate, strains within the bone or fracture gap motion and was therefore concluded to be unnecessary for the evaluation of screw positioning effects in the tibia.

8.5 Conclusions

- Working length is the primary determinant of plate stress; all other screw positioning variables have negligible influence.
- Several screw positioning variables influence the stress levels in the bone around screws under axial load: working length, the distance between the first and second screws. In terms of the total number of screws the reduction of stress within the bone is negligible beyond four screws.
- Plate rigidity can considerably influence stress levels within the bone.
- Bi-cortical fixation and separation between the first and second screws are more important in osteoporotic bone.

9

Mechanical Performance of Alternative Screw Types Used with the LCP

9.1 Introduction

When using plating the type of screw used is one of the biggest considerations as it determines how the plate will be used. There is debate surrounding the use of different screw types (Gautier, 2009); it is likely that different screws will be appropriate for different fracture patterns or locations. Since the advent of locking plates two particular developments use locking screws in a slightly different way to the usual bi-cortical fixation (LCP) (Figure 9.1a):

- Uni-cortical fixation (UCF) uses screws that penetrate the entrant cortex only (Figure 9.1b)

- Far-cortical locking (FCL) where screws engage the far cortex only (Figure 9.1c and 1d)

In this chapter, these two applications will be examined with regard to their mechanical performance in healthy and osteoporotic bone.

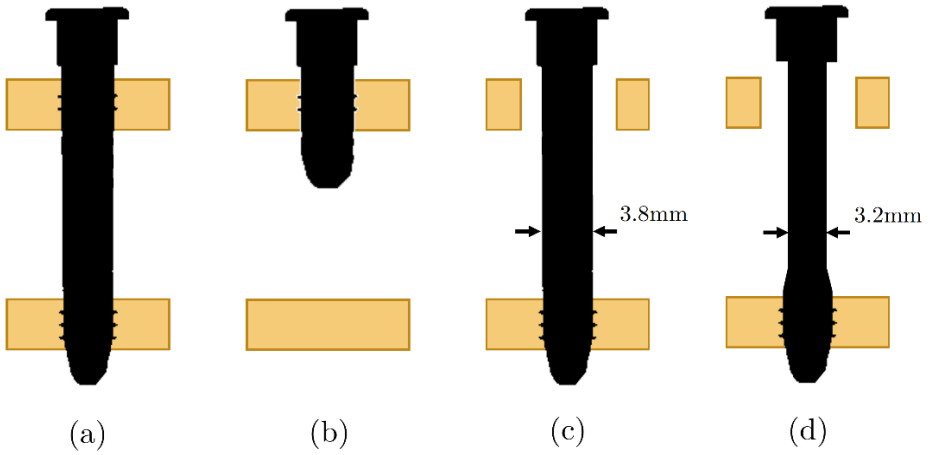

Figure 9.1 – Examples of locking screws with: (a) bi-cortical fixation (LCP); (b) uni-cortical fixation (UCF); (c) far-cortical locking (FCL); and (d) far-cortical locking using a screw with reduced core diameter (FCL-3.2).

9.1.1 Uni-Cortical Fixation

As locking plates maintain a secure screw-plate connection, the fixation does not rely on the exit cortex in the same manner as compression screws do (Gardner et al., 2004). This was demonstrated in Chapter 8 where the largest stress concentrations were found at the near cortex. Choosing the correct bi-cortical screw length is important as it safeguards against soft tissue damage on the exit cortex (Perren, 2002). Shorter uni-cortical screws do not suffer from this risk as only the entrant cortex is penetrated. Nevertheless, like compression screws, uni-cortical screws have been associated with poor performance in the metaphysis or in bone of poorer quality (Bucholz et al., 2006, Perren, 2002). This has been attributed to the reduced cortical thickness available to resist torsional loads (Gautier, 2009, Gautier and Sommer, 2003). Dunlap et al. (2011) found that when using uni-cortical screws the bending stiffness of plated bone is similar to that produced by bi-cortical locking screws; however, there is a reduction in the torsional stiffness. The inclusion of even a single bi-cortical locking screw has been shown

to greatly increase torsional stiffness of uni-cortical constructs (Roberts et al., 2007, Dunlap et al., 2011). Although UCF has been shown to have lower failure loads than the LCP (Afshar et al., 2012), a recent study found that there was no significant difference if the uni-cortical screws abut the exit cortex (Overturf et al., 2013). This shows that a contribution is made from the exit cortex, which cannot be guaranteed in UCF. Nevertheless, due to their clinical advantages, uni-cortical fixation will continue to be used.

9.1.2 **Far-Cortical Locking**

It is recognised that plating produces differential interfragmentary motion (IFM) (Bottlang et al., 2010a). It has recently been proposed that more parallel gap motion could be achieved with locking screws using the 'far cortical locking' concept (Bottlang et al., 2010a, Bottlang and Feist, 2011). Far-cortical locking screws engage with the far cortex of the bone only. This involves over-drilling the entrant cortex so that the screw shaft is not in contact with the bone allowing a much longer length of screw to bend under load, thereby increasing IFM. Similar techniques have been described by Gardner et al. (2010) utilising 'near cortical slots' and by Dobele et al. (2010) utilizing 'dynamic locking screws'. All studies demonstrate that this increases the motion at the fracture site, particularly at the near cortex (Bottlang et al., 2009b, Dobele et al., 2010, Gardner et al., 2010). The additional length of screw free to bend increases the flexibility of the construct while maintaining the same bone-plate off-set. This is beneficial as off-sets greater than 2mm have been shown to greatly compromise the load to failure (Ahmad et al., 2007). Huiskes et al. (1985) and Donaldson et al. (2012a), however, noted that reductions in stiffness of uni-lateral devices, such as using titanium screws, resulted in increased screw-bone interface stresses/strains. As FCL reduces construct stiffness it is likely that they will also produce greater stresses at the screw-bone interface. Moazen et al. (2013) predicted that FCL screws would greatly increase pull-out forces under

both axial and torsional loading. There is therefore a compromise between construct stiffness and the detrimental impact on the host bone, which must be considered.

Although the influence that uni-cortical and far-cortical locking screws have on the stiffness of bone-plate systems has been investigated their impact on the local strains within the bone has not. It is likely that the strains within the bone will be very different depending on the method of screw fixation and the bone quality.

9.1.3 Chapter Aim

The aim of the chapter is to examine the influence that uni-cortical fixation (UCF) and far-cortical locking (FCL) have on the performance of the LCP both in terms of motion across the fracture site and strains within the bone.

9.2 Methods

The finite element model developed in Chapter 6 was modified to simulate UCF and FCL (Figure 9.1a-d).

9.2.1 Geometry

Tibial cross-sectional geometries for healthy and osteoporotic bone were taken from Chapter 4. The various screw types were modelled with identical dimensions to those described in Chapter 5. The uni-cortical screw (Figure 9.1b) was identical to the bi-cortical screw (Figure 9.1a) but with reduced shaft length. Two geometries of FCL screw were considered: one with cross-sectional dimensions identical to the other screws (Figure 9.1c); and one with a reduced diameter of screw shaft, which will be referred to as FCL-3.2 (Figure 9.1d). Only screw threads in contact with the bone were modelled. The same screw configuration and a 13 hole plate were used for all screw types. Screw were used in the first, second and sixth holes on either side of the fracture gap with the central hole left empty.

9.2.2 Contact Interactions

The FCL screws were simulated by removing the contact interaction at the near cortex. In reality, over-drilling of the near cortex means that contact can occur at higher loads (Bottlang et al., 2010a), however, this aspect was not considered. In all cases the screw-bone interaction used a Coulomb frictional coefficient of 0.3.

9.2.3 Material Properties

The respective material properties for healthy and osteoporotic bone described in Chapter 4 were adopted for this study.

9.2.4 Loading

The bone-plate construct was loaded up to an axial load of 250N. An applied torque of 2Nm was also considered. The analysis was geometrically nonlinear and conducted using Abaqus 6.10 (Simulia, Providence, RI).

9.3 Results

The results of the UCL, FCL and FCL-3.2 simulations were compared against those for the bi-cortical LCP.

9.3.1 Gap Motion Comparison

The use of FCL screws more than doubled the IFM at the near cortex (103% increase) but only produced 14% greater motion at the far cortex at a load of 250N (Figure 9.2). The FCL-3.2 increased near and far cortex motion by 45% and 31% respectively versus the original FCL model; the increase versus the bi-cortical LCP was 193% and 50% respectively.

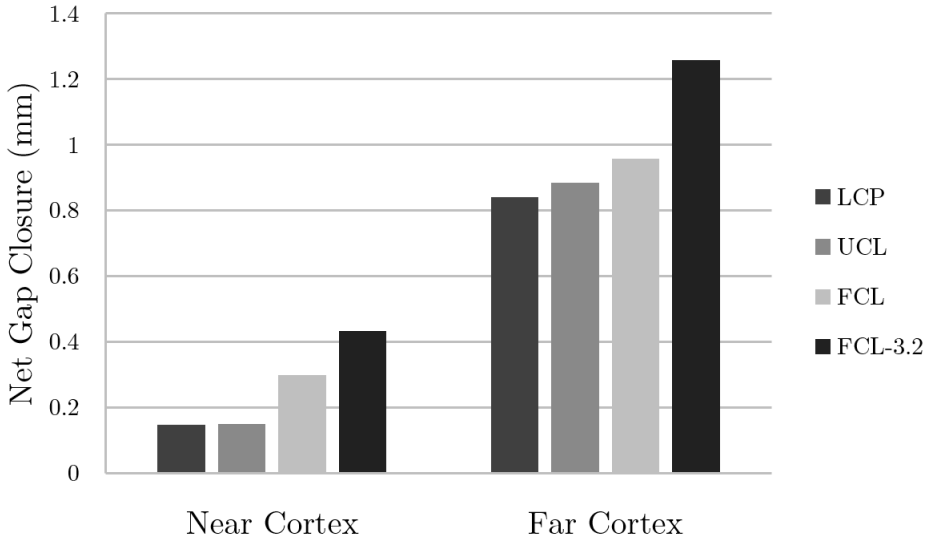

Figure 9.2 – Net gap closure at the near and far cortices for the difference screw types at 250N.

In all screw types, the majority of far cortex IFM was produced by plate bending. In the FCL models the relative movement between the FCL screws and the bone at the near cortex was 0.076mm representing 35% of the total near cortex IFM at 250N. Using the 3.2mm FCL screws, this relative movement increased to 0.105mm or 51% of near

cortex IFM. The gap opening around the near cortices of the FCL screw can be seen in the exaggerated deformed shapes shown in Figure 9.3.

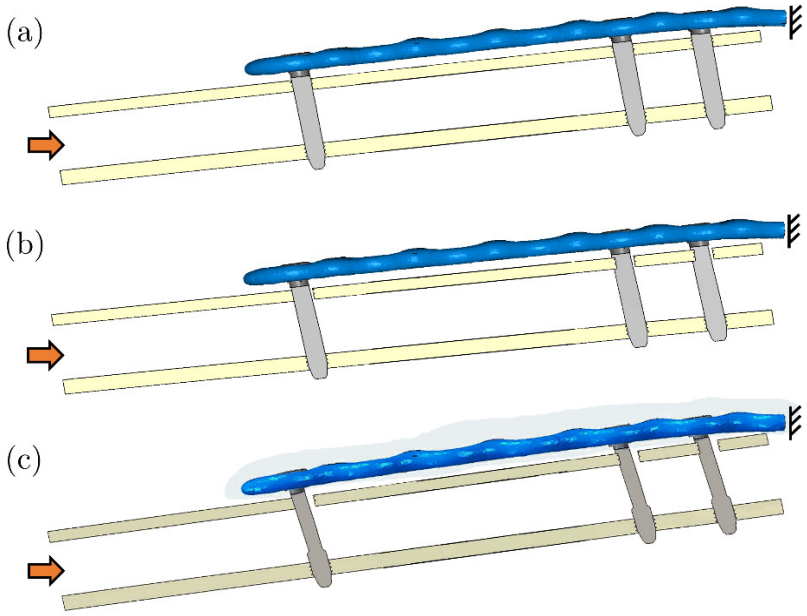

Figure 9.3 – Deformed shape of (a) the LCP model; (b) the FCL model and (c) the FCL model with reduced screw diameter. Deformation scale factor is ten times.

9.3.2 EqSV under Axial Loading

The minimum and maximum principle strains around the two screws closest to the fracture site under axial loading for all screw types and bone quality are shown in Figures 9.4 and 9.5. The LCP produced the smallest peak strains followed by UCF then FCL. All screw types produced larger strains in osteoporotic bone, although in the case of FCL-3.2 this increase was substantial.

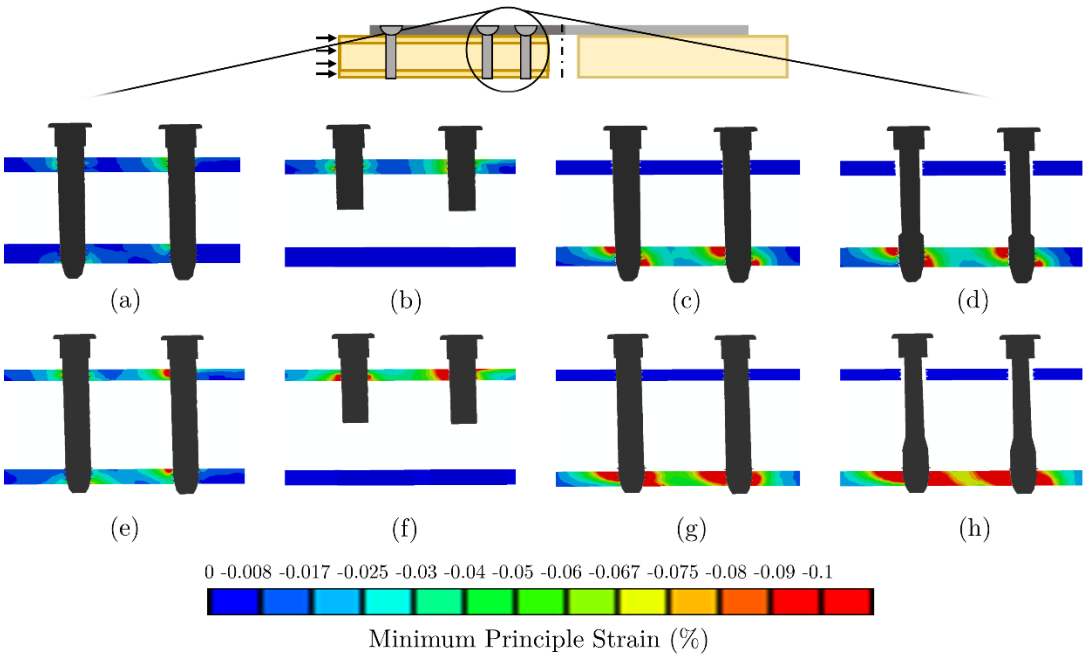

Figure 9.4 - Minimum principal strains for the different screw types: (a, e) Bicortical LCP; (b, f) UCF; (c, g) FCL; and FCL-3.2 (d, h) at a load of 250N for healthy bone (a-d) and osteoporotic bone (e-f).

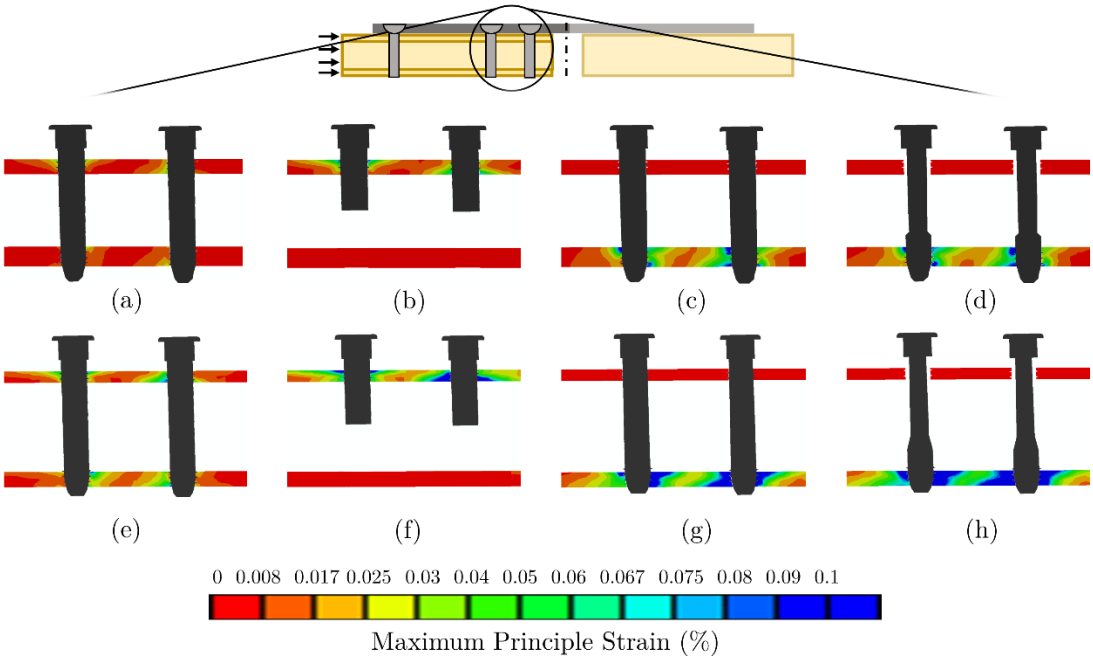

Figure 9.5 - Maximum principal strains for the different screw types: (a, e) Bicortical LCP; (b, f) UCF; (c, g) FCL; and FCL-3.2 (d, h) at a load of 250N for healthy bone (a-d) and osteoporotic bone (e-f).

The volume of bone around a screw with Von Mises stress greater than 6MPa was calculated for each screw type and bone quality and was termed EqSV (Equivalent stress volume). This value was chosen to clearly illustrate the differences between the screw types, which show considerable stress-strain variation. The EqSV can also vary considerably depending on which screw is chosen so the values for all three screws is shown for healthy bone (Figure 9.6) and osteoporotic bone (Figure 9.7). The value of EqSV for the bi-cortical LCP is the sum of the near and far cortices, whereas in all other screw types only a single cortex was used; despite this, in all cases the bi-cortical LCP produced the lowest EqSV. This was attributed to the better load distribution from two cortices sharing the load. UCF produced a similar EqSV distribution to the LCP with the first two screws transmitting the majority of the load. In both FCL screw types there was more even distribution of EqSV between the screws although the total magnitude was much greater. UCF generally produced smaller EqSV than both FCL screw types; however, under larger loads in osteoporotic bone they are comparable at the first screw nearest the fracture gap (Figure 9.7). Healthy bone appeared to tolerate the narrower FCL-3.2 screws better than osteoporotic bone; the average increase in EqSV produced by FCL-3.2 compared standard FCL was 22% in healthy bone compared to 54% in osteoporotic bone.

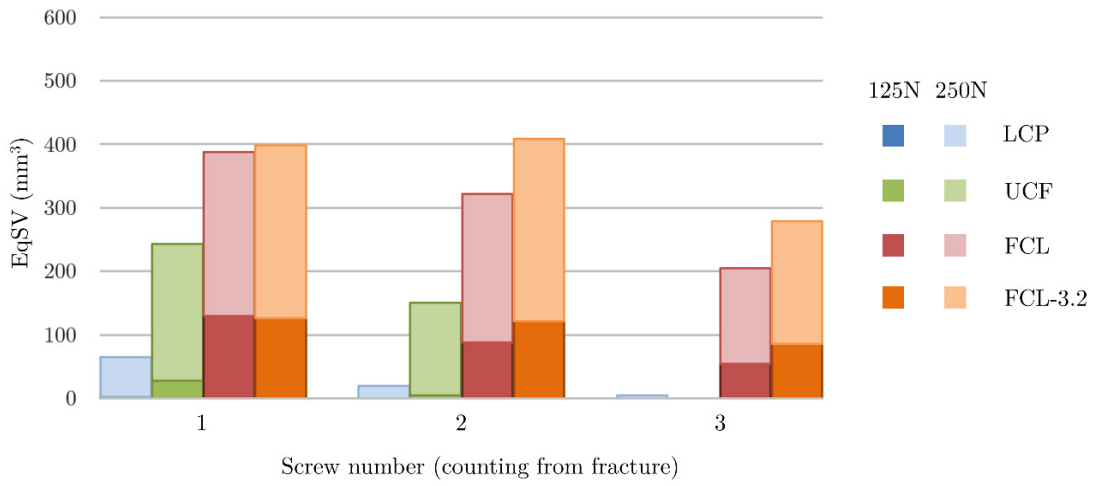

Figure 9.6 – Volume of elements with equivalent stress greater than 6MPa (EqSV) for the different screw types in healthy bone at 125N and 250N.

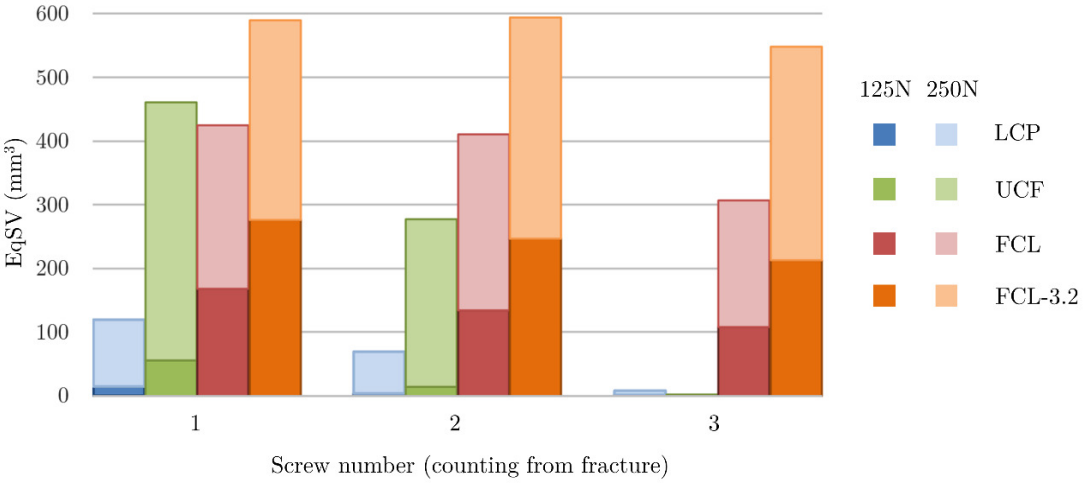

Figure 9.7 - Volume of elements with equivalent stress greater than 6MPa (EqSV) for the different screw types in osteoporotic bone at 125N and 250N.

Only the osteoporotic FCL models produced strains above than the tensile yield strain of cortical bone (0.5%) (Donaldson et al., 2012b) with a total bone volume of 0.074mm^3 exceeding this value. A slightly greater volume of bone (1.22mm^3) had exceeded the compressive yield strain (0.7%) (Donaldson et al., 2012b). In both cases the largest strains were located at the screw closest to the fracture.

9.3.3 EqSV under Torsional Loading

Under torsional loading the LCP produced the lowest EqSV and UCL fixation produced the largest (Figure 9.10 and Figure 9.10). Both types of FCL screw produced similar levels of EqSV but the distribution at each screw varied. The relative increases in EqSV between healthy and osteoporotic bone at the first screw were: -59% for the LCP; 34% for UCF; 106% for FCL; and 137% for FCL-3.2.

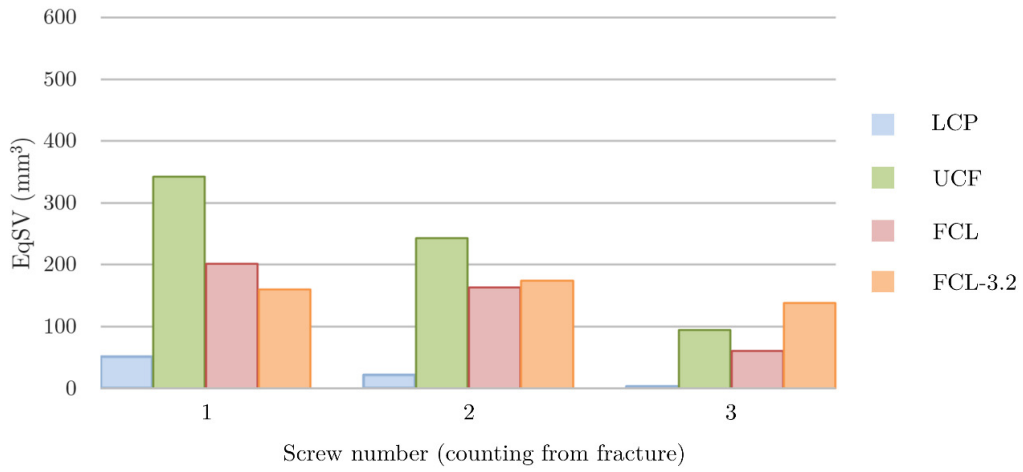

Figure 9.8 - Volume of elements with equivalent stress greater than 6MPa (EqSV) for the different screw types in healthy bone at 2Nm.

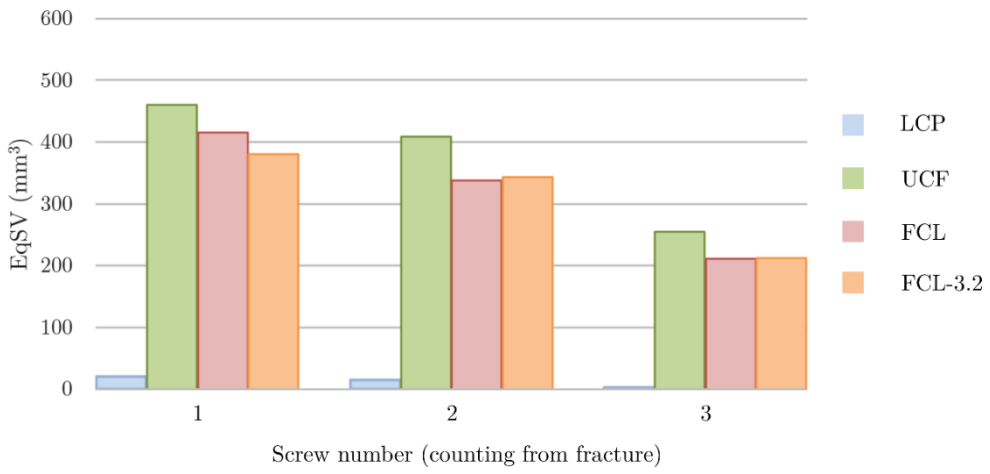

Figure 9.9 - Volume of elements with equivalent stress greater than 6MPa (EqSV) for the different screw types in osteoporotic bone at 2Nm.

9.4 Discussion

This study found that, compared to the bi-cortical LCP, far-cortical locking (FCL) screws increased IFM by 14-50% at the far cortex, whereas uni-cortical fixation (UCF) had minimal influence (<5% change). This means that FCL could have advantages for increasing mechanical stimulation at the fracture site. Both FCL and UCF, however, increased screw-bone interface stress. Under axial loading, EqSV levels were highest for the narrower FCL-3.2 screws; whereas under torsion, UCF produced the highest. Uni-cortical screws have been previously described as having inferior torsional resistance due to the smaller length of screw shaft engaged (Gautier and Sommer, 2003). Compared to the LCP, EqSV levels were 3.7 times larger for UCF screws and 5 times larger for FCL at the first screw closest to the fracture site. LCP and UCF screws had minimal EqSV at the third screw whereas FCL screws produced comparable levels at all screws.

In osteoporotic bone, UCF produced 3.9 times greater EqSV than the LCP under axial loading; similar to the increase observed in healthy bone. The relative increase in EqSV under torsion was nearly 7 times in healthy bone and 22 times in osteoporotic bone. This demonstrates that osteoporotic bone is not intrinsically sensitive to UCF; rather, UCF is highly sensitive to torsional loading and osteoporotic bone exaggerates this effect. This provides a biomechanical evidence to support the 'screw working length' explanation by Gautier (2009) where the reduced cortical thickness of osteoporotic bone reduces the lever arm with which torsional forces are resisted. Under torsional loading, the volume of EqSV for the LCP was actually lower in osteoporotic bone than in healthy bone. This was attributed to the greater cross-sectional dimensions of osteoporotic bone. Under axial loading, the tensile strain patterns observed are clearly indicative of push-in–pull-out (Figure 9.5a, b, e, f).

It should be noted that EqSV could be reduced in the LCP and UCF by using screw configuration C136 (Chapter 8); however, configuration C126 was chosen to make the

results more comparable (in magnitude) to the FCL. Screw configuration did not have a significant influence on EqSV when using FCL screws.

9.4.1 **Comparisons with Bottlang et al.**

Histological results from Bottlang et al. (2010b) do not show the dramatic difference that would be expected from Bottlang et al. (2009b) where the stiffness of the FCL was 88% lower (Figure 9.10). The results are more similar to those predicted by the present study's model which suggests, assuming the callus development to be proportional to the movement, the far cortex callus development would be marginally increased and the near cortex would be approximately double.

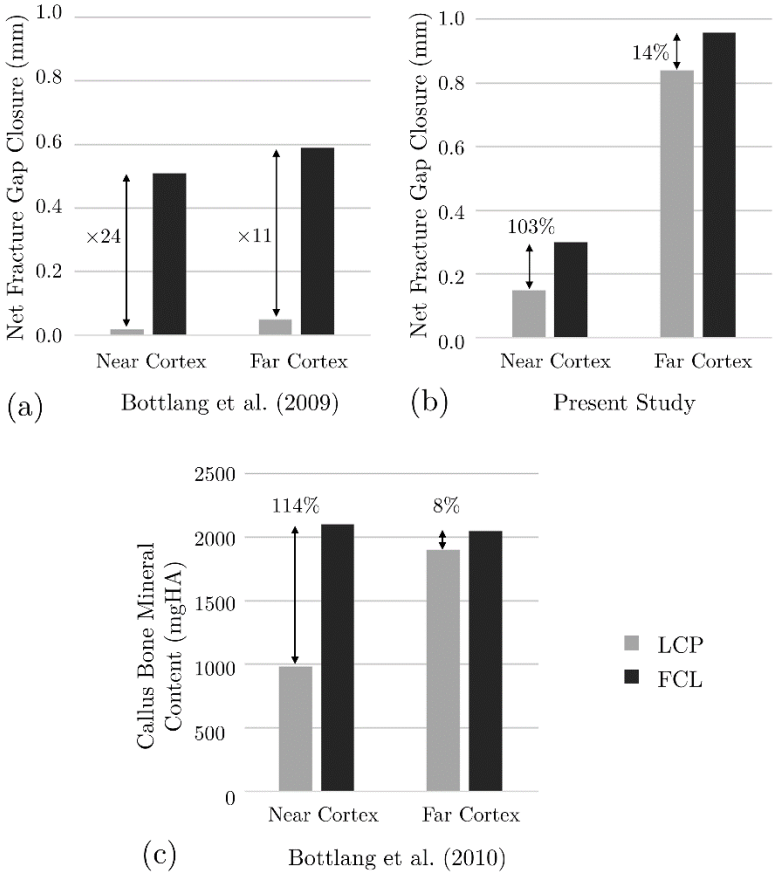

Figure 9.10 – Comparison of IFM predictions and callus bone mineral content for the LCP and FCL. (a) IFM predictions from Bottlang et al. 2009. (b) IFM predictions from the present study. (c) Histological assessment of sheep callus from Bottlang et al. 2010. The relative difference between LCP and FCL is annotated.

In the study by Bottlang et al. (2009) the unrealistic differences in predicted motion between the two screw types can be explained by particular aspects of the model:

- Rigid/clamped load application forces the bone fragments to remain perpendicular to the loading platform, which explains the observation of "parallel interfragmentary motion". It also severely restricts plate bending, which inhibits IFM in the LCP (Chapter 5)

- A very small working length was used, which is known to supress IFM (Stoffel et al., 2003);

- The selection of a 4.5 Broad LCP, typically used in the femur (Synthes®, 2003), produces less IFM than a 4.5 Narrow LCP recommended for the tibia.

- The FCL screw core diameter was smaller than the bi-cortical screw (3.2mm versus ~3.8mm) resulting in greatly increased flexibility (I=5.2mm^4 versus I=10.2mm^4). Using the 3.2mm FCL screw the increase in near and far cortex motion versus the original FCL model was 45% and 31% respectively;

For these reasons, the increase in IFM produced by the FCL compared with a bi-cortical LCP would have been exaggerated.

Bottlang et al. (2010b) suggest that findings regarding working length are "inconsistent" citing an article by Field et al. (1999) which evaluated the influence of screw position in compression plating. There are two key reasons why the study by Field et al. (1999) is not comparable to the locking plate study by Stoffel et al. (2003) and would therefore not provide consistent results: (1) the study did not evaluate axial loading; (2) the study used compression screws which result in bone-plate contact. This means that the working length is reduced to the size of the fracture gap and all screw configurations will produce very similar values of bending stiffness.

Finally, Bottlang et al. (2010a) predict that FCL produces "evenly distributed load sharing between screws" and reduces the stress concentration at the last screw compared with bi-cortical locking (Figure 9.11a). While this study also found that FCL screw produced a more even distribution of EqSV, the total magnitude was much larger than the LCP; it is therefore not clear why their FCL model produced smaller stresses. Additionally, in Chapter 6 it was found that the stress concentration at the last screw was an artifice of more rigid loading regimes.

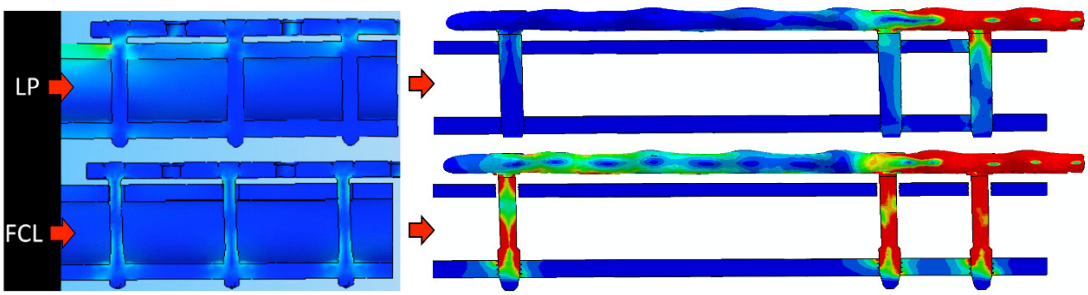

(a) (b)

Figure 9.11 - Prediction of von Mises stress in locking plates (LP) and far-cortical locking (FCL) from (a) Bottlang et al. 2010; and (b) the present study.

A related study was conducted within the Edinburgh Orthopaedic Engineering group using a principal strain-based healing algorithm to evaluate the influence of the different screw types on the fracture healing process (Kolev, 2014, Pantev, 2014). It was found that faster healing at the near cortex can actually inhibit healing at the far cortex. This may explain why the differences in the histological results from Bottlang et al. (2010b) are not as pronounced as would be expected from the differences in IFM. For example, this chapter predicts that the far cortex would have 14% greater IFM; however, the histology found only 8% more callus bone mineral content.

9.4.2 Summary of FCL

FCL can clearly produce larger fracture gap motion compared to bi-cortical locking; in some situations, however, the difference in motion may be very small. This study has shown that, using the same diameter of screw, the FCL increased the motion produced at the far cortex by only 14% compared to the bi-cortical LCP. In order to maximise the potential of FCL a screw with a narrower core diameter should be used. This was shown to generate up to 50% greater motion at the far cortex; however, it also increases the strain at the screw-bone interface, which is undesirable, particularly in osteoporotic bone. Even in healthy bone, the correct over-drill size at the near cortex must be evaluated to prevent excessive strain at the far cortex or stress within the screw.

9.4.3 Increasing Fracture Gap Motion without FCL

Far-cortical locking may be suitable for strong bone stock, however, due to the large strains induced it may be unsuitable in osteoporotic bone. Pull-out of diaphyseal screws has been observed when using locked plating in the femur (Button et al., 2004) meaning that far-cortical locking screws, which generate much larger pull-out forces (Moazen et al., 2013), may be unsuitable. An alternative means to generate increased fracture gap motion and reduce screw-bone interface strain would be to use bi-cortical locking screws and a less rigid plate—either by reducing its cross-sectional dimensions, choosing a less stiff material such as titanium, increasing the bone-plate off-set, or by using a larger working length (Miramini et al., 2013, Ahmad et al., 2007). These modifications would increase stress within the plate but maintain a strong screw-bone fixation.

9.4.4 What Causes Screw-Bone Interface Strains

Screw-bone interface strains are caused by two forces: pull-out and interface compression. These two phenomena explain why far-cortical locking screws produce larger strains at the screw-bone interface. The pull-out forces generated by a locking plate device are similar to those generated by external fixation. Considering a two screw

arrangement, the pull-out forces generated under axial load are related to the spacing of the screws and the off-set distance (Figure 9.12). Since the eccentricity off far-cortical locking screws is greater than bi-cortical locking screw, they produce greater pull-out forces.

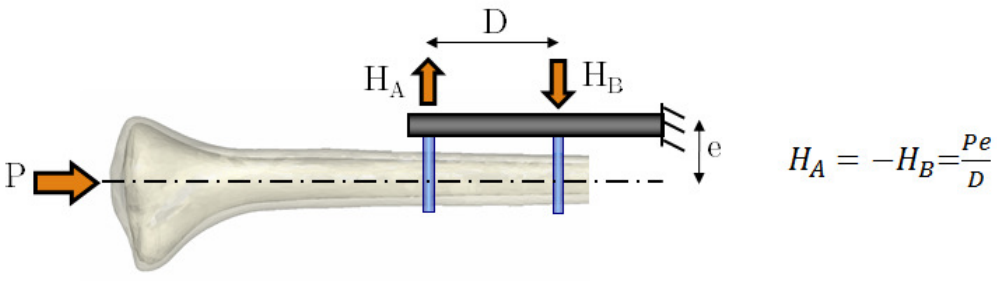

Figure 9.12 – Uni-lateral fixator depiction showing transverse pull-out forces due to axial loading.

Screw-bone interface compression is caused by axial loading and bending of screws. Huiskes et al. (1985) demonstrated that it is the bending forces rather than normal forces which dominate at the screw-bone interface. This results in a steeper gradient of stress and inefficient load transfer in external fixation devices (Figure 9.13a and b). Far-cortical locking screws exhibit similar characteristics to the unilateral device; however, they fasten to a single cortex (Figure 9.13d). As the bending restraint must be provided by a single cortex, the stress gradient is higher. In bi-cortical locking screw fixation, where the near cortex is engaged, these large bending forces are not generated as the off-set is much smaller (Figure 9.13c). The reduced stress gradient at the screw-bone interface is one of the reasons bi-cortical locking screws perform well in poorer quality bone. Uni-cortical screws produce a similar stress distribution to bi-cortical locking screws; however, pull-out forces are resisted by a single cortex resulting in increased strain.

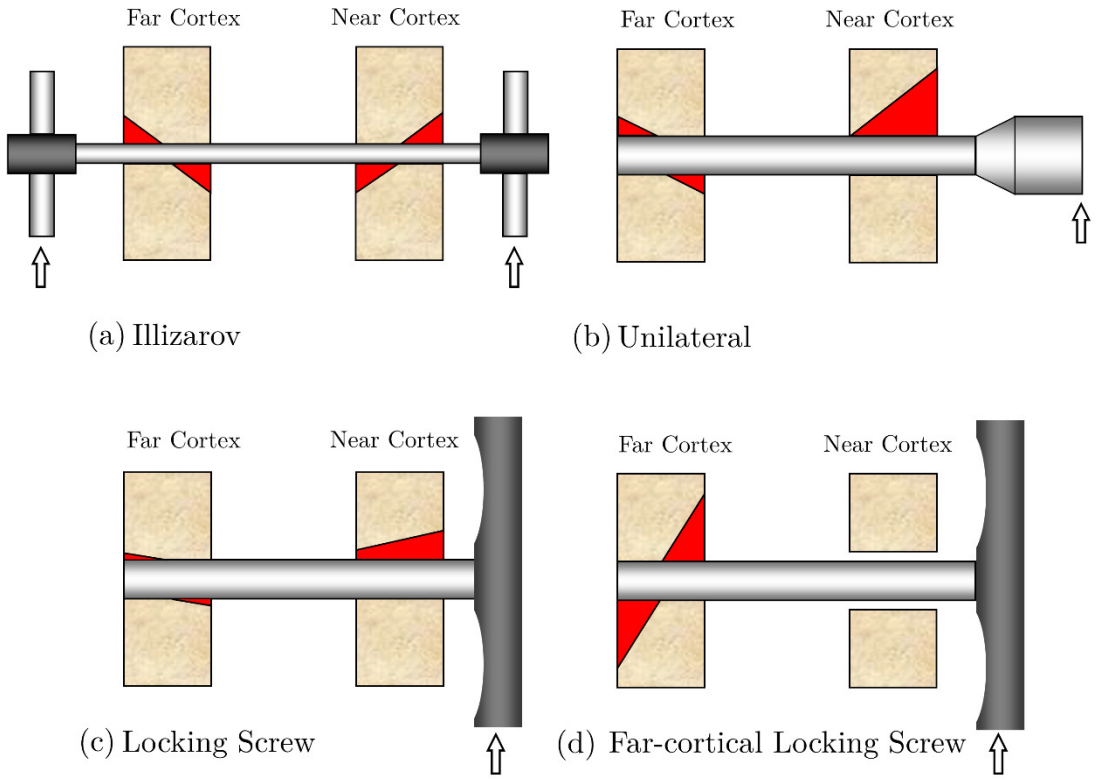

Figure 9.13 – Depiction of normal stress distribution at the screw-bone interface for (a) full-pin external fixators; (b) half-pin external fixators; (c) bi-cortical locking screws; and (d) far-cortical locking screws.

9.4.5 Limitations

Once screw-bone contact is made at the near cortex, the stiffness of the FCL would become identical to the bi-cortical LCP and the near cortex would begin to contribute to load-sharing (Bottlang and Feist, 2011). Examining the net motion between the screw and bone at the near cortex showed that loads of approximately 2000-3000N would be required to attain screw-bone contact using an over-drilled gap of 1mm, much larger than the load of 400N found by (Bottlang et al., 2010a). Therefore, incorporating this aspect of FCL screws would not have influenced the results for the levels of loads used in the study. After surgery, the over-drilled near cortex will begin to heal making the FCL more like the LCP, however, it is in the early stages with minimal callus development that strains around screws are largest.

9.4.6 **Conclusions**

- Uni-cortical screws do not significantly change the motion produced at the fracture site compared with the LCP (<5% difference);

- FCL screws can considerably increase the motion at the near cortex but motion at the far-cortex was less influenced;

- Both FCL and UCF considerably increase the levels of strain and stress around the screws compared with the LCP.

10

Predicting Implant Performance in Supracondylar Femoral Fractures

10.1 Introduction

10.1.1 Distal Femoral Fractures

Fractures of the distal femur are relatively rare, accounting for only 4-6% of femur fractures (Heiney et al., 2012, Wähnert et al., 2011, Obakponovwe et al., 2012, Pekmezci et al., 2014), but present significant surgical challenges (Ehlinger et al., 2011, Harder et al., 1999, Henry and Kregor, 1999, Obakponovwe et al., 2012, Kregor et al., 2001). While the total number is small there are a disproportionately high number of elderly sustaining them (over 50%), making them problematic due to the poor bone stock in conjunction with the large weight-bearing demands of the femur (Wähnert et al., 2011). Locked plating, in the form of the Less Invasive Stabilisation System (LISS), has replaced other treatment options such as intramedullary nails, blade plates and condylar screws as the most common treatment for distal femoral fractures (Granata et al., 2012, Hoffmann et al., 2013), particularly comminuted supracondylar femur fractures (Button

et al., 2004) and periprosthetic fractures (Kubiak et al., 2006, Henderson et al., 2010, Gebhard et al., 2008, Althausen et al., 2003). This is due to the anatomic alignment achieved compared with other fixation methods and the option of less invasive percutaneous surgery (Althausen et al., 2003, Button et al., 2004, Gebhard et al., 2008). Despite the success of the LISS in the distal femur plate failure rates are variable ranging from 2-18% (Button et al., 2004, Gao et al., 2013, Zlowodzki et al., 2004, Forster et al., 2006) and periprothetic fractures are known to present even higher complication rates, with plate failure reported in as many as 26% of cases (Ebraheim et al., 2012). Plate failure is commonly attributed to either incorrect screw placement or early weight-bearing in the presence of a delayed-union (Vallier et al., 2006, Button et al., 2004, Granata et al., 2012); this is intuitive as there is minimal load sharing with the bone and the loads are high. Screw loosening occurs in up to 7% of cases; when it does, it is generally proximal and has again been attributed to incorrect choice of screw configuration (Schandelmaier et al., 2001, Forster et al., 2006). In a study of 70 cases Henderson et al. (2011) found that fractures that went on to non-union were significantly ($p = 0.01$) more likely to have no screw empty holes adjacent to the fracture site, clearly indicating the importance of working length. Lujan et al. (2010) also found a correlation ($R2 = 0.09$) between bridging span and callus formation in a study of 64 cases. Additionally, titanium plates were shown to have significantly ($p < 0.05$) greater callus formation at 6 and 12 weeks after surgery. The success of the LISS is therefore largely dependent on pre-operative planning and screw positioning (Hierholzer et al., 2011, Leahy, 2010, Gautier, 2009). Several authors have advocated the use of larger working lengths or altered screw placement for better distribution of plate stress (Nassiri et al., 2012, Ehlinger et al., 2011). Interfragmentary contact occurring under load is known to shield plates from additional stress and provides biomechanical evidence for use of increased working length in situations where fragment contact can occur (Nassiri et al., 2012, Stoffel et al., 2003). In larger gap situations working length increases plate stress and can therefore be a cause of failure (Stoffel et

al., 2003). This has led to an apparent contradiction in results (Chao et al., 2013). It is also likely that a healing callus, even in the early stages, can enable a degree of load sharing (Vijayakumar et al., 2006) thereby producing a different environment to situations where callus is neglected. The influence that screw placement has on plate stress in vivo must be better understood to prevent these failures. Changes to construct strength, however, must also be weighed against any changes in mechanical stimulation produced at the fracture site (Zlowodzki et al., 2004).

10.1.2 **Modelling**

It is widely accepted that muscle contributions are key to biomechanical modelling of the femur (Phillips, 2009, Sverdlova and Witzel, 2010, Konstantinidis et al., 2012, Shih et al., 2008). Nevertheless, the vast majority of predictions of implant performance are made using in vitro models (or in vitro style models using FE) which neglect them (Granata et al., 2012, Hoffmeier et al., 2011, Talaia et al., 2007, Ebrahimi et al., 2012, Salas et al., 2011a, Completo et al., 2007, Heiney et al., 2012, Firoozabadi et al., 2012, Schmidt et al., 2013, Zlowodzki et al., 2004, Arnone et al., 2013, Tomaszewski et al., 2010, Wieding et al., 2012, Demos et al., 2012). While some studies have included the effect of key muscle groups for the proximal femur (Konstantinidis et al., 2012), in both computational and experimental models additional restraint is imposed which does not exist in vivo; these will influence the results (Phillips, 2009). The influence that this artificial restraint has on predictions such as implant failure has not been examined.

Several computational studies have examined the influence of muscle loading on the strain environment within an intact femur (Polgar et al., 2003, Duda et al., 1997, Speirs et al., 2007, Sverdlova and Witzel, 2010, Helwig et al., 2013, Phillips, 2009). Sverdlova and Witzel (2010) found that the muscles act to greatly reduce the bending forces in the diaphysis, producing a significantly different mechanical environment to in vitro tests of the bone in isolation where fixed boundary conditions induce large cantilever bending forces (Speirs et al., 2007). To the author's knowledge, no studies exist

evaluating the influence of muscle forces on a femur implanted with locked plating. It is therefore unclear whether the in vitro models used to provide predictions of locking plate fatigue strength, construct stiffness and strains within the bone are representative of the true physiology.

10.1.3 **Chapter Aim**

This chapter aimed to:

- Investigate whether a range of in vitro tests are representative of in vivo implant loading;
- Assess the ability of finite element modelling to predict clinical failures observed in selected LISS studies;
- Evaluate which screw configurations are most prone to plate breakage or delayed union and suggest alternatives that could be used.

10.2 Methods

10.2.1 **Geometry**

CT data of a femur was acquired from PhysiomeSpace[9] (Living Human Digital Library first donor: female; 81 year old; height: 1.67 m; weight: 63 kg). Three-dimensional finite element models were created using image processing software ScanIP (Simpleware Ltd., Exeter, UK). The average unicortical thickness of the model was 9mm in the diaphysis reducing to 5mm around the joints. The geometry of the 5.0mm Synthes® LISS plate was drawn from manufacturers dimensions (Synthes®, 2000). The locking screw dimensions were 5.0mm external and 4.3mm core diameter. Threads were modelled as

[9] SuperComputingSolutions, Bologna, 2013, last accessed 17/02/14 www.physiomespace.com/

idealised rings with a spacing of 1.2mm. A 6mm transverse osteotomy gap was created by partitioning the bone and specifying material properties of a healing callus in the relevant region (Figure 10.1). A recent study by Chen et al. (2013) found that there was only 1.5% difference between the predicted plate stress in oblique and transverse fractures; this demonstrates the relevance of osteotomies to other fracture patterns. Several screw configurations are examined throughout the study; however, in all cases four screws are used in the condyles.

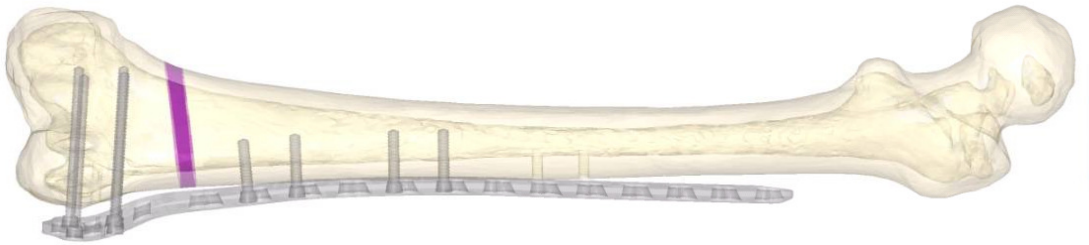

Figure 10.1 – Femur model implanted with LISS plate. Material properties have been specified in the purple region to represent healing callus.

10.2.2 Material Properties

All material properties were simplified to homogeneous isotropic and were assumed to be linear elastic. Cancellous bone was ignored and the screws and plate were initially considered to be titanium; the influence of steel plates was also considered subsequently. Cortical bone, titanium and steel were given Young's moduli of 17GPa, 105GPa and 180GPa respectively. All materials were given a Poisson's ratio of 0.3 (Steiner et al., 2014, Miramini et al., 2013).

In addition to gap defect models, the influence of healing callus within the fracture gap was also incorporated. This was to evaluate how the mechanical performance of locked plating can change throughout the healing period. Values of stiffness used for the healing callus vary considerably in the literature (Markel et al., 1990, Kim et al., 2010, Isaksson et al., 2006, Shefelbine et al., 2005, Fouad, 2010, Miramini et al., 2013, Steiner

et al., 2014). Three time-points of post-fracture healing were adopted (Table 10.1) and appropriate values of stiffness were approximated from the literature (Steiner et al., 2014, Isaksson et al., 2006). Weight-bearing (W.B.) returns approximately linearly (Cunningham et al., 1989, Isaksson et al., 2006) and full weight-bearing is generally restricted for 6-12 weeks (Granata et al., 2012). For the different time periods, all muscle forces and joint reactions were scaled linearly versus normal weight-bearing (section 10.2.6).

Table 10.1 – Assumed callus material properties and expected patient weight-bearing throughout the healing period.

Time post-surgery (weeks)	Callus Description	Expected weight-bearing (% of normal)	Callus Young's modulus (MPa)
0	Granulation/Fibrous Tissue	25	1
5	Cartilage	50	10
10	Woven Bone	100	100

10.2.3 **Interactions**

The screw-bone interaction used a coulomb friction coefficient of 0.3. The screw-plate connection was modelled using eight linear springs for each screw (four top and bottom) with a stiffness of 10,000N/mm (Chapter 6). The bone-plate offset was between 2mm and 5mm; no interaction was incorporated between these components.

10.2.4 **Meshing**

The model was meshed using 830,147 linear tetrahedral elements (351,524 in the bone; 218,551 in the plate; 23,668 for diaphyseal screws; and 41,350 for epiphyseal screws). The average element edge length around screw holes was 0.4mm. A mesh convergence study was performed and found that doubling the number of elements in the bone increased the fracture gap motion and plate stress predictions by 2.1% and 1.4%

respectively. Similarly, doubling the number of elements in the plate had a negligible influence on IFM but altered plate stress predictions by 3.7%.

10.2.5 **Restraint Conditions**

Several previous studies have modelled the femur in isolation by directly restraining nodes on the femur and using muscle forces applied as concentrated point loads (Figure 10.2a) (Speirs et al., 2007, Sverdlova and Witzel, 2010, Polgar et al., 2003). Phillips (2009) noted that there may be motion at the articular surfaces; however, clearly the acetabulum and tibial plateau provide considerable restraint (Sverdlova and Witzel, 2010). It is desirable to be able to analyse the femur in isolation but incorporating the pelvis, tibia and patella, as done in some studies (Phillips, 2009, Helwig et al., 2013), involves considerably more modelling effort and therefore limits the model's ability to be applied to multiple patient specific cases or load cases. Moreover, in spite of the additional modelling effort involved, it is not straightforward to validate these models. This study used a different approach, constraining the joints about their centres of rotation but allowing motion at the articular surfaces. This was done using multi-point constraints and rigid beam connections. The loading condition proposed by Speirs et al. (2007) has two degrees of freedom at the knee: rotation in the stagittal and coronal planes (Figure 10.2a). By including bi-condylar restraint (distributed across the articular surfaces), the present study has restrained an additional vertical degree of freedom, reducing the motion of the knee joint to a single degree of freedom hinge (Figure 10.2b). A similar loading condition was used in a recent experimental study of the distal femur by Assiri et al. (2013). When using a hinged condition, the orientation of the plate influences the IFM (Chapter 5). In the femur, the plate is generally placed laterally, at 90 degrees to the knee 'hinge'. This produces the stiffest possible response in terms of plate orientation as the direction of knee rotation is orientated with the strong axis of the plate.

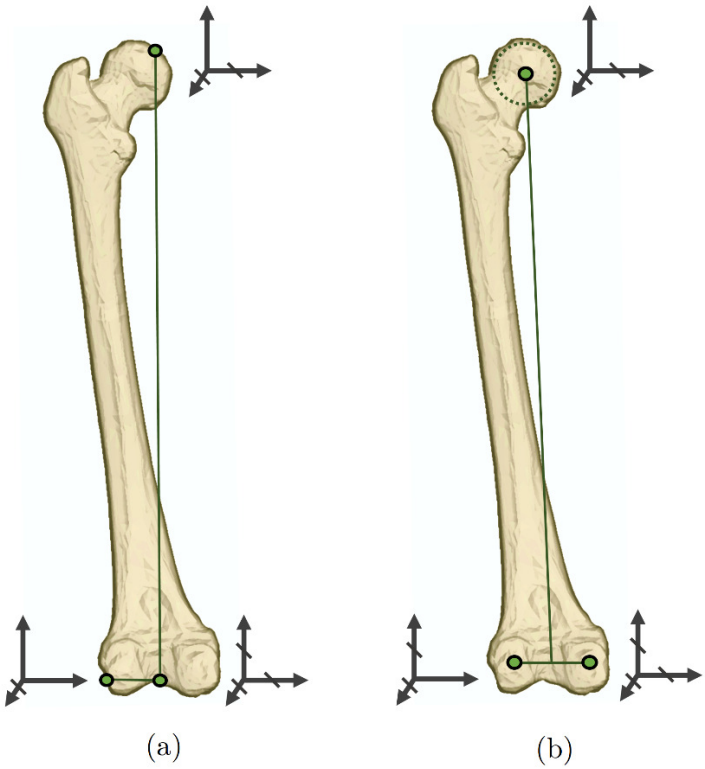

Figure 10.2 – The location of restrained nodes and translational degrees of freedom in (a) 'Case E' by Speirs et al. 2007 and (b) in the present study.

10.2.6 **Loading**

10.2.6.1 Hip Joint Loading

Mean, weight-averaged hip joint reaction forces were taken from the literature at 15% of walking gait (mid-stance) as this is the instance of maximum hip reaction force (Bergmann et al., 2001, Heller et al., 2001). A value of 238% body weight was used corresponding to 1471N for the subject's mass (63kg). The loading vector was taken as the mechanical axis through the centre of the femoral head to the centre of the condyles. In all analyses the hip was allowed to translate freely along the mechanical axis.

10.2.6.2 Muscles

Both Helwig et al. (2013) and Phillips (2009) used muscles modelled as spring elements. These produce passive forces by resisting displacements around the model. This approach is sensitive to the assumptions regarding muscle stiffness and required hip and knee structures to be modelled in addition to the femur for stability. Pankaj (2013) discussed two commonly used methods of incorporating muscle forces: force vectors and springs. This study modelled the muscles using point-to-point wire connectors (i.e. these were not springs as they have zero stiffness). The muscle forces were applied along the wires using 'connector forces' (ramped linearly through the loading step. This allowed the muscle forces to be specified, but also permitted the loading direction to change due to deformation. Muscle force data were taken from Sverdlova et al. (2010) using values for 15% of walking gait and scaled linearly based on the hip reaction forces. Muscle origin and insertion locations were taken from Dostal et al. (1981). The coordinates were scaled and transformed using a Matlab.

Muscle via points were created using coupling constraints. A via point was used to connect the gluteus maximus and illiotibial tract on the lateral aspect of the femoral shaft level with the lesser trochanter. A via point representing the patella was used to connect the patellar ligament and the quadriceps muscle group (including rectus femoris and three vastus muscles).

The analysis included nonlinear geometrical effects and was conducted using Abaqus 6.10 (Simulia, Providence, RI).

10.2.7 **Analyses**

10.2.7.1 Part 1 – In Vitro Conditions

In the first part of the study the influence of four 'in vitro' loading conditions (ignoring muscle contributions) used by previous studies were examined for a femur with gap defect stabilised with LISS (Figure 10.3):

(a) The distal femur is clamped; the hip is restrained in the coronal and stagittal planes (A-P and M-L) (Granata et al., 2012, Liang et al., 2012, Salas et al., 2011a).

(b) The distal femur is clamped; the hip is free to move in the coronal plane (M-L) and restrained in the stagittal plane (A-P) (Wieding et al., 2012).

(c) The knee is hinged; hip restraint is provided in the coronal and stagittal planes (A-P and M-L) (Assari et al., 2013).

(d) A node on the lateral condyle of the knee is pinned; a node on the medial condyle is restrained in the coronal plane; hip restraint is provided in the coronal and stagittal planes (A-P and M-L) (Speirs et al., 2007, Schmidt et al., 2013, Hoffmeier et al., 2011).

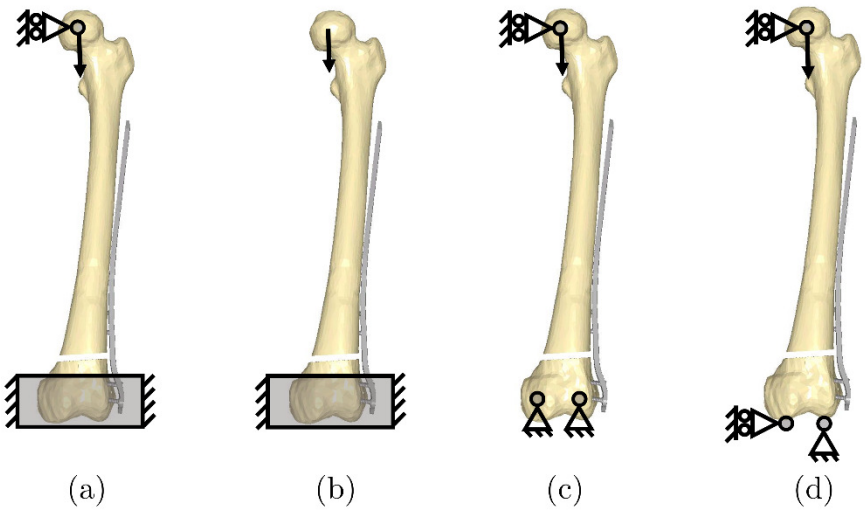

Figure 10.3 – The four in vitro loading conditions tested: a, b, c and d.

Screw configuration MX-2356 was used in all cases and the load applied was 368N. This value is ¼ of the total hip joint loading for the instance of gait considered. This load was chosen to ensure all cases produced stresses below the yield stress of titanium; previous experimental studies have found that titanium plates can yield or rupture at loads lower than this (Hoffmeier et al., 2011, Schmidt et al., 2013). Although condition (b) has been included as an in vitro condition, it is extremely difficult to implement experimentally and is usually only used in simulation.

10.2.7.2 Part 2 – In Vivo Conditions

In the second part of the study three further 'in vivo' loading conditions were evaluated including muscle force contributions for both intact and fractured cases. The loading and healing callus is intended to be representative of 5 weeks (736N; 10MPa). Three restraint conditions were examined (Figure 10.4):

(e) The knee is hinged; where the hip is free to move in the coronal plane and restrained in the stagittal plane (A-P and M-L).

(f) The knee is hinged; linear springs are used in both transverse directions at the hip

(g) The knee is hinged; where hip restraint is provided in the coronal and stagittal planes (A-P and M-L).

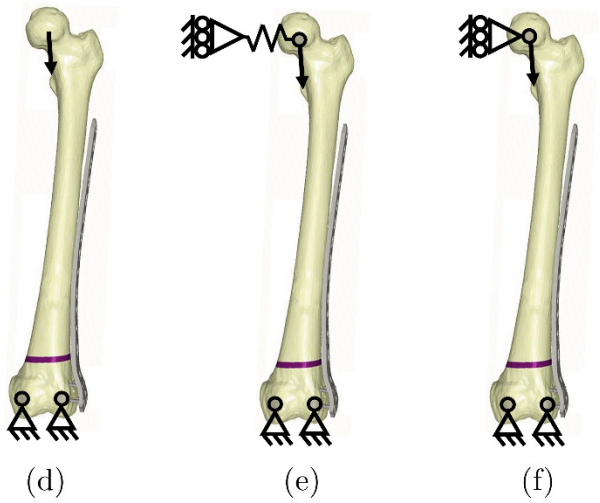

Figure 10.4 – The restraint conditions used in the in vivo loading conditions: (e), (f) and (g). The healing callus region is coloured in purple.

In all cases the screw configuration MX-2356 was used. The level of restraint imposed at the hip was found to be influential; it was postulated that the true environment was in-between the extremes represented by conditions (d) and (f). This was achieved using linear springs which dampen the movement but do not abolish it; the spring stiffness was evaluated using an intact femur. The value of stiffness was selected to give the ratio of medial and lateral joint reactions equal to 65:35 (Figure 10.5), which has been reported for this instance of gait (Halder et al., 2012, Kutzner et al., 2011). This value was calculated to be 30N/mm.

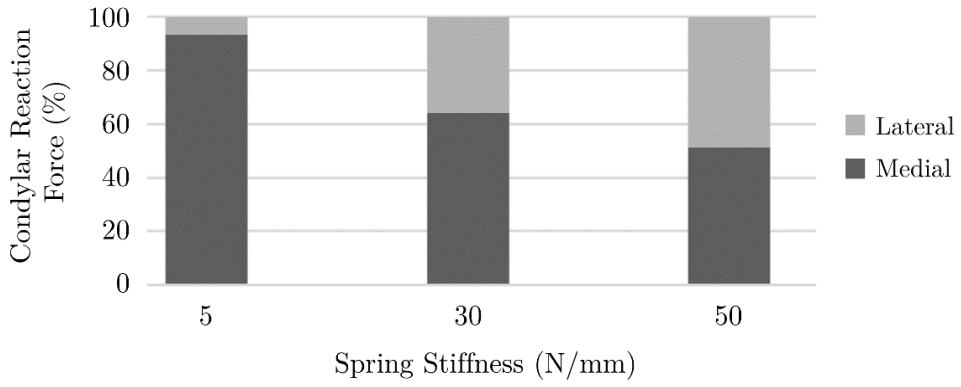

Figure 10.5 – Influence of hip spring stiffness on the medial and lateral load distribution at the knee for the intact femur cases.

10.2.7.3 Part 3 – Comparison of Different Screw Configurations

Finally, loading condition (f) was used to evaluate a range of different screw configurations. Comparisons are made with selected clinical cases from the literature.

10.3 Results

10.3.1 Part 1 - In Vitro Conditions

From the deformed shapes for the four in vitro loading conditions is shown in Figure 10.6, it was found that condition (a) produces the smallest IFM and condition (d) the largest. The absence of hip restraint in condition (b) allows the plate to bend freely; as deformation progresses the eccentricity of the load at the hip increases producing a nonlinear response. The IFM produced by condition (c) is larger than condition (a) due to the hinged restraint at the knee rather than the clamp. Condition (d) produced larger IFM than conditions (a) or (c) as it is free to rotate about the lateral condyle at the knee; it also demonstrated nonlinearity unlike conditions (a) or (c). These motions correspond to predictions of peak von Mises stress within the plate (Figure 10.7). Contour plots of the Von Mises stress distribution within the plate for the different conditions is provided in Appendix D.1.1.

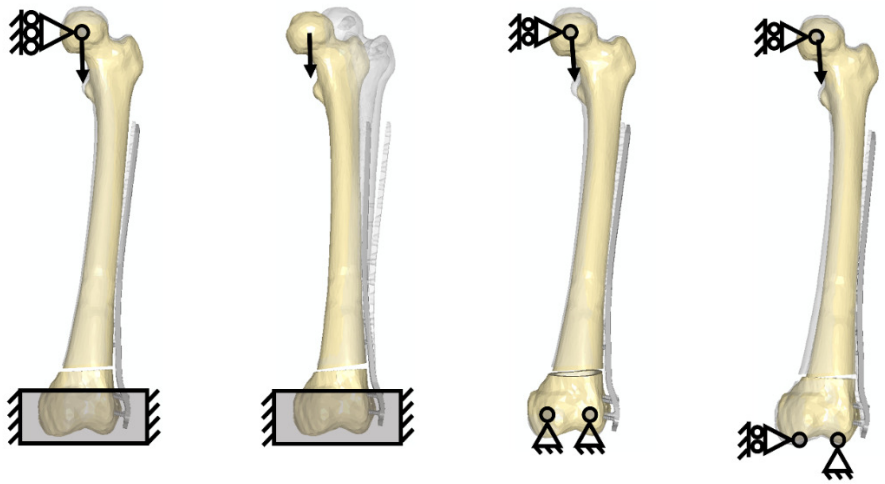

Figure 10.6 – Deformed shape for the in vitro loading conditions a, b, c and d. Exaggeration scale factors x50, x1, x50 and x5 respectively.

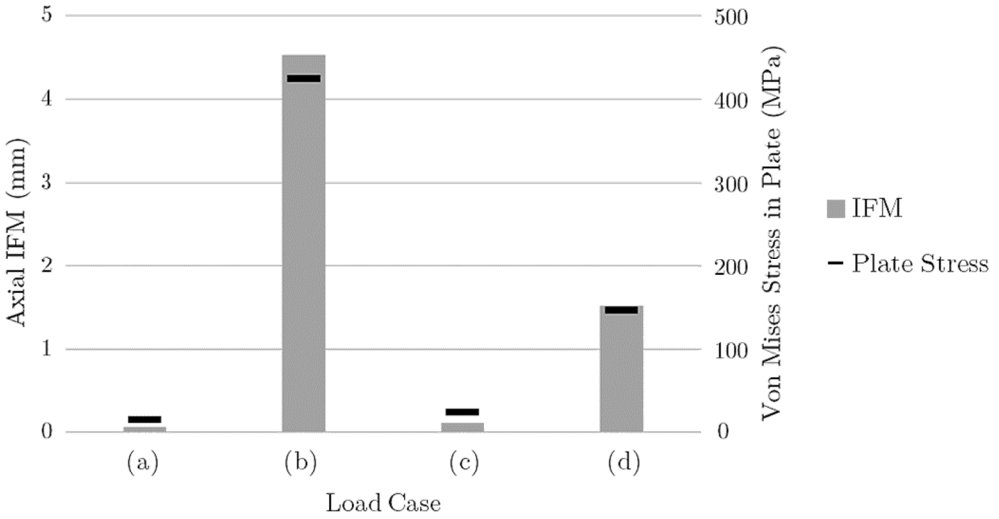

Figure 10.7 – Peak von Mises stress and IFM for the in vitro loading conditions a, b, c and d at a load of 368N.

It should be noted that case (d) was found to be sensitive to the position of the restrained node at the knee. This study restrained a node on the lateral condyle as it was closer to the plate; however, the medial condyle or a central node could have been chosen making the construct more flexible. This was tested and found to increase the plate stress and IFM by over 2.7 times. Only condition (c) provides information regarding medial-lateral condylar joint reactions. For this reason the in vivo simulations were based on condition (c); however, the influence of allowing transverse motion at the hip, such as in case (b), was also examined.

10.3.2 **Part 2 – In Vivo Conditions**

Before evaluating an implanted femur, the influence of the in vivo loading conditions (e, f and g) was examined for an intact case. For completeness, the values for case (f) with the femoral head restrained in the stagittal plane (A-P) has also been shown (second value), but has hereafter been ignored. The vertical deflections (along the mechanical axis) at the femoral head were measured for each in vivo loading case relative

to the centre of the femoral condyles (Figure 10.8). The loading conditions represent increasing degrees of hip restraint and the displacement predictions reflect this. Although the femoral head was free to rotate in all cases, loading condition (g) produced minimal rotation. Condition (f) produced a slightly negative displacement at some locations on the femoral head. This is simply because the upwards displacement due to rotation is greater than the downwards deflection of the centre of the head.

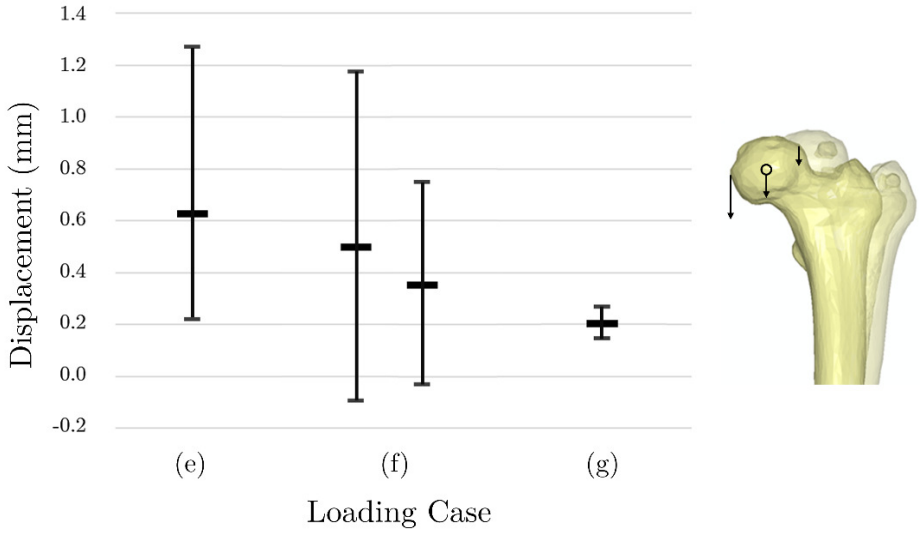

Figure 10.8 – Vertical displacements at the femoral head relative to the knee for the in vivo cases e, f and g, which use different restraint conditions at the hip. The central value is at the centre of the femoral head; the upper and lower values are the largest and smallest values of displacement measured.

The reaction forces produced at the femoral condyles for each in vivo loading case are shown in Figure 10.9 for intact and implanted cases. The intact cases show that increasing levels of restraint at the hip (left to right) cause a greater proportion of load to be transmitted laterally. Loading case (e) results in 89% of load transmitted medially whereas loading case (g) transmits 78% of load laterally. The intact case (f) produced a 65:35 medial-lateral loading distribution; when implanted, this changed to 45:55. Additionally, in the extreme loading cases, for loading conditions (e) and (g), negative reaction forces occur thereby increasing the net force on the joint. For example, intact loading case (e) produced 30% greater total knee joint reaction force than case (f); when

implanted, the reaction was 133% greater. The total magnitude of the joint reaction at the knee was 2810N (4.5 times B.W.), 2161N (3.5 times B.W.) and 2325N (3.8 times B.W.) for cases (e), (f) and (g) respectively.

Loading case (f) produced the distribution of knee joint reaction forces reported for this instance of gait (Halder et al., 2012, Kutzner et al., 2011) and displacements at the femoral head similar to previous studies (discussed further in 10.4.1). For this reason, it was considered to be closest to the true in vivo environment and used for part 3 of this chapter.

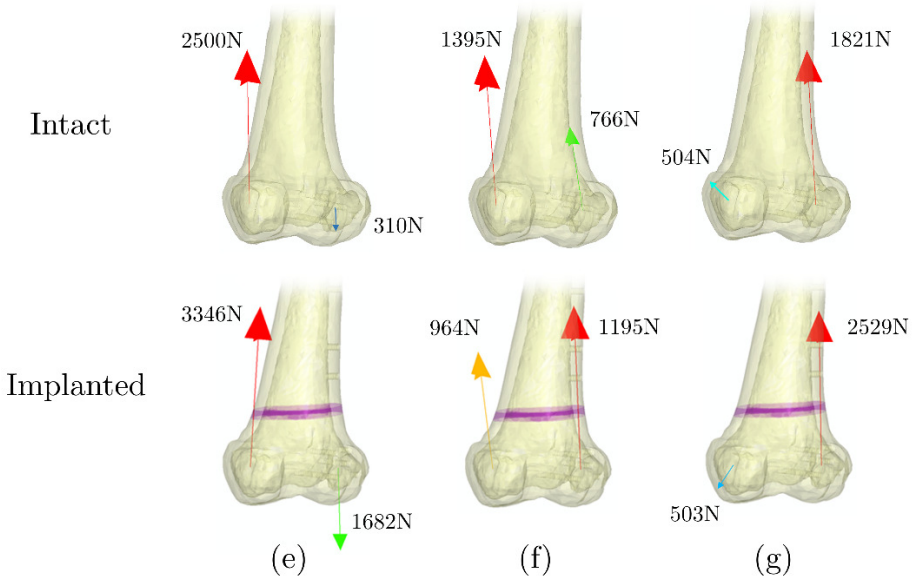

Figure 10.9 – Reaction forces at the femoral condyles for intact and implanted femurs using different restraint conditions at the hip. The arrows show the relative magnitude of the reaction forces (not to scale between cases). The medial condyle is located to the left. The healing callus region is coloured purple.

The influence of the varying degrees of hip restraint can be seen clearly from the deformed shapes for the three implanted in vivo loading conditions is shown in Figure 10.10. Values of IFM at the far cortex and maximum plate stress for the in vivo conditions (e, f and g) and in vitro conditions (a, b, c and d) are shown in Figure 10.11. Case (b) deformed excessively under the full load so the value for 368N is shown. The

load-deformation response of the in vivo cases was approximately linear; however, it was not for in vitro conditions (b) or (d). As expected, both IFM and plate stress reduced with increasing restraint at the hip.

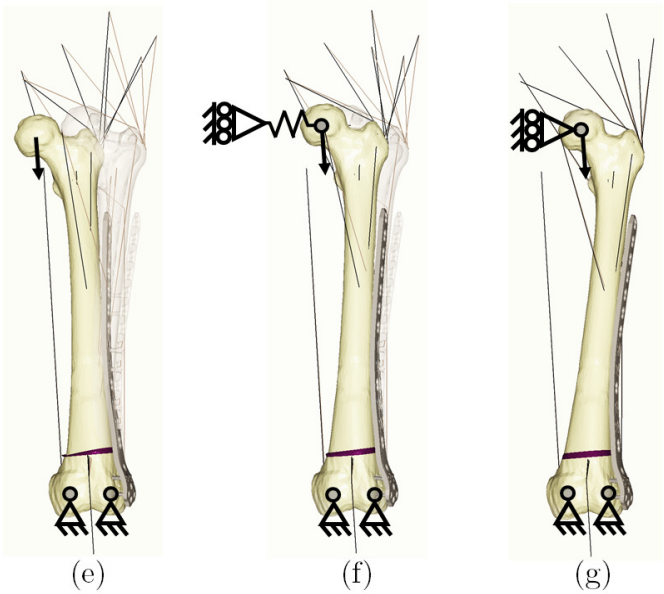

Figure 10.10 - Deformed shape and von Mises stress prediction in the plate for the in vivo loading conditions (e), (f) and (g) (exaggerated x2). The healing callus region is coloured in purple.

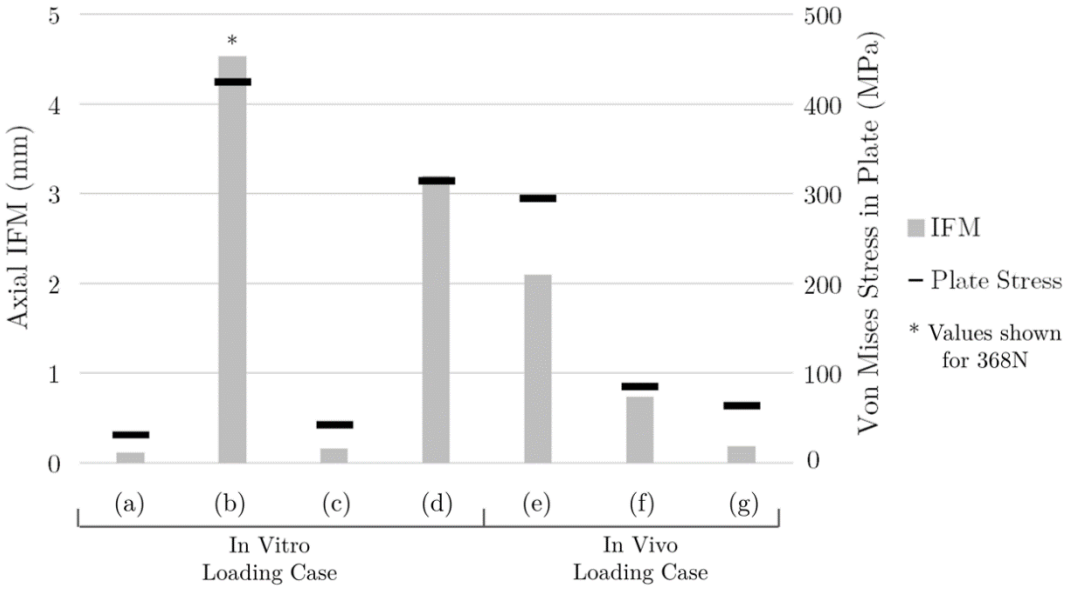

Figure 10.11 - Von Mises stress prediction in the plate for the in vitro (a-d) and in vivo (d-f) loading conditions. All cases are shown for a post-surgery time of 5 weeks;

all cases use a load of 736N at the hip and in vivo load cases also have callus (10MPa). Case (b) is shown for 368N.

Despite the in vivo loading conditions incorporating muscles which increase the total force in the femoral shaft, in vitro conditions (b) and (d) produced larger plate stress (Figure 10.11). Additionally, the predictions for in vivo simulations (e, f and g) were within the range of values predicted by the in vitro conditions (a, b, c and d).

There were also differences in plate stress distribution between the different loading conditions. Loading cases (b), (d) and (e) produced similar distributions with significant bending, whereas case (a) produced minimal bending. The more flexible conditions caused mainly minor axis plate bending whereas the stiffer responses exhibited significant bi-axial bending. All loading cases produced the peak stress at the hole in the mid-span of the bridging section with the exception of Case (g) where the largest stresses were located on the posterio-lateral edge of the plate adjacent to the first screw proximal to the fracture gap. Cases (c) and (f) also showed increased stress at the posterio-lateral edge, however, it was not the peak value. The level of load did not change the stress distribution significantly or the location of peak stress.

When the callus stiffness was reduced to 1MPa case (f) had the peak stress located at the first filled screw hole proximal to the fracture. Cases (e) and (g) had the peak stress located at the posterio-lateral edge next to this screw.

10.3.3 **Part 3 – Comparison of Different Screw Configurations**

A range of screw configurations was examined using loading condition (f) (Figure 10.12). IFM and plate stress were recorded for two fracture locations: metaphyseal (denoted MX) and diaphyseal (DX) (Figure 10.13 and Figure 10.14). The screw configurations were selected to examine the influence of different working lengths. The LISS is available in steel and titanium (Synthes®, 2000) but clinical reviews do not normally specify which material was used in cases of failure (Ehlinger et al., 2011, Button et al., 2004,

Hak et al., 2010b). Both materials were evaluated for two time-points: 0 weeks and 10 weeks post-operatively (see section 10.2.2). Axial IFM was expressed as maximal fracture gap closure measured using values of displacement at the far cortex. Shear IFM was taken as the magnitude of motion in the transverse plane at the same location used for axial IFM.

10.3.3.1 Results

For the initially post-operative period the axial IFM for each configuration is shown in Figure 10.13a. Although the differences between configurations were not large, working length generally increased axial IFM regardless of the fracture location (Figure 10.13a). This trend was not seen for shear IFM (Figure 10.13b). The strongest determinant of axial IFM was the number of free screw holes next to the fracture ($r^2 > 0.72$); this was also the case for shear IFM in diaphyseal fracture patterns but not for metaphyseal fractures. At 10 weeks, axial IFM was slightly reduced (Figure 10.14a), whereas shear IFM was substantially reduced (Figure 10.14b). Shear IFM did not correlate with axial IFM for either titanium or steel at 0 weeks ($r^2 < 0.05$) or at 10 weeks ($r^2 < 0.67$).

The peak von Mises stress within the plate was recorded for each of the different configurations (Figure 10.13c and Figure 10.14c). Two values of stress are shown representing different levels of weight-bearing for the same degree of healing (callus stiffness). In all cases steel produced larger plate stress than titanium. In the immediate post-operative period shorter working lengths produced smaller plate stress for titanium plates (Figure 10.13c); WL had less influence in steel plates. At ten weeks, however, the smallest working length produced the largest stresses for both materials. For both fracture patterns moderate WL (74mm) produced lower plate stress than small WL (55mm). In metaphyseal fractures with short working lengths steel plating produced up to 65% greater stress than titanium (Figure 10.13c). A similar increase of 47% was observed in diaphyseal fractures with short working lengths, although the total

magnitude was much greater (Figure 10.14c). For diaphyseal fractures, a WL of 80mm produced the lowest stress in both titanium and steel plates.

The location of peak stress was altered depending upon the configuration. In configurations DX-23-5689, DX-23-689 and DX-2-689 the peak stress was located at within the WL portion of the plate. If the plate is fixed at the condyles and there are no intermittent screws distally (all other configurations), the peak stress is through the first filled screw hole proximal to the fracture.

The location of the fracture within the working length can considerably influence the IFM and plate stress that the implant is exposed to. The differences in IFM and plate stress between cases MX-5689 and DX-5689 demonstrate this (Figure 10.13a and c).

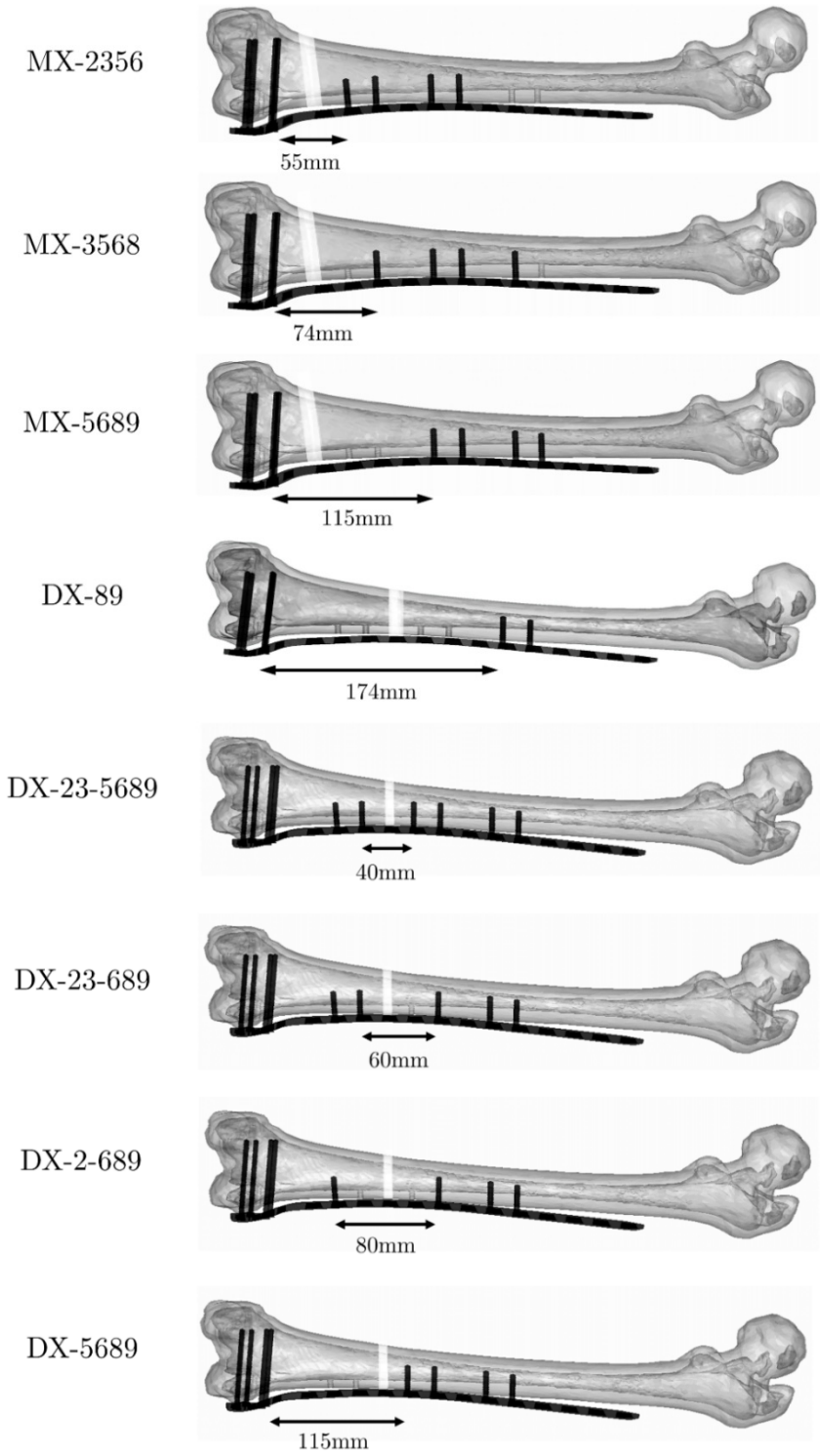

Figure 10.12 – The different screw configurations and fracture locations tested. Each configuration is referenced firstly by the fracture location (MX or DX) then by the position of screws counting from the knee.

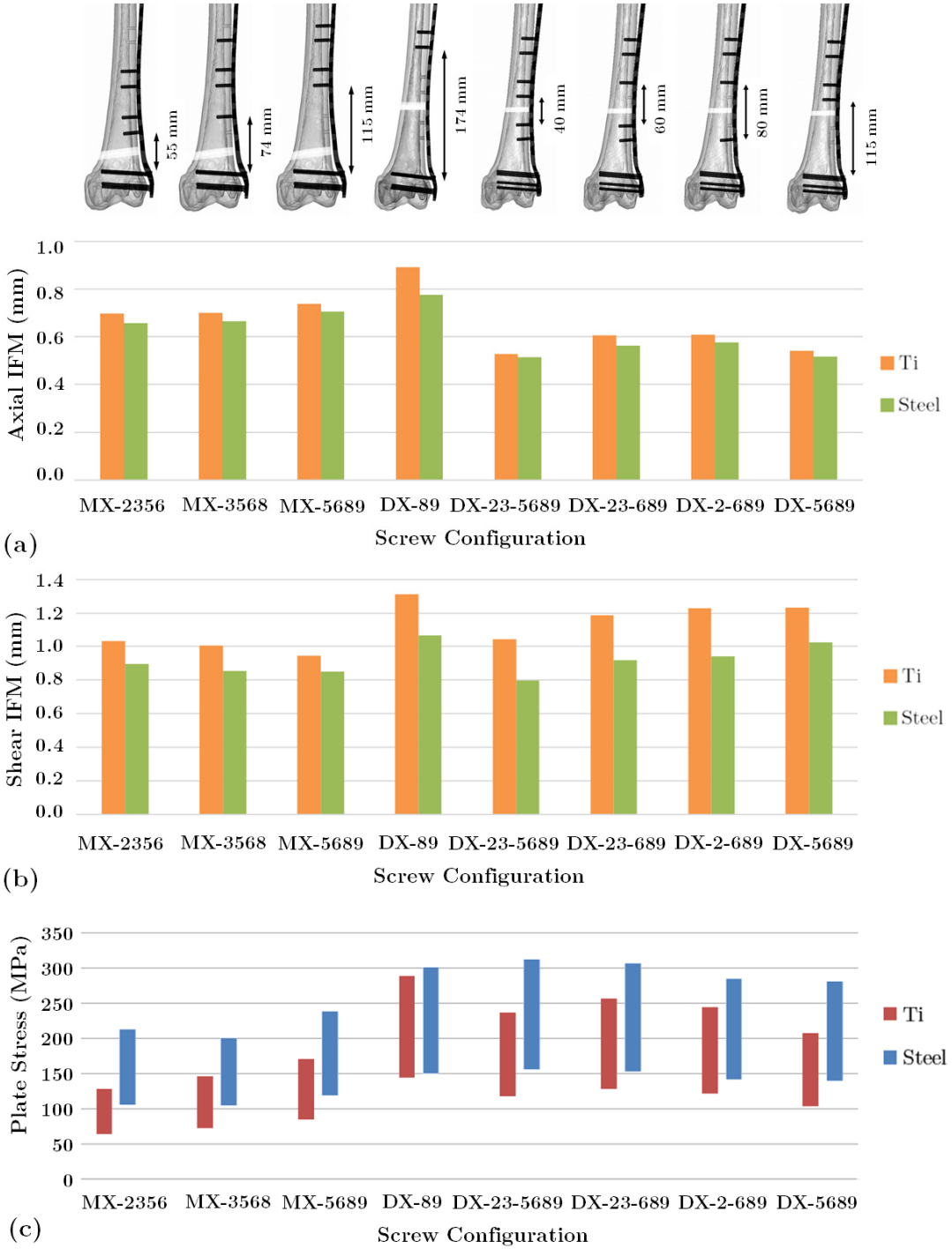

Figure 10.13 – (a) axial IFM; (b) shear IFM and (c) von Mises stress within the plate for different screw configurations and plate materials. IFM predictions are for the immediately post-operative period with 25% weight-bearing and a callus of 1MPa. Plate stress predictions provided for 25% and 50% weight-bearing (lower and upper values respectively), with 1MPa callus in both cases.

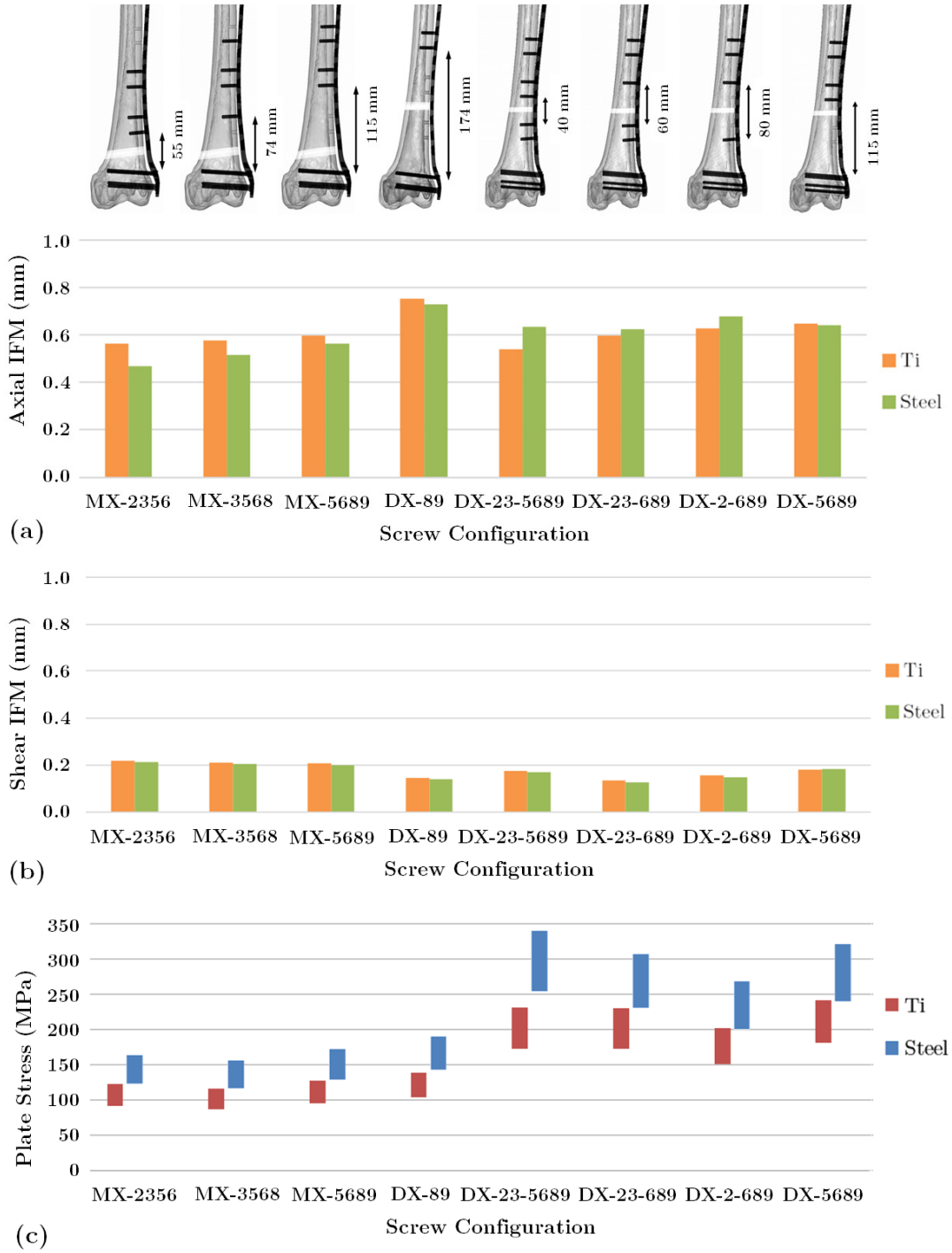

Figure 10.14 – (a) axial IFM; (b) shear IFM and (c) von Mises stress within the plate for different screw configurations and plate materials. IFM predictions are for 10 weeks post-surgery with 100% weight-bearing and a callus of 100MPa. Plate stress predictions provided for 75% and 100% weight-bearing (lower and upper values respectively), with 100MPa callus in both cases.

10.3.3.2 Comparison of Clinical Examples

Several examples of locking plate failure from the literature are compared. In every case, the working length (WL) has been annotated. Cases S1, S2, S3 and S4 have short working lengths preventing load sharing leading to plate breakage at 9, 10 and 6 months respectively (Figure 10.15) (Tan and Balogh, 2009, Button et al., 2004, Hak et al., 2010b). Case S5 and S6 failed due to insufficient motion leading to non-union (Gardner et al., 2009, Syed et al., 2004). Case S5 was declared a non-union at 5 months (Gardner et al., 2009). As this was a steel plate, it is likely that it too would have failed by fatigue in a matter of months (discussed further in 10.3.3.4).

In cases M1 and M2 a medium sized working length was used, with M1 failing at 14 months (Figure 10.16) (Vallier et al., 2006, Hunt and Buckley, 2013). In both of these cases, insufficient bone-plate off-set has effectively reduced the working length leading to plate failure. Case M3 was described as being overly-flexible having been declared a hypertrophic non-union at 6 months (Gardner et al., 2009). This demonstrates that sufficient IFM can be produced using working lengths of approximately 74mm; unfortunately, in this case IFM was not appropriate for the fracture pattern, which appears to be well reduced.

Cases L1, L2 and L3 (Hak et al., 2010b, Gardner et al., 2009, Syed et al., 2004) show significant callus development and went on to heal successfully (Figure 10.17). It appears that case L4 was healing, but failed due to screw loosening (Button et al., 2004). Chapter 7 demonstrated that both large working length and an insufficient gap between the first two screws can increase the strain within the bone around screws. This failure may, therefore, have been prevented by using fewer, well placed screws with a slightly shorter working length, similar to cases L1 and L2.

Ehlinger et al. (2011) demonstrate a case of plate breakage due to excessive WL and attributed this failure to “proximal and distal stiffening” due to screw placement (Figure

10.18). In this case an additional screw placed proximally with a one hole space between the existing screws could have increased the fatigue life of the construct, making it more like MX-5689.

The plate breakages seen in cases D1 and D2 (Apostolou et al., 2005, Park et al., 2011) were a result of traumatic loading due to a fall (Figure 10.19). Cases D3 and D4 show primary and revision operations in the same patient with the first failure due to fatigue and the second due to a fall (Kim et al., 2012). This was attributed to a large lateral bow in the femur considerably increasing the bending moment and therefore plate stress. There appears to be no radiographic evidence of healing at 3 months, which is expected due to the relatively small axial IFM produced by such configurations (Figure 10.13a). Based on the stress produced in diaphyseal fracture patterns (Figure 10.13c and Figure 10.14c), it may be safer to use a slightly longer working length (80mm) or a screw configuration that omits distal screws such as DX-5689. Additionally, a titanium plate would be recommended as they produce considerably smaller stress than steel in this situation (up to 32% less).

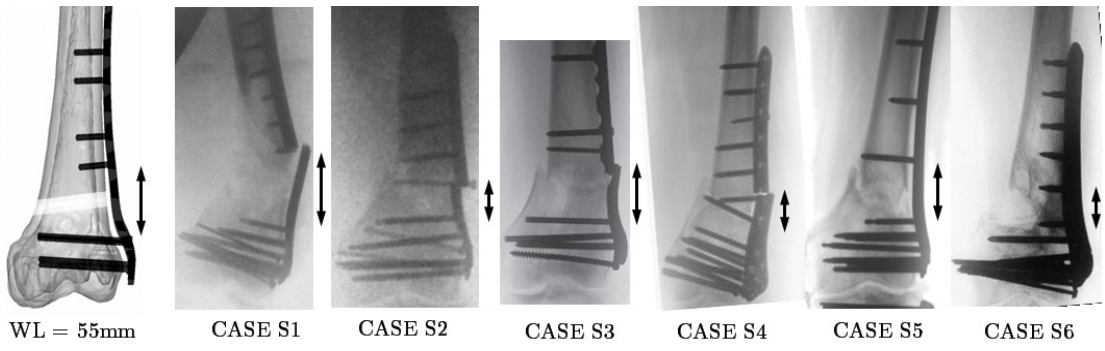

Figure 10.15 – Clinical examples of distal femur locking plates which used a short working length. The working length portion of the plate is annotated.

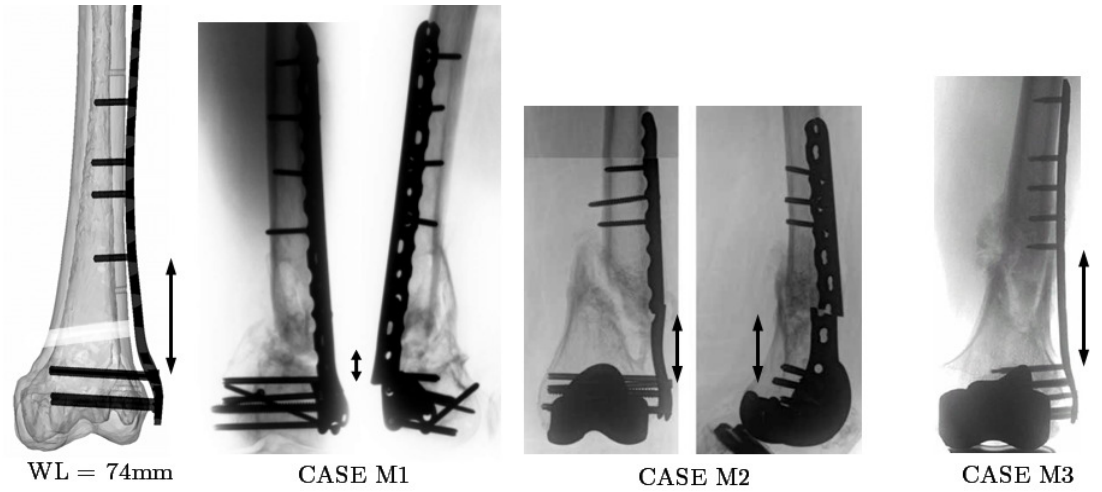

Figure 10.16 – Clinical examples of distal femur locking plates which used a moderate working length. The working length portion of the plate is annotated.

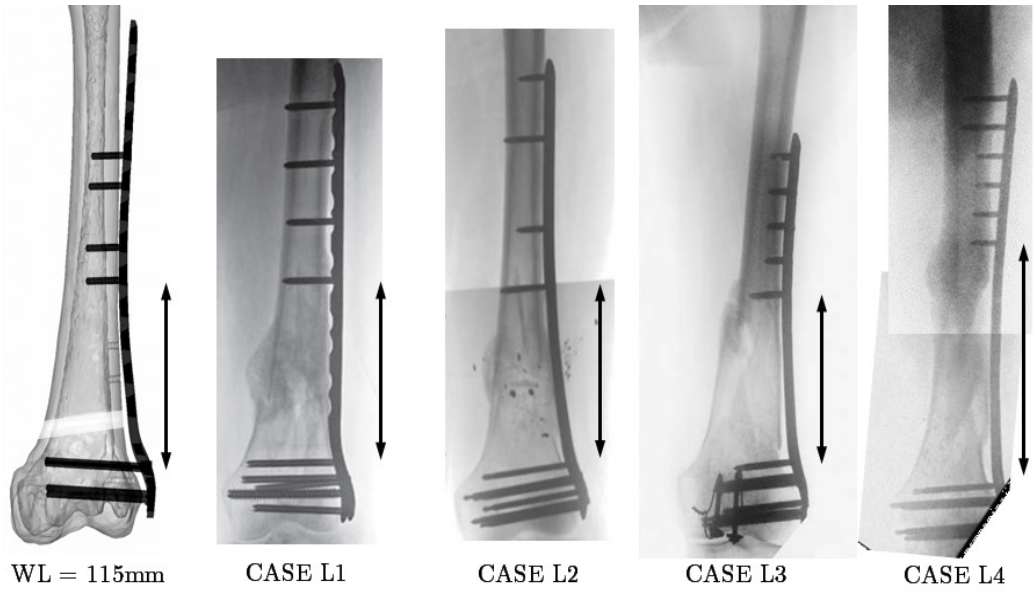

Figure 10.17 – Clinical examples of distal femur locking plates which used a long working length. The working length portion of the plate is annotated.

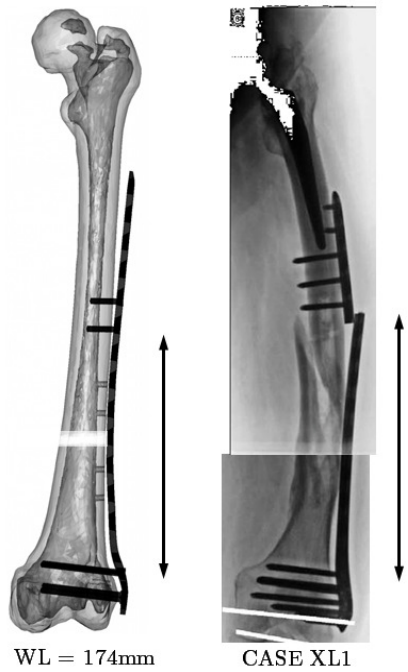

Figure 10.18 – Clinical example of a failed distal femur locking plate which used a very long working length. The working length portion of the plate is annotated.

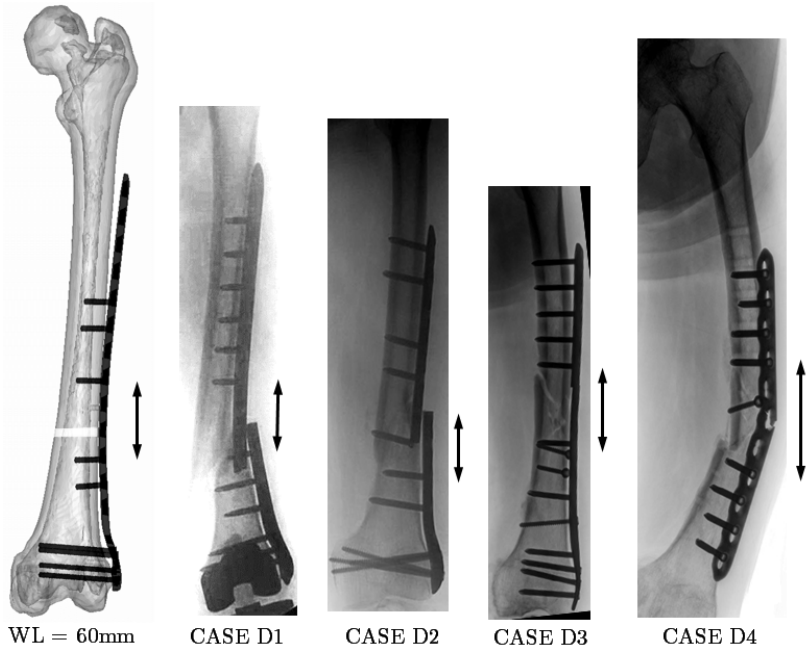

Figure 10.19 – Clinical example of a failed locking plates in the femoral diaphysis. The working length portion of the plate is annotated.

10.3.3.3 Prediction of Failure Location

The predicted failure location of configurations MX-2356, MX-3568, MX-5689, DX-5689 and DX-89 were all at the first filled screw hole proximal to the fracture. This is the failure location observed clinically in the short working length examples (Figure 10.15). The medium working lengths failed at the first point of bone-plate contact proximal to the fracture (Figure 10.16); the location is similar to the short working length cases. The extra-long working length failed at the most proximal empty screw hole in the working length (Figure 10.18). While this failure location was not correctly predicted by the model, the predicted stress at this location was only 12.3% lower than the peak stress in steel; for titanium plates this figure was 17%. The other configurations (DX-23-5689, DX-23-689, DX-2-689) were predicted to fail through a screw hole in the working length portion of the plate as observed in cases D1-D4 (Figure 10.19).

10.3.3.4 Prediction of Fatigue Strength

Titanium alloy is promoted as having superior strength to stainless steel (DePuy, 2005a); this is supported by the literature, even under cyclic loading (Niinomi, 2007, Okazaki, 2012). A study by Banovetz et al. (1996), however, found that titanium plates had a statistically ($p < 0.001$) higher rate of hardware failures (from 69 titanium and 200 steel cases). Moreover, several in vitro studies have found titanium plates to survive for fewer cycles and fail at lower loads than steel counterparts (Schmidt et al., 2013, Hoffmeier et al., 2011). Titanium and its alloys are known to be sensitive to fretting fatigue indicating that this phenomenon is present (Niinomi, 2007, Nakazawa et al., 2003). This is likely to occur either at the screw-plate junction or bone-plate interface (Niinomi, 2008).

The fatigue effects of commercially pure titanium (grade 2), Ti-6Al-4V and 316L stainless steel were considered (Niinomi, 2007, Disegi, 2008). Idealised power-law S-N curves were assumed for each metal based on the static yield stress and the respective fretting fatigue limit in a simulated body environment (Figure 10.20) (Niinomi, 2007).

Fretting fatigue is also known to be dependent upon the contact pressure between the two parts (Nakazawa et al., 2003); this aspect is uncertain and so was ignored. Assuming 10,000 cycles to represent a week (Heiney et al., 2012, Hoffmeier et al., 2011), predictions of time to failure were estimated for each configuration at different levels of weight bearing.

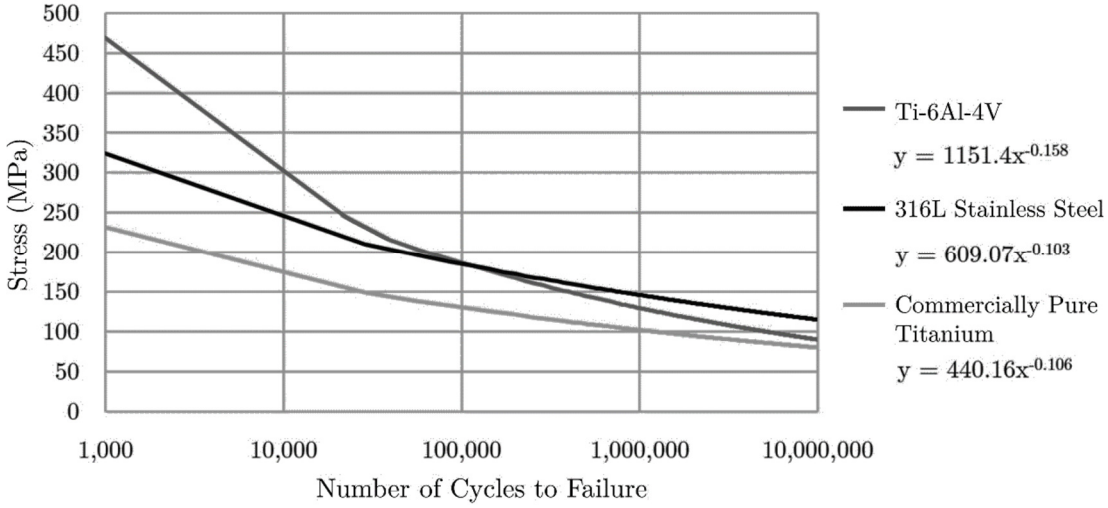

Figure 10.20 – The assumed S-N curves for fretting fatigue of the various materials used in the study.

The predicted fatigue life at different levels of weight-bearing incorporating a callus stiffness of 1MPa are shown in Table 10.2; Table 10.3 shows values using a callus stiffness of 100MPa. Cases where no failure was predicted within 24 months have been labelled 'OK'. Cases with an expected life of less than 0.1 month (4000 cycles) are labelled 'Fail'.

Table 10.2 – Predicted time to failure in months for different configurations and materials assuming a callus stiffness of 1MPa. Configurations that are predicted to last more than 24 months are denoted 'OK'.

	Weight-bearing level	MX-2356	MX-3568	MX-5689	DX-89	DX-23-5689	DX-23-689	DX-2-689	DX-5689
Ti-6Al-4V	25%	OK	OK	OK	OK	OK	OK	OK	OK
	50%	OK	OK	17.5	0.6	2.2	1.3	1.8	5.1
	75%	8.1	3.6	1.3	Fail	0.2	0.1	0.1	0.4
316L Stainless Steel	25%	OK	OK	OK	OK	OK	OK	OK	OK
	50%	2.8	4.9	0.9	0.1	0.1	0.1	0.2	0.2
	75%	0.1	0.1	Fail	Fail	Fail	Fail	Fail	Fail
Commercially Pure Titanium	25%	OK	OK	OK	3.7	24.0	11.2	17.7	OK
	50%	11.0	3.3	0.7	Fail	Fail	Fail	Fail	0.1
	75%	0.2	0.1	Fail	Fail	Fail	Fail	Fail	Fail

Table 10.3 – Predicted time to failure in months for different configurations and materials assuming a callus stiffness of 100MPa. Configurations that are predicted to last more than 24 months are denoted 'OK'.

	Weight-bearing level	MX-2356	MX-3568	MX-5689	DX-89	DX-23-5689	DX-23-689	DX-2-689	DX-5689
Ti-6Al-4V	75%	OK	OK	OK	OK	16.2	16.3	OK	12.1
	100%	OK	OK	OK	OK	2.6	2.6	6.2	2.0
316L Stainless Steel	75%	OK	OK	OK	OK	0.5	1.2	4.7	0.8
	100%	OK	OK	20.9	7.9	Fail	0.1	0.3	0.1
Commercially Pure Titanium	75%	OK	OK	OK	OK	0.7	0.7	2.4	0.4
	100%	17.0	OK	12.2	5.4	Fail	Fail	0.2	Fail

Despite steel producing larger stress in all configurations, commercially pure titanium is predicted to fail first in the majority of configurations using a callus of 1MPa (Table 10.2). In cases where it did not produce the lowest life expectancy for 1MPa, it was lowest for a 100MPa callus (Table 10.3). Ti-6Al-4V was predicted to have the best

fatigue performance in all cases even though it has an inferior fatigue strength at a high number of cycles compared with steel.

The diaphyseal fracture pattern from the literature (D3) failed by fatigue at between 3 months (Kim et al., 2012). The predictions for steel and pure titanium indicate that this configuration is only safe with 25% weight-bearing; using Ti-6Al-4V, failure is only predicted within 1-2 months at 50% W.B. (Table 10.2). While the metaphyseal gap defects were more tolerant to 50% weight-bearing, all steel and pure titanium cases were expected to fail within 1-11 months; predictions for Ti-6Al-4V were similar at 75% W.B. In the literature, cases of short working length failure occurred between five and ten months post-surgery (Gardner et al., 2009, Hak et al., 2010b, Button et al., 2004). The extra-long WL case failed in 2 months (Ehlinger et al., 2011). In this case all materials were predicted to fail within 1 month at 50% W.B.

10.3.3.5 Understanding the Differences between Configurations

The influence of different callus stiffness' was investigated further using the idealised model developed in Chapter 8. To represent the healing period, callus properties were varied through the step time, increasing exponentially up to 100MPa (Figure 10.21a) (Comiskey et al., 2010, Steiner et al., 2014); the applied load was increased linearly throughout the step up to 250N (Figure 10.21b). Two working lengths were investigated (36mm and 108mm) using a titanium plate and a fracture gap 10mm.

The results showed IFM decreases sharply with step time for both working lengths even though the load is increasing (Figure 10.21). The increase in stiffness observed for the larger working length is similar to the S-shape shown by Claes and Cunningham (2009) and Epari (2013). It also shows that longer working lengths produce larger plate stress earlier in the healing process whereas shorter working lengths produce larger stress later (Figure 10.21b). The point of transition is likely to be dependent upon many variables (gap and callus size, device stiffness, applied load); however, in this case it occurred at

a callus stiffness of approximately 2-3MPa. This explains the observations of steel plates producing larger stress than titanium despite producing smaller IFM. It also demonstrates that the plate stress produced by flexible devices is more sensitive to callus formation than for more rigid devices.

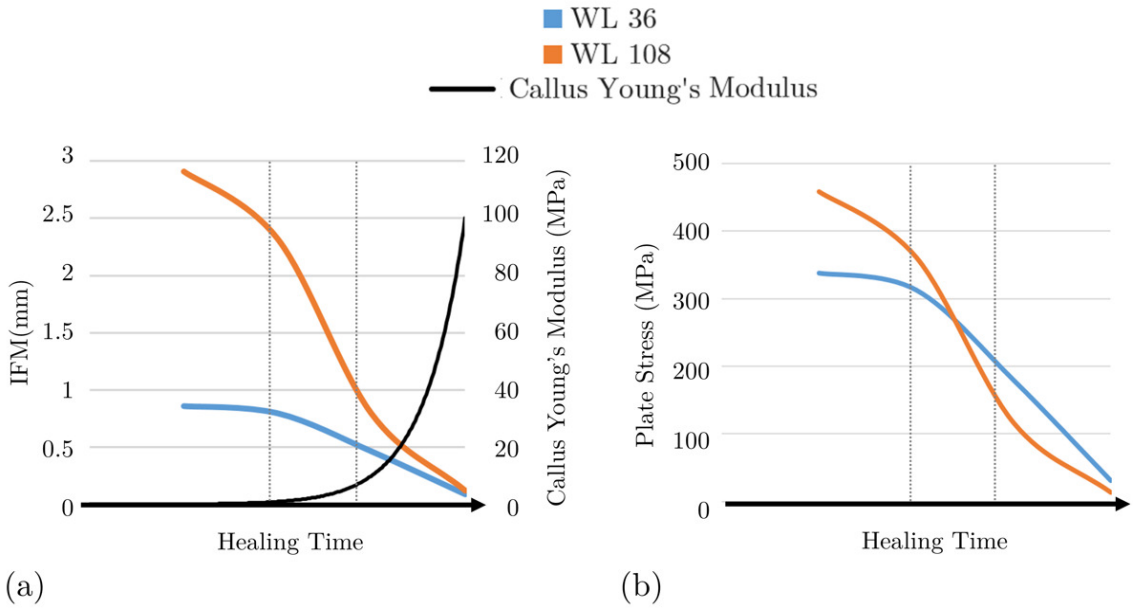

Figure 10.21 – Comparison of different plate rigidities, represented by two working lengths (36mm and 108mm), showing: (a) the assumed increase in callus stiffness and the reduction in IFM over the healing period; (b) the reduction in plate stress over the healing period.

10.3.3.6 Titanium versus Steel in Vitro

Several studies have compared the performance of titanium and steel plates in vitro (Schmidt et al., 2013, Hoffmeier et al., 2011). Configurations MX-2356, DX-23-5689 and DX-2-689 were examined using in vitro loading case (d), which is similar to the experimental conditions used in previous studies (Schmidt et al., 2013, Hoffmeier et al., 2011). Figure 10.22 shows that titanium produces larger plate stress than steel for all configurations (with a gap osteotomy). This is due to the increased lateral deflections and bending moment produced. As the differences in stress are caused by deformation,

the level of load and flexibility of the construct can influence the stress produced by titanium and steel. This was confirmed with the relative difference in stress between titanium and steel more than doubling between 368N and 736N. This also explains why the differences are very small for the configuration MX-2356; the fracture is very close to the joint so rotation due to deformation does not add significantly to the loading eccentricity. On the other hand, in the diaphyseal configurations (DX) larger differences are observed as the length of bone on either side of the fracture is greater.

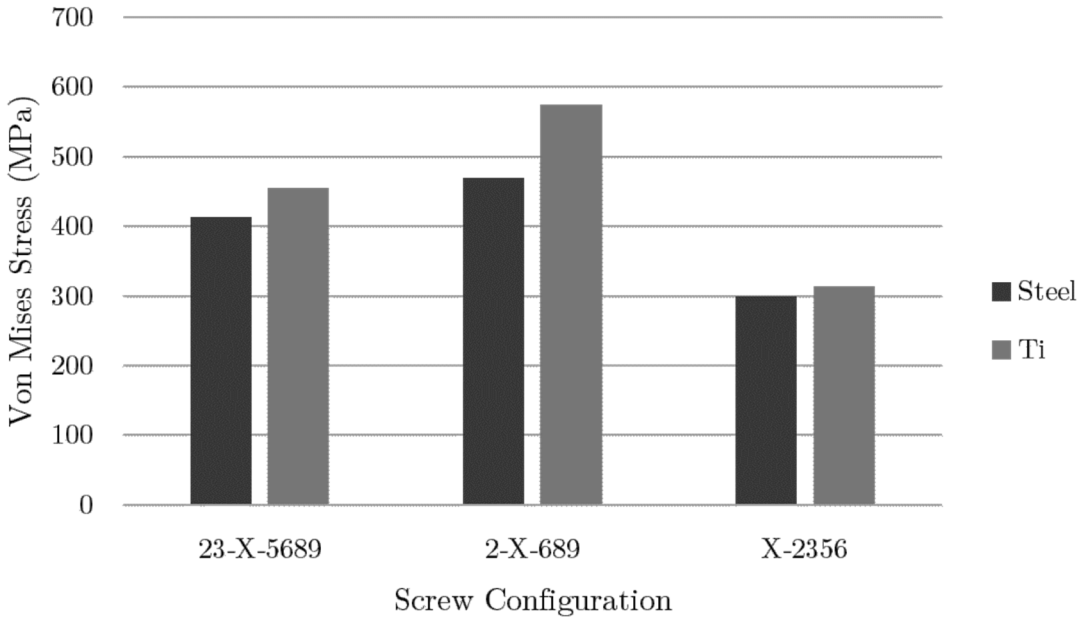

Figure 10.22 – Plate stress produced by different plate materials and configurations using in vitro loading case (d).

10.4 Discussion

This study found that the choice of restraint conditions substantially altered the biomechanical behaviour of femora, both intact and implanted with locked plating. Predictions of IFM, location and magnitude of peak stress within the plate and the joint reactions at the knee were all influenced. The inclusion of muscle forces also had an influence on these variables, however, it was much less pronounced. The developed in vivo model used spring elements at the hip and produced a mechanical environment that was within the extremes presented by the in vitro conditions and is considered to be more physiological.

10.4.1 Displacement and Strain Predictions (Intact Femur)

Taylor et al. (1996) examined femoral head displacements due to single-legged stance using radiographs; the single-legged stance instance of gait (15%) used in this study was assumed to be comparable (Debevec et al., 2010). While it is difficult to draw any strong conclusions from the radiological measurements by Taylor et al. (1996), taking an average of the two subjects, the maximum vertical displacement of the femoral head was 1.5mm. The intact cases (e) and (f) produced maximum vertical displacements of 1.3mm and 1.2mm respectively; however, only case (f) produced negative (upwards) displacement which was observed by Taylor et al. (1996) in subject 2. These values of vertical displacement are considerably less than that of Speirs et al. (2007) at around 3.2mm who used the relatively flexible restraint condition (d).

The present study predicted vertical and medial displacements at the centre of femoral head of 0.5mm and 3.2mm respectively. The transverse (M-L) motions are comparable to the value of 2.9mm predicted by Helwig et al. (2013) in the single-legged stance phase during walking, however, in this study vertical displacements were not provided. Considering both displacement directions, the results are most similar to those of Polgar et al. (2003) with vertical displacement of 0.6mm and medial displacement of 2.1mm.

Despite the fact that a slightly different instance of gait (10%) was used for muscle activity, it is still likely that these similarities in deformation behaviour are mostly due similar restraint conditions. Polgar et al. (2003) also used a hinge at the knee by directly restraining nodes on each of the condyles in the vertical direction. Most other simulations in the literature predict smaller transverse displacements at the femoral head than in the shaft (Phillips, 2009, Speirs et al., 2007). These predictions are consistent with a pinned column approach where bowing of the femur would be expected and tensile and compressive strains are of similar magnitude within the femoral shaft (Phillips, 2009, Duda et al., 1998, Speirs et al., 2007). Conditions (a), (c), (d) and (g) produce this response whereas conditions (b), (e) and (f) produce greater displacement at the femoral head. Some studies advocate that muscle forces act to reduce the bending forces in the femoral shaft, which would reduce the bowing under load (Duda et al., 1998, Sverdlova and Witzel, 2010). While there was still bending in the femoral shaft, the present model was predominantly in axial compression with a peak compressive strain in the femoral shaft of 0.124% or 1240μstrain. Other than at muscle attachment locations, the peak tensile strain was around 30% lower than the compressive strain at 0.087% or 870μstrain matching predictions by Helwig et al. (2013). The cross-sectional strain distribution at different locations within the femur is shown in Appendix D.1.2.

The hip springs resulted in some horizontal reaction force at the hip and also absorbed a small part of the applied force (along the mechanical axis). The resulting hip vectors for the present study were found to match closely to those measured by Bergmann et al. (2001). Both studies used the same coordinate system and the resulting hip joint vectors expressed as % B.W. were [41.6, 73.4, 224.2] and [24.9, 67.8, 232.0] respectively.

10.4.2 **Interfragmentary Motion**

Several studies have suggested that locking plates can be overly-rigid, which can be detrimental to healing (Granata et al., 2012, Bottlang et al., 2010a, Kubiak et al., 2006, Henderson et al., 2010). In a study of sixty-six distal femoral fractures treated with

locked plating Lujian (2010) found that 37% had a deficient bridging callus at six months postoperatively. Plate material was found to be important with this figure reducing to 26% for titanium plates and increasing to 49% for steel plates ($p = 0.01$). In addition to reduced callus formation, studies have found that steel plates present slightly increased risk of non-union, although this is not significant (Hoffmann et al., 2013, Henderson et al., 2011). On the other hand, Henderson et al. (2011) found that non-unions were significantly ($p = 0.01$) more likely to have no empty plate holes on either side of the fracture. While Lujian et al. (2010) found only a modest correlation between bridging span and callus formation, working length can be suppressed if there is bone-plate contact (Hoffmeier et al., 2011), which may explain the weakness of this result ($r = 0.3$).

The increased callus formation associated with titanium plates (Lujan et al., 2010, Bottlang et al., 2010a) was reflected in the larger IFM predictions of titanium, particularly with smaller WL. The smallest working lengths also produced the smallest IFM for similar fracture patterns; however, axial IFM was found to vary less than would be expected from in vitro predictions (Stoffel et al., 2003). At 10 weeks, the maximum axial IFM was 41% larger than the minimum IFM for titanium configurations (range of WL: 40mm-174mm); for steel this difference was 34%. The 90° orientation of the plate produced a relatively stiffer mechanical environment compared with Chapter 5. Additionally, previous computational studies that have incorporated healing callus show a similarly small influence of screw configuration on IFM in plating (Wongchai, 2012, Duda et al., 2002, Miramini et al., 2013). To further examine this, gap defect models using the same boundary conditions as case (f) were run and much larger difference in axial IFM were observed. The increase in IFM between MX-2356 and MX-5689 (100% increase in WL) was 33%; in the in vivo simulation using 1MPa callus, the increase was only 5.7%. This demonstrates that even modest callus formation can significantly impact on axial IFM. Predictions of plate stress and IFM are similar in magnitude to those by

Duda et al. (2002) in an FE simulation of the tibial shaft. Miramini et al. (2013) also included callus formation and found that working length did not alter IFS, however, plate material did. While their callus stiffness was slightly lower (0.05MPa), there was a much larger volume of callus surrounding the fracture.

This study has found that the shear movement is influenced by the choice of WL in the early stages of healing, although it is not necessarily related to axial IFM. All configurations produced larger shear IFM than axial IFM in the early stages of healing. This contrasts with the in vitro loading conditions tested in Chapter 5 where relative transverse motions at the fracture site were very small. The role of shear movement in fracture healing is still unclear; this is due to contradictory results in the literature (Augat et al., 2003, Park et al., 1998) most likely caused by differing test procedures (magnitudes and directions of applied load) and fracture patterns (i.e. reduced or gap, transverse or oblique) (Steiner et al., 2014). The combination of shear movement with axial movement has not been shown to be detrimental (Park, 2004, Augat, 2004); intramedullary nails have been shown to have larger shear motions than axial motions, yet have similar rates of non-union to locking plates, which are thought to produce a low shear environment (Duda et al., 2001, Henderson et al., 2010). Locking plates, on the other hand, have been associated with a greater incidence of non-union when using small working lengths (Henderson et al., 2011).

10.4.3 **Plate Stress**

Several studies state that too many screws can concentrate stress within the plate leading to plate breakage (Tan and Balogh, 2009, Ehlinger et al., 2011). In Chapter 8 it was shown that, other than working length, screw position has no influence on plate stress. In the literature, most examples of plate breakage were found to use a short working length (up to 55mm). Two medium working length cases had insufficient bone-plate off-set, which reduced the working length and failed in a similar manner to the short working length examples (Vallier et al., 2006, Hunt and Buckley, 2013). No cases

of plate breakage were found that used a moderate or long working length (approx. 74-115mm), however, there was one that used a very long WL (approx. 174mm) (Ehlinger et al., 2011).

In the context of in vitro gap defect models, the relationship between IFM and plate stress is straightforward; more flexible systems produce larger plate stress. Early weight-bearing in the presence of delayed healing is described as a cause of plate failure (Gardner et al., 2009, Granata et al., 2012); however, this study has shown that excessive plate rigidity can increase plate stress even in the presence of healing. The presence of callus allows more flexible systems to load-share reducing plate stress. In terms of stress reduction, there appears to be a compromise between allowing sufficient load-sharing and limiting the stress produced by flexure.

The presence of callus causes in vitro and in vivo tests to result in contradictory conclusions regarding the relative performance of steel and titanium. The in vitro conditions predicted that titanium plates produced larger plate stress than steel in all cases. The increase depended upon the working length of the configuration and the location of the fracture. The difference is most marked in the diaphysis because deformation under loading represents a larger proportion of the loading eccentricity. Conversely, the in vivo simulations predicted that titanium produced lower plate stress for all of the configurations examined. This is because in vivo simulations incorporate callus formation allowing load sharing even with modest callus formation. the difference in stress between steel and titanium was smallest (4%) when using configuration DX-89 demonstrating that steel may be beneficial for longer bridging spans, particularly early during the healing period. This is due to the greater stiffness of steel reducing the deformation and thus stress.

The effect of load-sharing at the fracture site was more pronounced when the callus was stiffer. In these situations, plate stress in shorter working lengths became larger than

that of moderate working lengths; indeed, the largest plate stress prediction was for the shortest working length case: DX-23-5689. Based on these findings it appears that moderate working lengths are less likely to break than short working lengths in vivo. It should be noted that more flexible plates can have different failure modes; for example, in Chapter 8 it was found that additional plate flexibility increases the strain within the bone around screw holes. Additionally, the predictions of plate stress indicate that early weight-bearing is likely to be better tolerated in metaphyseal fractures compared with diaphyseal patterns.

The difference in plate stress between small and moderate working lengths was small (5.3-5.8%); this is because the callus stiffness was identical for every configuration. In reality, the increased IFM of larger WL could promote faster healing (Comiskey et al., 2010), thereby reducing plate stress. Nevertheless, even small differences in stress have an impact on fatigue resistance;

10.4.4 **Fatigue Failure**

A recent in vitro study by Schmidt et al. (2013) found that stiffer steel plates demonstrate better survivability than the less stiff titanium plates. Although this was attributed to implant design rather than material, Hoffmeier et al. (2011) also demonstrated that stiffer steel plates perform better than titanium under fatigue using plates of identical cross-section. The results from these two previous studies are compared with the in vitro gap defect model using loading case (d) restrained vertically at the lateral condyle. The axial stiffness of the plated bone using configuration MX-2356 was 85N/mm for titanium and 138N/mm for steel. These values are comparable to those of Hoffmeier et al. (42-57N/mm), Schmidt et al. (50-100N/mm) and Zlowodzki et al. (64-213N/mm) who used similar working lengths (~55mm). Interestingly, under a cyclic load of 368N, Ti-6Al-4V is predicted to last for 37% fewer cycles than steel. Although different loads were used, Schmidt et al. (2013) found that Ti-6Al-4V plates (POLYAX and Synthes) endured an average of 17.4% fewer cycles than steel

counterparts (AxSOS and PERI-LOC). Similarly, Hoffmeier et al. (2011) found that steel plates withstood 1.6 times as many cycles of loading using a load of 265N for commercially pure titanium plates and 420N for steel plates. Using loads of 273N and 400N, an identical prediction was made for screw configuration DX-2-689. The larger differences between steel and titanium found by Hoffmeier et al. (2011) are therefore due to the use of a mid-diaphyseal fracture.

The predictions of fatigue strength in vivo, however, contradict the results of the in vitro style tests, with Ti-6Al-4V performing best in all cases. Callus formation reduces the mechanical demands placed on the plate, which inhibits fatigue failure. This implies that less stiff plates with lower in vitro fatigue resistance may not fail in vivo; conversely, stiffer plates may have larger fatigue resistance in in vitro tests, but supress healing, restrict load-sharing and ultimately fail earlier in vivo.

All Ti-6Al-4V and steel cases examined could support 25% weight-bearing in the early stages without exceeding the relevant fatigue stress. Diaphyseal fracture patterns generally had lower fatigue resistance than metaphseal fractures; using pure titanium some failures were predicted within 24months, even with 25% weight-bearing. For metaphyseal fractures using a moderate WL of 74mm, pure titanium was expected to last 3.3 months compared with steel at 5 months.

No configuration or material was able to withstand full weight-bearing without substantial callus healing. In an in vitro study, Granata et al. (2012) advised against immediate full W.B. despite finding a fatigue strength of 1329N using an in vitro gap defect model. While the majority of specimens survived over 200,000 cycles, nearly half of the specimens failed before 125,000 cycles (3 months). This study used a clamped condition at the knee, which will increase the failure load of the plate (Chapter 5) and explains the increased fatigue life estimates compared with this study (around 1-5 months for 50% W.B. using steel).

It is intuitive that longer working length increases plate stress due to flexure, however, the fatigue predictions demonstrated that both short and long working lengths can fail by fatigue before a moderate working length. With increased healing in the diaphysis, plates with moderate WL (80mm) were expected to survive 3 months longer than short WL (40mm). This was true for all materials. Nevertheless, an optimum was shown to exist where, both in the earlier and later stages of healing, plate stress is minimised. This minimum was predicted to be approximately 74-80mm for all fracture patterns. Despite the modelling results, however, no case of plate failure were found in the literature that used a long working length (approximately 115mm) indicating that this may also be in the optimal range. Two other cases of meta-diaphyseal fractures, MD1 and MD2, (Sirbu et al., 2011, Syed et al., 2004) used working lengths of approximately 108mm and 144mm; both healed despite massive comminution (Figure 10.23). Another case with a large displaced fragment, MD3, healed with the aid of bone graft using a long working length (~126mm) (Sirbu et al., 2011).

Unexpectedly, there was no difference in optimum working length between titanium and steel plates; however, Ti-6Al-4V produced lower plate stress in every case examined and is therefore likely to be less sensitive to screw placement generally. Based on these findings a higher incidence of plate breakage in steel plates would be expected. Banovetz (1996), however, found that titanium plates suffered from a higher incidence of hardware failure. It may be that these cases of failure used pure titanium and not Ti-6Al-4V. The design of implants also clearly plays an important part of fatigue strength; not all Ti-6Al-4V implants will perform better than all stainless steel implants (Schmidt et al., 2013).

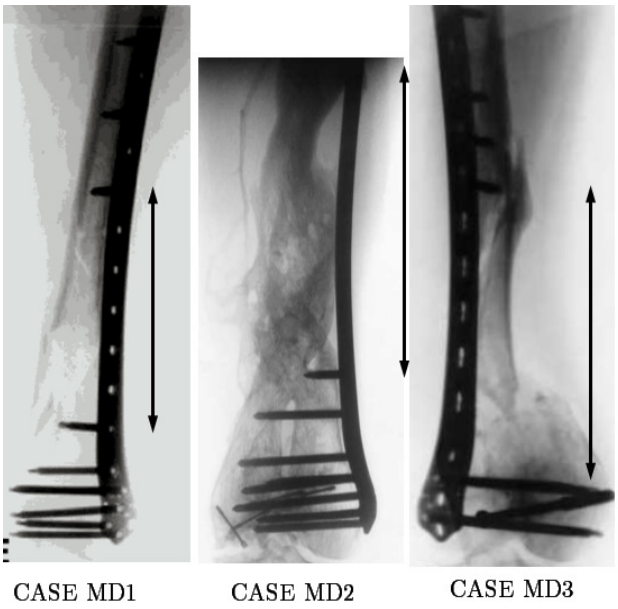

Figure 10.23 – Severely comminuted distal femur fractures that used a long working length. The working length is annotated.

This study generally underestimated of the fatigue life of the clinical examples; this is to be expected as immature callus was assumed for the duration of the loading period; nevertheless, they demonstrate that clinically useful predictions can be made, if the loading regime and callus properties are known.

10.4.5 Are In Vitro Tests Representative of the In Vivo Environment?

This study has found that in vitro test conditions produce a significantly different mechanical environment to the in vivo conditions; predictions of IFM and location and magnitude of plate stress were considerably altered. Loading condition (a) and (c) produced much lower plate stress than the other conditions evaluated. Studies which choose to use these conditions should be aware that it may not, therefore, be appropriate for the prediction of fatigue strength or loads to failure (Granata et al., 2012, Liang et al., 2012, Salas et al., 2011a). Differences in loading conditions also explain the differences in failure loads of the pinned studies such as Hoffmeier et al. (2011) and

Zlowodkzi et al. (2004) who predicted static failure loads of 385-1126N compared with Liang et al. (2012), who found failure loads of at least 4000N, and Granata et al. (2012) who predicted a fatigue strength of 1361N.

The influence of a healing callus is difficult to incorporate in in vitro tests; however, its absence changes the mechanical environment. Other than the profound effect this has on the relative performance of steel and titanium plates, this study has found other limitations of in vitro conditions. For all in vitro style test regimes, IFM correlates with plate stress; this correlation, however, does not exist for the in vivo simulations. None of the in vitro cases predicted the peak stresses at the failure location observed in clinical failures of metaphyseal fractures. Condition (c) produced a location of high stress on the posterior-lateral edge of the plate next to the first screw proximal to the fracture, however, the magnitude of the stress was much smaller (50-63%) than the in vivo model (f). Case (b) used an unrestrained hip and case (d) allowed free rotation at the knee; both predicted very large stresses and they were located within the working length of the plate.

Some previous studies have developed three-dimensional finite element models of a plated fractured femur and have employed different loading conditions (Figure 10.24). Using in vitro loading condition (a), Arnone et al. (2013) found peak plate stresses at the same location as this study (Figure 10.24a). Anitha et al. (2013) found the peak stress at the mid-span of the working length using a test set-up similar to in vitro condition (b) (Figure 10.24b). Chen et al. (2013) used the inverse of condition (b) where the proximal end of the femur was clamped and the load applied at the femoral condyles; in this case the location of peak stress was not consistent with the predictions of this study (Figure 10.24c). It is, however, intuitive that the peak stress should be closest to the restraint, and the result in the present study may be due to geometrical changes in the plate near the condyles. Salas et al. (2011a) found that the femur fractured at the end screw using a condition similar to case (a); this location of increased strain within

the bone was observed in conditions (a) and (c) but not in the more flexible loading conditions. It was, however, most pronounced in the in vivo conditions (e) and (g), and to a lesser extent case (f).

Using a pinned condition, medial condylar restraint produced 2.7 times greater plate stress than lateral condylar restraint (Figure 10.24d and e). It can be inferred that treating the knee as a ball joint, or the use of proximal and distal hinges, which are in the plane of the plate bending, would produce a result in-between these values. This demonstrates the sensitivity of experimental fatigue life predictions to the test set-up, even for similar loading regimes.

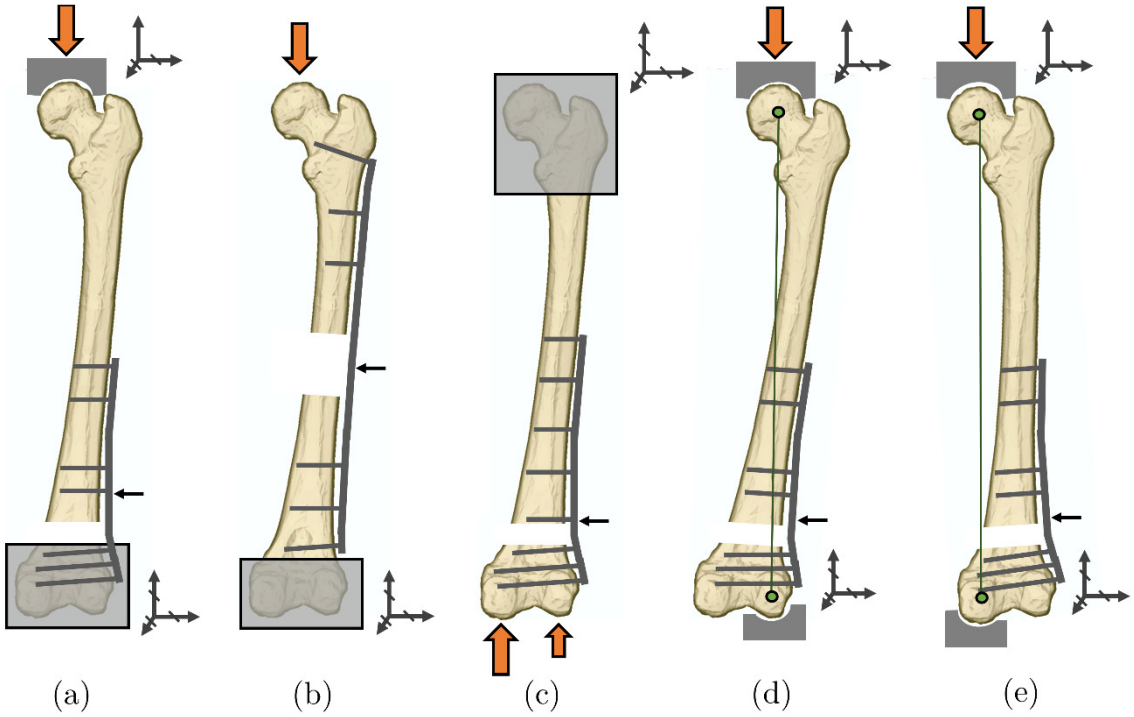

Figure 10.24 – Test set-up depictions for (a) Arnone et al. (2012); (b) Anitha et al. (2013); (c) Chen et al. (2013); (d) laterally restrained pinned case; and (e) medially restrained pinned case. The location of peak stress is annotated with a black arrow.

10.4.6 **Modelling of the Femur**

Modelling the knee with bicondylar support (Polgar et al., 2003) instead of a single node as done by many previous authors (Duda et al., 1997, Behrens et al., 2009, Lerch et al., 2012, Speirs et al., 2007) enables the model to predict medial and lateral condylar joint reactions. It also increases the sensitivity of the model to conditions at the hip. Changing the angle of the loading vector by 3.7° valgus resulted in 100% of the load being transmitted medially. Malpositioning of tibial components of total knee arthroplasty have been found to produce similar changes in load distribution (Werner et al., 2005). Therefore, the use of a single knee joint reaction can mask mal-alignment in models. This also highlights the importance of mechanical alignment in operative plate positioning.

Changes in the properties of articular cartilage have been recently shown to considerably alter force transmission at the knee joint (Adouni and Shirazi-Adl, 2013). It is, therefore, not surprising that incorporating subsidence in the acetabulum through the use of a spring-based restraint is so influential in the model. This may be a more important factor for the global mechanical behaviour than other features such as preloaded ligaments around the hip capsule that Helwig et al. (2013) incorporated.

10.4.7 **Limitations**

The use of linear springs at the hip was based on producing the known knee joint reactions for a specific load case (15% gait). It may be that there is a nonlinear spring relationship that would be suitable for all load cases. Day et al. (1975) measured hip forces and the settlement of wet acetabular cartilage under load. The load-deformation response was significantly non-linear with a sharp increase in stiffness at approximately 0.25mm. While springs have been included for the hip, they could also be incorporated for the knee.

Muscle activity in the immediate post-operative period is unlikely to be the same as normal weight-bearing; however, to the author's knowledge, no muscle force data for this period is available. Nevertheless, muscle forces were found to be less influential than the restraint conditions.

It should be noted that throughout this study no contact between the bone and plate was modelled. In reality this could substantially reduce motions. Additionally, a bone-plate off-set was used (approximately 4.0-9.6mm at the condyles; 0.5-2.0mm in the shaft); this could potentially add some movement to all cases due the additional bone-plate off-set. The deformation of the screws between the plate and bone, however, was found to contribute approximately 0.01mm to IFM.

The model was not directly validated. Many of the modelling aspects, however, have been evaluated earlier in this thesis including the screw-bone interaction (Chapter 2.1) and screw-plate interaction (Chapter 5.2).

10.5 Conclusions

- The restraint conditions are the primary determinant in predictions of IFM, plate stress and locations of failure when using biomechanical models of locked plating.
- In vitro models are not representative of the in vivo fracture environment where callus is present. This study can help to inform experimental studies about the consequences of the assumptions being made with regard to restraint conditions and the simplifications required for in vitro testing.
- Failure locations and expected fatigue failure times were predicted for a range of screw configurations. The predictions matched clinical findings closely.
- Bone-plate contact appears to be a prominent cause of failure in locked plating.

11 Conclusions

The primary aim of this study was evaluate and optimise the performance of locked plating using finite element analysis, which permits consideration of a wide range of scenarios with relative ease. In order to achieve this aim, it was necessary to address a range of complex modelling issues that have not so far received the attention they deserve.

11.1 Interface Modelling

Various approaches to modelling the screw-bone interface were evaluated. Subsequent studies can now make informed modelling decisions based on their variables of interest. If interfragmentary motion (IFM) is the focus of the study then tied interactions are generally sufficient; if local stress-strain distribution is required then nonlinear contact interactions should be used. Where extremely rigid boundary conditions exist or the bone is much softer than cortical bone, separation arising at contact interfaces can become more significant.

It is important to note that contact interactions should not be used to 'fine tune' numerical models to experimental data. In the majority of situations, changes in contact

interactions should not cause noticeable differences. Moreover, geometric nonlinearity is likely to be much more influential than contact modelling.

Localised bone damage around the screw-bone interface can occur even before weight-bearing loads due to screw fastening. A novel approach to modelling the effect of undersized pilot holes was proposed and evaluated. The approach, which uses anisotropic thermal expansion to produce the interference fit, has several advantages: it simplifies the modelling process, particularly where screw threads are included; it allows several levels of interference to be simulated by changing only a single value; and is straightforward to implement.

The effect of including inelasticity was investigated using plasticity. Furthering studies could also incorporate visco-elasticity to evaluate the longer-term response.

11.2 Modelling Conventional and Locking Screws

Locking screws are promoted as being superior to conventional screws in osteoporotic bone; however, their advantages are not clear in healthy bone. Locking screws function differently to conventional screws and the entire bone-plate construct must be considered for any comparison. The typical qualitative explanation for the difference is that locking screws function as a single 'fixed angle' unit and therefore must all fail simultaneously; conventional screws fail by pull-out individually. This explains increases in failure load, but not the differences between the bone qualities. This study provided a biomechanical basis for this discrepancy. Both screw types produce greatly increased strains in osteoporotic bone. While locking screws produced larger compressive strains in some situations, conventional screws always produce much larger tensile strains than locking screws. In osteoporotic bone the magnitude of the tensile strain produced by conventional screws was relatively unaffected by fracture gap reduction. This demonstrates that screw tightening preload is essential to capturing the strain environment produced by the conventional screws. Additionally, the impact of different

aspects of the modelling was examined: material and geometric changes associated with osteoporosis were found to be equally influential in strain predictions.

Future studies could use these findings to optimise new screw types for tensile strain minimisation.

11.3 Loading and Boundary Conditions

The study found that the range of stiffness predictions from previous studies examining locking plates varied by three orders of magnitude. This wide variation can be explained largely by the choice of boundary condition. Studies using similar loading regimes but different materials and geometries generally fall within a single order of magnitude. The extent to which the boundary conditions can influence the mechanical response was quantified; in experimental tests the variation was over six times. As expected, finite element simulations were more sensitive to the boundary conditions and produced differences of over twenty-four-fold.

At present, studies draw contrary conclusions regarding effectiveness of screw placement, locations of peak strain, failure load and stiffness due to differences in boundary conditions. For example: working length has been shown to have substantial impact in some studies but not in others; peak strains can be located at the screw nearest or farthest from the fracture; predicted failure loads in femoral locked plating can vary by be ten-fold.

Due to the sensitivity of the bone-plate system to the boundary conditions used it is recommended that experimental boundary conditions are standardised, thus enabling comparisons between studies. Under axial loading, the only boundary condition that can be used for this purpose is the pinned condition as others leave clamp tightness as an unknown variable. The limitation of this boundary condition is that it does not allow for the bi-condylar restraint provided by the knee.

The boundary conditions used in experimental tests represent extremes — either freely rotating or overly rigid. Numerically, it is possible to produce a boundary condition in-between these extremes by incorporating springs. This approach was used in this study to produce results comparable to more involved modelling techniques, such as including the surrounding hip and knee structures with ligaments. For studies wishing to create the in vivo condition, this presents an efficient means of modelling the bone in isolation while including the effects of restraint from neighbouring bodies. Unfortunately, the spring stiffness is dependent upon the entire system and must be evaluated for the specific model. Future studies could also incorporate nonlinear springs and use springs at the knee as well as at the hip.

11.4 Analytical Modelling of the LCP

This thesis demonstrates that for the prediction of fracture gap motion, a simplified two-dimensional approximation can be sufficient. This is especially true when simulating lab experiments where the plate bending is predominantly about the weak axis. In clinical practice, there are a very large number of biological, psychological and mechanical variables that influence the course of healing. While other factors may be out of the surgeon's control, the mechanical environment can be controlled to a degree by device configuration. As this simple model can reliably predict lab experiments using only seven variables, it has the potential to be used as a tool to predict the mechanical environment in vivo with much less effort than other methods. Due to its simplicity, the present model has some limitations. It is sensitive to the input parameters. Some of these variables could be obtained from manufacturers' data such as second moment of area, young's modulus and plate depth; however, some others may need to be obtained from radiographs. The model assumes symmetry. This did not appear to influence the results significantly, however, a-symmetry is something that could be incorporated by the addition of two variables: second fragment length and relative position of working length span. A method of incorporating bone quality into the analytical model was

developed; the elastic modulus of the bone was found to influence axial stiffness predictions far more than gap stiffness.

11.5 Optimising Screw Placement

The pinned boundary conditions, recommended in Chapters 5 and 6 were used to evaluate a range of screw configurations and screw types. For prediction of fracture gap motion, the working length was by far the most influential screw positioning variable. This is convenient as it shows that IFM can be optimised using working length and then the remaining screws can be positioned to reduce strain levels within the bone. Strain levels within the bone were highest at the first two screws closest to the fracture site. Under axial loading, three screws produced substantially lower strains than two screws but the addition of more screws yielded only slight reductions. Osteoporotic bone was found to be more susceptible to pull-out forces, and therefore sensitive to screw placement, than healthy bone. Due to the mix of pull-out forces and normal contact forces at screws, there was found to be an optimum distance between the two screws closest to the fracture gap; a spacing of one or two holes produced the lowest peak strains at the first two screws. Working length and plate rigidity also influenced strain levels.

In healthy bone the far cortex was exposed to much smaller strains than the near cortex; in osteoporotic bone, the distribution was much more even. This supports clinical guidance that bi-cortical screws should be used in bone of poorer quality and explains why osteoporotic bone is more sensitive to the alternative screw types that fasten to a single cortex. Different locking screw types also influenced mechanical behaviour. Far-cortical locking screws (FCL) increased IFM but greatly increased strain levels; uni-cortical screws (UCL) did not increase IFM but increased strain levels.

An interesting finding from the experimental tests conducted was that filled screw holes do not increase the bending rigidity of a locking plate and that screws have some elastic

movement within the screw hole. This finding had modelling implications that were subsequently addressed.

One factor that can dramatically alter the mechanical behaviour of locked plating is the presence of bone-plate contact. If the plate is touching the bone, it can reduce the working length to the size of the fracture gap. If this situation occurs, screw placement will have much less significance. This may explain some locking plate failures that appear to have used larger working lengths.

11.6 Understanding Failures

A range of distal femur locked plating failures were examined. The majority of failures used working lengths that were relatively small (<55mm). Previous studies' experimental models, however, have predicted that small working lengths and more rigid devices generally perform better under fatigue conditions. Chapter 10 demonstrated that the results from current in vitro testing are misleading. Using in vitro models that ignore the presence of fracture callus, titanium plates produce higher stress. Conversely, with the inclusion of callus at the fracture site, steel plates produced higher stress. This is because the callus transmits some of the load and titanium allows greater load-sharing. In a similar manner, shorter working lengths produce lower stresses than larger lengths initially. As the callus stiffness increases, however, this trend is reversed. Therefore, models that neglects callus formation can actually draw contrary conclusions, regarding the fatigue strength of fracture devices, to those that include it.

Using a different screw configuration will influence the course of healing and perhaps even alter patient weight-bearing. For comparisons, however, the applied load and callus stiffness were consistent between configurations. This may, therefore, over-estimate the fatigue performance of the configurations with lower levels of callus stimulation. Future studies may wish to develop time-dependent simulations where increases in callus

stiffness are dependent upon strain exposure; these, however, would involve many more assumptions and could make interpretation more difficult.

11.7 Limitations

Only a diaphyseal tibial fracture and metaphyseal distal femur fracture were considered. It would be beneficial to investigate plating in the upper extremity as conclusions for lower limb loading may not fully apply.

In femur models muscles were included as preloaded wires. This representation could be improved by including wrapping using via points. Only a specific load case (single legged stance) was considered. Clearly the entire gait cycle could be examined, however, it was expected that the peak hip force would be the largest load that the implant would be exposed to. This would be representative for peak stress and fatigue estimates, and the upper limit of IFM exposure at the fracture site.

Although strain levels under static load are a good indicator of regions susceptible to screw loosening, it is something that occurs gradually over time. To simulate this is not straightforward, requiring plasticity, viscoplasticity or damage and a dynamic loading regime. Nevertheless, to fully understand loosening phenomena these aspects should be considered.

References

Adouni, M. & Shirazi-Adl, A. Computational biomechanics of the knee joint in gait - osteoarthritic and asymptomatic subjects. 19th Congress of the European Society of Biomechanics, 25-28th August 2013 Patras, Greece.

Afshar, R., Fong, T. S., Latifi, M. H., Kanthan, S. R. & Kamarul, T. 2012. A biomechanical study comparing plate fixation using unicortical and bicortical screws in transverse metacarpal fracture models subjected to cyclic loading. *J Hand Surg Eur,* 37**,** 396-401.

Ahmad, M., Nanda, R., Bajwa, A. S., Candal-Couto, J., Green, S. & Hui, A. C. 2007. Biomechanical testing of the locking compression plate: When does the distance between bone and implant significantly reduce construct stability? *Injury-International Journal of the Care of the Injured,* 38**,** 358-364.

Alho, A., Benterud, J. G., Hogevold, H. E., Ekeland, A. & Stromsoe, K. 1992. Comparison of functional bracing and locked intramedullary nailing in the treatment of displaced tibial shaft fractures. *Clinical Orthopaedics and Related Research***,** 243-250.

Allgöwer, M., Perren, S. & Matter, P. 1970. A new plate for internal fixation—the dynamic compression plate (dcp). *Injury,* 2**,** 40-47.

Alonso-Vazquez, A., Lauge-Pedersen, H., Lidgren, L. & Taylor, M. 2004. The effect of bone quality on the stability of ankle arthrodesis. A finite element study. *Foot & Ankle International,* 25**,** 840-850.

Althausen, P. L., Lee, M. A., Finkemeier, C. G., Meehan, J. P. & Rodrigo, J. J. 2003. Operative stabilization of supracondylar femur fractures above total knee arthroplasty: A comparison of four treatment methods. *The Journal of Arthroplasty,* 18**,** 834-839.

An, Y. H., Burgoyne, C. R., Crum, M. S. & Glaser, J. A. 2002. Current methods and trends in fixation of osteoporotic bone. *In:* AN, Y. H. (ed.) *Internal fixation in osteoporotic bone.* New York: Thieme Medical Publishers Inc.

Andrea, C. R., Stover, S. M., Galuppo, L. D., Taylor, K. T. & Rakestraw, P. C. 2002. Comparison of insertion time and pullout strength between self-tapping and non-self-tapping ao 4.5-mm cortical bone screws in adult equine third metacarpal bone. *Veterinary Surgery,* 31**,** 189-194.

Anitha, D., Das De, S., Sun, K. K., Doshi, H. K. & Lee, T. 2013. Improving stability of locking compression plates through a design modification: A computational investigation. *Comput Methods Biomech Biomed Engin,* 14**,** 14.

Apivatthakakul, T., Anuraklekha, S., Babikian, G., Castelli, F., Pace, A., Phiphobmongkol, V., White, R., Kojima, K. & Camuso, M. 2012. *Ao surgery reference: Tibial shaft* [Online].

Apostolou, C. D., Papavasiliou, A. V., Aslam, N., Handley, R. C. & Willett, K. M. 2005. Preliminary results and technical aspects following stabilisation of fractures around the knee with liss. *Injury Extra,* 36**,** 529-536.

Arnone, J. C., Sherif El-Gizawy, A., Crist, B. D., Della Rocca, G. J. & Ward, C. V. 2013. Computer-aided engineering approach for parametric investigation of locked plating systems design. *Journal of Medical Devices,* 7**,** 021001-021001.

Assari, S., Kaufmann, A., Darvish, K., Park, J., Haw, J., Safadi, F. & Rehman, S. 2013. Biomechanical comparison of locked plating and spiral blade retrograde nailing of supracondylar femur fractures. *Injury,* 44**,** 1340-5.

Augat, P. 2004. Reply to letter to the editor: Shear movement at the fracture site delays healing in a diaphyseal fracture model. *Journal of Orthopaedic Research,* 22**,** 1158-1159.

Augat, P., Burger, J., Schorlemmer, S., Henke, T., Peraus, M. & Claes, L. 2003. Shear movement at the fracture site delays healing in a diaphyseal fracture model. *Journal of Orthopaedic Research,* 21**,** 1011-1017.

Bae, J. H., Oh, J. K., Chon, C. S., Oh, C. W., Hwang, J. H. & Yoon, Y. C. 2011. The biomechanical performance of locking plate fixation with intramedullary fibular strut graft augmentation in the treatment of unstable fractures of the proximal humerus. *Journal of Bone and Joint Surgery-British Volume,* 93B**,** 937-941.

Baggi, L., Cappelloni, I., Di Girolamo, M., Maceri, F. & Vairo, G. 2008. The influence of implant diameter and length on stress distribution of osseointegrated implants related to crestal bone geometry: A three-dimensional finite element analysis. *Journal of Prosthetic Dentistry,* 100**,** 422-431.

Bähr, W. 1990. Pretapped and self-tapping screws in the human midface: Torque measurements and bone screw interface. *International Journal of Oral and Maxillofacial Surgery,* 19**,** 51-53.

Banovetz, J. M., Sharp, R., Probe, R. A. & Anglen, J. O. 1996. Titanium plate fixation: A review of implant failures. *J Orthop Trauma,* 10**,** 389-94.

Bartonicek, J. 2010. Early history of operative treatment of fractures. *Arch Orthop Trauma Surg,* 130**,** 1385-96.

Battula, S., Schoenfeld, A. J., Sahai, V., Vrabec, G. A., Tank, J. & Njus, G. O. 2008. The effect of pilot hole size on the insertion torque and pullout strength of self-tapping cortical bone screws in osteoporotic bone. *Journal of Trauma-Injury Infection and Critical Care,* 64**,** 990-995.

Baumgart, F. W., Cordey, J., Morikawa, K., Perren, S. M., Rahn, B. A., Schavan, R. & Snyder, S. 1993. Ao/asif self-tapping screws (sts). *Injury-International Journal of the Care of the Injured,* 24**,** S1-S17.

Bayraktar, H. H., Morgan, E. F., Niebur, G. L., Morris, G. E., Wong, E. K. & Keaveny, T. M. 2004. Comparison of the elastic and yield properties of human femoral trabecular and cortical bone tissue. *Journal of Biomechanics,* 37**,** 27-35.

Beardmore, R. 2013. *Thick walled cylinders* [Online]. [Accessed 04/06/2013.

Beaupre, G. S., Carter, D. R., Orr, T. E. & Csongradi, J. 1988. Stresses in plated long-bones: The role of screw tightness and interface slipping. *Journal of Orthopaedic Research,* 6**,** 39-50.

Beaupre, G. S., Giori, N. J., Caler, W. E. & Csongradi, J. 1992. A comparison of unicortical and bicortical end screw attachment of fracture fixation plates. *J Orthop Trauma,* 6**,** 294-300.

Behrens, B. A., Nolte, I., Wefstaedt, P., Stukenborg-Colsman, C. & Bouguecha, A. 2009. Numerical investigations on the strain-adaptive bone remodelling in the periprosthetic femur: Influence of the boundary conditions. *Biomedical Engineering Online,* 8.

Bell, J. C. & Ness, M. G. 2007. A mechanical evaluation of pre-tapped and self-tapped screws in small bones. *Vet Comp Orthop Traumatol,* 20**,** 277-80.

Benli, S., Aksoy, S., Havitcioglu, H. & Kucuk, M. 2008. Evaluation of bone plate with low-stiffness material in terms of stress distribution. *Journal of Biomechanics,* 41**,** 3229-3235.

Bergmann, G., Deuretzbacher, G., Heller, M., Graichen, F., Rohlmann, A., Strauss, J. & Duda, G. N. 2001. Hip contact forces and gait patterns from routine activities. *Journal of Biomechanics,* 34**,** 859-871.

Bhandari, M., Guyatt, G. H., Swiontkowski, M. F., Tornetta, P., Hanson, B., Weaver, B., Sprague, S. & Schemitsch, E. H. 2001. Surgeon's preferences for the operative treatment of fractures of the tibial shaft - an international survey. *Journal of Bone and Joint Surgery-American Volume,* 83A**,** 1746-1752.

Biliouris, T. L., Schneider, E., Rahn, B. A., Gasser, B. & Perren, S. M. 1989. The effect of radial preload on the implant-bone interface: A cadaveric study. *J Orthop Trauma,* 3**,** 323-32.

Bitsakos, C., Kerner, J., Fisher, I. & Amis, A. A. 2005. The effect of muscle loading on the simulation of bone remodelling in the proximal femur. *Journal of Biomechanics,* 38**,** 133-139.

Blecha, L. D., Zambelli, P. Y., Ramaniraka, N. A., Bourban, P. E., Manson, J. A. & Pioletti, D. P. 2005. How plate positioning impacts the biomechanics of the open wedge tibial osteotomy; a finite element analysis. *Comput Methods Biomech Biomed Engin,* 8**,** 307-13.

Board, T. N., Yang, L. & Saleh, M. 2007. Why fine-wire fixators work: An analysis of pressure distribution at the wire-bone interface. *Journal of Biomechanics,* 40**,** 20-25.

Bottlang, M., Doornink, J., Byrd, G. D., Fitzpatrick, D. C. & Madey, S. M. 2009a. A nonlocking end screw can decrease fracture risk caused by locked plating in the osteoporotic diaphysis. *J Bone Joint Surg Am. ,* 91**,** 620-627.

Bottlang, M., Doornink, J., Fitzpatrick, D. C. & Madey, S. M. 2009b. Far cortical locking can reduce stiffness of locked plating constructs while retaining construct strength. *Journal of Bone and Joint Surgery-American Volume,* 91A**,** 1985-1994.

Bottlang, M., Doornink, J., Lujan, T. J., Fitzpatrick, D. C., Marsh, L., Augat, P., Von Rechenberg, B., Lesser, M. & Madey, S. M. 2010a. Effects of construct stiffness on healing of fractures stabilized with locking plates. *Journal of Bone and Joint Surgery-American Volume,* 92A**,** 12-22.

Bottlang, M. & Feist, F. 2011. Biomechanics of far cortical locking. *Journal of Orthopaedic Trauma,* 25**,** S21-S28.

Bottlang, M., Lesser, M., Koerber, J., Doornink, J., Von Rechenberg, B., Augat, P., Fitzpatrick, D. C., Madey, S. M. & Marsh, J. L. 2010b. Far cortical locking can improve healing of fractures stabilized with locking plates. *Journal of Bone and Joint Surgery-American Volume,* 92A**,** 1652-1660.

Bower, A. F. 2010. Applied mechanics of solids. CRC Press.

Brown, C. U., Norman, T. L., Kish, V. L., Gruen, T. A. & Blaha, J. D. 2002. Time-dependent circumferential deformation of cortical bone upon internal radial loading. *Journal of Biomechanical Engineering-Transactions of the Asme,* 124**,** 456-461.

Bucholz, R. W., Heckman, J. D. & Court-Brown, C. M. (eds.) 2006. *Rockwood & green's fractures in adults 6th edition*.

Button, G., Wolinsky, P. & Hak, D. 2004. Failure of less invasive stabilization system plates in the distal femur: A report of four cases. *J Orthop Trauma,* 18**,** 565-70.

Carter, D. R., Blenman, P. R. & Beaupré, G. S. 1988. Correlations between mechanical stress history and tissue differentiation in initial fracture healing. *Journal of Orthopaedic Research,* 6**,** 736-748.

Chao, P., Conrad, B., Lewis, D., Horodyski, M. & Pozzi, A. 2013. Effect of plate working length on plate stiffness and cyclic fatigue life in a cadaveric femoral fracture gap model stabilized with a 12-hole 2.4 mm locking compression plate. *BMC Veterinary Research,* 9**,** 1-7.

Cheal, E. J., Hayes, W. C., White, A. A. & Perren, S. M. 1985. Stress-analysis of compression plate fixation and it's effects on long-bone remodeling. *Journal of Biomechanics,* 18**,** 141-150.

Chen, G., Schmutz, B., Wullschleger, M., Pearcy, M. J. & Schuetz, M. A. 2009. Computational investigations of mechanical failures of internal plate fixation. *Proceedings of the Institution of Mechanical Engineers Part H-Journal of Engineering in Medicine,* 224**,** 119-126.

Chen, J. C., Beaupré, G. S. & Carter, D. R. 2010a. An approach to quantifying bone overloading and hypertrophy with applications to multiple experimental studies. *Bone,* 46**,** 322-329.

Chen, S.-H., Chiang, M.-C., Hung, C.-H., Lin, S.-C. & Chang, H.-W. 2013. Finite element comparison of retrograde intramedullary nailing and locking plate fixation with/without an intramedullary allograft for distal femur fracture following total knee arthroplasty. *The Knee,* 21**,** 224-31.

Chen, S. J., An, Q., Zhang, Y., Gao, L. X. & Li, Q. 2010b. Loading analysis on the thread teeth in cylindrical pipe thread connection. *Journal of Pressure Vessel Technology-Transactions of the Asme,* 132.

Cheung, G., Zalzal, P., Bhandari, M., Spelt, J. K. & Papini, M. 2004. Finite element analysis of a femoral retrograde intramedullary nail subject to gait loading. *Medical Engineering & Physics,* 26**,** 93-108.

Claes, L. E. & Cunningham, J. L. 2009. Monitoring the mechanical properties of healing bone. *Clin Orthop Relat Res,* 467**,** 1964-71.

Claes, L. E., Heigele, C. A., Neidlinger-Wilke, C., Kaspar, D., Seidl, W., Margevicius, K. J. & Augat, P. 1998. Effects of mechanical factors on the fracture healing process. *Clinical Orthopaedics and Related Research,* 355**,** S132-S147.

Comiskey, D. P., Macdonald, B. J., Mccartney, W. T., Synnott, K. & O'byrne, J. 2010. The role of interfragmentary strain on the rate of bone healing-a new interpretation and mathematical model. *Journal of Biomechanics,* 43**,** 2830-2834.

Completo, A., Fonseca, F. & Simoes, J. A. 2007. Experimental validation of intact and implanted distal femur finite element models. *J Biomech,* 40**,** 2467-76.

Compte, P. & Straumann, F. 1985. Influence of unoccupied holes on the fatigue behaviour of bone fixation plates. *Proceedings of the European Society of Biomechanics: Current Interdisciplinary Research***,** 459-464.

Court-Brown, C. M., Aitken, S., Hamilton, T. W., Rennie, L. & Caesar, B. 2010. Nonoperative fracture treatment in the modern era. *J Trauma,* 69**,** 699-707.

Cristofolini, L., Schileo, E., Juszczyk, M., Taddei, F., Martelli, S. & Viceconti, M. 2010. Mechanical testing of bones: The positive synergy of finite-element models and in vitro experiments. *Philos Trans A Math Phys Eng Sci,* 368**,** 2725-63.

Cristofolini, L. & Viceconti, M. 2000. Mechanical validation of whole bone composite tibia models. *Journal of Biomechanics,* 33**,** 279-288.

Cristofolini, L., Viceconti, M., Cappello, A. & Toni, A. 1996. Mechanical validation of whole bone composite femur models. *Journal of Biomechanics,* 29**,** 525-535.

Cronier, P., Pietu, G., Dujardin, C., Bigorre, N., Ducellier, F. & Gerard, R. 2010. The concept of locking plates. *Orthopaedics & Traumatology: Surgery & Research,* 96**,** S17-S36.

Cunningham, J. L., Evans, M. & Kenwright, J. 1989. Measurement of fracture movement in patients treated with unilateral external skeletal fixation. *Journal of Biomedical Engineering,* 11**,** 118-122.

Dammak, M., Shiraziadl, A. & Zukor, D. J. 1997. Analysis of cementless implants using interface nonlinear friction - experimental and finite element studies. *Journal of Biomechanics,* 30**,** 121-129.

Davenport, S. R., Lindsey, R. W., Leggon, R., Miclau, T. & Panjabi, M. 1988. Dynamic compression plate fixation: A biomechanical comparison of unicortical vs bicortical distal screw fixation. *J Orthop Trauma,* 2**,** 146-50.

Davis, C., Stall, A., Knutsen, E., Whitney, A., Becker, E., Hsieh, A. H. & O'toole, R. V. 2012. Locking plates in osteoporosis: A biomechanical cadaveric study of diaphyseal humerus fractures. *Journal of Orthopaedic Trauma,* 26**,** 216-221.

Dawson, J. M. & Bartel, D. L. 1992. Consequences of an interference fit on the fixation of porous-coated tibial components in total knee replacement. *Journal of Bone and Joint Surgery-American Volume,* 74A**,** 233-238.

Day, W. H., Swanson, S. A. & Freeman, M. A. 1975. Contact pressures in the loaded human cadaver hip. *J Bone Joint Surg Br,* 57**,** 302-13.

Debevec, H., Pedersen, D. R., Iglic, A. & Daniel, M. 2010. One-legged stance as a representative static body position for calculation of hip contact stress distribution in clinical studies. *J Appl Biomech,* 26**,** 522-5.

Decoster, T. A., Heetderks, D. B., Downey, D. J., Ferries, J. S. & Jones, W. 1990. Optimizing bone screw pullout force. *J Orthop Trauma,* 4**,** 169-74.

Defino, H., Wichrchrchr, C., Shimano, A. & Kandziorara, F. 2007. The influence of pilot hole diameter on screw pullout resistance. *Acta Ortopédica Brasileira,* 15**,** 76-79.

Demos, H. A., Briones, M. S., White, P. H., Hogan, K. A. & Barfield, W. R. 2012. A biomechanical comparison of periprosthetic femoral fracture fixation in normal and osteoporotic cadaveric bone. *The Journal of Arthroplasty,* 27**,** 783-788.

Depuy 2005a. Polyax surgical technique. Distal femoral locked plating system.

Depuy 2005b. Surgical technique: Distal femoral locked plating system.

Depuy 2009. Small fragment plating system: Anatomic surgical locked plating surgical technique.

Disegi, J. 2008. Implant materials. Unalloyed titanium.

Dobele, S., Horn, C., Eichhorn, S., Buchholtz, A., Lenich, A., Burgkart, R., Nussler, A. K., Lucke, M., Andermatt, D., Koch, R. & Stockle, U. 2010. The dynamic locking screw (dls) can increase interfragmentary motion on the near cortex of locked plating constructs by reducing the axial stiffness. *Langenbecks Archives of Surgery,* 395**,** 421-428.

Doblaré, M., GarcíA, J. M. & Gómez, M. J. 2004. Modelling bone tissue fracture and healing: A review. *Engineering Fracture Mechanics,* 71**,** 1809-1840.

Donaldson, F. E., Pankaj, P. & Simpson, A. H. R. W. 2012a. Bone properties affect loosening of half-pin external fixators at the pin-bone interface. *Injury,* 43(10)**,** 1764-70.

Donaldson, F. E., Pankaj, P. & Simpson, A. H. R. W. 2012b. Investigation of factors affecting loosening of ilizarov ring-wire external fixator systems at the bone-wire interface. *Journal of Orthopaedic Research,* 30**,** 726-32.

Dostal, W. F. & Andrews, J. G. 1981. A three-dimensional biomechanical model of hip musculature. *Journal of Biomechanics,* 14**,** 803-812.

Dubov, A., Kim, S. Y. R., Shah, S., Schemitsch, E. H., Zdero, R. & Bougherara, H. 2011. The biomechanics of plate repair of periprosthetic femur fractures near the tip of a total hip implant: The effect of cable-screw position. *Proceedings of the*

Institution of Mechanical Engineers Part H-Journal of Engineering in Medicine, 225**,** 857-865.

Duda, G. N., Heller, M., Albinger, J., Schulz, O., Schneider, E. & Claes, L. 1998. Influence of muscle forces on femoral strain distribution. *Journal of Biomechanics,* 31**,** 841-846.

Duda, G. N., Mandruzzato, F., Heller, M., Goldhahn, J., Moser, R., Hehli, M., Claes, L. & Haas, N. P. 2001. Mechanical boundary conditions of fracture healing: Borderline indications in the treatment of unreamed tibial nailing. *Journal of Biomechanics,* 34**,** 639-650.

Duda, G. N., Mandruzzato, F., Heller, M., Kassi, J. P., Khodadadyan, C. & Haas, N. P. 2002. Mechanical conditions in the internal stabilization of proximal tibial defects. *Clinical Biomechanics,* 17**,** 64-72.

Duda, G. N., Schneider, E. & Chao, E. Y. S. 1997. Internal forces and moments in the femur during walking. *Journal of Biomechanics,* 30**,** 933-941.

Dunlap, J. T., Lucas, G. L., Chong, A. C. M., Cooke, F. W. & Tiruvadi, V. 2011. Biomechanical evaluation of locking plate fixation with hybrid screw constructs in analogue humeri. *American journal of orthopedics (Belle Mead, N.J.),* 40**,** E20-5.

Ebacher, V., Tang, C., Mckay, H., Oxland, T. R., Guy, P. & Wang, R. Z. 2007. Strain redistribution and cracking behavior of human bone during bending. *Bone,* 40**,** 1265-1275.

Ebraheim, N. A., Liu, J., Hashmi, S. Z., Sochacki, K. R., Moral, M. Z. & Hirschfeld, A. G. 2012. High complication rate in locking plate fixation of lower periprosthetic distal femur fractures in patients with total knee arthroplasties. *The Journal of Arthroplasty,* 27**,** 809-813.

Ebrahimi, H., Rabinovich, M., Vuleta, V., Zalcman, D., Shah, S., Dubov, A., Roy, K., Siddiqui, F. S., H. Schemitsch, E., Bougherara, H. & Zdero, R. 2012. Biomechanical properties of an intact, injured, repaired, and healed femur: An experimental and computational study. *Journal of the Mechanical Behavior of Biomedical Materials,* 16**,** 121-135.

Efunda. *Columns: Eccentric loads* [Online]. eFunda Inc. Available: https://www.efunda.com/formulae/solid_mechanics/columns/eccentric.cfm 2014].

Egol, K. A., Kubiak, E. N., Fulkerson, E., Kummer, F. J. & Koval, K. J. 2004. Biomechanics of locked plates and screws. *Journal of Orthopaedic Trauma,* 18**,** 488-493.

Ehlinger, M., Adam, P., Arlettaz, Y., Moor, B. K., Dimarco, A., Brinkert, D. & Bonnomet, F. 2011. Minimally-invasive fixation of distal extra-articular femur fractures with locking plates: Limitations and failures. *Orthopaedics & Traumatology: Surgery & Research,* 97**,** 668-674.

Eichinger, J. K., Herzog, J. P. & Arrington, E. D. 2011. Analysis of the mechanical properties of locking plates with and without screw hole inserts. *Orthopedics,* 34**,** 01477447-20101123.

Ellis, T., Bourgeault, C. A. & Kyle, R. F. 2001. Screw position affects dynamic compression plate strain in an in vitro fracture model. *Journal of Orthopaedic Trauma,* 15**,** 333-337.

Epari, D. R., Kassi, J. P., Schell, H. & Duda, G. N. 2007. Timely fracture-healing requires optimization of axial fixation stability. *Journal of Bone and Joint Surgery-American Volume,* 89A**,** 1575-1585.

Epari, D. R., Wehner, T., Ignatius, A., Schuetz, M. A. & Claes, L. E. 2013. A case for optimising fracture healing through inverse dynamization. *Medical Hypotheses,* 81**,** 225-227.

Erhardt, J. B., Stoffel, K., Kampshoff, J., Badur, N., Yates, P. & Kuster, M. S. 2012. The position and number of screws influence screw perforation of the humeral head in modern locking plates: A cadaver study. *J Orthop Trauma,* 26**,** e188-92.

Eser, A., Tonuk, E., Akca, K. & Cehreli, M. C. 2010. Predicting time-dependent remodeling of bone around immediately loaded dental implants with different designs. *Medical Engineering & Physics,* 32**,** 22-31.

Evans, M., Spencer, M., Wang, Q., White, S. H. & Cunningham, J. L. 1990. Design and testing of external fixator bone screws. *Journal of Biomedical Engineering,* 12**,** 457-462.

Feerick, E. M. & Mcgarry, J. P. 2012. Cortical bone failure mechanisms during screw pullout. *Journal of Biomechanics,* 45**,** 1666-1672.

Ferguson, S. J., Wyss, U. P. & Pichora, D. R. 1996. Finite element stress analysis of a hybrid fracture fixation plate. *Medical Engineering & Physics,* 18**,** 241-250.

Field, J. R., Törnkvist, H., Hearn, T. C., Sumner-Smith, G. & Woodside, T. D. 1999. The influence of screw omission on construction stiffness and bone surface strain in the application of bone plates to cadaveric bone. *Injury,* 30**,** 591-598.

Filipowicz, D., Lanz, O., Mclaughlin, R., Elder, S. & Werre, S. 2009. A biomechanical comparison of 3.5 locking compression plate fixation to 3.5 limited contact dynamic compression plate fixation in a canine cadaveric distal humeral metaphyseal gap model. *Veterinary and Comparative Orthopaedics and Traumatology,* 22**,** 270-277.

Firoozabadi, R., Mcdonald, E., Nguyen, T. Q., Buckley, J. M. & Kandemir, U. 2012. Does plugging unused combination screw holes improve the fatigue life of fixation with locking plates in comminuted supracondylar fractures of the femur? *J Bone Joint Surg Br,* 94**,** 241-8.

Fitzpatrick, D. Potential benefits of computer models in orthopaedics. OTC workshop on future of numerical modelling in trauma care, 2009 Boston.

Fitzpatrick, D. C., Doornink, J., Madey, S. M. & Bottlang, M. 2009. Relative stability of conventional and locked plating fixation in a model of the osteoporotic femoral diaphysis. *Clinical Biomechanics,* 24**,** 203-209.

Forster, M. C., Komarsamy, B. & Davison, J. N. 2006. Distal femoral fractures: A review of fixation methods. *Injury,* 37**,** 97-108.

Fouad, H. 2010. Effects of the bone-plate material and the presence of a gap between the fractured bone and plate on the predicted stresses at the fractured bone. *Medical Engineering & Physics,* 32**,** 783-789.

Fragomen, A. T. & Rozbruch, S. R. 2007. The mechanics of external fixation. *Hospital for Special Surgery (HSS Journal),* 3**,** 13-29.

Frigg, R. 2001. Locking compression plate (lcp). An osteosynthesis plate based on the dynamic compression plate and the point contact fixator (pc-fix). *Injury,* 32, Supplement 2**,** 63-66.

Gaebler, C., Speitling, A., Milne, E. L., Stanzl-Tschegg, S., Vécsei, V. & Latta, L. L. 2001. A new modular testing system for biomechanical evaluation of tibial intramedullary fixation devices. *Injury,* 32**,** 708-712.

Ganesh, V. K., Ramakrishna, K. & Ghista, D. N. 2005. Biomechanics of bone-fracture fixation by stiffness-graded plates in comparison with stainless-steel plates. *Biomed Eng Online,* 4.

Gantous, A. & Phillips, J. H. 1995. The effects of varying pilot hole size on the holding power of miniscrews and microscrews. *Plast Reconstr Surg,* 95**,** 1165-9.

Gao, K., Gao, W., Huang, J., Li, H., Li, F., Tao, J. & Wang, Q. 2013. Retrograde nailing versus locked plating of extra-articular distal femoral fractures: Comparison of 36 cases. *Med Princ Pract,* 22**,** 161-6.

GarcíA, J. M., Doblaré, M. & Cegoñino, J. 2002. Bone remodelling simulation: A tool for implant design. *Computational Materials Science,* 25**,** 100-114.

Gardner, M. J., Evans, J. M. & Dunbar, R. P. 2009. Failure of fracture plate fixation. *Journal of the American Academy of Orthopaedic Surgeons,* 17**,** 647-657.

Gardner, M. J., Helfet, D. L. & Lorich, D. G. 2004. Has locked plating completely replaced conventional plating? *American journal of orthopedics (Belle Mead, N.J.),* 33**,** 439-46.

Gardner, M. J., Nork, S. E., Huber, P. & Krieg, J. C. 2010. Less rigid stable fracture fixation in osteoporotic bone using locked plates with near cortical slots. *Injury-International Journal of the Care of the Injured,* 41**,** 652-656.

Gaston, M. S. & Simpson, A. H. R. W. 2007. Inhibition of fracture healing. *J Bone Joint Surg Br,* 89-B**,** 1553-1560.

Gautier, E. 2009. Bridge plating. *AO Dialogue.*

Gautier, E., Perren, S. M. & Cordey, J. 2000. Strain distribution in plated and unplated sheep tibia - an in vivo experiment. *Injury-International Journal of the Care of the Injured,* 31**,** 37-44.

Gautier, E. & Sommer, C. 2003. Guidelines for the clinical application of the lcp. *Injury,* 34 Suppl 2**,** B63-76.

Gebert, A., Peters, J., Bishop, N. E., Westphal, F. & Morlock, M. M. 2009. Influence of press-fit parameters on the primary stability of uncemented femoral resurfacing implants. *Medical Engineering & Physics,* 31**,** 160-164.

Gebhard, F., Kregor, P. & Oliver, C. 2008. *Distal femur 33-a2 crif - reduction & internal fixation* [Online]. Available: www2.aofoundation.org [Accessed 22/04/13.

Gefen, A. 2002. Optimizing the biomechanical compatibility of orthopedic screws for bone fracture fixation. *Medical Engineering & Physics,* 24**,** 337-347.

Genna, F., Paganelli, C., Salgarello, S. & Sapelli, P. 2003. Mechanical response of bone under short-term loading of a dental implant with an internal layer simulating the nonlinear behaviour of the periodontal ligament. *Computer Methods in Biomechanics and Biomedical Engineering,* 6**,** 305-318.

Gerber, C., Mast, J. W. & Ganz, R. 1990. Biological internal fixation of fractures. *Archives of Orthopaedic and Trauma Surgery,* 109**,** 295-303.

Giannoudis, P. V. & Schneider, E. 2006. Principles of fixation of osteoporotic fractures. *Journal of Bone and Joint Surgery-British Volume,* 88B**,** 1272-1278.

Giotakis, N. & Narayan, B. 2007. Stability with unilateral external fixation in the tibia. *Strategies in trauma and limb reconstruction (Online),* 2**,** 13-20.

Goffin, J. M., Pankaj, P. & Simpson, A. H. 2014. Are plasticity models required to predict relative risk of lag screw cut-out in finite element models of trochanteric fracture fixation? *J Biomech,* 47**,** 323-8.

Goodship A, E. & Cunningham J, L. (eds.) 2001. *Pathology and function adaption of bone remodelling and repair in vivo,* New York: CRC Press.

Goodship, A. E. & Kenwright, J. 1985. The influence of induced micromovment upon the healing of experimental tibial fractures. *The Journal of Bone and Joint Surgery (American).* 0301 620X8S/41 14.

Granata, J. D., Litsky, A. S., Lustenberger, D. P., Probe, R. A. & Ellis, T. J. 2012. Immediate weight bearing of comminuted supracondylar femur fractures using locked plate fixation. *Orthopedics,* 35**,** E1210-E1213.

Grawe, B., Le, T., Williamson, S., Archdeacon, A. & Zardiackas, L. 2012. Fracture fixation with two locking screws versus three non-locking screws. *Bone and Joint Research,* 1**,** 118-24.

Gray, H. A., Taddei, F., Zavatsky, A. B., Cristofolini, L. & Gill, H. S. 2008. Experimental validation of a finite element model of a human cadaveric tibia. *Journal of biomechanical engineering,* 130**,** 031016.

Grewal, A. S. & Sabbaghian, M. 1997. Load distribution between threads in threaded connections. *Journal of Pressure Vessel Technology-Transactions of the Asme,* 119**,** 91-95.

Hak, D. J., Althausen, P. & Hazelwood, S. J. 2010a. Locked plate fixation of osteoporotic humeral shaft fractures: Are two locking screws per segment enough? *J Orthop Trauma,* 24**,** 207-11.

Hak, D. J., Toker, S., Yi, C. & Toreson, J. 2010b. The influence of fracture fixation biomechanics on fracture healing. *Orthopedics,* 33**,** 752-755.

Halder, A., Kutzner, I., Graichen, F., Heinlein, B., Beier, A. & Bergmann, G. 2012. Influence of limb alignment on mediolateral loading in total knee replacementin

vivo measurements in five patients. *The Journal of Bone & Joint Surgery,* 94**,** 1023-1029.

Halloran, J. P., Petrella, A. J. & Rullkoetter, P. J. 2005. Explicit finite element modeling of total knee replacement mechanics. *Journal of Biomechanics,* 38**,** 323-331.

Halsey, D., Fleming, B., Pope, M. H., Krag, M. & Kristiansen, T. 1992. External fixator pin design. *Clinical Orthopaedics and Related Research***,** 305-312.

Harder, Y., Martinet, O., Barraud, G. E., Cordey, J. & Regazzoni, E. 1999. The mechanics of internal fixation of fractures of the distal femur: A comparison of the condylar screw (dcs) with the condylar plate (cp). *Injury,* 30, Supplement 1**,** SA31-SA39.

Heidemann, W., Gerlach, K. L., Grobel, K. H. & Kollner, H. G. 1998. Effect of the diameter of various bore holes on retention of osteosynthesis screws. *Mund Kiefer Gesichtschir,* 2**,** 136-40.

Heiney, J. P., Battula, S., O'connor, J. A., Ebraheim, N., Schoenfeld, A. J. & Vrabec, G. 2012. Distal femoral fixation: A biomechanical comparison of retrograde nail, retrograde intramedullary nail, and prototype locking retrograde nail. *Clinical Biomechanics,* 27**,** 692-696.

Heller, M. O., Bergmann, G., Deuretzbacher, G., Durselen, L., Pohl, M., Claes, L., Haas, N. P. & Duda, G. N. 2001. Musculo-skeletal loading conditions at the hip during walking and stair climbing. *Journal of Biomechanics,* 34**,** 883-893.

Helwig, P., Hindenlang, U., Hirschmuller, A., Konstantinidis, L., Sudkamp, N. & Schneider, R. 2013. A femoral model with all relevant muscles and hip capsule ligaments. *Comput Methods Biomech Biomed Engin,* 16**,** 669-77.

Henderson, C. E., Lujan, T., Bottlang, M., Fitzpatrick, D. C., Madey, S. M. & Marsh, J. L. 2010. Stabilization of distal femur fractures with intramedullary nails and locking plates: Differences in callus formation. *The Iowa orthopaedic journal,* 30**,** 61-68.

Henderson, C. E., Lujan, T. J., Kuhl, L. L., Bottlang, M., Fitzpatrick, D. C. & Marsh, J. L. 2011. 2010 mid-america orthopaedic association physician in training award: Healing complications are common after locked plating for distal femur fractures. *Clin Orthop Relat Res,* 469**,** 1757-65.

Henry, S. L. & Kregor, P. J. 1999. Supracondylar femur fractures. *Operative Techniques in Orthopaedics,* 9**,** 177-196.

Hertel, R., Eijer, H., Meisser, A., Hauke, C. & Perren, S. M. 2001. Biomechanical and biological considerations relating to the clinical use of the point contact-fixator--evaluation of the device handling test in the treatment of diaphyseal fractures of the radius and/or ulna. *Injury,* 32 Suppl 2**,** B10-4.

Hierholzer, C., Rüden, C., Pötzel, T., Woltmann, A. & Bühren, V. 2011. *Outcome analysis of retrograde nailing and less invasive stabilization system in distal femoral fractures: A retrospective analysis.*

Hoffmann, M. F., Jones, C. B., Sietsema, D. L., Tornetta, P., 3rd & Koenig, S. J. 2013. Clinical outcomes of locked plating of distal femoral fractures in a retrospective cohort. *J Orthop Surg Res,* 8**,** 8-43.

Hoffmeier, K. L., Hofmann, G. O. & Mückley, T. 2011. Choosing a proper working length can improve the lifespan of locked plates: A biomechanical study. *Clinical Biomechanics,* 26**,** 405-409.

Hogel, F., Hoffmann, S., Weninger, P., Buhren, V. & Augat, P. 2012. Biomechanical comparison of two locking plate systems for the distal tibia. *European Journal of Trauma and Emergency Surgery,* 38**,** 53-58.

Hsu, C.-C., Wang, J.-L., Hou, S.-M., Chao, C.-K. & Lin, J. 2003. Pushout strength of tibial locking screws: Development of finite element models. Jounral of the Chinese Institute of Engineers.

Hughes, A. N. & Jordan, B. A. 1972. Mechanical properties of surgical bone screws and some aspects of insertion practice. *Injury-the British Journal of Accident Surgery,* 4**,** 25-&.

Huiskes, R., Chao, E. Y. S. & Crippen, T. E. 1985. Parametric analyses of pin-bone stresses in external fracture fixation devices. *Journal of Orthopaedic Research,* 3**,** 341-349.

Hunt, S. B. & Buckley, R. E. 2013. Locking plates: A current concepts review of technique and indications for use. *Acta Chir Orthop Traumatol Cech,* 80**,** 185-91.

Hyldahl, C., Pearson, S., Tepic, S. & Perren, S. M. 1991. Induction and prevention of pin loosening in external fixation: An in vivo study on sheep tibiae. *Journal of Orthopaedic Trauma,* 5**,** 485-92.

Isaksson, H., Wilson, W., Van Donkelaar, C. C., Huiskes, R. & Ito, K. 2006. Comparison of biophysical stimuli for mechano-regulation of tissue differentiation during fracture healing. *Journal of Biomechanics,* 39**,** 1507-1516.

Izaham, R. M. a. R. & Kadir, M. R. A. Screws placement effect on locking compression plate (lcp) for tibial oblique fracture fixation. Conference on Biomedical Engineering & Sciences (IECBES 2010), 2010 Kuala Lumpur, Malaysia, 30th November 2010.

James, T. P. & Andrade, B. A. 2013. Modeling bicortical screws under a cantilever bending load. *J Biomech Eng,* 135**,** 4025651.

Karunratanakul, K., Schrooten, J. & Van Oosterwyck, H. 2010. Finite element modelling of a unilateral fixator for bone reconstruction: Importance of contact settings. *Medical Engineering & Physics,* 32**,** 461-467.

Kenwright, J. & Gardner, T. 1998. Mechanical influences on tibial fracture healing. *Clinical Orthopaedics and Related Research***,** S179-S190.

Kerner, J., Huiskes, R., Van Lenthe, G. H., Weinans, H., Van Rietbergen, B., Engh, C. A. & Amis, A. A. 1999. Correlation between pre-operative periprosthetic bone density and post-operative bone loss in tha can be explained by strain-adaptive remodelling. *J Biomech,* 32**,** 695-703.

Kershaw, C. J., Cunningham, J. L. & Kenwright, J. 1993. Tibial external fixation, weight bearing, and fracture movement. *Clinical Orthopaedics and Related Research*, 28-36.

Kim, D. S., Kim, Y. M., Choi, E. S., Shon, H. C., Park, K. J., Cho, B. K., Park, J. K., Lee, H. C. & Hong, K. H. 2012. Repeated metal breakage in a femoral shaft fracture with lateral bowing - a case report - *Journal of the Korean Fracture Society,* Apr, 136-141.

Kim, H.-J., Kim, S.-H. & Chang, S.-H. 2011a. Finite element analysis using interfragmentary strain theory for the fracture healing process to which composite bone plates are applied. *Composite Structures,* 93, 2953-2962.

Kim, J.-D., Kim, N.-S., Hong, C.-S. & Oh, C.-Y. 2011b. Design optimization of a xenogeneic bone plate and screws using the taguchi and finite element methods. *International Journal of Precision Engineering and Manufacturing,* 12, 1119-1124.

Kim, S. H., Chang, S. H. & Jung, H. J. 2010. The finite element analysis of a fractured tibia applied by composite bone plates considering contact conditions and time-varying properties of curing tissues. *Composite Structures,* 92, 2109-2118.

Kim, T., Ayturk, U. M., Haskell, A., Miclau, T. & Puttlitz, C. M. 2007. Fixation of osteoporotic distal fibula fractures: A biomechanical comparison of locking versus conventional plates. *J Foot Ankle Surg,* 46, 2-6.

Koca, O. L., Eskitascioglu, G. & Usumez, A. 2005. Three-dimensional finite-element analysis of functional stresses in different bone locations produced by implants placed in the maxillary posterior region of the sinus floor. *Journal of Prosthetic Dentistry,* 93, 38-44.

Koistinen, A. P., Korhonen, H., Kiviranta, I., Kroger, H. & Lappalainen, R. 2011. Analysis of plastic deformation in cortical bone after insertion of coated and non-coated self-tapping orthopaedic screws. *Proceedings of the Institution of Mechanical Engineers Part H-Journal of Engineering in Medicine,* 225, 629-639.

Kolev, B. 2014. *Numerical simulation of bone fracture healing.* BEng, University of Edinburgh.

Konowalchuk, B. K., Wills, N. J., Tollefson, B. & Swiontkowski, M. 2009. Tibial shaft fractures. *Medscape.*

Konstantinidis, L., Papaioannou, C., Hirschmuller, A., Pavlidis, T., Schroter, S., Sudkamp, N. P. & Helwig, P. 2012. Effects of muscle-equivalent forces on the biomechanical behavior of proximal femur fracture models: A pilot study on artificial bones. *Proc Inst Mech Eng H,* 226, 681-5.

Kregor, P. J., Hughes, J. L. & Cole, P. A. 2001. Fixation of distal femoral fractures above total knee arthroplasty utilizing the less invasive stabilization system (l.I.S.S.). *Injury,* 32, SC64-75.

Krettek, C., Haas, N. & Tscherne, H. 1991. The role of supplemental lag-screw fixation for open fractures of the tibial shaft treated with external fixation. *Journal of Bone and Joint Surgery-American Volume,* 73A, 893-897.

Krishna, K. R., Sridhar, I. & Ghista, D. N. 2008. Analysis of the helical plate for bone fracture fixation. *Injury,* 39**,** 1421-1436.

Kubiak, E. N., Fulkerson, E., Strauss, E. & Egol, K. A. 2006. The evolution of locked plates. *The Journal of Bone and Joint Surgery (American),* 88**,** 189-200.

Kuhn, A., Mc Iff, T., Cordey, J., Baumgart, F. W. & Rahn, B. A. 1995. Bone deformation by thread-cutting and thread-forming cortex screws. *Injury,* 26, Supplement 1**,** 12-20.

Kunkel, K. A., Suber, J. T., Gerard, P. D. & Kowaleski, M. P. 2011. Effect of pilot hole diameter and tapping on insertion torque and axial pullout strength of 4.0-mm cancellous bone screws. *Am J Vet Res,* 72**,** 1660-5.

Kutzner, I., Küther, S., Heinlein, B., Dymke, J., Bender, A., Halder, A. M. & Bergmann, G. 2011. The effect of valgus braces on medial compartment load of the knee joint – in vivo load measurements in three subjects. *Journal of Biomechanics,* 44**,** 1354-1360.

Lanyon, L. E. & Rubin, C. T. 1984. Static vs dynamic loads as an influence on bone remodelling. *J Biomech,* 17**,** 897-905.

Leahy, M. 2010. When locking plates fail. *AAOS Now,* 4.

Leng, H., Dong, X. N. & Wang, X. 2009. Progressive post-yield behavior of human cortical bone in compression for middle-aged and elderly groups. *Journal of Biomechanics,* 42**,** 491-497.

Lerch, M., Kurtz, A., Stukenborg-Colsman, C., Nolte, I., Weigel, N., Bouguecha, A. & Behrens, B. A. 2012. Bone remodeling after total hip arthroplasty with a short stemmed metaphyseal loading implant: Finite element analysis validated by a prospective dexa investigation. *Journal of Orthopaedic Research,* 30**,** 1822-1829.

Lethaby, A., Temple, J. & Santy, J. 2011. Pin site care for preventing infections associated with external bone fixators and pins (review). *The Cochrane Collaboration,* The Cochrane Library.

Li, G., Kozanek, M., Hosseini, A., Liu, F., Velde, S. & Rubash, H. 2009. New fluoroscopic imaging technique for investigation of 6dof knee kinematics during treadmill gait. *Journal of orthopaedic surgery and research,* 4**,** 1-5.

Liang, B. W., Ding, Z. Q., Shen, J. G., Zhai, W. L., Kang, L. Q., Zhou, L., Sha, M. & Liang, D. Z. 2012. A distal femoral supra-condylar plate: Biomechanical comparison with condylar plate and first clinical application for treatment of supracondylar fracture. *International Orthopaedics,* 36**,** 1673-1679.

Lujan, T. J., Henderson, C. E., Madey, S. M., Fitzpatrick, D. C., Marsh, J. L. & Bottlang, M. 2010. Locked plating of distal femur fractures leads to inconsistent and asymmetric callus formation. *J Orthop Trauma,* 24**,** 156-62.

Luo, C. A., Hua, S. Y., Lin, S. C., Chen, C. M. & Tseng, C. S. 2013. Stress and stability comparison between different systems for high tibial osteotomies. *BMC Musculoskelet Disord,* 14**,** 1471-2474.

Ma, C.-H., Wu, C.-H., Tu, Y.-K. & Lin, T.-S. 2013. Metaphyseal locking plate as a definitive external fixator for treating open tibial fractures—clinical outcome and a finite element study. *Injury,* 44**,** 1097–1101.

Macleod, A. R., Pankaj, P. & Simpson, A. H. R. W. 2012. Does screw–bone interface modelling matter in finite element analyses? *Journal of Biomechanics,* 45**,** 1712-1716.

Markel, M. D., Wikenheiser, M. A. & Chao, E. Y. S. 1990. A study of fracture callus material properties - relationship to the torsional strength of bone. *Journal of Orthopaedic Research,* 8**,** 843-850.

Mathurin, F., Guillot, J., Stephan, P. & Daidie, A. 2009. 3d finite element modeling of an assembly process with thread forming screw. *Journal of Manufacturing Science and Engineering,* 131**,** 041015.

Mauntler, N. A., Schmitz, T. L. & Ziegert, J. C. 2008. The influence of process variation on a cortical bone interference fit pin connection. *J Manuf Sci Eng,* 130**,** 024501-024507.

Mcgrath, L. & Royston, S. 2003. Fractures of the tibial shaft (including acute compartment syndrome). *Surgery (Oxford),* 21**,** 231-235.

Mckibbin, B. 1978. The biology of fracture healing in long bones. *J Bone Joint Surg Br,* 60-B(2)**,** 150-62.

Mercer, C., He, M. Y., Wang, R. & Evans, A. G. 2006. Mechanisms governing the inelastic deformation of cortical bone and application to trabecular bone. *Acta Biomaterialia,* 2**,** 59-68.

Merino, M. K. A., Rahal, S. C., Ribeiro, C. R. & Padovani, C. R. 2013. The effect of locked screw angulation on the biomechanical properties of the s.P.S. Free-block plate. *Veterinary and comparative orthopaedics and traumatology : V.C.O.T,* 26**,** 117-22.

Miller, D. L. & Goswami, T. 2007. A review of locking compression plate biomechanics and their advantages as internal fixators in fracture healing. *Clinical Biomechanics,* 22**,** 1049-1062.

Miramini, S., Zhang, L., Richardson, M., Pirpiris, M., Mendis, P., Oloyede, K. & Edwards, G. 2013. Computational simulation of the early stage of bone healing under different configurations of locking compression plates. *Comput Methods Biomech Biomed Engin,* 21**,** 21.

Moazen, M., Jones, A. C., Leonidou, A., Jin, Z., Wilcox, R. K. & Tsiridis, E. 2012. Rigid versus flexible plate fixation for periprosthetic femoral fracture-computer modelling of a clinical case. *Med Eng Phys,* 34**,** 1041-8.

Moazen, M., Mak, J. H., Jones, A. C., Jin, Z., Wilcox, R. K. & Tsiridis, E. 2013. Evaluation of a new approach for modelling the screw-bone interface in a locking plate fixation: A corroboration study. *Proc Inst Mech Eng H,* 227**,** 746-56.

Moroni, A., Vannini, F., Mosca, M. & Giannini, S. 2002. Techniques to avoid pin loosening and infection in external fixation. *Journal of Orthopaedic Trauma,* 16**,** 189-195.

Morrison, J. B. 1970. The mechanics of the knee joint in relation to normal walking. *Journal of Biomechanics,* 3**,** 51-61.

Müller, M. E. & Perren, S. M. 1991. Implants. *In:* ALLGOËWER, M. (ed.) *Manual of internal fixation: Techniques recommended by the ao-asif group.* 3rd ed. 1991 ed.: Springer.

Mullins, L. P., Bruzzi, M. S. & Mchugh, P. E. 2009. Calibration of a constitutive model for the post-yield behaviour of cortical bone. *Journal of the Mechanical Behavior of Biomedical Materials,* 2**,** 460-470.

Murray, D. W., Wilson-Macdonald, J., Morscher, E., Rahn, B. A. & Kaslin, M. 1996. Bone growth and remodelling after fracture. *J Bone Joint Surg Br,* 78**,** 42-50.

Mushtaq, A., Shahid, R., Asif, M. & Maqsood, M. 2009. Distal tibial fracture fixation with locking compression plate (lcp) using the minimally invasive percutaneous osteosynthesis (mipo) technique. *European Journal of Trauma and Emergency Surgery,* 35**,** 159-164.

Nagatani, T., Mori, R., Wang, Y., Nakai, T., Ozoe, N. & Uchio, Y. 2010. Optimum predrilled hole size for bone screws used in osteochondral fixation: In vitro biomechanical study and clinical case. *Journal of Orthopaedic Science,* 15**,** 245-250.

Nakazawa, K., Maruyama, N. & Hanawa, T. 2003. Effect of contact pressure on fretting fatigue of austenitic stainless steel. *Tribology International,* 36**,** 79-85.

Nassiri, M., Macdonald, B. & O'byrne, J. M. 2013. Computational modelling of long bone fractures fixed with locking plates - how can the risk of implant failure be reduced? *J Orthop,* 10**,** 29-37.

Nassiri, M., Macdonald, B. & O'byrne, J. 2012. Locking compression plate breakage and fracture non-union: A finite element study of three patient-specific cases. *European Journal of Orthopaedic Surgery & Traumatology,* 22**,** 275-281.

Natali, A. N. 1992. Nonlinear interaction phenomena between bone and pin. *Clinical Materials,* 9**,** 109-114.

Newman, S. D. S., Mauffrey, C. P. C. & Krikler, S. 2010. Distal metadiaphyseal tibial fractures. *Injury,* In Press, Corrected Proof.

Nhs. *Osteoporosis* [Online]. Available: http://www.nhs.uk/Conditions/Osteoporosis/Pages/Introduction.aspx.

Nicayenzi, B., Crookshank, M., Olsen, M., Schemitsch, E. H., Bougherara, H. & Zdero, R. 2012. Biomechanical measurements of cortical screw stripping torque in human versus artificial femurs. *Proc Inst Mech Eng H,* 226**,** 645-51.

Nice 2012. Osteoporosis: Assessing the risk of fragility fracture. *Nice clinical guideline 146.* National Institute for Health and Care Excellence.

Niinomi, M. 2007. Fatigue characteristics of metallic biomaterials. *International Journal of Fatigue,* 29**,** 992-1000.

Niinomi, M. 2008. Biologically and mechanically biocompatible titanium alloys. *Materials Transactions,* 49**,** 2170 - 2178.

Norman, T. L., Ackerman, E. S., Smith, T. S., Gruen, T. A., Yates, A. J., Blaha, J. D. & Kish, V. L. 2006. Cortical bone viscoelasticity and fixation strength of press-fit femoral stems: An in-vitro model. *Journal of Biomechanical Engineering-Transactions of the Asme,* 128**,** 13-17.

Obakponovwe, O., Kallala, R., Stavrou, P. Z., Harwood, P. & Giannoudis, P. 2012. (iv) the management of distal femoral fractures: A literature review. *Orthopaedics and Trauma,* 26**,** 176-183.

Oh, J. K., Sahu, D., Ahn, Y. H., Lee, S. J., Tsutsumi, S., Hwang, J. H., Jung, D. Y., Perren, S. M. & Oh, C. W. 2010. Effect of fracture gap on stability of compression plate fixation: A finite element study. *Journal of Orthopaedic Research,* 28**,** 462-467.

Okazaki, Y. 2012. Comparison of fatigue properties and fatigue crack growth rates of various implantable metals. *Materials,* 5**,** 2981-3005.

Ons 2011. Statistical bulletin: Older people's day. *In:* STATISTICS, O. F. N. (ed.).

Orthoinfo. 2007. *Orthoinfo: Internal fixation for fractures* [Online]. American Academy of Orthopaedic Surgeons. Available: http://orthoinfo.aaos.org/topic.cfm?topic=A00196.

Overturf, S., Morris, R., Gugala, Z. & Lindsey, R. 2013. Biomechanical properties of bicortical screws versus unicortical far cortex abutting screws for locking plate fixation in a radius comminuted fracture model. *Orthopaedic Research Society.* San Antonio.

Pacific Research Laboratories, I. 2013. Sawbones catalog.

Pankaj, P. 2013. Patient-specific modelling of bone and bone-implant systems: The challenges. *International Journal for Numerical Methods in Biomedical Engineering,* 29**,** 233-49.

Pankaj, P. & Donaldson, F. E. 2012. Algorithms for a strain-based plasticity criterion for bone. *International Journal for Numerical Methods in Biomedical Engineering,* 29**,** 40–61.

Pantev, I. 2014. *Numerical simulation of bone fracture healing.* BEng, University of Edinburgh.

Park, S.-E., Kang, H.-T., Kim, Y.-Y., Jeong, J.-J., Lee, J.-U. & Kim, W.-Y. 2011. Treatment of distal femoral fractures using polyaxial locking plate. *Journal of the Korean Fracture Society,* Oct**,** 321-327.

Park, S. H. 2004. "Shear movement at the fracture site delays healing in a diaphyseal fracture model" by peter augat, johannes buger, sandra schorlemmer, thomas henke, manfred peraus, lutz claes j orthop res 2003;21 : 1011-17. *Journal of Orthopaedic Research,* 22**,** 1156-1157.

Park, S. H., Llinas, A., Goel, V. & Keller, J. 2000. Hard tissue replacements. *In:* BRONZINO, J. D. (ed.) *The biomedical engineering handbook, second edition. 2 volume set.* CRC Press.

Park, S. H., O'connor, K., Mckellop, H. & Sarmiento, A. 1998. The influence of active shear or compressive motion on fracture-healing. *J Bone Joint Surg Am,* 80**,** 868-78.

Pekmezci, M., Mcdonald, E., Buckley, J. & Kandemir, U. 2014. Retrograde intramedullary nails with distal screws locked to the nail have higher fatigue strength than locking plates in the treatment of supracondylar femoral fractures: A cadaver-based laboratory investigation. *Bone & Joint Journal,* 96-B**,** 114-121.

Perren, S. M. 2002. Evolution of the internal fixation of long bone fractures. *Journal of Bone and Joint Surgery-British Volume,* 84B**,** 1093-1110.

Pessoa, R. S., Muraru, L., Marcantonio, E., Vaz, L. G., Sloten, J. V., Duyck, J. & Jaecques, S. V. N. 2010. Influence of implant connection type on the biomechanical environment of immediately placed implants - ct-based nonlinear, three-dimensional finite element analysis. *Clinical Implant Dentistry and Related Research,* 12**,** 219-234.

Pettine, K. A., Chao, E. Y. S. & Kelly, P. J. 1993. Analyses of the external fixator pin bone interface. *Clinical Orthopaedics and Related Research***,** 18-27.

Phillips, A. T. M. 2009. The femur as a musculo-skeletal construct: A free boundary condition modelling approach. *Medical Engineering and Physics,* 31**,** 673-680.

Phillips, A. T. M., Pankaj, P., Howie, C. R., Usmani, A. S. & Simpson, A. H. R. W. 2007. Finite element modelling of the pelvis: Inclusion of muscular and ligamentous boundary conditions. *Medical Engineering and Physics,* 29**,** 739-748.

Polgar, K., Gill, H. S., Viceconti, M., Murray, D. W. & O'connor, J. J. 2003. Strain distribution within the human femur due to physiological and simplified loading: Finite element analysis using the muscle standardized femur model. *Proceedings of the Institution of Mechanical Engineers, Part H: Journal of Engineering in Medicine,* 217**,** 173-189.

Prendergast, P. J. 1997. Finite element models in tissue mechanics and orthopaedic implant design. *Clinical Biomechanics,* 12**,** 343-366.

Ramakrishna, K., Sridhar, I., Sivashanker, S., Khong, K. S. & Ghista, D. N. 2004. Design of fracture fixation plate for necessary and sufficient bone stress shielding. *Jsme International Journal Series C-Mechanical Systems Machine Elements and Manufacturing,* 47**,** 1086-1094.

Reeves, N. P., Narendra, K. S. & Cholewicki, J. 2007. Spine stability: The six blind men and the elephant. *Clin Biomech,* 22**,** 266-74.

Reilly, D. T. & Burstein, A. H. 1975. The elastic and ultimate properties of compact bone tissue. *Journal of Biomechanics,* 8**,** 393-405.

Roberts, J. W., Grindel, S. I., Rebholz, B. & Wang, M. 2007. Biomechanical evaluation of locking plate radial shaft fixation: Unicortical locking fixation versus mixed bicortical and unicortical fixation in a sawbone model. *The Journal of Hand Surgery,* 32**,** 971-975.

Rs 2003. Ferri precision universal joints.

Ruffoni, D., Wirth, A. J., Steiner, J. A., Parkinson, I. H., Muller, R. & Van Lenthe, G. H. 2012. The different contributions of cortical and trabecular bone to implant anchorage in a human vertebra. *Bone,* 50**,** 733-8.

Russo, C. R., Lauretani, F., Seeman, E., Bartali, B., Bandinelli, S., Di Iorio, A., Guralnik, J. & Ferrucci, L. 2006. Structural adaptations to bone loss in aging men and women. *Bone,* 38**,** 112-118.

Rybicki, E. F. & Simonen, F. A. 1977. Mechanics of oblique fracture fixation using a finite-element model. *Journal of Biomechanics,* 10**,** 141-148.

Sabharwal, S. & Root, M. Z. 2012. Impact of obesity on orthopaedics. *J Bone Joint Surg Am,* 94**,** 1045-52.

Salas, C., Mercer, D., Decoster, T. A. & Taha, M. M. R. 2011a. Experimental and probabilistic analysis of distal femoral periprosthetic fracture: A comparison of locking plate and intramedullary nail fixation. Part a: Experimental investigation. *Computer Methods in Biomechanics and Biomedical Engineering,* 14**,** 157-164.

Salas, C., Mercer, D., Decoster, T. A. & Taha, M. M. R. 2011b. Experimental and probabilistic analysis of distal femoral periprosthetic fracture: A comparison of locking plate and intramedullary nail fixation. Part b: Probabilistic investigation. *Computer Methods in Biomechanics and Biomedical Engineering,* 14**,** 175-182.

Scanlan, S. F., Chaudhari, A. M. W., Dyrby, C. O. & Andriacchi, T. P. 2010. Differences in tibial rotation during walking in acl reconstructed and healthy contralateral knees. *Journal of Biomechanics,* 43**,** 1817-1822.

Schandelmaier, P., Partenheimer, A., Koenemann, B., Grün, O. A. & Krettek, C. 2001. Distal femoral fractures and liss stabilization. *Injury,* 32, Supplement 3**,** 55-63.

Schatzker, J., Horne, J. G. & Sumnersmith, G. 1975a. Effect of movment on the holding power of screws in bone. *Clinical Orthopaedics and Related Research***,** 257-262.

Schatzker, J., Sanderson, R. & Murnaghan, J. P. 1975b. Holding power of orthopaedic screws in vivo. *Clinical Orthopaedics and Related Research***,** 115-126.

Schileo, E., Taddei, F., Malandrino, A., Cristofolini, L. & Viceconti, M. 2007. Subject-specific finite element models can accurately predict strain levels in long bones. *J Biomech,* 40**,** 2982-9.

Schmidt, H., Alber, T., Wehner, T., Blakytny, R. & Wilke, H.-J. 2009. Discretization error when using finite element models: Analysis and evaluation of an underestimated problem. *Journal of Biomechanics,* 42**,** 1926-1934.

Schmidt, U., Penzkofer, R., Bachmaier, S. & Augat, P. 2013. Implant material and design alter construct stiffness in distal femur locking plate fixation: A pilot study. *Clin Orthop Relat Res,* 471**,** 2808-14.

Schnaser, E. & Vallier, H. 2013. Corr insights: Locking buttons increase fatigue life of locking plates in a segmental bone defect model. *Clin Orthop Relat Res,* 471**,** 1045-6.

Schneider, E., Goldhahn, J. & Burckhardt, P. 2005. The challenge: Fracture treatment in osteoporotic bone. *Osteoporosis International,* 16**,** S1-S2.

Seide, K., Triebe, J., Faschingbauer, M., Schulz, A. P., Puschel, K., Mehrtens, G. & Jurgens, C. 2007. Locked vs. Unlocked plate osteosynthesis of the proximal humerus - a biomechanical study. *Clinical Biomechanics,* 22**,** 176-182.

Seral, B., GarcíA, J. M., Cegoñino, J., Doblaré, M. & Seral, F. 2004. Finite element study of intramedullary osteosynthesis in the treatment of trochanteric fractures of the hip: Gamma and pfn. *Injury,* 35**,** 130-135.

Shah, S., Kim, S. Y. R., Dubov, A., Schemitsch, E. H., Bougherara, H. & Zdero, R. 2011. The biomechanics of plate fixation of periprosthetic femoral fractures near the tip of a total hip implant: Cables, screws, or both? *Proceedings of the Institution of Mechanical Engineers Part H-Journal of Engineering in Medicine,* 225**,** 845-856.

Shefelbine, S. J., Simon, U., Claes, L., Gold, A., Gabet, Y., Bab, I., Müller, R. & Augat, P. 2005. Prediction of fracture callus mechanical properties using micro-ct images and voxel-based finite element analysis. *Bone,* 36**,** 480-488.

Shih, K.-S., Tseng, C.-S., Lee, C.-C. & Lin, S.-C. 2008. Influence of muscular contractions on the stress analysis of distal femoral interlocking nailing. *Clinical Biomechanics,* 23**,** 38-44.

Shultz, T. R., Blaha, J. D., Gruen, T. A. & Norman, T. L. 2006. Cortical bone viscoelasticity and fixation strength of press-fit femoral stems: A finite element model. *Journal of Biomechanical Engineering-Transactions of the Asme,* 128**,** 7-12.

Simulia 2009. Defining a contact interaction property. *Abaqus 6.9 online documentation.* Dassault Systèmes.

Sirbu, P. D., Petreus, T., Asaftei, R., Berea, G. & Botez, P. 2011. Minimally invasive plate osteosynthesis (mipo) in long bone fractures – biomechanics – design – clinical results.

Smidt, G. L. 1973. Biomechanical analysis of knee flexion and extension. *J Biomech,* 6**,** 79-92.

Smith, W. R., Ziran, B. H., Anglen, J. O. & Stahel, P. F. 2007. Locking plates: Tips and tricks. *Journal of Bone and Joint Surgery-American Volume,* 89A**,** 2298-2307.

Sommer, C., Babst, R., Muller, M. & Hanson, B. 2004. Locking compression plate loosening and plate breakage - a report of four cases. *Journal of Orthopaedic Trauma,* 18**,** 571-577.

Sommer, C., Gautier, E., Müller, M., Helfet, D. L. & Wagner, M. 2003. First clinical results of the locking compression plate (lcp). *Injury,* 34, Supplement 2**,** 43-54.

Speirs, A. D., Heller, M. O., Duda, G. N. & Taylor, W. R. 2007. Physiologically based boundary conditions in finite element modelling. *Journal of Biomechanics,* 40**,** 2318-2323.

Steeves, M., Stone, C., Mogaard, J. & Byrne, S. 2005. How pilot-hole size affects bone-screw pullout strength in human cadaveric cancellous bone. *Can J Surg,* 48**,** 207-12.

Steiner, M., Claes, L., Ignatius, A., Simon, U. & Wehner, T. 2014. Disadvantages of interfragmentary shear on fracture healing-mechanical insights through numerical simulation. *J Orthop Res,* 32**,** 865-72.

Stoffel, K., Dieter, U., Stachowiak, G., Gächter, A. & Kuster, M. S. 2003. Biomechanical testing of the lcp - how can stability in locked internal fixators be controlled? *Injury,* 34**,** 11-19.

Stoffel, K., Klaue, K. & Perren, S. M. 2000. Functional load of plates in fracture fixation in vivo and its correlate in bone healing. *Injury,* 31, Supplement 2**,** 37-86.

Strauss, E. J., Alfonso, D., Kummer, F. J., Egol, K. A. & Tejwani, N. C. 2007. The effect of concurrent fibular fracture on the fixation of distal tibia fractures: A laboratory comparison of intramedullary nails with locked plates. *Journal of Orthopaedic Trauma,* 21**,** 172-177.

Strauss, E. J., Schwarzkopf, R., Kummer, F. & Egol, K. A. 2008. The current status of locked plating: The good, the bad, and the ugly. *J Orthop Trauma,* 22**,** 479-86.

Stryker 2007. Axsos locking plate system: Operative technique distal lateral femur.

Sugiura, T., Horiuchi, K., Sugimura, M. & Tsutsumi, S. 2000. Evaluation of threshold stress for bone resorption around screws based on in vivo strain measurement of miniplate. *Journal of Musculoskeletal & Neuronal Interactions,* 1**,** 165-170.

Sverdlova, N. S. & Witzel, U. 2010. Principles of determination and verification of muscle forces in the human musculoskeletal system: Muscle forces to minimise bending stress. *Journal of Biomechanics,* 43**,** 387-396.

Syed, A. A., Agarwal, M., Giannoudis, P. V., Matthews, S. J. E. & Smith, R. M. 2004. Distal femoral fractures: Long-term outcome following stabilisation with the liss. *Injury,* 35**,** 599-607.

Synthes® 2000. Less invasive stabilization system (liss): Distal femur technique guide.

Synthes® 2002. Synthes screw reference chart: Screws, drill bits, taps and guide wires.

Synthes® 2003. Locking compression plate (lcp) system.

Szypryt, P. & Forward, D. 2009. The use and abuse of locking plates. *Orthopaedics and Trauma,* 23**,** 281-290.

Taheri, E., Sepehri, B., Ganji, R. & Nasirai, C. 2012. Effect of screws placement on locking compression plate for fixating medial transverse fracture of tibia. *Biomedical Engineering Research,* 1**,** 13-18.

Takebe, K., Nakagawa, A., Minami, H., Kanazawa, H. & Hirohata, K. 1984. Role of the fibula in weight-bearing. *Clinical Orthopaedics and Related Research***,** 289-292.

Talaia, P. M., Ramos, A., Abe, I., Schiller, M. W., Lopes, P., Nogueira, R. N., Pinto, J. L., Claramunt, R. & Simoes, J. A. 2007. Plated and intact femur strains in fracture fixation using fiber bragg gratings and strain gauges. *Experimental Mechanics,* 47**,** 355-363.

Taljanovic, M. S., Jones, M. D., Ruth, J. T., Benjamin, J. B., Sheppard, J. E. & Hunter, T. B. 2003. Fracture fixation. *Radiographics,* 23**,** 1569-90.

Tan, S. L. E. & Balogh, Z. J. 2009. Indications and limitations of locked plating. *Injury-International Journal of the Care of the Injured,* 40**,** 683-691.

Taylor, M. E., Tanner, K. E., Freeman, M. a. R. & Yettram, A. L. 1996. Stress and strain distribution within the intact femur: Compression or bending. *Medical Engineering & Physics,* 18**,** 122-131.

Templeton, D. L., Kelly, A. S., Steinberger, J. & Dengel, D. R. 2010. Lower relative bone mineral content in obese adolescents: Role of non-weight bearing exercise. *Pediatr Exerc Sci,* 22**,** 557-68.

Thiele, O. C., Eckhardt, C., Linke, B., Schneider, E. & Lill, C. A. 2007. Factors affecting the stability of screws in human cortical osteoporotic bone: A cadaver study. *J Bone Joint Surg Br,* 89**,** 701-5.

Tomaszewski, P., Verdonschot, N., Bulstra, S. & Verkerke, G. 2010. A comparative finite-element analysis of bone failure and load transfer of osseointegrated prostheses fixations. *Annals of Biomedical Engineering,* 38**,** 2418-2427.

Tompkins, M., Paller, D. J., Moore, D. C., Crisco, J. J. & Terek, R. M. 2013. Locking buttons increase fatigue life of locking plates in a segmental bone defect model. *Clin Orthop Relat Res,* 471**,** 1039-44.

Tornkvist, H., Hearn, T. C. & Schatzker, J. 1996. The strength of plate fixation in relation to the number and spacing of bone screws. *Journal of Orthopaedic Trauma,* 10**,** 204-208.

Tsai, W. C., Chen, P. Q., Lu, T. W., Wu, S. S., Shih, K. S. & Lin, S. C. 2009. Comparison and prediction of pullout strength of conical and cylindrical pedicle screws within synthetic bone. *BMC Musculoskeletal Disorders,* 10.

Turner, C. H., Anne, V. & Pidaparti, R. M. 1997. A uniform strain criterion for trabecular bone adaptation: Do continuum-level strain gradients drive adaptation? *J Biomech,* 30**,** 555-63.

Turner, C. H. & Burr, D. B. 1993. Basic biomechanical measurements of bone: A tutorial. *Bone,* 14**,** 595-608.

Uhl, J. M., Seguin, B., Kapatkin, A. S., Schulz, K. S., Garcia, T. C. & Stover, S. M. 2008. Mechanical comparison of 3.5 mm broad dynamic compression plate, broad limited-contact dynamic compression plate, and narrow locking compression plate systems using interfragmentary gap models. *Veterinary Surgery,* 37**,** 663-673.

Uhthoff, H. K. 1973. Mechanical factors influencing the holding power of screws in compact bone. *J Bone Joint Surg Br,* 55**,** 633-9.

Uhthoff, H. K., Poitras, P. & Backman, D. S. 2006. Internal plate fixation of fractures: Short history and recent developments. *Journal of Orthopaedic Science,* 11**,** 118-126.

Vallier, H. A., Hennessey, T. A., Sontich, J. K. & Patterson, B. M. 2006. Failure of lcp condylar plate fixation in the distal part of the femur. A report of six cases. *J Bone Joint Surg Am,* 88**,** 846-853.

Vasarhelyi, A., Baumert, T., Fritsch, C., Hopfenmüller, W., Gradl, G. & Mittlmeier, T. 2006. Partial weight bearing after surgery for fractures of the lower extremity – is it achievable? *Gait & Posture,* 23**,** 99-105.

Veziroglu, F., Uckan, S., Ozden, U. A. & Arman, A. 2008. Stability of zygomatic plate-screw orthodontic anchorage system - a finite element analysis. *Angle Orthodontist,* 78**,** 902-907.

Viceconti, M., Ansaloni, M., Baleani, M. & Toni, A. 2003. The muscle standardized femur: A step forward in the replication of numerical studies in biomechanics. *Proc Inst Mech Eng H,* 217**,** 105-10.

Vijayakumar, V., Marks, L., Bremmer-Smith, A., Hardy, J. & Gardner, T. 2006. Load transmission through a healing tibial fracture. *Clinical Biomechanics,* 21**,** 49-53.

Wagner, M. 2003. General principles for the clinical use of the lcp. *Injury,* 34**,** 31-42.

Wähnert, D., Hoffmeier, K., Fröber, R., Hofmann, G. O. & Mückley, T. 2011. Distal femur fractures of the elderly—different treatment options in a biomechanical comparison. *Injury,* 42**,** 655-659.

Wehner, T., Claes, L. & Simon, U. 2009. Internal loads in the human tibia during gait. *Clinical Biomechanics,* 24**,** 299-302.

Weinans, H., Huiskes, R. & Grootenboer, H. J. 1993. Quantative analysis of bone reactions to relative motions at implant bone interfaces. *Journal of Biomechanics,* 26**,** 1271-1281.

Werner, F. W., Ayers, D. C., Maletsky, L. P. & Rullkoetter, P. J. 2005. The effect of valgus/varus malalignment on load distribution. *Journal of Biomechanics,* 38**,** 349-355.

Wheeless, C. R. Screws. *Wheeless' Textbook of Orthopaedics.* Duke Orthopaedics.

Who 1994. Assessment of fracture risk and its application to screening for postmenopausal osteoporosis. Report of a who study group. *World Health Organ Tech Rep Ser,* 843**,** 1-129.

Wieding, J., Souffrant, R., Fritsche, A., Mittelmeier, W. & Bader, R. 2012. Finite element analysis of osteosynthesis screw fixation in the bone stock: An appropriate method for automatic screw modelling. *PloS one,* 7**,** e33776.

Wilke, H. J., Heuer, F. & Schmidt, H. 2009. Prospective design delineation and subsequent in vitro evaluation of a new posterior dynamic stabilization system. *Spine,* 34**,** 255-61.

Williams, T. H. D. & Schenk, W. 2008. Bridging-minimally invasive locking plate osteosynthesis (bridging-milpo): Technique description with prospective series of 20 tibial fractures. *Injury-International Journal of the Care of the Injured,* 39**,** 1198-1203.

Wirth, A. J., Muller, R. & Lenthe, G. H. V. 2010. Computational analyses of small endosseous implants in osteoporotic bone. *European Cells & Materials,* 20**,** 58-71.

Wongchai, B. 2012. The effect of the configuration of the screw fixation on the interfragmentary strain. *American Journal of Applied Sciences,* 9**,** 842-845.

Woo, S. L. Y., Lothringer, K. S., Akeson, W. H., Coutts, R. D., Woo, Y. K., Simon, B. R. & Gomez, M. A. 1983. Less rigid internal fixation plates: Historical perspectives and new concepts. *Journal of Orthopaedic Research,* 1**,** 431-449.

Woon, C. Y., Wong, M. K. & Howe, T. S. 2010. Lcp external fixation--external application of an internal fixator: Two cases and a review of the literature. *J Orthop Surg Res,* 5**,** 5-19.

Ya'ish, F. M. M., Nanu, A. M. & Cross, A. T. 2011. Can dcp and lcp plates generate more compression? The effect of multiple eccentrically placed screws and their drill positioning guides. *Injury,* 42**,** 1095-1100.

Yanez, A., Carta, J. A. & Garces, G. 2010. Biomechanical evaluation of a new system to improve screw fixation in osteoporotic bones. *Medical Engineering & Physics,* 32**,** 532-541.

Yánez, A., Cuadrado, A., Carta, J. A. & Garcés, G. 2012. Screw locking elements: A means to modify the flexibility of osteoporotic fracture fixation with dcps without compromising system strength or stability. *Medical Engineering and Physics,* 34**,** 717-724.

Yang, G. Y., Kabel, J., Van Rietbergen, B., Odgaard, A., Huiskes, R. & Cowin, S. C. 1999. The anisotropic hooke's law for cancellous bone and wood. *Journal of Elasticity,* 53**,** 125-146.

Yang, P. F., Bruggemann, G. P. & Rittweger, J. 2011. What do we currently know from in vivo bone strain measurements in humans? *J Musculoskelet Neuronal Interact,* 11**,** 8-20.

Yu, W.-J., Kim, M.-R., Park, H.-S., Kyung, H.-M. & Kwon, O.-W. 2011. Finite element analysis of peri-implant bone stresses induced by root contact of orthodontic microimplant. *Korean J Orthod,* 41**,** 6-15.

Zamani, A. R. & Oyadiji, S. O. 2009. Analytical modelling of kirschner wires in ilizarov circular external fixator as pretensioned slender beams. *Journal of the Royal Society Interface,* 6**,** 243-256.

Zand, M. S., Goldstein, S. A. & Matthews, L. S. 1983. Fatigue failure of cortical bone screws. *Journal of Biomechanics,* 16**,** 305-311.

Zdero, R., Rose, S., Schemitsch, E. H. & Papini, M. 2007. Cortical screw pullout strength and effective shear stress in synthetic third generation composite femurs. *J Biomech Eng,* 129**,** 289-93.

Zehnder, S., Bledsoe, J. G. & Puryear, A. 2009. The effects of screw orientation in severely osteoporotic bone: A comparison with locked plating. *Clinical Biomechanics,* 24**,** 589-594.

Zhang, G.-L. & Ge, B.-F. 2009. Overseas advance on the use of locking plates. *Zhongguo Gu Shang,* 22**,** 643-5.

Zlowodzki, M., Williamson, S., Cole, P. A., Zardiackas, L. D. & Kregor, P. J. 2004. Biomechanical evaluation of the less invasive stabilization system, angled blade plate, and retrograde intramedullary nail for the internal fixation of distal femur fractures. *J Orthop Trauma,* 18**,** 494-502.

A
Appendix

A.1. Tensor Interpolation Results

The influence of tensor interpolation versus component-wise interpolation is shown in Figure A.1. The maximum error between the two forms of interpolation was 4.34% for Young's moduli and 7.2% for poisson's ratios.

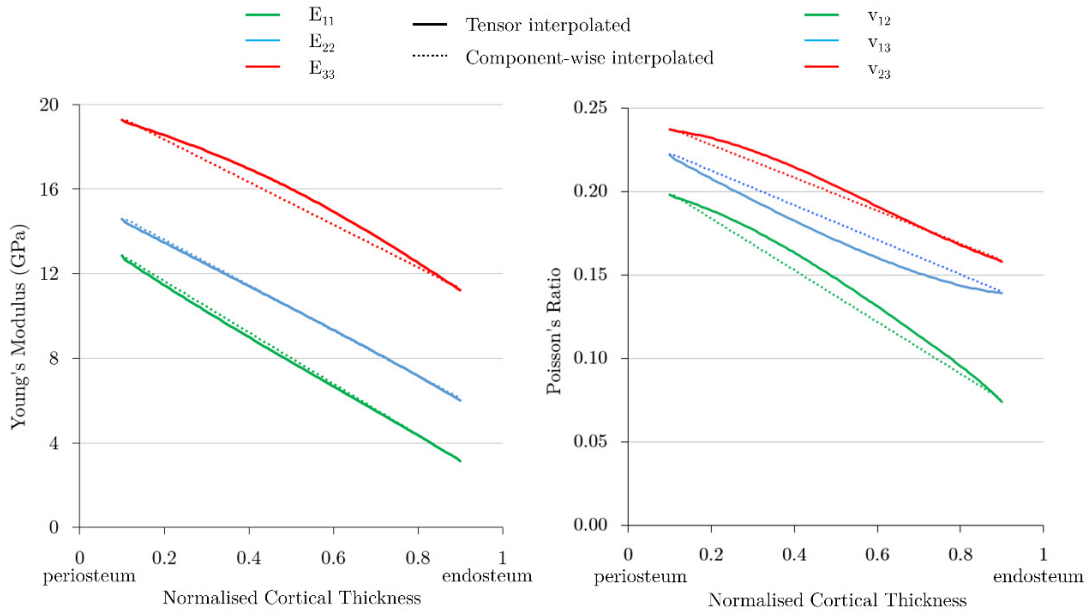

Figure A.1 – Tensor interpolated constants versus linearly interpolated constants through the cortical thickness of osteoporotic bone.

B
Appendix

B.1. Transverse IFM Results

Transverse IFM predictions of the FE simulations are shown next to the experimental measurements for the four loading conditions for narrow plates (Figure B.1) and broad plates (Figure B.2). The transverse IFM predictions of the experimental tests show a similar trend to the axial IFM results in Chapter 5 with increasing restraint reducing IFM. The FE results also find this relationship for axial IFM but not for transverse IFM, where condition (b) produces the largest value.

It was established that the experimental clamped conditions were considerably more flexible than the FE equivalent; however, the FE simulation predicted larger transverse IFM for case (b) than the equivalent experimental test. This can be attributed to the deformation mode. The FE simulation clearly shows that case (b) produces greater relative transverse motion at the fracture site due to the presence of the clamp (Figure B.3). The flexibility of the experimental clamps meant that this deformation mode did not occur. Differences in deformation mode, however, do not account for the large differences observed in the pinned case (c). The transverse IFM is much more similar for C1234, indicating that some of the difference between the FE and experimental results may have been due to bone-plate contact occurring with longer working lengths. This is confirmed in Figure B.3 where the shortest working length, screw configuration C1234, matches the FE prediction closely for all restraint conditions. If bone-plate contact occurs on one side of the fracture and not the other, a deformation mode similar to case (b) is observed (Chao et al., 2013).

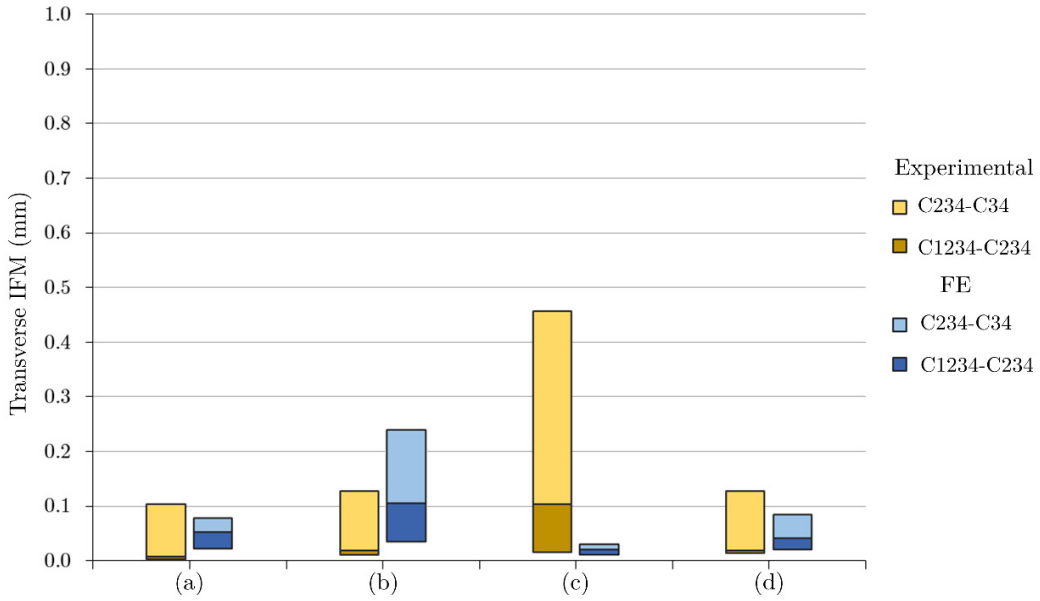

Figure B.1 – Experimental and FE predictions of transverse IFM for narrow plates using the four loading conditions (a-d) at a load of 100N.

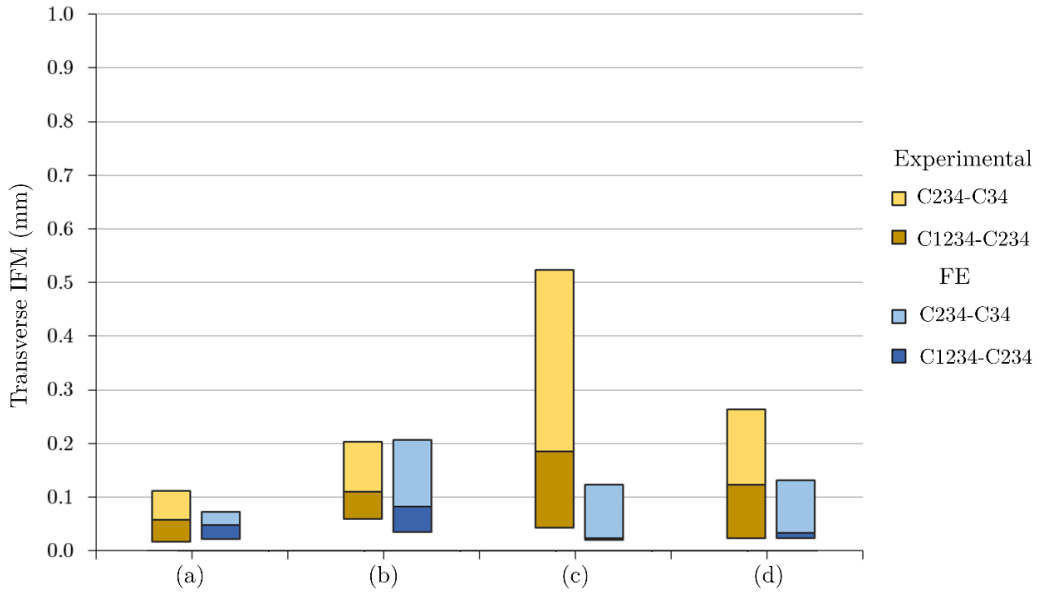

Figure B.2 – Experimental and FE predictions of transverse IFM for broad plates using the four loading conditions (a-d) at a load of 200N.

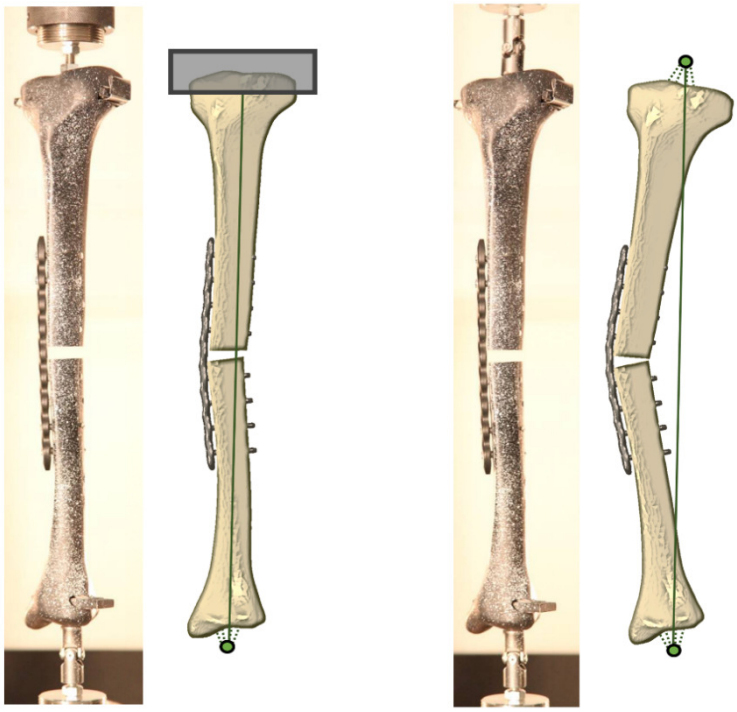

Figure B.3 – Experimental and FE deformed shapes for loading cases (b) and (c). The FE deformed shapes have been exaggerated to see the deformation mode more clearly.

C
Appendix

C.1. Mechanical Explanation for Observations

Cronier et al. (2010) demonstrated that, under bending loads, greater spacing of screws can distribute forces, reducing the localised strain within the bone (or surrogate) around screws. This study has shown that under axial loading the mechanical behaviour can be different. The first two screws on either side of the fracture site were found to have the largest EqSV associated with them under axial loading, regardless of the total number of screws or their position. This finding is counter-intuitive and was investigated further.

An idealised two-dimensional beam model of the bone plate system was created. The plate was given a cross-sectional area of 48.1mm^2 and a second moment of area of 60.3mm^4. Screws were modelled as solid cylinders with diameter 4.5mm. The implants were assumed to be steel (E = 205GPa). The bone was considered to be rigid and was modelled as cross-braced rectangles using members with cross-sectional area much greater than the plate or screws. The bone-plate off-set was 10mm. The total length of the bone-plate system was 350mm with a working length of 30mm. The model was meshed with 206 quadratic shear flexible beam elements. The analysis was conducted up to a load of 100N which was applied on a single node located at the centre of the 40mm wide bone section.

C.1.1. Pull-out Forces

If the fixation device is considered to be rigid, as is often done in uni-lateral external fixation studies (Donaldson et al., 2012a, Huiskes et al., 1985), the influence of the screw positioning is intuitive. Consider a door with three hinges: if the central door hinge is positioned nearer to the top of the door the top two hinges will share the tensile pull-out force; if it is located closer to the bottom hinge, it will share compressive load. If it is located exactly in the middle it will transmit only shear forces. If the fixator is assumed to be rigid the result matches the door hinge scenario (Figure C.1).

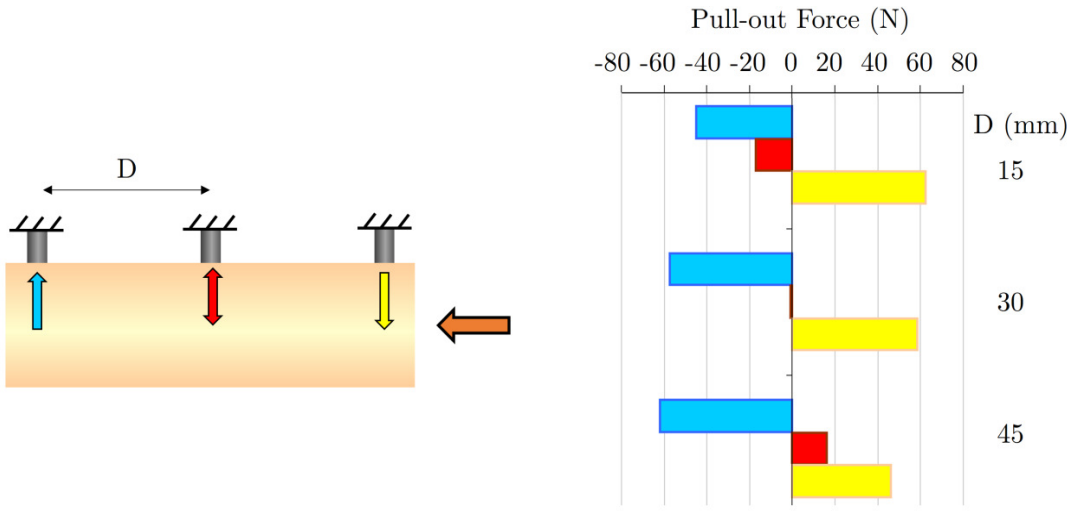

Figure C.1 – Pull-out forces for different positions of the central screw assuming the fixator to be rigid

Although locked plating is structurally similar to uni-lateral fixation, the influence of the reduced bone plate off-set is significant. The majority of the fracture gap motion is generated by plate bending and so it cannot be considered to be rigid. The plate has considerably lower flexural rigidity than the bone and deformation is most noticeable over the working length region of the plate. To better view the deformed shape of the plate, the plate was restrained up to the first screw (Figure C.2). The bending of the first screw closest to the fracture gap causes the bone to rotate versus the restrained plate. The plate must then bend to remain flush with the bone. This results in increased

pull-out forces as the screw must restrain the plate bending. Figure C.2 shows the pull-out force for each screw depending on the location of the middle screw. Interestingly, the first screw is the only one in compression (push-in); the other screws are in tension. The closer the second screw is to the first screw, the larger the peak pull-out forces. This explains the predictions of larger EqSV in the relevant screw configurations.

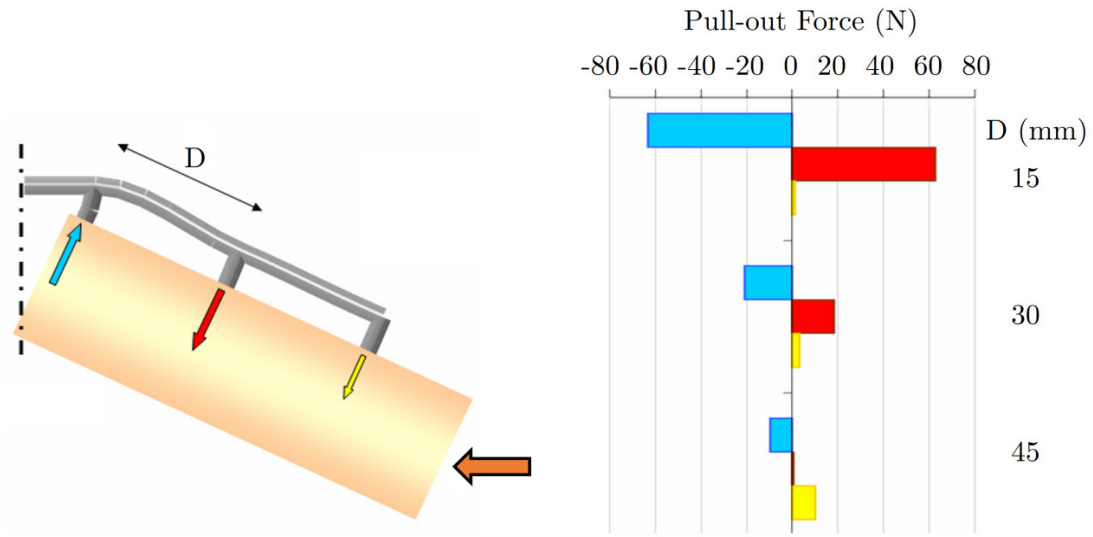

Figure C.2 – Pull-out forces for different positions of the central screw incorporating the flexural rigidity of the fixator

To examine the influence of plate dimensions, more rigid plate properties were used for comparison ($I = 129.1$ mm^4 $A = 76$ mm^2) and resulted in increased pull-out forces. This supports the conclusion regarding plate rigidity drawn by the Perren (2002) in a cantilever bending example. Therefore, the reductions in EqSV seen by using a more rigid plate are due to better distribution of normal forces at the screw-bone interface and not changes in pull-out forces. For interest, the analysis was re-run using an increased bone-fixator off-set of 30mm; the trends remained the same.

C.1.2. Shear load transfer

Unlike axial load transfer, shear load transfer remains similar for all screw positions. The portion of the plate spanning between the first and second screws, D, was found to be in tension, which is counter-intuitive as the loading is compressive. The reason for this is because of the bending occurring at the first screw. Figure C.3a shows the undeformed shape of the bone plate construct where the bone is assumed to be rigid. If a single screw is considered the deformation expected is illustrated in Figure C.3b. Due to the bending of the first screw an angle is formed between the plate and the bone. If a second screw is added, the plate is pulled back towards the bone. This produces both pull-out forces and tension in the plate due to the extension, δ (Figure C.3c). The first screw, therefore, transfers the total applied plus forces induced due to the plate extension. This can result in shear forces greater than the total applied load.

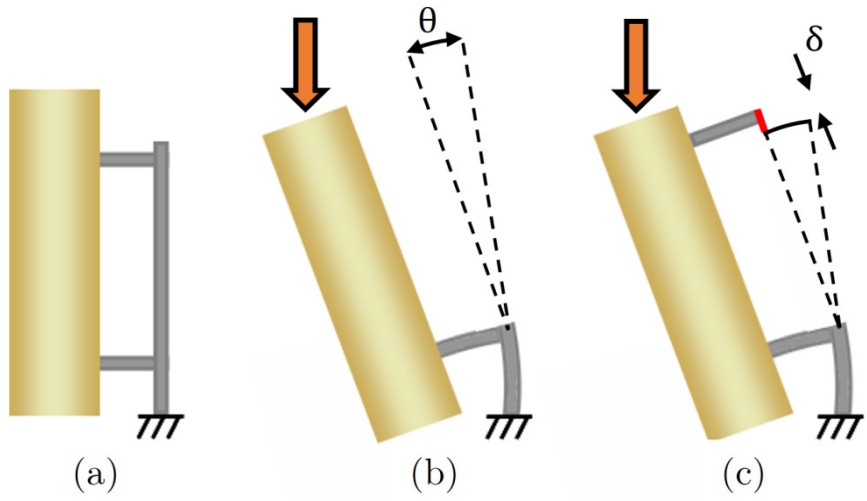

Figure C.3 – Depiction of the bone plate system (a) unloaded; (b) loaded showing the angle of rotation at the first screw and (c) the extension of the plate, δ, caused by the screw bending.

C.2. Influence of Muscle Forces

In the previous chapter different loading conditions were tested and it was concluded that the hinge-pin condition could be more physiological at larger loads. If full weight-bearing is imposed muscle forces may become significant. Therefore the effect that muscle forces had on the hinge-pin system was investigated using muscle forces quoted by Duda et al. (2002). Muscles attachment locations were scaled to the bone and were included as concentrated nodal loads (Figure C.4).

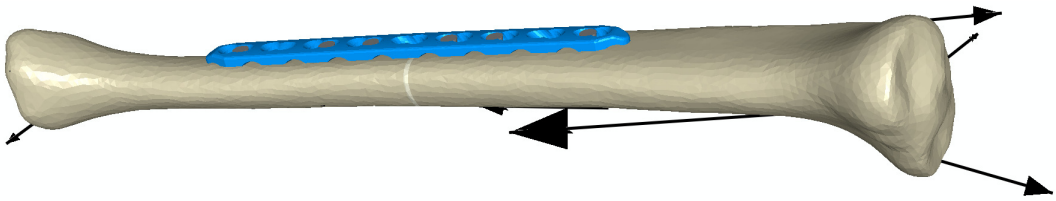

Figure C.4 – Muscle forces incorporated in a tibial model using concentrated point loads.

It was found that muscle forces induced torsional forces at the knee that were not present without muscle forces (Figure C.5). These changes in reaction force, however, did not significantly change the behaviour of the bone-plate system; IFM, plate stress and strains around screws were not significantly affected (Figure C.6 and Figure C.7). This is not surprising as the dominant loads in the tibia are from the joint reactions forces at the knee and ankle. The ankle reaction is 2079N whereas the soleus produces the largest muscle force at 684N (Duda et al., 2002). These muscle forces also act predominantly axially. The more flexible the restraint conditions, the greater influence muscles forces are likely to have. In order to use muscle forces in a pinned loading condition, however, additional restraint would have to be incorporated to prevent spinning about the Z axis; the bone would then no longer be entirely free to rotate and thus not a true pinned condition.

Figure C.5 – Condylar reaction forces in the fractured tibia (a) without muscle forces and (b) with muscle forces.

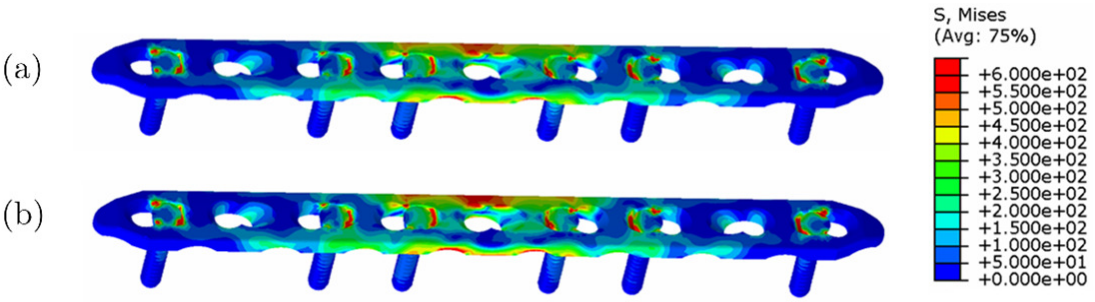

Figure C.6 – Von Mises stress in the plate (a) without and (b) with muscle inclusions.

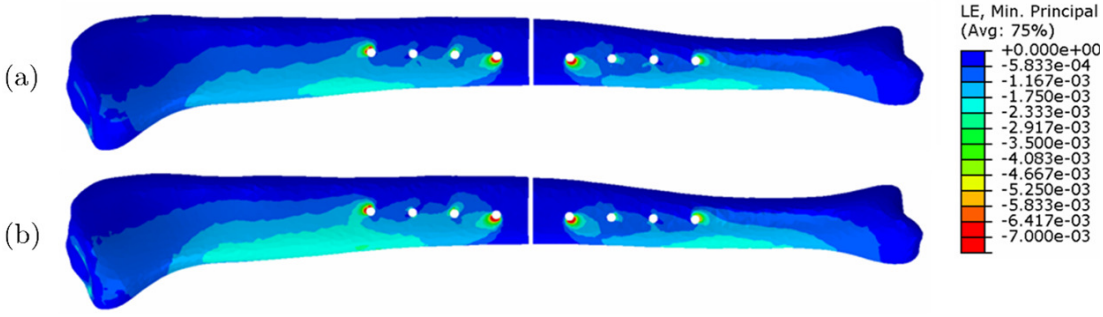

Figure C.7 – Minimum principal strain within the bone (a) without and (b) with muscle inclusions.

D
Appendix

D.1. Chapter 10

D.1.1. Stresses Within the Plate

The von Mises stress distribution within the plate for different in vitro loading conditions is shown in Figure D.1.

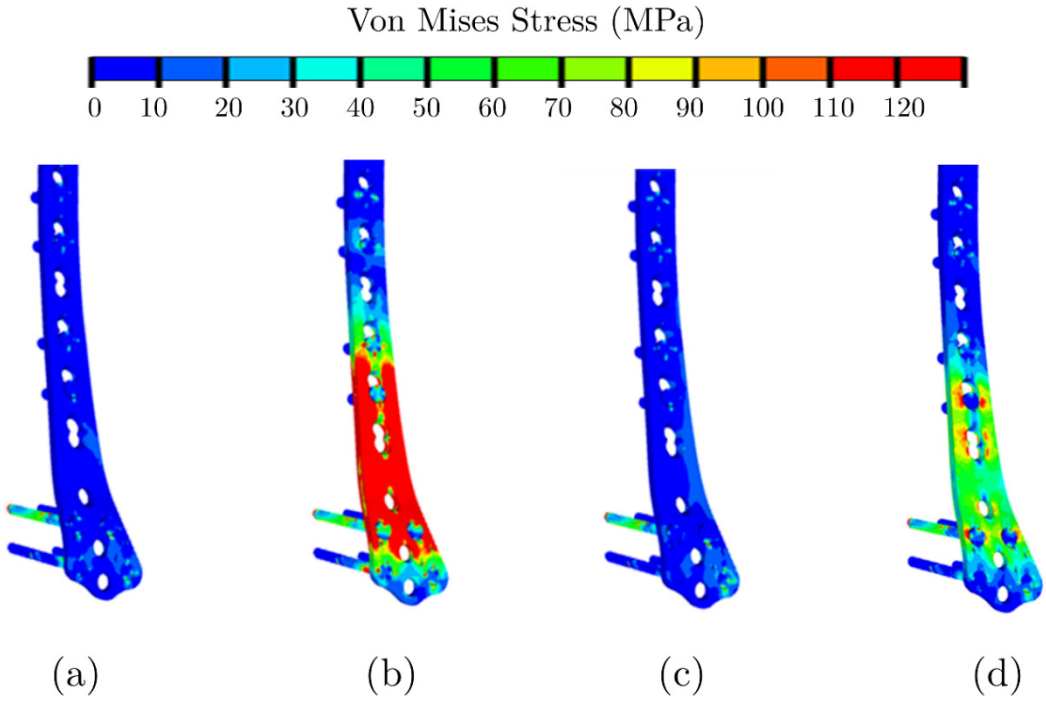

Figure D.1 – Von Mises stress in the plate for the in vitro loading conditions (a) (exaggerated x50), (b) (x1); (c) (x50); and (d) (x5). The applied load is 368N.

D.1.2. Strains Throughout the Femur

The minimum principal strain at different locations through the intact femur is shown in cross-sectional slices (Figure D.2).

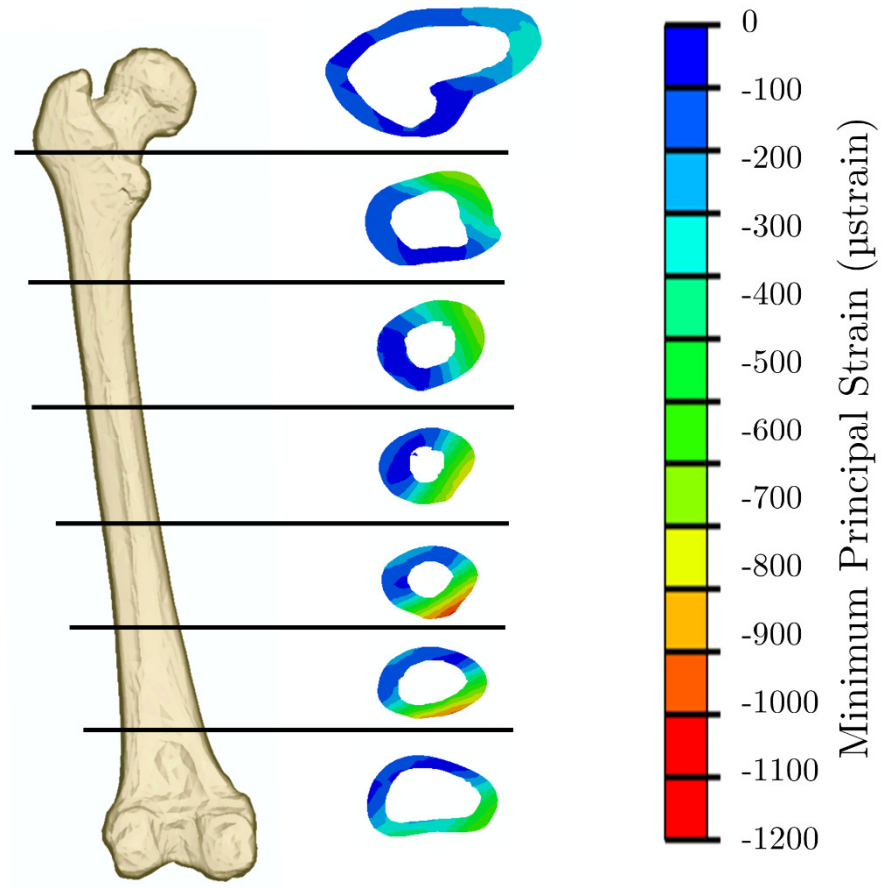

Figure D.2 – Minimum principal strain at different cross-sections through the femur under 15% walking gait loading using restraint condition (f).

Publications

This research has resulted in the following publications to date:

Journal Articles

Alisdair R. MacLeod, Pankaj Pankaj, A. Hamish R.W. Simpson, The reasons conventional screws are inferior to locking screws in osteoporotic bone: a finite element explanation, Computer methods and in Biomechanics and Biomedical Engineering, 2014; 18(16):1818-25. DOI: 10.1080/10255842.2014.974580.

Alisdair R. MacLeod, Pankaj Pankaj, A. Hamish R.W. Simpson, Does screw-bone interface modelling matter in finite element analyses?, Journal of Biomechanics 2012; 45(9):1712-6. http://dx.doi.org/10.1016/j.jbiomech.2012.04.008

Book Chapter

MacLeod A, Pankaj P, 2014, Computer simulation of fracture fixation using-extra-medullary devices: an appraisal. In Computational Biomechanics in Medicine, Springer, 87-99.

Published Conference Proceedings

MacLeod, A., Pankaj, P., and Simpson, H., 2012, The Effect of Varying Screw Configuration of the Mechanical Response of Locking Plate Fixators. Journal of Biomechanics, 45, Supplement 1(0), S218. http://dx.doi.org/10.1016/S0021-9290(12)70219-1

MacLeod, A., Pankaj, P., and Simpson, H., 2012, Screw-Bone Interface Modelling in Locking Plate FE Models. Journal of Biomechanics, 45, Supplement 1(0), S333. http://dx.doi.org/10.1016/S0021-9290(12)70334-2

MacLeod, Alisdair; Pankaj, Pankaj; Simpson, Hamish, A. Finite Element Comparison of Locking Plate and Compression Plate Fracture Fixation, The Proceedings of the 10th International Symposium on Computer Methods in Biomechanics and Biomedical Engineering, 357-362, Berlin, 2012.

Alisdair R. MacLeod, Pankaj Pankaj, A. Hamish R.W. Simpson, The Importance of Modelling Bone-Implant Interface in Locking Plate FE Models, Journal of Bone Joint Surgery (British) 2012 vol. 94-B no. SUPP XXXVI 84.

Conference Oral Presentations

Alisdair R. MacLeod, Pankaj Pankaj, A. Hamish R.W. Simpson, Axial Compression Tests of Plated Bone: the Influence of the Loading Conditions on the Mechanical Response, IIE Scotland Postgraduate Conference, June 2013, Edinburgh, UK.[10]

MacLeod, A., Pankaj, P., and Simpson, H., 2012, The Effect of Varying Screw Configuration of the Mechanical Response of Locking Plate Fixators, European Society of Biomechanics, July 2012, Lisbon, Portugal.

Alisdair R. MacLeod, Pankaj Pankaj, A. Hamish R.W. Simpson, Finite element comparison of locking plate and dynamic compression plate fracture fixation, Computer Methods in Biomechanics and Biomedical Engineering, April 2012, Berlin, Germany.

[10] Awarded best presentation prize (£100).

Conference Poster Presentations

Alisdair R. MacLeod, Pankaj Pankaj, A. Hamish R.W. Simpson, A simple analytical tool to optimise locking plate configuration. Accepted to World Congress of Biomechanics, July 2014, Boston, USA.

Alisdair R. MacLeod, Pankaj Pankaj, Incorporating the effect of osteoporotic microstructure in musculoskeletal bone models. Anisotropic, heterogeneous and cellular materials, December, 2013, Edinburgh, UK.

Alisdair R. MacLeod, Pankaj Pankaj, A. Hamish R.W. Simpson, Predicting fracture gap motion using plating; working towards patient specific clinical weight bearing guidelines, 4th Joint BRS-BORS meeting, September 2013, Oxford, UK.

MacLeod, A., Pankaj, P., Simpson, H., Axial compression tests of plated bone: A numerical study to investigate the effect of loading conditions on the mechanical response, European Society of Biomechanics, August 2013, Patras, Greece.

Alisdair R. MacLeod, Pankaj Pankaj, A. Hamish R.W. Simpson, Screw-Bone Interface Modelling in Locking Plate FE Models, European Society of Biomechanics, July 2012, Lisbon, Portugal.

Alisdair R. MacLeod, Pankaj Pankaj, A. Hamish R.W. Simpson, Choosing an appropriate screw configuration for osteoporotic long bone fractures, Computer Methods in Biomechanics and Biomedical Engineering, April 2012, Berlin, Germany.

Alisdair R. MacLeod, Pankaj Pankaj, A. Hamish R.W. Simpson, The Importance of Modelling Bone-Implant Interface in Locking Plate Finite Element Models, 2nd EPSRC meeting on patient specific modelling, September, 2011, Edinburgh, UK.